CATALYTIC THERMAL DECOMPOSITION OF THE MUNICIPAL MIXED PLASTIC WASTE INTO SUSTAINABLE ALTERNATIVE FUEL FOR MODIFIED CI ENGINE

A Thesis submitted to the

UPES

For the Award of
Doctor of Philosophy

in

Mechanical Engineering

By

Shashank Pal

June 2024

Supervisor
Dr. Anil Kumar

External Supervisor
Dr. Shyam Pandey

Department of Mechanical Engineering

School of Advanced Engineering (SOAE)
UPES
Dehradun- 248007: Uttarakhand

CATALYTIC THERMAL DECOMPOSITION OF THE MUNICIPAL MIXED PLASTIC WASTE INTO SUSTAINABLE ALTERNATIVE FUEL FOR MODIFIED CI ENGINE

A Thesis submitted to the

UPES

For the Award of
Doctor of Philosophy

in

Mechanical Engineering

By

Shashank Pal

SAP ID- 500080562

June 2024

Supervisor
Dr. Anil Kumar
Associate Professor
Department of
Mechanical Engineering, UPES

External Supervisor
Dr. Shyam Pandey
Principal at
Yogoda Satsanga Mahavidyalaya

Department of Mechanical Engineering

School of Advanced Engineering (SOAE)
UPES
Dehradun- 248007: Uttarakhand

DECLARATION

I declare that the thesis entitled "**Catalytic Thermal Decomposition of the Municipal Mixed Plastic Waste into Sustainable Alternative Fuel for Modified CI Engine**" has been prepared by me under the guidance of Dr. Anil Kumar (Supervisor). Associate professor of the Mechanical Engineering Department, at UPES, Dehradun and Dr. Shyam Pandey (External supervisor), former Professor of the Mechanical Engineering Department, at UPES, Dehradun, Currently – Principal at Yogoda Satsanga Mahavidyalaya, Ranchi. No part of this thesis has formed the basis for the award of any degree or fellowship previously.

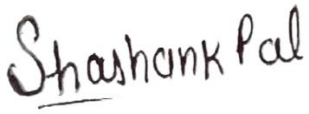

Shashank Pal
Department of Mechanical Engineering
UPES,
Bidholi Campus, Dehradun
Uttarakhand, India

DATE: June 6, 2024

UPES
UNIVERSITY OF TOMORROW

Great Place To Work. Certified

CERTIFICATE

I certify that **Shashank Pal** has prepared his thesis entitled "**Catalytic Thermal Decomposition of the Municipal Mixed Plastic Waste into Sustainable Alternative Fuel for Modified CI Engine**" for the award of PhD degree of the UPES, under my guidance. He has carried out the work at the Department of **Mechanical Engineering**, UPES.

Internal Supervisor

Dr. Anil Kumar
Associate professor
Department of Mechanical Engineering
UPES, Bidholi Campus, Dehradun

Energy Acres: Bidholi Via Prem Nagar, Dehradun - 248 007 (Uttarakhand), India, T: +91 135 2770137, 2776053/54/91, 2776201, M: 9997799474, F: +91 135 2776090/95
Knowledge Acres: Kandoli Via Prem Nagar, Dehradun - 248 007 (Uttarakhand), India, M: +91 8171979021/2/3, 7060111775

Yogoda Satsanga Mahavidyalaya
(Established in 1967)
NAAC Accredited B++ (CGPA 2.89)
Affiliated to Ranchi University & registered under 2 (F) & 12 (B) of UGC Act

CERTIFICATE

I certify that **Shashank Pal** has prepared his thesis entitled **"Catalytic Thermal Decomposition of The Municipal Mixed Plastic Waste into Sustainable Alternative Fuel for Modified CI Engine"** for the award of PhD degree of the UPES, under my guidance. He has carried out the work at the Department of **Mechanical Engineering, UPES**.

External Supervisor

Dr. Shyam Pandey
Principal at
Yogoda Satsanga Mahavidyalaya
Ranchi, Jharkhand 834004

Jagannathpur, Dhurwa, Ranchi 834 004, Jharkhand
Email: ysm.principal@ysei.edu.in, Web: www.ysmranchi.net
Under the auspices of YOGODA SATSANGA SOCIETY OF INDIA
Founder: SRI SRI PARAMAHANSA YOGANANDA • President: SRI SRI SWAMI CHIDANANDA GIRI

ABSTRACT

The recovery of fuel oil and gas from waste has sparked global interest in energy security and environmental problems. It has encouraged researchers to investigate affordable alternative fuels, such as alcohol and biodiesel, that have qualities similar to standard petroleum-based fuels, particularly for use in internal combustion engines. The abundant availability of municipal mixed plastic waste (MMPW), containing high calorific value hydrocarbons, makes them ideal sources of alternative fuels. MMPW consists of low-density polyethylene (LDPE), Polyethylene (PE), High-density polyethylene (HDPE), Polystyrene (PS), Polyethylene terephthalate (PET), polyvinyl chloride (PVC) and Polypropylene (PP) along with filler and binders. Plastic waste is primarily generated from different sectors, including agriculture, construction, industry, food packaging, and household consumption. Once these plastic products fulfill their intended purposes, they are typically discarded, collected by the municipality, and dumped into municipal garbage houses. However, this indiscriminate disposal poses a significant environmental and public health threat. Therefore, recycling MMPW is necessary to reduce the quantity of plastic waste. There are various thermochemical recycling roots, such as incineration, combustion, gasification, hydrolysis, pyrolysis, etc., for fuel generation. However, pyrolysis is the most pertinent technology that involves heating MMPW at elevated temperatures in an inert atmosphere to produce solid, gas, and liquid fuel.

The current study investigated both conventional and advanced (catalytic) pyrolysis processes. Two types of catalysts, namely commercial FCC catalyst and fuller earth, were employed, significantly influencing the yield of plasto oil (PO), char, and gas formation. Initially, conventional pyrolysis of the MMPW was conducted at 400 °C, 450 °C, 500 °C, 550 °C and 600 °C temperatures with 10 °C/min heating rate for 3 hours of residence time. It resulted in plastic oil yield of 43.2 wt.%, 47.7 wt.%, 52.1 wt.%, 53.9 wt.%, and 48.3 wt.%, respectively and observed that on increasing the temperature, the gaseous yield also increased, while concurrently decreasing the yield of PO. Catalytic thermal degradation of

the MMPW was carried out with different proportions of fuller earth and Commercial FCC catalyst (2 wt.%, 4 wt.%, 6 wt.%, 8 wt.%, 10 wt.% of feedstock) at 500 °C temperature at 10 °C/min heating rate for 3 hr. residence time. The highest yield of PO was achieved with 8 wt.% of Fuller Earth, resulting in yields of 78.9 wt.% and 76.2 wt.% for Fuller Earth and Commercial FCC catalyst, respectively. Further investigations were carried out on a higher yield of PO obtained by 8 wt.% fuller earth as a catalyst. The fractional distillation of the obtained PO was carried out at temperature ranges 20 to 180 °C and 180 to 340 °C and yielded 340 gm/kg plasto oil light (POL) in gasoline range and 580 gm/kg plasto oil heavy (POH) in diesel range respectively. Additionally, 70 gm/kg of tar or residue was obtained as the remaining byproduct. The physicochemical characteristics of the POH were assessed using ASTM methods. A single-cylinder 4-stroke compression ignition (CI) engine was tested with PO and diesel blends such as PO25D75, PO50D50, PO75D25, and neat plasto oil. PO fueled in CI engine produced lower brake thermal efficiency (BTE) by 6.90% than diesel at higher engine load. This is caused by higher viscosity and longer hydrocarbon chains (C_{10}–C_{30}), leading to inadequate fuel atomization and ineffective combustion in the cylinder. However, increasing the PO in the diesel blend increased the Hydrocarbon (HC), carbon monoxide (CO), and oxide of nitrogen (NO_x). However, carbon dioxide (CO_2) was decreased by 5.60, 10.87%, 19.06%, and 21.81% for PO25D75, PO50D50, PO75D25, and PO100, respectively, at higher engine load. It has been observed that PO produced from the MMPW pyrolysis has higher density and viscosity, which may cause higher emissions and poor combustibility. Therefore, fractional distillation of PO was carried out at 20-180 ^oC and 180-340 ^oC temperatures to obtain the plasto oil light (POL) and plasto oil heavy (POH), respectively. The heavier plasto oil was utilized in the modified CI engine. The conventional direct injection (DI) compression ignition engine was modified to a partially premixed charge compression ignition (PCCI) engine by incorporating the fuel vaporizer. The experimental study was conducted in PCCI engine mode with 2 and 3 ml/min induction of POH vapor through the

intake manifold with direct injection of diesel, POH10D90, and POH20D80. In PCCI mode, employing 2 and 3 ml/min of POH vapor induction with diesel (DI) resulted in a lower BTE by 2.96% and 4.64%, respectively, than conventional CI engine fueled with diesel at full engine load. In PCCI engine mode, direct injection of POH10D90 with 2 and 3 ml/min POH vapour induction decreased the BTE by 3.42% and 6.33%, respectively, compared to the POH10D90 fueled in a conventional CI engine. However, direct injection of POH20D80 with 2 and 3 ml/min POH vapour induction decreased the BTE by 4.63% and 7.20%, respectively. The NO_x emission was reduced by 16.78% and 25.65% for 2 ml and 3 ml POH vapor induction with diesel (DI), compared to the conventional CI engine fueled with diesel at maximum engine load. However, the smoke opacity was diminished by 16.98% and 22.64% for the same conditions. Similarly, the direct injection of POH20D80 with 3 ml of POH vapour induction decreased the NO_x by 19.86% compared to the conventional CI engine fueled with POH20D80 at a higher engine load. However, combining 10% EGR reduced the NO_x emission and inversely increased the smoke opacity without much affecting the BTE in PCCI engine mode.

ACKNOWLEDGEMENT

I hereby acknowledge with deep appreciation the excellent supervision of Dr. Anil Kumar and Prof. Dr. Shyam Pandey for the past four years at UPES. His untiring creative and innovative drive, Wisdom, and invaluable insights contributed enormously to the success of this work. His consistent emphasis on practicality has ignited my enthusiasm for learning and applying acquired knowledge to address modern societal issues in a simplified and practical way. They consistently provided opportunities to enhance paper writing and presentation skills, fostering confidence and nurturing the growth of a proficient researcher. Their unwavering support was indispensable; completing a PhD would have been impossible without it. The wealth of knowledge and guidance they imparted has made me today and will continue to enlighten me in the future to achieve the best in my life.

I extend my gratitude to the R&D team at UPES for providing the SEED grant facility to accomplish the work without any financial obstacles. I also appreciate the ongoing encouragement provided by Dr. Devesh Kumar Awasthi, Dr. Syed Mohammad Tauseef, and Dr. Pankaj Thakur throughout this work. I especially want to thank Dr. Swapnil Sureshchandra Bhurat for transferring the fuel vaporizer technology. He also provided technical guidance in experiments and research paper writing and always stood by me like an elder brother.

I extend my heartfelt appreciation to the members of my Doctoral Research Committee, namely Dr. Gopalakrishnan Govindasamy from the Chemical Engineering Department, and Dr. Ram Kunwer and Dr. Rajesh Maithani from the Mechanical Engineering Department. Their invaluable suggestions and guidance at various stages of my work have been instrumental in shaping the research work. I am also grateful to the Head of the Mechanical cluster Dr. Ashish Karn and the Research Coordinator Dr. Adesh Kumar, for their encouragement and insightful suggestions. They all have played a significant role in polishing my

research writing skills. Their enduring guidance will remain unforgettable throughout my lifetime.

I am also pleased to thank Dr. Praveen Kumar Ghodke of the Chemical Engineering Department at NIT Calicut and Dr. Amit Kumar Sharma of the Chemistry Department and Center for Renewable Energy Research at UPES. Who made my access simpler to the research facilities and laboratory and gave an opportunity to become part of their team. Special thanks to Mr. Pardeep Singh, the engine lab technician, for his unwavering assistance throughout my engine experimentation. I am also thankful to all the dedicated lab staff at our Institute (UPES) for their continuous support. Additionally, I want to recognize APEX Innovation Pvt. Ltd. in Sangli, Maharashtra, for providing the lab facility and research assistance for the PCCI engine project. During this time, I have collaborated with IIT, Roorkee for TGA analysis, Wadiya Institute of Himalyan Geology, Dehradun for XRF analysis, UIT, Dehrdaun for SEM analysis and Material Analysis and Research Centre, Banglore for BET and NH_3 TPD analysis I regard this greatly. I wish to extend my warmest thanks to all those who have helped me directly or indirectly.

I extend my heartfelt appreciation to my grandfather Shri Phool Singh Pal and grandmother Late Shrimati Vimla Devi. He aspired to see his grandson awarded a doctorate. I would like to thank my father Shri Pramod Kumar and mother Shrimati Sushila Devi for their unwavering support and love throughout every stage of my life. Completing this degree would have been impossible without their encouragement. Lastly, I am deeply grateful to my dear colleagues Dr. Caneon Kurein, Prashant Kumar S, Rishabh Agarwal, Krishna Moorthy Rajendran and Akshit Trada for their consistent assistance and support.

TABLE OF CONTENTS

LIST OF FIGURES

LIST OF TABLES

LIST OF SYMBOLS

A-F	Air fuel ratio
BET	Brunauer–Emmett–Teller
BTE	Brake thermal efficiency
BSFC	Brake-specific fuel consumption
CA	Crank Angle
CHNS-O	Carbon hydrogen nitrogen and oxygen
CI	Compression ignition
CO	Carbon monoxide
CO_2	Carbon dioxide
DI	Direct injection
DAQ	Data Acquisition system
EDX	Energy Dispersive X-Ray
EGR	Exhaust gas recirculation
EGT	Exhaust gas temperature
ECU	Electronic control unit
FTIR	Fourier Transform Infrared Spectroscopy
FBR	Fixed bed reactor
GCV	Gross calorific value
GC-MS	Gas chromatography and mass spectroscopy
HCCI	Homogeneous charge compression ignition
HC	Hydrocarbon
IC	Internal combustion
IVC	Inlet valve close
NOx	Oxides of nitrogen
NHRR	Net heat release rate
OEMs	Original equipment manufacturer
PM	Particulate matter
PCCI	Partially premixed charge compression ignition engine
PO	Plasto oil
POL	Plasto oil light

POH	Plasto oil heavy
RT	Residence time /retention time
SEM	Scanning Electron Microscopy
SoI	Strat of injection
aTDC	After top dead centre
TGA	Thermo gravimetric analysis
TPD	Temperature programmed distribution
VE	Volumetric efficiency
XRF	X-ray fluorescence
XRD	X-ray diffraction

CHAPTER 1: INTRODUCTION

1.1 Necessity of developing sustainable alternative fuel

Transportation has become an essential energy-consuming sector, accounting for 30% of global energy consumption (*Energy Institute*, 2022). Despite the introduction of a fleet of new E-vehicles, 90% of transportation is currently powered by oil to sustain the staggering 1.4 billion automobiles, 100,000 ships, and 29,000 aircraft currently in use (*The Drive*, 2023). A statistical report revealed that global proven oil in 2023 was 1.6 trillion barrels and consumption was 0.03 trillion barrels per annum, suggesting that it may last barely for 50 more years (Statistical Review of World Energy, 2022). On the other hand, the total CO_2 emission from fossil fuels' energy use reached 39 giga tons. Thus, the twin sustainability issues of the long-term availability of petroleum and global warming caused by CO_2 emission from its use have created energy security and environmental concerns. The increasing population and transportation needs, particularly in the aviation and shipping sectors, which are not expected to be electrified soon due to technological constraints, will increase oil consumption further. Fossil fuel resources, also suffer from supply interruptions and price volatility often due to geopolitical conflicts. Petroleum is non-renewable as it takes millions of years to form from plant and animal remnants by the action of high pressure and heat that prevails at the earth's subsurface compared to its consumption rate (Okolie et al., 2020; Dey et al., 2021). Therefore, a sustainable alternative fuel is required to reduce the dependency on petroleum-derived transportation fuel. Biomass-derived fuels such as bioethanol, biodiesel, and biogas are the important solution to the stated problem as they are renewable and carbon neutral from a life cycle viewpoint and easily adopted by the automobile sector.

However, biomass suffers from low energy density, higher oxygen content, feedstock availability, and supply chain constraints, appropriate pretreatment methods, and operational issues involving biomass conversion to biofuels.

On the other hand, the production of synthetic plastics, fiber, and rubber is increasing, most of which is produced from petroleum. Plastics have become an integral part of society due to their wide use in everyday life owing to their lightweight, moldability, pliability, durability, versatility, and economic viability. Hence, plastic utilization increased from 6,800 kilotons per annum in 2010 to 20898 kilotons per annum in 2021, as a result per capita plastic consumption increased from 5.5 kg in 2010 to 15 kg in 2021 in India (Figure 1.1). However, plastics produced in 2022 reached 430 million metric tons due to its increased packaging application.

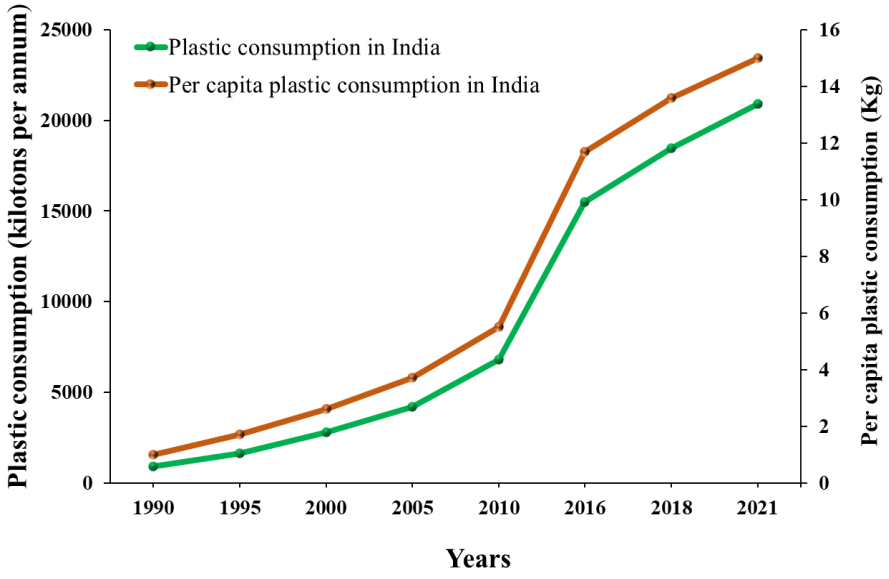

Figure 1.1: Plastic consumption and per capita plastic consumption in India (*India - Net Plastic Consumption 2021 | Statista*, 2024*; India - per Capita Plastic Consumption in India | Statista*, 2024)

There are various sectors, such as packaging, automotive, electrical and electronics, agriculture, building and construction, and household, where plastics are used. Figure 1.2 shows the plastic consumption by the different sectors in

India shows that approximately 59% of plastics are consumed by the packaging industry. The average service life required for packaging is hardly minutes to days, whereas the average lifetime of plastics that make up the packaging varies from a minimum of 20 years to several hundred years, resulting in waste. It is evident from the fact that global plastic waste was 6.3 billion metric tons in 2015, and is expected to reach 12 billion metric tons by 2050.

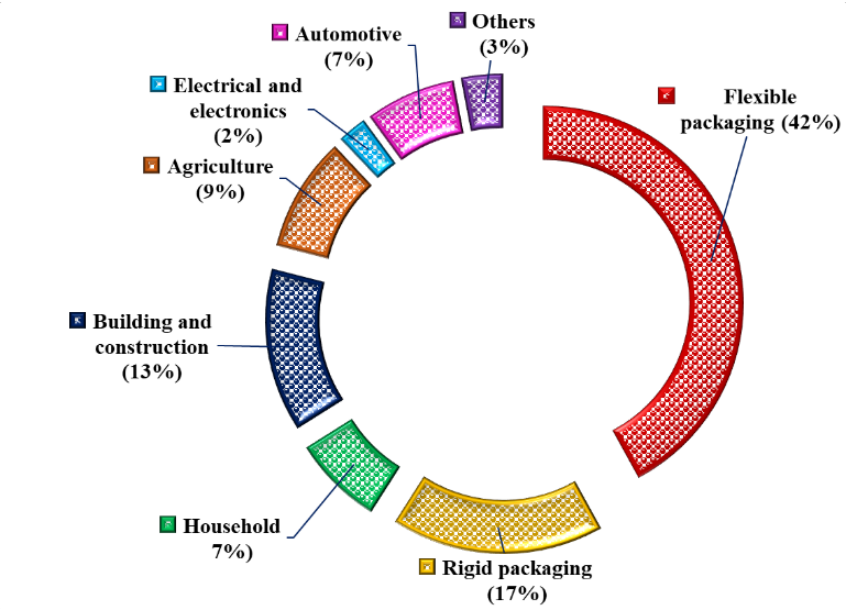

Figure 1.2: Plastic consumption by different sectors in India by 2018 (*India: Plastic Consumption Share by Sector | Statista*, 2024)

Plastics discarded into wastes include single-use plastic products, end-of-life products, manufacturing waste, packaging waste, and improperly disposed items. These are typically collected by local authorities and disposed of alongside other solid waste, known as municipal solid waste (MSW). Within MSW, there exists a category termed municipal mixed plastic waste (MMPW), which encompasses plastic waste originating from households, offices, and institutions within a municipality or city (Figure 1.3).

Figure 1.3: Municipal solid waste (Nitter Kathrine, 2022)

Municipal mixed plastic waste can be challenging to manage because of its heterogeneity and non-plastic contaminants such as food residues, paper, glass, and metals, as shown in Figure 1.4.

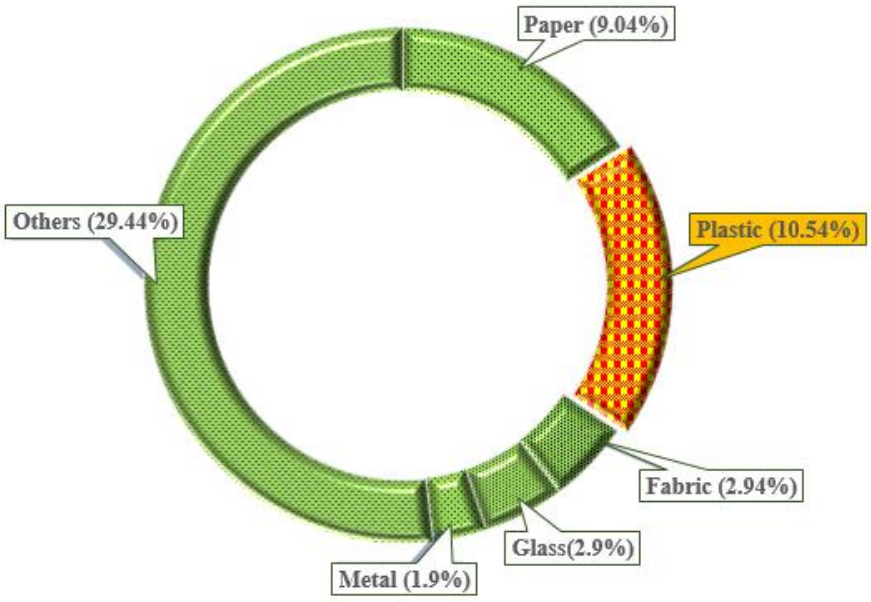

Figure 1.4: Composition of municipal solid waste (Srivastava et al., 2020)

Figure 1.5 illustrates the categorization of plastics present in the 10.54% of plastic waste found within MSW, mainly HDPE (57.4%) and LDPE (17.4%), owing to their wide usage in the packaging industry. Different types of plastic waste pose

various challenges due to their composition, recycling feasibility, and environmental impact. Plastic waste contaminates ecosystems, including seas, rivers, and land. Plastic waste presents a significant threat to marine life as animals often confuse it with food, leading to ingestion and entanglement. Moreover, the prolonged decomposition process of plastic, spanning hundreds of years, not only occupies land space but also damages the environment and poses risks to wildlife and human health. Tackling these issues requires a comprehensive strategy encompassing regulations to segregate plastic waste from the rest of MSW at source, restriction on its disposal by landfill, plastic waste utilization, investment in recycling infrastructure, development of sustainable materials, and public awareness initiatives promoting responsible waste management practices.

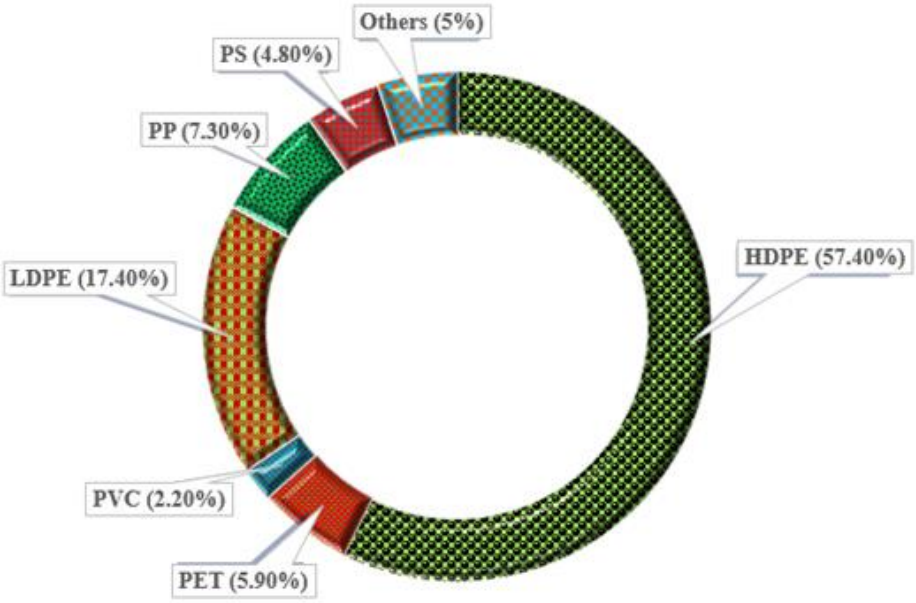

Figure 1.5: Classification of various types of plastic waste (Areeprasert et al., 2017)

Hence, there has been a heightened emphasis on developing suitable techniques for utilizing waste plastic and preventing its harmful effects on the environment. Therefore, several thermochemical technologies such as incineration (Franke et al., 1999; Murakami et al., 2009; Dong et al., 2018), gasification (Lee et al., 2014;

Lopez et al., 2015; Bai et al., 2019), plasma gasification (Q.Zhang et al., 2012; Sanlisoy et al., 2017; Munir et al., 2019), pyrolysis (Davi et al., 2019; Kofi et al., 2019; Won et al., 2020) and hydrogenation (Aznar et al., 2006) have been developed to utilize the MMPW for the energy recovery. Among them, pyrolysis was reportedly the most viable and promising technology (Ali et al., 2022).

1.2 Significance of Pyrolysis of MMPW

Pyrolysis of MMPW is the heating of plastic waste at 350-800 ^{o}C in an inert atmosphere leading to its thermal decomposition into plasto oil (PO), gases, and solid (residue char) (Fernandez et al., 2022; Walendziewski et al., 2002). Among the products, plasto oil is a potential transportation fuel and thus substantially reduces the reliance on finite conventional fossil fuel resources. Pyrolysis of MMPW facilitates waste material reuse, recycling, and recovery, thereby closing the loop and paving the way for a circular economy (Yang et al., 2022). Thus it provides a strategy for adequately managing this waste stream into energy and mitigating the greenhouse gas emissions. Further, it provides a pivotal solution to address the aforementioned environmental challenges involving MMPW disposal by diverting the MMPW from ending up in landfills, as litter in land and marine environments. Thus, the pyrolysis of MMPW is a single-point solution to multiple challenges such as MMPW management, environmental impact, energy security, and circular economy.

Researchers have introduced the premise hypotheses and innovation for converting MMPW into plasto oil. Many small-scale pyrolysis plants have been developed in different countries and copious studies were conducted on the pyrolysis of unmixed and MPW collected from various sources (Kaminsky et al., 1996; S.M. Al-Salem et al., 2019; Bhoi & Rahman et al., 2022; Lubongo et al., 2022; Y. Wu et al., 2022). Introducing the catalyst into the pyrolysis process diminishes the required temperature, and residence time and increases the yield of plasto oil making it more energy and material-efficient.

1.3 Significance of catalyst in pyrolysis of MMPW

Catalytic pyrolysis also known as the catalytic thermal degradation process, involves the use of a catalyst to enhance the rate of reaction and increase the plasto oil yield at lower temperatures and reaction time. Catalysts are often employed to improve the conversion and product selectivity by lowering the process's activation energy. Thus catalytic pyrolysis increases the yield of C_2-C_4 olefins having high demand since they are the feedstock for the manufacture of plastics themselves (Elordi et al., 2009). This will again reduce the consumption of fresh petroleum as its distillate naphtha is the feedstock for the production of C_2-C_4 olefins. Besides the quality of plasto oil obtained by catalytic pyrolysis of MMPW is high and comparable to conventional petroleum-derived fuels including gasoline and diesel.

1.4 Compression ignition (CI) engine and emissions

A CI engine is a mechanical device used to convert the fuel chemical energy into mechanical output. CI engines are widely utilized for electricity and transportation due to their high combustion efficiency and cost-effectiveness. According to the statistical review of world energy, the transportation sector used 42.8% of world liquid fuel in 2022. If current trends continue, liquid fuel utilization in the transportation industry may reach 72% by 2035 (M. Z. A. Khan et al., 2023). The IC engines harm the environment, prompting several countries to impose limitations on exhaust pollutants. CI engines emit harmful emissions such as NO_x, CO, HC, and smoke opacity. Therefore, higher power output and reduction in emissions are the key research aspects for the CI engine. Engines are designed to be efficient while meeting emission standards. However, there is a trade-off between emissions performance and efficiency. Diesel particulate filters (DPF) and selective catalytic reduction (SCR) catalysts are employed to minimize NO_x, HC, CO, and soot (Guan et al., 2014). However, The primary cause continues to be CO_2, a greenhouse gas that is responsible for global warming. CI engines have an essential role in the Indian transportation industry as original

equipment manufacturers (OEMs) aim for high performance and low emissions to fulfill Bharat stage-VI pollution requirements starting April 1, 2020. However, due to engine performance limitations, clogging of the filter generates backpressure; nevertheless, it requires periodic maintenance.

Several experimental studies have been conducted on the plasto oil application in CI engine. Chalita kaewbuddee et al. investigated CI engine fueled with plasto oil, resulting in higher NO_x, HC, and CO emissions than diesel (Kaewbuddee et al., 2020). This is caused by the higher density, viscosity, and lower calorific value of the plasto oil. Damodharna et al. studied the plasto oil application in CI engine and observed that NO_x emission increased by 6.39 % more than diesel. This may lead to a higher proportion of premixed combustion and a longer ignition delay, which raises the temperature of the cylinder and heat release rate (Damodharan et al., 2018).

Moreover, the nitrogen content in the plasto oil may increase the nitrogen oxides by the fuel mechanism. However, the Smoke opacity was 21.5% and 57.6 % for diesel and plasto oil, respectively. The higher smoke opacity occurs due to aromatic compounds, which increases the delay period, which could lead to the incomplete combustion of the fuel. Various studies have been conducted on plasto oil and have been observed that high viscosity, density, lower calorific value, and higher aromatic compounds available in plasto oil increase the exhaust pollutants. Higher emissions from plasto oil are necessary to be controlled. This may be achieved by modifying the engine technology. It seems more viable if newer advanced engine technology can be made to be retrofitted to existing and future engines. Studies show that vehicle exhaust regulations have constantly challenged engine design. Since internal combustion engine emissions, especially the NO_x and smoke opacity from diesel are harmful to human health, it becomes inevitable to reduce emissions emitting from the engine. Exhaust gas recirculation (EGR) effectively reduces NO_x emissions in DI diesel engines by diluting excess O_2 in the intake air. The heterogeneous mixture of diesel and air represents another crucial factor, influencing the atomization and vaporization of injected fuel,

pivotal in forming a combustible mixture thus affecting ignition delay, and NO_x, PM, and HC emissions.

Homogeneous charge compression ignition (HCCI) is a potential approach to improve CI engine performance and emissions. The HCCI combustion technology reduces NO_x and PM emissions without compromising thermal efficiency. However, it has significant drawbacks, including high HC and CO emissions and uncontrolled combustion when using high-cetane-rating diesel. A minor modification in the existing CI engine modifies the combustion strategy and is operated in HCCI mode. However, the combustion chamber is crucial in improving the engine characteristics. However, due to the uncontrolled combustion, lean mixture formation restricts the HCCI engine at all engine load conditions. The HCCI technique is very effective in reducing NO_x and smoke opacity. However, the uncontrolled combustion phase is the main flaw in HCCI mode. This led to the development of a new combustion strategy, i.e. PCCI combustion. Modifying in-cylinder parameters provides a more cost-effective and practical alternative to HCCI combustion. PCCI combustion is an advanced prioritizing premixed combustion over mixing controlled combustion. PCCI combustion produces slightly more particulate and NO_x emissions than HCCI combustion but is substantially lower than conventional CI combustion. PCCI engine could be another useful strategy for existing engines. The primary aim of this technique is to achieve low emissions without compromising engine thermal efficiency as compared to CI engine. This may be done by using a homogenous mixture. Two methods for achieving PCCI combustion are internal in-cylinder preparation and external mixture preparation. Internal mixture formation may occur either by late or early fuel injection throughout a cycle. Kanda et alinvestigated the impact of earlier start-of-injection (SoI) timing on diesel PCCI engine performance. Optimising SoI timings and retarding inlet valve closure (IVC) timings significantly reduced NO_x emissions during low-temperature combustion (LTC) in the engine cylinder. (Kanda et al., 2005). Jia et al. studied the effect of IVC and SoI timing on engine combustion characteristics of PCCI

engine fueled with diesel (Jia et al., 2011; Kanda et al., 2005). However, advanced start of main injection (SoMI) timings led to a slight reduction in indicated specific fuel consumption (ISFC).

The external mixture formation approach involves attaching a low-pressure fuel injection system with an air intake manifold and fumigation (Pandey et al., 2019) or by port fuel injection (F.Q. Zhao et al., 1995). Using an external mixture formation approach has significantly reduced NO_x and smoke in CI engines. However, both CO and HC emissions increased in the same way. To overcome this constraint, the fuel must be partly injected by the intake manifold and the rest via conventional DI, with limited exhaust gas recirculation (EGR). Using a limited amount of EGR in the PCCI engine addresses two key issues: reducing NO_x and net heat release rate by charge dilution.

1.5 Research gaps

- Virgin and source-segregated household plastic municipal mixed plastic waste have been studied extensively for their pyrolysis to plasto oil. A handful of researchers have studied the pyrolysis of the MMPW comprised of plastics differing in chemical composition and thermal decomposition behavior in the presence of different catalysts under different process conditions.
- Researchers have conducted pyrolysis with different catalysts such as Zeolite, clay and bimetallic material, fly ash, sulphated zirconia, zeolite-Y, and ZSM-5 to improve the PO yield. These catalysts have higher production costs, which enhance the cost of liquid fuel production through the pyrolysis process. Hence, there is a scope for exploring cost-effective catalysts to enhance the yield of PO from the MMPW pyrolysis.
- Characteristics of crude PO obtained by the pyrolysis of MMPW do not match petroleum-derived transportation fuels. Hence, they are unsuitable for direct use in the IC engine. Therefore, distillation of the crude plasto oil may improve the physicochemical characteristics by separating the lighter and heavier fractions in the plasto oil.

- A conventional compression ignition engine produces higher NOx and smoke emissions, which depend on fuel injection parameters, ignition parameters, different inlet conditions of air and fuel, etc. Research needs to be done to reduce the emission characteristics of the CI engine by a few modifications. To the best of our understanding, no attempt has been made over modification of the CI engine to examine the engine characteristics fueled with sustainable alternative fuel.

1.6 Problem statement

The escalating worry over the depletion of natural resources is evidenced globally. Rapid population growth and the intensification of industrial activity place significant stress on the planet's finite resources, leading to shortages in many areas. This is particularly relevant for critical resources like soil, water, and energy (J. Wang et al., 2024). The loss of these essential resources seriously threatens the existence of humans and the economy's advancement. The scarcity of fossil fuel resources is a significant concern in maintaining energy requirements. Achieving sustainability independent of fossil fuels necessitates the adoption of an eco-friendly alternative fuel. This fuel must fulfill these criteria, including economic viability, abundance, and the ability to regenerate from natural sources (Rui et al., 2017; Z. Zhang et al., 2018; Bukkarapu et al., 2018). Moreover, using fossil fuels is a significant source of CO_2, a greenhouse gas contributing to global warming and other environmental issues. Although, for the past three decades, plastic production has had a consistent annual growth of approximately 3-4% (Bukkarapu et al., 2018). This increase in plastic production can be attributed to factors such as its versatility, longevity, and resistance to corrosion. These characteristics have motivated various sectors to incorporate plastic into their processes. Thus, plastic is used in various sectors to manufacture useable products for consumers. The excessive application of plastic in households, industries, agriculture, and other sources generates waste plastic dumped into nearby municipal dumping yards mixed with municipal solid waste (Munir et al., 2019). Besides being non-degradable, waste plastic affects the food

cycle of living beings by harming nature. Thus, municipal mixed plastic waste is a challenge to society due to the exceeding production and consumption of plastic materials by various growing sectors. However, a hydrocarbon long chain in MMPW is the better source of alternative fuel production. Therefore, chemical recycling of waste plastic may be crucial for MMPW. Pyrolysis is the most promising approach for the chemical recycling of the MMPW to produce valuable products, especially plasto oil (Onu et al., 1999). Plasto oil overcome the dependency on conventional fossil fuels, which are on the verge of ending on earth. Although the world population is increasing rapidly, sustainable alternative fuel is required to meet the growing population's energy demand. Therefore, catalytic thermal degradation of the MMPW may play a vital role in producing a higher yield of the plasto oil. The application of the plasto oil in the CI engine is not viable caused of poor fuel characteristics. A modified CI engine may overcome the difficulty of lower thermal efficiency and higher emissions. Therefore, the PCCI engine has been used to improve thermal efficiency, and the gas emission recirculation system has been used to reduce NOx emissions. Hence, the overall aim was to recycle the MMPW for fuel recovery and its application in CI engine for energy recovery.

1.7 Motivation

The increasing global population has sparked significant concern. Plastic items, utilized across diverse sectors like packaging, construction, and healthcare, are indispensable for maintaining human living standards. Hence, a pressing requirement for heightened plastic production is needed to meet this growing population's demands. Although higher production of plastic would increase the rate of plastic waste, it will increase pollution. However, a growing population would also affect natural resources. There will be a need for extensive energy to meet the energy demand of the growing population. Therefore, increasing population and plastic waste will spoil the balance of the environment. Although it will be a challenge for the world to transform these severe problems into opportunities (Chintala Subramanian et al., 2014). In recent years, various

techniques have been utilized to recycle plastic waste through incineration, landfilling, gasification, and other processes but these are not sufficient to reduce the plastic waste, and somewhere they pollute the atmosphere. Therefore, a viable option is needed to utilize plastic waste appropriately to fulfill the emerging demand of the population. Extensive utilization of traditional materials and depletion of the materials globally have affected the perspective of the various sectors, including transport. Thus, all kinds of waste materials should be utilized in other valuable applications that have become a necessity. Among these waste materials, plastic waste has the potential to be used as an energy source in the transportation sector as well as construction industries. Plastic is more durable and it takes billions of years to decompose, it inevitably encounters wide applications in different aspects of our everyday lives (Aisien et al., 2021). Although our dependency has increased, the growing population is depleting conventional fossil fuel and this is due to extensive consumption. Plastic waste is generally made of hydrocarbon molecules in chains the same as petroleum-based fuel. There are various technologies to produce energy from waste like incineration, hydrolysis, combustion, and gasification. However, pyrolysis is pivotal in recycling plastic waste and providing energy for the transportation sector (Huang et al., 2022).

The current research work aims at the collection and characterization of MMPW, subjecting the same to catalytic pyrolysis using economically viable catalysts to get plasto oil, its characterization, and evaluation in CI engines under varying conditions as detailed below.

1.8 Objective

1. To enhance the yield of the plasto oil from the thermal decomposition of municipal mixed plastic waste by using the catalyst.
2. To modify the physicochemical properties of the obtained plasto oil through fractional distillation.
3. Performance evaluation of modified fuel derived from municipal mixed plastic waste in CI engine modified with fuel vaporizer.

CHAPTER 2: LITERATURE REVIEW

The chapters described the literature review pertaining to municipal mixed plastic waste, the pyrolysis process, and the catalytic effect on the end product yield. Moreover, reviewing the performance of plasto oil as fuel in the CI engine and evaluating the engine characteristics and how the PCCI approach can fill the gap of higher CI engine emission, especially NO_x and smoke.

2.1 Municipal mixed plastic waste

MMPW is obtained from municipal solid waste (MSW). MSW contains various wastes including food, paper, glass, metals, and plastics. Despite sorting attempts, some plastic waste remains mixed owing to causes such as contamination, poor disposal, or the difficulty of sorting specific types of plastics. This mixed plastic waste may include a variety of plastics with different properties, colors, and compositions. The selection of waste plastic, the mixture of PET, PP, HDPE, PS, LDPE, PP, PE and PVC is known as municipal mixed plastic waste.

2.2 Worldwide scenario of plastic waste

Plastics are rapidly displacing conventional materials in all segments due to advancements in polymer science, processing machinery, and cost-effective manufacturing methods. Continuous innovation accounts for the nearly 10% average annual increase in plastic production globally since 1950. Figure 2.1 illustrates the regional share of global plastic production over five years. It has been observed that China emerged as the leading producer, contributing 32% to the world's plastic production. The rest of the Asian countries collectively account for 19% of global production, while North America contributes 17%.

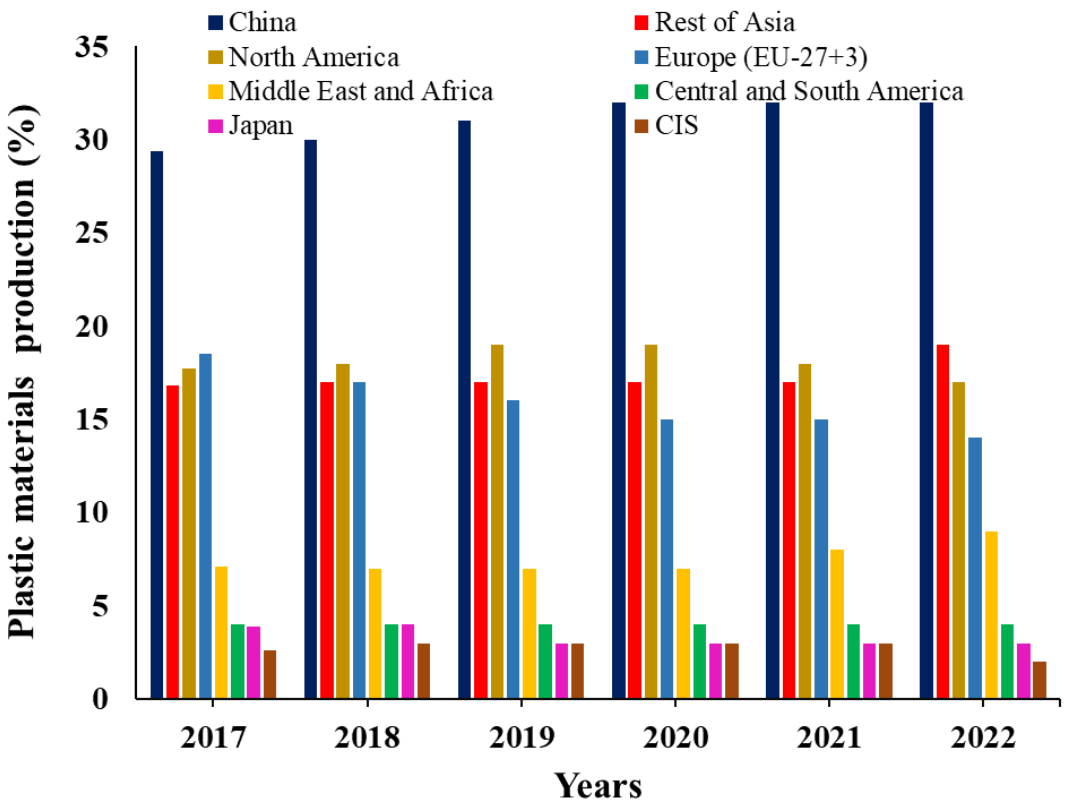

Figure 2.1: Global plastic materials production (Madhumitha Jaganmohan, 2024)

In 2019, the United States claimed the top spot as the globe's foremost generator of plastic waste, churning out more than 73 million metric tons (MMT), while China trailed closely behind at nearly 65 MMT. Together, these nations accounted for 40% of that year's plastic waste production. Meanwhile, India's contribution stood at 18.52 MMT. (Bruna Alves et al., 2023) . In 2015, global plastic waste generation soared to 6.3 billion tons. However, 9% of this waste was recycled, 12% incinerated and 79% ended up in landfills or the natural environment (Ncube et al., 2021). Projections indicate that the global volume of plastic waste will triple by 2060, surpassing the one billion metric ton mark. This dramatic surge is anticipated to be propelled by increasing demographics and economic progress. Effective waste management will mitigate the environmental threat due to this escalating waste output. Nevertheless, forecasts indicate that landfilling will remain globally's primary disposal method by 2060, with recycling accounting for

less than 20%. Packaging is poised to significantly contribute to the substantial growth of plastic waste generated over the next four decades (Bruna Alves et al., 2023). Plastic waste generation is the most significant global environmental challenge because plastic products have become integral to our daily lives. MMPW is produced from various sources, such as residential sources, including plastic bottles, containers, bags, wrappers, disposable cutlery, plates, cups, straws, packaging materials from groceries, household goods, and personal care products. Commercial sources include retail and supermarkets: packaging materials, plastic bags, and containers used for product display and transportation contribute to plastic waste. Restaurants and food services: Single-use plastic items like food containers, cups, lids, and utensils are prevalent in the food service industry. Institutional activities include plastic packaging from office supplies, electronics, and other workplace materials, contributing to municipal plastic waste. Moreover, construction and demolition, public space and events and illegal dumping and littering contribute to the MMPW. The generation of MMPW varies substantially across the globe and within individual countries, depending on population size, level of economic development, consumption patterns, waste management infrastructure, and cultural norms. Efforts to reduce municipal mixed plastic waste generation rely on waste reduction, reuse, recycling, and effective waste management techniques. Some measures to reduce plastic waste generation in communities include education and awareness campaigns, policies promoting the adoption of alternatives to single-use plastics, and increasing recycling infrastructure.

2.3 Municipal mixed plastic waste plastic affects the environment and public health

Plastics are valuable in several applications, and their post-use may significantly impact the world's parameters if not managed appropriately. Some of these consequences could affect the environment. To effectively manage waste plastic, it is essential to understand the adverse effects of improper handling. Poor waste

management and non-biodegradability may pose environmental risks, including clogging drains in metropolitan areas (Gu et al., 2021). Plastic physicochemical characteristics contribute to their utility, while their products after usage are discarded. Around 10-12% of municipal mixed waste comprises plastic waste, which undergoes combustion. The gases discharged into the atmosphere during burning contribute to air pollution and greenhouse impacts. The elements discharged into the atmosphere include dioxins, polychlorinated biphenyls, furans and mercury. Immediate action is required to handle and manage these issues effectively, ensuring environmental protection. Plastic products in aquatic environments can absorb hydrophobic toxins, reducing their availability to wildlife, particularly when these plastics are buried on the seafloor (Abdul–Latif et al., 2021). Improper discarding and mistreatment of waste plastic may negatively impact animals, public health, and the environment. Pollution is the disposal of unneeded or dangerous products into the environment after usage. Pollutants are non-used items that harm natural or artificial arrangements. They can be categorized as natural (such as plants, volcanic ash, and animal secretions) or artificial (including waste and byproducts from food, beverage, pharmaceutical, and cosmetics). Pollutants from these activities significantly affect the quality of water, marine life, air quality, and land use posing challenges for agriculture. Land pollution is caused by anthropogenic activities such as city development, using organic fertilizers, and introducing artificial chemicals into the soil, which can alter its acidity and alkalinity levels (Zubris et al., 2005). Plastic waste contaminates land through chemical degradation during organic decomposition. Plastic waste contains plastics, which are easily penetrated and make their way into the environment. Plastics in aquatic ecosystems, air, and soil have received little attention in environmental contamination studies. Microplastics have been found in several products, including sea salt, bottled water, tap water, sugar, and honey, raising concerns about their possible influence on human health and the environment (Pannetier et al., 2019). The earth's ecosystem, primarily water at 70%, is dispersed across water reservoirs, rivers and seas. Water pollution arises

when detrimental substances, predominantly chemicals and microorganisms, infiltrate streams, rivers, seas, and other small water bodies, deteriorating their quality and posing toxicity risks to living beings and the environment (Bhateria et al., 2016). Due to its chemical composition, the breakdown of plastic waste emits various toxic gases that can impact the atmosphere. The release of gases such as carbon dioxide can lead to several issues, including climate change, acidic rain, global warming, and nosocomial infections. Additionally, it aids in the spreading of airborne diseases like COVID-19, which is currently impacting globally (Ahmed et al., 2019). Inadequate waste disposal can have varying effects on animals, serving as vectors for pathogens and parasites and exposing them to chemical toxicity (Vanapalli et al., 2021). Plastic waste interacting with other antigen bodies within animals, such as cattle, can significantly affect their physiological functions in various ways. Specifically, the digestive systems of animals are unable to break down plastics. Anatomically, cattle possess various parts, including 3- non-glandular fore-stomach compartments: the rumen, reticulum, and omasum. These compartments aid in the digestion of various molecules, excluding plastic materials (De Weerdt et al., 2020). Inadequately disposal methods of waste plastics pose severe health risks, both directly and indirectly (Bilal et al., 2020). Carbon-based plastics include a variety of harmful components, including bisphenol-A, polyfluorinated, phthalates compounds, antimony trioxide and brominated flame retardants, all of which may harm the environment and human health. Chemical pollution or exposure may have both immediate and long-term negative consequences. These impacts may include reproductive and genital organ abnormalities in both men and women, as well as malignant tumors, weakened immunity, congenital disabilities, endocrine disorders, ophthalmological disorders, leukemia, and other infectious illnesses. Plastic may be a disease vector between persons and animals (Evode et al., 2021). Electronics waste plastic products are a massive global environmental and public health concern, primarily due to their extensive manufacturing and insufficient waste management strategies globally (V. Yadav et al., 2020).

2.4 Management of MMPW

Managing municipal mixed plastic waste involves strategies to promote recycling and implement proper waste management practices. Two factors merit attention when managing waste plastics. Firstly, if not promptly and thoroughly managed, waste plastic can undergo slow decomposition, resulting in the wastage of significant energy and resources. Secondly, improper recycling techniques may lead to adverse environmental impacts or escalate treatment costs. Methods for managing municipal mixed plastic waste encompass landfilling, incineration, mechanical recycling, and chemical recycling.

Landfills are a simple and easy way to dispose of plastic waste, but they are not the best option since plastics take a long time to degrade and pose a danger to the sustainability of the ecosystem. Due to its low density, plastic waste has a huge volume and fills landfills, exacerbating the already dire situation of limited land resources (Ware et al., 2017). However, plastic waste is difficult to decompose, making it permanent waste after landfilling. This significantly reduces the ability of surface water to seep in and groundwater to circulate. Hazardous plastic composition seeps into the soil, endangering the ecology and agricultural fields (Swift et al., 2015). Moreover, plasticizers and pigments are examples of additives in plastics that may lead to secondary contamination, which is contrary to sustainable development. In incineration, plastic waste is burned at high temperatures to produce energy, usually heat or electricity. At the same time, it could offer an efficient means to diminish the quantity of waste transported to landfills while generating energy. In the process, the main products of plastic waste are CO_2 and water. However, polycyclic aromatic hydrocarbon compounds, carbon monoxide, and other harmful substances are also produced due to changes in plastic composition and incineration conditions. For example, hydrochloric acid is produced when polyvinyl chloride breaks down thermally and polyacrylonitrile that produces hydrogen cyanide (Huang et al., 2018).

Additionally, the waste plastics could include compounds made of heavy metals, including lead (Pb), cadmium (Cd) and mercury (Hg). These heavy metal compounds are released into the air during the incineration process together with the soot, where they remain as incineration residues and continue to contaminate the surroundings (Ni et al., 2016). As a result, incineration of waste plastics is not the ideal way to dispose of waste plastic since it needs a sophisticated system for treating and purifying pollutants.

Mechanical recycling is essential to sustainable waste management initiatives, which process the waste plastic into secondary raw materials or products without changing the chemical structure (Ragaert et al., 2017). It provides a realistic and scalable method to reduce plastic pollution and promote resource efficiency. Plastics with low carbon footprints are ideal for reducing overall environmental effects. For instance, the deposit return plan, which collects plastic drink bottles selectively, can potentially build an efficient recycling loop. The material may be reprocessed back into plastic bottles with minimum quality loss. The process steps include sorting, cleaning, shredding, melting, extrusion and manufacturing (Briassoulis et al., 2013). The quality of plastic materials tends to deteriorate with each recycling cycle because of various factors like contamination, processing-related deterioration, and additive accumulation. Eventually, plastic could become unusable for high-value applications due to quality degradation, which would need downcycling or disposal.

Chemical recycling, often called feedstock advanced recycling, is an alternate method of handling plastic waste by decomposing polymers into their component chemicals or converting them into energy products such as fuel (Rahimi et al., 2017). Chemical recycling procedures often begin with depolymerization. This may be performed in numerous ways, such as gasification, hydrolysis and pyrolysis (Hahladakis et al., 2018).

Gasification is the process by which plastic waste is transformed into a synthesis gas, or syngas, that contains several gases such as CO and H_2. The syngas may be

processed further to produce chemicals and fuels, or it may be used as a fuel to produce heat and electricity (Acomb et al., 2014).

In hydrolysis, water or acids break the waste plastic into monomers or oligomers. The resultant monomers may be refined and utilized to create new polymers and materials (Silva et al., 2023).

Pyrolysis is the thermal degradation process, a continuous chemical reaction process in which organic waste polymer is decomposed into combustible gas, oil, and solid carbon by heating at elevated temperatures without oxygen (Osman Y. Yansaneh et al., 2022).

These methods involve exposing waste plastic to elevated temperatures in the absence of O_2, producing PO or synthetic diesel. These options are viable alternatives to replace conventional fossil fuels (Nasution et al., 2022). Among all the technologies available for treating municipal mixed plastic waste, pyrolysis emerges as the most suitable and promising option, capable of generating valuable products such as plasto oil, solids, and gases (P. K. Ghodke et al., 2021). Many studies have investigated the economic, environmental, and technical aspects of pyrolysis as a method of transforming waste plastic into sustainable alternative fuels (Onu et al., 1999; Saad et al., 2015; I. Mohan et al., 2023). Kaminsky et al. carried out a study on pyrolysis of the MMPW containing 25% polystyrene (PS) and 75% polyolefins (PE, PP) with a minimal amount of polyvinyl chloride (PVC) at 730 ^{o}C. They obtained 48.4 wt% of plasto oil (Kaminsky et al., 1996). Demirbas et al. examined the pyrolysis of MMPW and found 46.6 wt% plasto oil, 35 wt.% gas, and 2.2 wt.% solid char. The PO contained 4 ppm of chlorine (Cl), attributed to the presence of residual PVC materials (Demirbas et al, 2004). The presence of Cl did not affect the oil quality, as it was below the minimum Cl limit typically required in petrochemical processing, which is usually less than 10 ppm. However, the remaining Cl was found in the solid char. Researchers deduced that to ensure the production of high-quality oil, the Cl content in the feedstock should not be more than 1 wt.%. Donaj et al. also investigated the pyrolysis potential of

polyolefin-mixed polymers. LDPE comprised 75% of the MPW, HDPE 30%, and PP 24%. The experiment was conducted at 650 ^{o}C and 730 ^{o}C. They revealed that plasto oil was 48.4 wt.% and gas was 36.9 wt.% at 650 ^{o}C. Nonetheless, heavy fractions such as carbon black, heavy oil, and wax made up 52% of the oil fraction (Donaj et al., 2012). In comparison, the pyrolysis plasto oil was 44.7 wt.% and 42.4 wt.% at an operating temperature of 730 ^{o}C. This may conclude that pyrolysis is the most viable technology to obtain sustainable alternative fuel at elevated temperatures. However, increasing the temperature raised the gas's product yield.

2.5 Economic feasibility of MMPW pyrolysis

The chemical recycling of MMPW into a petrochemical feedstock that can be utilized as fuel or as a starting substance for chemicals and polymers. Pyrolysis is the thermal degradation of materials at elevated temperatures without an oxidant.. Other chemical recycling included gasification. In the process, waste plastic reacted with the gasified agents, i.e. oxygen, air and steam, at higher temperatures up to 1300 ^{o}C to produce flue gases. Moreover, chemolysis converts the PET into the monomers. The return on investment of gasification and chemolysis is lower than that of the pyrolysis process. Moreover, landfilling and incineration of waste plastic is threatening the environment. However, the pyrolysis process is more eco-friendly than other processes. Although, the pyrolysis process has been reported for mixed or multi-layered plastic waste. Very few studies have been carried out to address the economic feasibility. Riedewald et al. conducted an economic analysis for a 40,000-ton/year MPW pyrolysis facility in Belgium. An internal rate of return was 20% estimated (i.e., the plant had a positive net present value up to a 20% waiver), with revenue of €210/t, even though the price of PO was considered in the calculations at a 15-year low (Frank Riedewald et al., 2021). The study revealed that the economic viability was influenced by factors such as the quality and volume of plastic waste, feedstock expenses, capital, and operational costs, revenues generated from the PO sale, tipping fees, and the feasibility of co-locating the plant. Fivga and Dimitriou et al. investigated the

economic viability of converting waste plastic to PO fuel at 1,000, 10,000, and 100,000 kg/h sizes (Fivga & Dimitriou et al., 2018). The various authors conducted techno-economic assessments of waste plastic-to-fuel plants, and their findings showed that, in most cases, competition from traditional refineries and prices for produced oil and feedstock limit the profitability of waste plastic to PO conversion (Fivga & Dimitriou, 2018; Larrain et al., 2020; Qureshi et al., 2020; Frank Riedewald et al., 2021). M. Ghodrat et al. analyzed the techno economics of waste plastic pyrolysis plants established in Australia. The economic study was conducted on 40 tons of waste plastic feed per day. Equipment prices are either derived from literature or computed. The economic study indicates that collecting, transporting, and shipping waste plastic to the plant location for free can result in a 54% ROI over 25 years for a capital expenditure of AUD 5220531. Scaling up the suggested plastic pyrolysis factory can increase its return on interest (ROI) (Ghodrat et al., 2019). The techno-economic study was carried out in Aspen Plus for pyrolysis, which processes 10,000 tons of HDPE waste annually. The pyrolysis product's minimum selling price was $302.50 per ton, with a net present value of the process costing $12,594,659.7, and the profit period was 15 months. The results show that pyrolysis is economically feasible and potentially profitable (Hasan et al., 2024). Westerhout et al. performed a techno-economic study of MPW pyrolysis for PO production in the Netherlands, using ROI as an economic performance indicator. Therefore, we examined how ROI varies with MPW feeding capacity for three pyrolysis plants: Bubbling Fluidized Bed (BFB), Circulating Fluidized Bed (CFB), and Rotating Cone Reactor (RCR), respectively. The plant capacity significantly impacts the economics of plastic pyrolysis facilities. The profitability of PO from urban waste plastics depends on the pyrolysis process types and parameters. The pyrolysis plant with RCR technology for 20k ton/year plant capacity at an operating temperature of 625 ^{o}C, which has the highest ROI, followed by CFB and BFB operating temperatures of 740 and 840 ^{o}C. The necessity of high temperatures in CFB and BFB reactors needs significant capital investments and energy expenses. The MMPW pyrolysis

may be economical at a scale of 30 kTon/year. Still, the least possible process capacity of 50 kTon/year is required to attain a 25% ROI before tax return on investment. Hence, studies have been carried out on MPW pyrolysis, which has the potential to produce energy with economic viability and profitability (Westerhout et al., 1998).

2.6 Analysis of the MMPW

2.6.1 Proximate analysis

A proximate analysis of the different waste plastic and MPW is given in Table 2.1. Proximate analysis is a chemical analysis determining the number of various components in a sample. In the case of MMPW, proximate analysis can provide important information about the composition and properties of the plastic, which can help identify potential uses or recycling options. Some of the critical information that can be obtained through proximate analysis of waste plastic includes:

Moisture content: The amount of water in the MMPW can affect its physical and mechanical properties. Proximate analysis can help determine the moisture content, which can be useful in determining the appropriate processing conditions for recycling.

Volatile matter: Volatile matter refers to plastic components that can be vaporized under specific conditions. The amount of volatile matter can indicate the quality of MMPW.

Fixed carbon: Fixed carbon refers to the non-volatile components of the MMPW, which can provide information about the chemical composition of the MMPW.

Ash content: The ash content of the MMPW can indicate the impurities, such as `inorganic fillers or contaminants.

The volatile matter content of plastic can have an impact on the plasto oil yield during pyrolysis. Usually, higher volatile matter content in the plastic can lead to a higher plasto oil yield during pyrolysis. This is because volatile matter refers to

plastic components that can be vaporized under specific conditions, such as high temperatures. During pyrolysis, the plastic is heated to high temperatures, causing the volatile components to evaporate and form a vapor phase. This vapor phase can then be condensed to form a liquid product, which can be used as a feedstock for other processes. Therefore, if a plastic sample has a higher volatile matter content, it can result in a higher PO yield during pyrolysis, as more volatile components are available to be condensed into a liquid product.

Table 2.1: Proximate analysis of the plastic waste

Type of plastic	Fixed carbon	Moisture content	Ash	Volatile matter	References
PET	13.9	NA	NA	84.1	(Chattopadhyay et al., 2016)
PET	14.5	NA	0.7	84.8	(Suriapparao et al., 2022)
HDPE	NA	NA	0.8	97.15	(Chattopadhyay et al., 2016)
HDPE	0.00	0.00	0.01	99.99	(Rahman et al., 2021)
HDPE	16.85	NA	NA	83.15	(Bhoi & Rahman, 2022)
LDPE	0.051	0.11	0.023	99.816	(Janajreh et al., 2020)
LDPE	0.68	0.30	3.37	95.61	(H wijayanti, C Irawan, 2022)
PP	1.0	NA	NA	96.9	(Chattopadhyay et al., 2016)
PP	1.62	0.16	4.45	93.77	(Hakeem et al., 2018)
PP	0.5	NA	0.00	99.5	(X. Liu et al., 2020)
PP	0.43	0.29	0.00	99.28	(Bai et al., 2020)
PS	0.071	0.09	0.025	99.814	(Janajreh et al., 2020)
PS	0.22	0.00	0.00	99.78	(N. Ahmad et al., 2020)
PS	1.05	0.32	0.09	98.54	(S. Zhao et al., 2022)

PE	0.00	0.2	0.4	99.4	(Duque et al., 2020)
PE	0.07	NA	NA	99.93	(Y. Wu et al., 2022)
PVC	4.10	0.00	0.01	95.89	(Q. Wang et al., 2018)
PVC	1.97	0.65	0.11	97.92	(Wei et al., 2022)
PA	0.69	0.00	0.00	99.7	(Wan Nurdyana wan mansor et al., 2021)
ABS	0.04	0.10	0.99	98.87	(Kasar et al., 2020)
ABS	9.6	0.00	13.6	76.8	(Mortezaeikia & Tavakoli, 2022)
PBT	2.88	0.16	0.00	97.12	(Kasar et al., 2020)
MPW	3.5	0.00	3.3	93.2	(Lazzarotto et al., 2020)
MPW	5.34	0.86	1.21	93.45	(P. K. Ghodke, 2021)

2.6.2 Elemental analysis (CHNS-O)

CHNS-O analysis is a type of elemental analysis that reports the amounts of carbon (C), hydrogen (H), nitrogen (N), sulfur (S), and oxygen (O) present in a sample. This type of analysis can be useful for characterizing the composition of plastic waste and understanding its potential applications or recycling options, as given in Table 2.2. CHNS-O analysis of plastic waste can provide information about the types of polymers that are present, as well as any impurities or additives that may be present in the plastic. For example, the carbon content of the plastic can provide information about the amount of polymer present. In contrast, the hydrogen and oxygen content can provide information about the degree of polymerization and additives including plasticizers. Additionally, the nitrogen and sulfur content can provide information about any impurities that may be present in the plastic waste. For example, some plastics may contain sulfur-based additives for UV stabilization or flame retardancy, which can be detected through CHNS-O

analysis. CHNS-O analysis can be a valuable tool for characterizing plastic waste composition and understanding its potential uses or recycling options. By understanding the elemental composition of plastic waste, researchers and waste management professionals can develop more effective strategies for recycling or disposing of this material.

Table 2.2: Elemental analysis (Moorthy Rajendran et al., 2020)

Type of plastic	Carbon	Hydrogen	Nitrogen	sulfur	Oxygen
Polypropylene	77.52-86.1	14.22-13.7	0.1	0	7.46-0.2
Polystyrene	83.10-92.7	7.82-7.9	0.21	0.0	0-8.88
Polyethylene	69.67-85.4	10.12-14.4	0.09	0.0	0.03-18.5
HDPE	83.9	14.9	0.05	0.0	0.74
LDPE	69.67-85.7	10.12-13.0	0.09	0.00	0.9-18.5
MMPW	70.14	6.81	3.27	0.00	14.73

Proximate and elemental analysis is critical for understanding the composition and characteristics of feedstock before introducing it to pyrolysis. This feedstock analysis is required to develop efficient and sustainable pyrolysis processes, optimize product yields, and reduce environmental impact.

2.7 Pyrolysis process

Pyrolysis is the thermal decomposition of feedstock materials in a non-oxidizing environment at elevated temperatures. Heating material is the cause of physical (e.g., deformation, melting) and chemical (e.g., bond breaking) changes, depending on its characteristics and heating circumstances. The broken bonds form radicals, which may propagate across the chemical structure and recombine with other radicals. Heat breaks bonds, producing tiny products that evaporate and leave a solid residue. The volatilized products may degrade and react with other products to generate different chemical compounds. Some compounds can be condensed into liquid form, whereas others are permanent gases. The final products include liquid, solid residue (char), and gases.

$$Feedstock \xrightarrow{Elevated\ temperature} Liquid + Solid + Gases \qquad \text{Eqn. (2.1)}$$

2.8 Conventional (Thermal) pyrolysis of MMPW

Conventional pyrolysis refers to the thermal degradation of MMPW that employs an electrical heater as a heating source. Numerous studies have investigated conventional pyrolysis using various types of plastics, e.g., PS, LDPE, PS, PP, HDPE, and MPW (Kaminsky et al., 2000; Obeid et al., 2014; I. Ahmad et al., 2015; R. K. Singh et al., 2022). Plastic pyrolysis can be conducted using semi-batch, batch, or continuous reactors, which have their pros and cons.

Ghodke et al. conducted the conventional pyrolysis of virgin mixed plastic and MMPW at 500 ^{o}C and found 62.5 wt.% PO yield with MMPW. Heating is the primary source and bottleneck in pyrolysis (P. K. Ghodke et al., 2021). The substantial costs associated with conventional pyrolysis methods stem from ineffective heating mechanisms and heat loss. Therefore, researchers are switched to utilizing other heating sources, such as solar (Chintala et al., 2017), microwave (Suriapparao et al., 2018), and other renewable energy sources, (Moorthy Rajendran et al., 2020; Sivagami et al., 2021).

2.8.1 Type of Pyrolysis Process

The pyrolysis process decomposes organic matter by heating it to an elevated temperature without atmospheric oxygen. Heat is essential to break down the hydrocarbon molecules at suitable temperatures in the pyrolysis reactor and produce solid, liquid, and gaseous fuels. The quantity of these pyrolysis products is influenced by factors such as the feedstock, temperature, heating rate, and the type of reactor employed for the process. Pyrolysis is classified as a slow, fast, and flash process based on reaction temperature and heating rate. The product distribution of slow, fast and flash pyrolysis processes with their respective temperature range is given in Table 2.3. However, the pros and cons of different pyrolysis processes are outlined in Figure 2.2.

Table 2.3: Recent developments in the pyrolysis process (Sipra et al., 2018; Lu et al., 2020)

Name of pyrolysis	Temperature range	Residence time	Heating rate (°C/sec)	Feedstock size (Mm)	Liquid (wt%)	Solid (wt%)	Gases (wt%)
Slow pyrolysis	300-700 °C	10-100 Minute	0.1 -1	5-50	30	35	35
Fast pyrolysis	400-800 °C	0.5-2 sec	10-100	< 3	40-70	15-25	10-20
Flash pyrolysis	700- 1200 °C or above	< 0.5 sec	1000	< 0.2	10-20	10-15	60-80

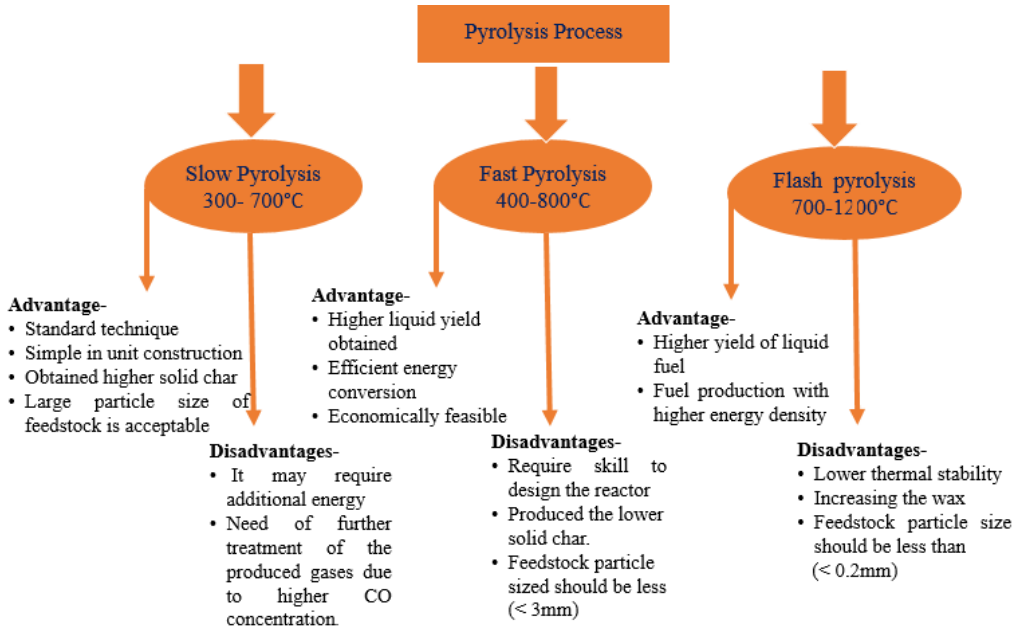

Figure 2.2: Development in pyrolysis technique (Pal et al., 2022)

2.8.1.1 Slow Pyrolysis Process

Slow pyrolysis occurs at lower operating temperatures and slower heating rates, promoting the production of coke, tar, and char (Sogancioglu et al., 2017). During

slow pyrolysis, the feedstock is subjected to a low heating rate ranging from approximately 0.1 to 0.8 $^{o}C\ s^{-1}$. This slow heating rate, coupled with an extended residence time of the feedstock, leads to increased char production. Slow pyrolysis is conducive to synthesizing H_2, CO, CH_4, and C_5H_{12} and is aided by a significantly lower non-isothermal heating rate, while fast pyrolysis yields predominantly gases (Harussani et al., 2022). Das et al. demonstrated in their study that thermally degraded PP and PE wastes produce light hydrocarbon plasto oil fractions (C_6–C_{20}) at low temperatures (400 ^{o}C) (P. Das et al., 2018). Conversely, slow pyrolysis results in higher char yields. Therefore, the carbonization method was introduced as an innovative approach for producing charcoal as a valuable product for underserved areas. The process requires a proximate feedstock analysis to analyze the moisture, ash, fixed carbon, and volatile matter. Although temperature has an essential role in product distribution, particle size, heating rate and moisture content also substantially influence the outcome of pyrolysis products (Moorthy Rajendran et al., 2020).

2.8.1.2 Fast pyrolysis

Fast pyrolysis represents an advanced and promising technology that contemplates rapid thermal degradation with increased heating rates and high process temperatures, followed by swift product quenching to facilitate liquid product formation. This process enables good-quality liquid fuel (R. K. Singh et al., 2019). Fast pyrolysis of plastic waste results in the yielding of gas with minimal char and plasto oil yields. This rapid decomposition process facilitates the breakdown of plastic molecules into more minor carbon chain compounds such as methane, ethane, propane and others. During fast heating, the dissociation reaction of the waste plastics triggers β-scission, followed by inter- and intramolecular H_2 transfer, leading to a larger quantity of short-chain hydrocarbons (R. K. Singh et al., 2019). The process requires a higher heating rate of around 10 to 100 $^{o}C\ s^{-1}$, and the feedstock particle size must be less than 3 mm. Mass transfer rate, heat, and chemical kinetics are essential in deciding the pyrolysis product chemistry. Various researchers conducted studies on fast

pyrolysis and produced higher plasto oil yield at a temperature range of 500–550 ^{o}C (Sharuddin et al., 2018; Sipra et al., 2018; R. K. Singh et al., 2019; Hussein et al., 2021; Lubongo et al., 2022). The process produces byproducts such as residue char and gases. The state-of-the-art shows that the generation of pyrolytic gases increases as the yield of plastic oil and solid char decreases (Sharuddin et al., 2018; Kasar et al., 2020; Hussein et al., 2021).

2.8.1.3 Superfast/Ultra-Fast / Flash pyrolysis

Superfast pyrolysis is the most advanced technique, renowned for producing higher amounts of operable PO and gases with lower water content. Operating with a high-temperature range of 700 to 1200 ^{o}C or above, which requires a higher heating rate of approximately 1000 ^{o}C s^{-1} or above to achieve the requisite temperatures for the feedstock. Particle size is crucial, with feedstock particles ideally less than 0.2 mm due to the accelerated heating rate (Kataki et al., 2018). The pyrolysis process efficiently converts 80% energy contained in feedstock into valuable products, producing higher energy-dense products than the raw feedstock. However, the plasto oil often contains a significant amount of oxygen content, rendering the product unstable for further use. Additionally, it may contain impurities such as nitrogen and heavy metals. Removing these pollutants requires a substantial amount of H_2, which can increase the overall cost of the process (Fang et al., 2018).

2.9 Effect of process parameter in pyrolysis

Pyrolysis of MMPW has been affected by the process parameters essential in optimizing product yield and quality. The parameters include temperature, pressure, residence time, type of reactor, and catalyst.

2.9.1 Effect of Temperature

Temperature is the essential parameter for MMPW pyrolysis due to its regulation of polymer chain cracking and its influence on product distribution. Temperature controls the breakdown process of the hydrocarbon molecules, thereby adjusting the amount of gaseous and plasto oil. Moreover, it also affects the char produced.

The Vander Waals force attracts molecules together, preventing them from collapsing (Mahdavi et al., 2022).

As the system temperature increases, molecules experience heightened vibration and tend to evaporate from the feedstock surface. The energy produced by the Vander Waals force along polymer chains increased the enthalpy of the C-C bond, leading to the break of the carbon chain. In polymers, carbon bonds are nonpolar, stable, and highly tight, requiring much energy to break. Therefore, 300–800 ^{o}C temperature is required. Various studies demonstrate the effect of temperature on plasto oil yield with various feedstocks (Mastral et al., 2002; Kalargaris et al., 2017; Susastriawan Sandria et al., 2020). For instance, Adnan et al. studied polystyrene waste material at 500 ^{o}C, obtaining more than 80 wt.% PO. The lower temperature range resulted in the formation of a long hydrocarbon chain. However, a higher temperature range resulted in the short carbon chain formation caused by the breaking of C–C bonds and the production of aromatic hydrocarbons (Adnan et al., 2015).

2.9.2 Effect of Pressure

Pyrolysis is usually performed at atmospheric pressure, leading to limited exploration of the effect of pressure on pyrolysis in existing literature and presenting a significant research gap. However, some researchers have performed pyrolysis under vacuum (lower than atmospheric pressure) or higher-pressure conditions (higher than 1 atm). Low pressures favor forming primary products, such as monomers, whereas high pressures favor complex liquid fractions. Increasing pressure increases pyrolytic compounds' boiling point, resulting in heavy hydrocarbons being hydrolyzed rather than vaporized at a given operating temperature (Osman Y. Yansaneh et al., 2022). Lopez et al. examined the waste tire pyrolysis process under vacuum at 25 kPa and 50 kPa under atmospheric pressure at 500 ^{o}C (Lopez et al., 2010). Their findings revealed a higher yield of diesel fraction similar to plasto oil above the atmospheric pressure. The principal impact of a vacuum pressure over an atmospheric pressure is the yielding of

liquid fuel. Additionally, Minimizing pore blockage enhanced the surface area of the carbon black, positively affecting the porous structural characteristics of the remaining carbon black. Vacuum conditions facilitate the devolatilization of the feedstock and promote the diffusion of volatiles inside the particle. Conversely, increasing pressure resulted in higher production of gaseous products and a higher yield of lower molecular weight of PO (Krishnamoorthy et al., 2018).

2.9.3 Residence time

The residence time (RT) is stated as the duration of time of MMPW spent in a pyrolysis reactor as long as the products continue to be produced and have a high impact on product yield and quality (Kalargaris et al., 2017; P. Ghodke & Krishna etal., 2018). Higher residence times tend to increase the higher liquid production due to the pyrolysis reactor's secondary reaction. Al-Salem et al conducted a study on residence time, demonstrating that increasing the residence time led to a higher yield of plasto oil. Studies have shown that residence time influences plasto oil yield at a given temperature and that increasing residence time may ultimately decrease the yield of plasto oil (Al-Salem et al., 2017). Similarly, Mastral et al. examined the thermal cracking of HDPE and observed the impact of RT. The experiments were performed at temperatures ranging from 650 ^{o}C to 850 ^{o}C, with residence time ranging from 0.64 s to 2.6 s. It has been observed that plasto oil yield was 79.7 wt.% at 650 ^{o}C for 0.64 s., which decreased by 14.05% with increasing the residence time by 2.6 s at the same temperature (Mastral et al., 2002). Moreover, the yielded gas was 11.4 wt.% and 31.5 wt.% at an RT of 1 sec and 1.5 sec, respectively. At 780°C, a lower plasto oil yield of 9.6 wt.% was achieved, accompanied by a substantial increase in gaseous hydrocarbons, reaching 86.4 wt.%. This increase primarily stemmed from heightened methane, ethane, and hydrogen yields (Al-Salem et al., 2017). Hence, increasing residence times led to higher gaseous products. However, along with residence time, other factors, including heating rate, temperature, catalyst, and reactor design exert significant concurrent influences on hydrocarbon fuel quality (R. K. Singh et al., 2022).

2.9.4 Type of Reactor

Fluidized bed (bubbling and circulation), rotary kiln, ablative, screw, and auger reactors are among the most typical pyrolysis reactors used to produce PO from MMPW. To ensure successful pyrolysis, two essential design characteristics must be addressed. Firstly, the reactor should efficiently blend the feedstock with the catalyst, ensuring uniform distribution. Secondly, it must effectively deliver substantial heat to the feedstock while maintaining a short residence period within the reactor (Musale et al., 2013). Extended residence times coupled with low heat transfer rates can generate large volumes of solid and gaseous hydrocarbons.

2.9.4.1 Fixed-Bed Reactor

The pyrolysis process commonly employs a fixed-bed reactor (FBR), often operated in batch mode. The reactor design is simple to construct and suitable for the uniform size of the feedstock, as shown in Figure 2.3. However, larger particles or polymers lead to feeding issues into reactors. Heat is supplied to the reactor for the thermal breakdown of feedstock either externally or by minimal combustion. As the gas volume expands, the products flow out of the pyrolyzer reactor, while char remains stored at the bottom of the reactor. However, a sweep gas is often employed to remove the volatiles from the reactor effectively (Hasan et al., 2021). In a few cases, a solid catalyst was used as a packed bed, allowing the volatiles to pass over the bed and improve the efficiency. However, FBR is often associated with the challenges related to feeding irregularly shaped polymers with poor heat conductivity. Moreover, researchers entertained the FBR for secondary pyrolysis, facilitating the primary product to be easily transferred to the secondary reactor (Fogler et al., 2016). The catalytic process of polyethylene with Y-zeolite produced 85 wt.% plasto oil. However, the plasto oil increased to 95 wt.% at 500 ^{o}C without a catalyst. Additionally, they concluded that increasing the temperature decreased plasto oil yield, accompanied by higher production of gaseous products (Palomar-Torres et al., 2022). Traditional fixed-bed reactors encounter several limitations, including a slow heating rate, an extended residence

period, and uneven sample temperatures within the reactor. Moreover, their batch-scale nature renders them economically inefficient.

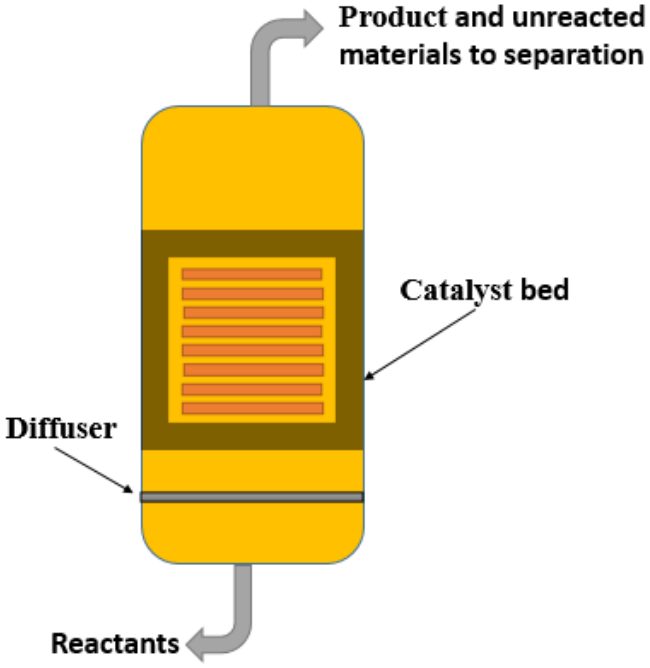

Figure 2.3: Fixed bed reactor (Pal et al., 2022)

2.9.4.2 Fluidized-Bed Reactor

A fluidized-bed reactor, as presented in Figure 2.4, is the most viable reactor and is being used on the industrial scale to process crude oil. The reactor is utilized comprehensively in industries due to the continuous provision of feedstock to produce plasto oil. The upward motion of the co-reactant feed in the reactor suspends tiny catalyst particles in suspension. A gas is frequently employed as the fluid in a fluidized-bed reactor, which promotes particle mixing by maintaining a high flow rate within the reactor. The particle size is much lower than in FBR, ranging from 10 to 300 µm with a constant temperature. Thermal and catalytic thermal processes can occur at 290–850 ^{o}C in the reactor (Palomar-Torres et al., 2022). Luo et al. conducted a comparative study on LDPE on a fluidized-bed react, producing a higher plasto oil yield (Luo et al., 2021). Additionally, the fluidized-bed reactor provides considerably more significant mass enhancement and heat transmission, thereby reducing temperature gradients within the reactor

(Elordi et al., 2009; Chetna Mohabeer et al., 2022). This implies that fluidized bed reactors may offer greater economic sustainability for large-scale operations, despite batch reactors being equally efficient at the laboratory scale.

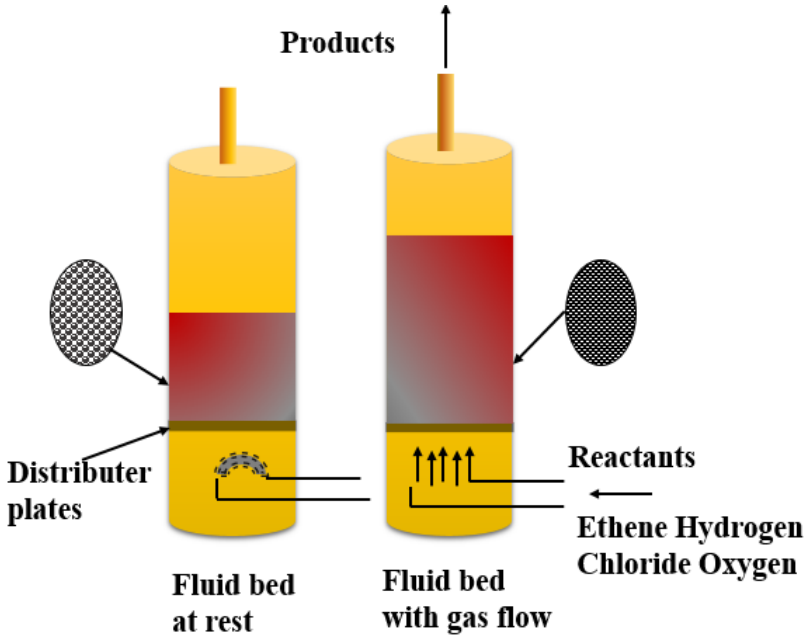

Figure 2.4: Fluidized bed reactor (Pal et al., 2022)

2.9.4.3 Conical Spouted-Bed Reactor (CSBR)

CSBR is employed in the pyrolysis and gasification of waste plastic. As illustrated in Figure 2.5, the CSBR comprises several components such as a hopper, feeding system, gas mixture, gas preheater, reactor, and condenser. The conical spouted reactor is conical from the end and has a cylindrical part at the top (Moorthy Rajendran et al., 2020). The CSBR finds application in processing materials with a wide particle size distribution while ensuring adequate mixing. The principal advantages of the CSBR over the fluidized-bed reactor include fast heat transfer rates and negligible defluidization issues, particularly when handling highly sticky inputs such as PE and PP at specific temperatures. The reactor uses a slow pyrolysis process at low temperatures, yielding higher wax content. A study investigating the pyrolysis of HDPE with HZSM-5, HY, and Hβ zeolite-based catalysts in a conical spouted-bed reactor (CSBR) at 500°C and

atmospheric pressure found that the HZSM-5 zeolite-based catalyst was highly selective for light olefins, Conversely, the Hβ and HY zeolite-based catalysts were notably successful in generating non-aromatic C_5–C_{11} products (Orozco et al., 2021). Elordi et al. conducted a study on the catalytic pyrolysis of polyethylene (PE) in a CSBR using an FCC catalyst (Elordi et al., 2009). Conversely,Hβ and HY produce high yields of non-aromatic C_5–C_{11} products (approximately 45 wt.%). However, catalyst deactivation due to coke generation increased wax yield as the reactions progressed, particularly notable with HY and Hβ zeolite-based catalysts. Fernandez et al. studied biomass steam pyrolysis in a CSBR and achieved 75.4 wt.% bio-oil at 500–800 ^{o}C temperature range (Fernandez et al., 2022). Arabiourrutia et al. employed CSBR to obtain wax products from polyolefin plastics. Their findings revealed that the design of the spouted bed was particularly well-suited for extracting wax through pyrolysis at low temperatures, as the wax yield decreased with increasing temperature. (Arabiourrutia et al., 2012).

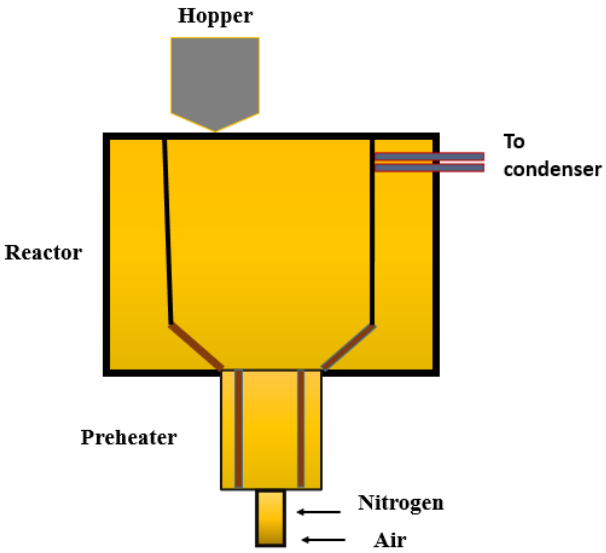

Figure 2.5: Conical spouted-bed reactor (Pal et al., 2022)

The decrease in wax yield with increasing temperature could be attributed to the higher likelihood of waxes breaking down into liquid or gaseous products as temperatures rise. Hence, it can be inferred that CSBR provides efficient heat

transmission between phases, ensures proper mixing, and can handle large particles of varying densities. However, challenges persist with feeding and entrapping the catalyst within the reactor.

2.9.4.4 Rotary Kiln Reactor

Figure 2.6 depicts the schematic diagram of the rotary kiln reactor. A rotary kiln reactor is more efficient due to its proper mixing. The reactor efficiently mixes feedstock very well compared to other reactors. However, these reactors operate on a slow pyrolysis process, indicating moderate heating rates. The heating rate is typically limited to 100 °C/min, with a residence time of one hour (Fantozzi et al., 2006). Rotary drums, furnaces, and kilns are steel drums walled internally with high resistance. Reactors are intended for prolonged RT of 20 min or exceed and feature inclined low-speed rotational movements. The product in rotary kilns varies significantly due to the huge temperature differential in the system. The rotation of the kiln aids in the appropriate mixing of the feedstock. Then, it is progressively heated as pyrolysis gases are produced as it moves down the cylinder and carbonizes (D. Chen et al., 2014).

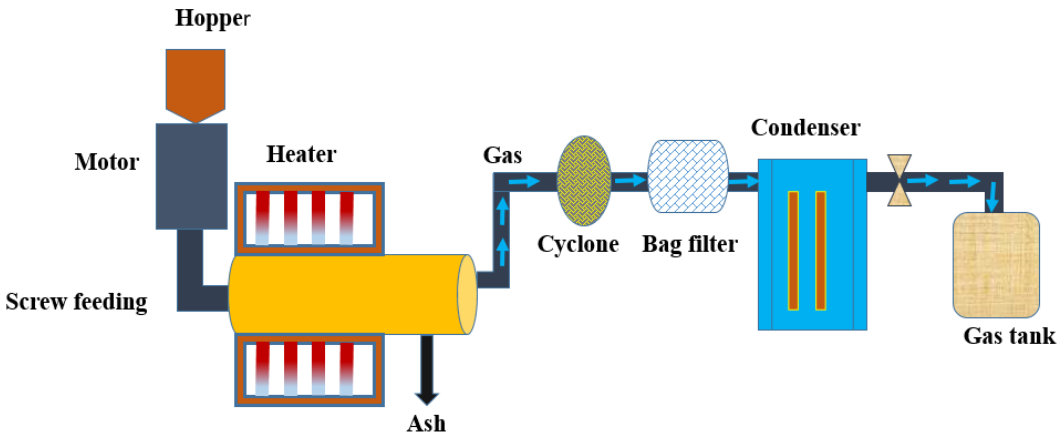

Figure 2.6: Rotary kiln reactor (Pal et al., 2022)

Several advantages are evident, such as ensuring proper feedstock mixing, offering flexibility in adjusting residence time, accommodating heterogeneous

materials, eliminating the necessity for feedstock pre-treatment, and facilitating maintenance tasks.

2.9.4.5 Auger Reactor

The auger reactor is also known as the screw reactor because of having a screw, as shown in Figure 2.7. The reactor consists of various components, such as a hopper, a tubular shape, and a screw responsible for continuously transporting the feedstock during operation. The spinning of the screw facilitates the transfer of feedstock, while the necessary heat for pyrolysis is transferred by the reactor tubular wall. Remarkably, external heat sources have proven adequate for heating reactor tubes with smaller diameters (Park et al., 2022). This design allows for closer contact between feedstock particles as they go through the reactor tubes. Solid carriers can be built of steel or ceramic pellets. An auger reactor can be constructed to be extremely small and even portable in certain situations. It can also be strategically located near municipal plastic waste (MPW) disposal sites.

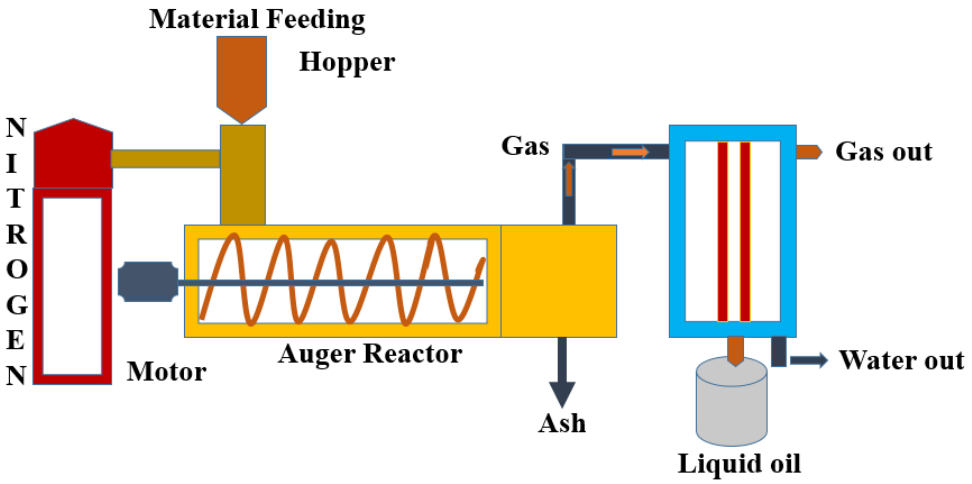

Figure 2.7: Auger reactor (Pal et al., 2022)

Hence, different reactors may be used in the pyrolysis process. The most employed reactors for the pyrolysis process are given in Table 2.4. It has been observed that batch reactors are more feasible for the waste plastic pyrolysis process to obtain a higher plasto oil yield than other reactors.

Table 2.4: Product yield distribution with different reactors

Reactor type	Heating rate (^{O}C/min)	Reaction temperature (^{O}C)	Concentration of catalyst	Type of catalyst	Liquid (%)	Solid (%)	Gas (%)	References
Semi batch reactor	20	440	10%	ZSM-5	56.9	3.2	40.4	(Lopez-Urionabarrenechea et al., 2012)
Batch reactor	-	240	-	Activated carbon	82.43	15.22	2.35	(Senthil Kumar et al., 2017)
Batch reactor	-	240	-	Charcoal	95.54	2.33	2.13	(Senthil Kumar et al., 2017)
Batch reactor	20	500	33.3%	Calcium bentonite	81.3	12.7	6	(K.panda, 2018)
Batch reactor	15	510	5% 1:1:2	Red mud : Ca(OH) : Ni/SAPO	64.2-71.9	-	-	(Fekhar et al., 2019)
Batch glass reactor	5	350	10%	Al-Si	93.11	9.27	0.36	(Sangpatch et al., 2019)
Batch reactor	10	500	Pelletized	MgO	88	10	2	(Inayat et al., 2021)
Batch reactor	5.5	400	-	-	86	8	6	(Paula costa et al., 2021)
Fixed bed reactor	10	600	100%	FCC	69	28	3	(Onwudili et al., 2019)

Vertical tube reactor	-	600	100%	$Ca(OH)_2$	52.2	9.0	27.7	(Kumagai et al., 2015)
Vertical tube reactor	-	600	100%	CaO	46.7	31.8	17.6	(Kumagai et al., 2015)
Vertical reactor	-	500	10%	USY -Zeolite	70-80			(Kassargy et al., 2018)
Vertical tube reactor	20	500	-	$CaCO_3$	68	5.7	26.3	(R. K. Singh et al., 2022)
Stirred tank reactor	10	450	1kg/hour – 60 gm catalyst	Fe-restructured clay	83.73	-	-	(Lei et al., 2018)
TL- 200 Tube furnace	10	480	10%	Organic vermiculite	80.6	0.1	19.4	(zicai chen, Yiqian wang, 2021)
TL-200 Tube furnace	10	480	10%	Co/Vermiculites	73.2	0.1	26.7	(zicai chen, Yiqian wang, 2021)
TL-200 Tube furnace	10	480	10%	Ni/Vermiculites	70.7	1.3	28.0	(zicai chen, Yiqian wang, 2021)
TL-200 Tube furnace	10	480	10%	Co-Ni/Vermiculites	73.9	0.1	26.0	(zicai chen, Yiqian wang, 2021)
Continuous microwave-assisted pyrolysis system	-	620	200gm pelletized form	ZSM-5	48.9	-	49.0	(N. Zhou et al., 2021)

2.10 Catalytic Thermal Degradation (CTD)

The catalytic thermal degradation (CTD) process represents a significant advancement over the conventional pyrolysis process as it occurs within a catalyst environment, leading to enhanced quality of liquid fuels compared to traditional thermal methods. Hence, selecting a suitable catalyst plays a vital role throughout the process. By employing a catalyst, the reaction rate of thermal degradation is heightened. Catalysts lower the activation energy and the process temperature required to improve the pyrolysis process and conversion efficiency. The thermal degradation process demands substantial energy input, as it necessitates high temperatures to degrade waste plastic and produce a high-quality end product, potentially obviating the need for additional upgrading processes (Hussein et al., 2021). Therefore, the CTD process is economically feasible for yielding valuable products like low molecular weight plasto oil with enhanced quality, requiring less thermal and energy input. This plasto oil boasts a higher heating value (HHV) of 38–46 MJ kg^{-1}, nearly comparable to conventional diesel, which has an HHV of 45.5 MJ kg^{-1} (Hafeez et al., 2018). The first stage is related to the disintegration of short-length branches, whereas the second stage is associated with the degradation of the molecular backbone of the main chain. Moreover, increasing the wt.% of the catalyst leads to increased solid residue char due to non-decomposable content within the catalyst and carbon deposition on the catalyst surface. Hence, it can be inferred that catalyst concentration directly influences thermal degradation. The significance of the catalyst lies in its ability to initiate decomposition at a lower temperature, a characteristic that is directly proportional to the concentration of the catalyst.

2.10.1 Type of Catalyst

Catalysts enhance product quality while reducing the temperature and retention time, thereby optimizing the overall process. Catalytic thermal degradation is more appealing than thermal cracking alone since it is faster and needs lower temperatures, resulting in considerable energy savings. Furthermore, catalytic cracking using catalysts such as zeolites produces high-quality products in a range

of motor engine fuels, reducing the need for additional upgrading processes. Thermal pyrolysis is limited to areas with existing oil refineries since its products require additional refining (Hafeez et al., 2019). Catalysts have several beneficial effects in the pyrolysis process: they lower the required pyrolysis temperature, shorten reaction times, facilitate the formation of diesel within the optimal boiling point range of 390–425°C, enhance selectivity towards gasoline, and expedite isomerization reactions (Butler et al., 2011). Catalysts are widely employed in refineries and in waste plastic pyrolysis to recover hydrocarbons from waste. The global market for refinery catalysts has experienced significant growth despite stringent regulations and rising demand for petroleum products. This growth is primarily driven by the increasing need for transportation fuel. Additionally, stringent emission control regulations worldwide have highlighted the necessity for efficient, sustainable, and high-yield techniques, driving advancements in the market. As a consequence of this environmental concern, demand for refinery catalysts has increased, enhancing the efficiency of the process. The type of catalyst used has a considerable influence on the process outcome, since the catalyst's large surface area can change the nature of pyrolysis and hence considerably impact the products (Lin et al., 2010; Yang et al., 2022). Thermal degradation of plastic waste used two primary types of catalysts: heterogeneous and homogeneous. Heterogeneous catalysts involve reactions where the catalyst and reactant exist in different phases, while homogeneous catalysts operate within a single phase (where the reactant and catalyst are in the same phase). The Fe/Al_2O_3 ratio catalysts are a prevalent form of homogeneous catalysts employed in plastic waste pyrolysis (Yang et al., 2022). However, heterogeneous catalysts are predominantly favored by plastic waste pyrolysis due to their ability to facilitate easy separation of the liquid product from the catalyst, along with convenient regeneration and reuse. Among the most widely used heterogeneous catalysts are nanocrystalline zeolites, ordinary acid solids, and mesostructured catalysts such as metal-supported carbon and basic oxides (Rasul Jan et al., 2013) Heterogeneous catalysts have been demonstrated to withstand extreme reaction

conditions of up to 1300°C and 35 MPa while being easily separated from the gaseous and liquid reactants and products. Acid solids, mesostructured catalysts, and nanocrystalline zeolites are typical heterogeneous catalysts (Ruhul et al., 2015). Various researchers have shown interest in nanocrystalline zeolites due to their significant role in product distribution (Figueiredo et al., 2016; Ubando et al., 2022; Yansaneh et al., 2022). In addition, various other catalysts, such as fly ash, bentonite, silicate, silica-alumina, ceramic, activated char, and MVM-41, have recently attracted researchers' attention. Table 2.4 summarizes the catalytic effect on solid, liquid, and gaseous hydrocarbons with different heating rates and reactors.

2.10.1.1 Zeolite Catalyst

In thermo-catalytic processes, zeolite has been extensively recognized as an efficient and selective material catalyst for biofuel production. Due to its robust catalytic properties, ZSM-5 is a comparatively inexpensive catalyst for converting waste plastic into plasto oil. The catalyst has greater thermal stability, activity, selectivity, and coke deactivation than others (Hedlund et al., 2022). Zeolites, also known as aluminosilicate crystalline sieves, are solid crystalline structures defined by a 3-D framework in which O_2 atoms link tetrahedral sides with open pores and ion exchange capabilities. The reactivity and efficacy of zeolite are influenced by the SiO_2/Al_2O_3 ratio, which influences the type and quality of the pyrolysis-yielded products. The proportion of silica-alumina in various zeolites varies, and the ratio has a distinct reactivity. Ates et al. proved this with varied $SiO_2/Al2O_3$ ratios of 30, 80, and 280, utilizing the catalyst HZSM-5 zeolite. $SiO_2/Al2O_3$ (30) has an average pore diameter, higher surface area and higher acid strength. Higher acidity of the catalyst is obtained with a SiO_2/Al_2O_3 ratio of 30, sufficient to crack the wax and lead to the yielding of light olefins and lower the heavy fraction (C_{12}–C_{20}) . Conversely, decreasing the SiO_2/Al_2O_3 ratio from 280 to 30 led to an increase in light olefins output from 35.5 to 58 wt.%, accompanied by a decrease in the C_{12}–C_{20} and C_5–C_{11} from 28 to 5.3 wt.% and 28.8 to 15.2 wt.%, respectively (Ateş et al., 2013). Various zeolite base catalysts' pore size and

acidity vary, affecting the final product. For instance, catalysts with larger pore sizes facilitate plastic conversion into polyalkyl aromatics, whereas those with smaller pore sizes primarily produce aromatic compounds with small dynamic diameters. According to his findings, choosing the appropriate zeolite catalyst in the pyrolysis reaction significantly influences the resulting end product. The variation in pore size and acidity among different zeolite-based catalysts directly impacts the yield (Fadillah et al., 2021). Wong et al. studied LDPE pyrolysis over ZSM-5 zeolite and found that catalytic cracking produced the C_1–C_8 hydrocarbons caused by effective heat exchange between the catalyst and polymer chain (Wong et al., 2017). Sivagami et al. The pyrolysis of LDPE with synthesized ZSM 5 catalysts at 500 ^{o}C temperature produced 70 wt.% plasto oil yield with 16 wt.% gas and 14 wt.% solid char (Sivagami et al., 2021). The strong acidic properties and microporous crystalline structure of the synthesized ZSM-5 catalyst enabled enhanced cracking and isomerization reactions, leading to more significant fragmentation of larger molecules into smaller ones and increased oil production during pyrolysis experiments. Susastriawan et al. studied the impact of zeolite size on the low-temperature pyrolysis of LDPE. The researchers observed that reducing the size of the zeolite could enhance reaction rates, pyrolysis temperature, heat transfer rates, and oil production during the pyrolysis process, attributed to the larger surface area-to-volume ratio associated with smaller particles. Maximum oil yields were obtained when the zeolite particle size was 1 mm; however, the difference in oil production was insignificant when the particle size ranged from 1 to 3 mm (Susastriawan et al., 2020). A related study by Kim et al. suggested that phenolic functional groups in lignin may increase the aromatic hydrocarbons by 39% in the final products over zeolite catalysts. The available hydroxyl group on the zeolite surface accelerates the condensation, facilitating the formation of aromatic hydrocarbon molecules through pathways such as oligomerization, isomerization, aromatization, and dihydroxylation (J. Y. Kim et al., 2018). Moreover, researchers have demonstrated that heat and acid activation can enhance the zeolite properties (Miandad et al., 2016). However, researchers

have also proven that heat and acid activation may improve the catalytic capabilities of natural zeolite. Rashid et al. investigated natural zeolite modified by heat and acid activation, which was used in the pyrolysis of MPW. It was discovered that acid-activated zeolite has higher catalytic activity than thermally-activated zeolite (Miandad et al., 2019). Another benefit of this catalyst is that the used zeolite catalyst may be recovered and used in a similar process with the same purpose, but with different performance. Additionally, it helps reduce sulfur impurities in the liquid product generated (Subhaschandra et al., 2020).

2.10.1.2 Fluid Catalytic Cracking Catalyst

The fluid catalytic cracking (FCC) catalyst is vital in cracking the heavier petroleum fractions into valuable fuels, viz. LPG, gasoline, and diesel (Saeaung et al., 2021). FCC catalysts have been widely reported, primarily consisting of zeolite Y modified to enhance effectiveness, cracking activity, coke selectivity, and stability. These modifications typically involve introducing an additional aluminum framework into the zeolite structure (Palos et al., 2022). Aisien et al. evaluated that pyrolysis of PE with FCC catalyst reduced the PO yield from 83.3 wt.% to 77.6 wt.%; however, it led to an increase in the gaseous hydrocarbons from 13.2 wt.% to 19.7 wt.% and decreased in solid char formation from 3.0 wt.% to 2.7 wt.% (Aisien et al., 2021). Similarly, Abbas et al. examined the FCC catalyst in the proportion of 10 wt.% to 60 wt.% at 450 ^{o}C and found no significant impact on the non-condensable gaseous hydrocarbons (Abbas-Abadi et al., 2013). However, the FCC catalyst increased the solid char, potentially due to enhanced dehydrogenation and aromatization processes occurring on the catalyst surfaces. This phenomenon led to an accumulation of solid hydrocarbons on the catalyst surface. Moreover, coke deposition on the catalyst resulted in deactivation, rendering it less effective in breaking down waxes. Monitoring of catalyst activity indicated that an equilibrated catalyst exhibited favorable performance for MPW pyrolysis. Abadi et al. suggested that the FCC catalyst is particularly effective in polypropylene (PP) pyrolysis, enabling a yield of plasto oil exceeding 90 wt.% (Abbas-Abadi et al., 2014). Sharuddin et al. examined the

use of wasted FCC catalysts in the pyrolysis of waste plastics, obtaining an 80 wt.% yield of PO. As pyrolysis evolves as a technique for recycling plastic waste, FCC catalysts have gained prominence in this industry (Anuar Sharuddin et al., 2016). The fluid catalytic cracking unit (FCCU) turns heavy oil fractions into high-octane petrol, augmenting the refinery gasoline pool. This underscores the potential of FCC catalysts in the pyrolysis of plastic waste in the foreseeable future (Orozco et al., 2021).

2.10.1.3 Bimetallic Catalyst

Bimetallic catalysts have been used in the pyrolysis reaction to produce plasto oil from plastic waste. Wen et al. investigated Ni-loaded carbon nanotubes (CNTs) for polyolefin pyrolysis and reported favorable outcomes attributed to the higher carbon content present in the catalyst. This is caused by high surface area and stability, bimetallic catalysts offer a synergistic effect in pyrolysis (Wen et al., 2014). Chen et al. studied the effects of Fe-Ni bimetallic alteration of MCM-41, with each metal containing 10 wt.%, resulting in a large 49.9 wt.% liquid hydrocarbon yield, 65.9% of which was composed of single styrene hydrocarbons (T. Chen et al., 2020). The large surface area allows polymers to penetrate the pore structure and break. While Fe functions as a catalyst for converting raw materials into styrene, the inclusion of nickel metal oxides improves the acidity of the catalyst, permitting the transformation of multi-ring compounds into single hydrocarbon structures. The chemisorption process is governed by the external surface properties and pore size, which may be controlled using synthetic techniques. In this case, higher pore widths in the FeNi catalyst result in enhanced hydrogen desorption. Similar to the high pore size of Co/SBA-15 (Han et al., 2018). Additionally, Mo and Ni have various benefits as pyrolysis catalysts, including cheap cost absorbent, excellent stability and performance, large surface area, and simplicity of manufacture (Sridhar et al., 2020). However, the sulfurization procedure influences the bimetallic catalyst's reactivity. The improved sulfurization process may consistently improve the proportion of oil conversion to fuel oil, which now stands at 86.9%. Zhou et al. conducted the

study on the Ni–Fe/ZrO2 catalyst, resulting in the excellent degradation of the polystyrene (PS) at a temperature of 500 ^{o}C. Hence, the bimetallic catalyst has good selective conversion in the pyrolysis process and may improve the catalytic activity (H. Zhou et al., 2020). The combined characteristics of Ni–Fe might lower the water gas shift reaction and other reforming reaction activation energies (P. Wu et al., 2020).

2.10.2 Catalyst effect on physicochemical characteristics of the plasto oil

Table 2.5. presents the physicochemical characteristics of the PO produced from municipal plastic waste pyrolysis with and without a catalyst. The physicochemical properties of gasoline and diesel fuels play a vital role in their utilization in the transport sector. In recent years, alternative fuels have been used in engine vehicles. It has been observed from the table that conventional fuel density for diesel and gasoline is 0.807 gcm^{-3} and 0.780 $gcm^{-3,}$ respectively, which is in line with fuels produced from plastic wastes with zeolite and kaolin catalysts of 0.871 and 0.800 gcm^{-3}, respectively (Damodharan et al., 2019). Herein, in a combustion chamber, the kinematic viscosity of the fuel appears as a spray pattern and atomization behavior. Excessively viscous oil can lead to inadequate fuel atomization and fuel injector leakage, consequently compromising engine performance (Sharma et al., 2016; K. Khan et al., 2018). Therefore, the kinematic viscosity of the fuel should be lower for proper atomization and complete fuel combustion in an engine cylinder. Pyrolysis with a zeolite catalyst obtained a 1.99 cSt lower than other catalysts and close to the diesel viscosity. Calorific value is the essential characteristic of the obtained plasto oil. The calorific value of the plasto oil obtained with zeolite and kaolin is 46.67 MJ/kg and 46.47 MJ/kg, close to the conventional diesel.

Moreover, studies have shown that higher calorific values consume less fuel than lower calorific values, leading to complete combustion in the cylinder and improving the power efficiency of the engine (Chintala et al., 2019; Sharma et al., 2020). However, the higher pour point of the plastic plasto oil lowers the flow

characteristic because it may cause the wax to form in the cylinder and make it troublesome in the engine. However, plastic pyrolysis with kaolin clay obtained the pour point at a very low temperature of 18 ^{o}C. The flashpoint of the liquid hydrocarbon is much less than conventional diesel, indicating the safety hazards of plasto oil in terms of explosion and fire during fuel transportation (Sharma et al. 2016; Sekar et al., 2021). Hence, it is concluded from Table 2.5 that plasto oil has the same characteristics as conventional fuel, so plasto oil may be used to blend diesel and some additives for transportation.

Table 2.5: Physicochemical characteristics of the plasto oil

Characteristics Properties	**No catalyst** (P. K. Ghodke, 2021)	**Silica–alumina** (Choi et al., 2010)	**Natural Zeolite** (Syamsiro et al., 2014)	**Fly ash** (Nalluri et al., 2020)	**FCC** (N. Zhou et al., 2021)	**Kaolin** (Wan Nurdyana wan mansor et al., 2021)	**Calcium bentonite** (Aisien et al., 2021)	**Gasoline** (I. Ahmad et al., 2015)	**Diesel** (I. Ahmad et al., 2015)
Density @ 15°C (g/cm^3)	0.860	0.770	0.868	0.800	0.752	0.800	NA	0.780	0.807
Viscosity (cSt)	2.48	2.21	2.191	0.145	2.273	2.72	2.32	1.17	1.9-4.1
Calorific value (MJ/kg)	40.42	NA	45.58	41.93	43.28	46.479	43.28	42.5	43.5
Octane number	NA	NA	NA	NA	NA	NA	NA	81-85	NA
Pour point (°C)	18	NA	24	NA	-11	-18	NA	NA	6
Flash point (°C)	35	NA	<10	NA	29	40	NA	42	52
Aniline point (°C)	60	NA	NA	NA	NA	NA	NA	71	77.5
API gravity@ 60°F	38.1	NA	NA	NA	NA	NA	NA	55	38
Moisture % vol	2.4	NA	NA	NA	NA	NA	NA	0.4-0.5	0.1-0.3

2.10.3 By-products of the catalytic pyrolysis process

The catalytic pyrolysis of municipal mixed plastic waste yields plasto oil as the main product, along with by-products such as solid char and gaseous hydrocarbons. The effects of catalysts on byproducts are described in the following.

2.10.3.1 Catalyst effect on solid residue and its potential

The solid residue, char, represents the unburnt waste plastic remnants in the pyrolysis reactor. The solid char formation is contingent upon temperature, heating rate, and residence time. Generally, lower values of these parameters correspond to a higher proportion of char formation (Thahir et al., 2019). The state-of-the-art has reported that char is comparatively lower than the gas and liquid yield (Senthil Kumar et al., 2017; Kassargy et al., 2018; Sangpatch et al., 2019). The presence of a catalyst tends to increase the hydrocarbon content in the char residue. However, char deposition on the catalyst surface can diminish the effectiveness of the reaction, potentially leading to reduced pyrolysis efficiency and increased production of ash content as byproducts (Ratnasari et al., 2017; Sembiring et al., 2018; Qiu et al., 2018). Jamradloedluk et al. conducted pyrolysis of HDPE at 400 and 450°C, collecting and analyzing the resulting char. Proximate and elemental analysis revealed that the solid char contained a significant proportion of volatile matter (51.40%), moisture content (2.41%), fixed carbon (46.03%) and ash content (0.61%) (Jamradloedluk et al., 2014). The char-derived briquettes demonstrated promising potential as a solid fuel for heating applications. Additionally, some studies have suggested its utility as a heavy metal absorbent in industrial wastewater and for removing toxic gases or in graphene production (Jamradloedluk et al., 2014; Moorthy Rajendran et al., 2020).

2.10.3.2 Catalytic effect on gaseous hydrocarbons and its potential

Gaseous hydrocarbons represent one of the byproducts of the pyrolysis process, and their production is affected by the type of waste plastic and the temperature range. Polyolefins and polystyrene typically yield gaseous hydrocarbons from 5%

to 20% by weight. Pyrolysis of MPW at 350°C yields more gaseous products than individual waste plastics, with an increase of 8.5% by weight observed upon raising the temperature. It has been observed that 1 kg of feedstock generates approximately 13% to 26% of gaseous products by weight. Furthermore, the catalyst significantly influences the production of gaseous hydrocarbons compared to plasto oil. While it enhances gaseous product yield through increased cracking processes, it simultaneously reduces plasto oil yield, thus improving the quality of the resulting plasto oil (Sivagami et al., 2021). In conventional pyrolysis of municipal plastic waste, CO, CO_2, hydrogen, methane, ethane, propane, butane, and other gaseous hydrocarbons are a source of gaseous products from the pyrolysis. The presence of a catalyst leads to the decarboxylation route, which may reduce the concentration of CO_2 and increase the CO in the gaseous products. However, the state-of-the-art shows that the most significant impact of kaolin and zeolite on the produced gases increases the H_2 and carbon frame isomerization, which increases i-butane concentration (López, Adrados, et al., 2011; P. K. Ghodke et al., 2021). The gases produced by plastic garbage have a significant calorific value. Gases generated by the pyrolysis of agricultural waste plastic include 45.9 and 46.6 MJ/kg HHV, respectively (Zicai Chen et al., 2021). Moreover, the HHV of gases produced by PP and PE pyrolysis is 50 and 42 MJ/kg, respectively (Jung et al., 2010). In addition, there are comparable findings for HHV of tire pyrolysis (45 MJ/kg) (Leng et al., 2015). As a result, the generated gases can be used in boilers for heating or gas turbines for power generation. Moreover, because of their composition, 1-butene and isoprene may be recovered by condensation and used to make tires. After being separated from other gases, propane, and ethane can be utilized as chemical feedstock to produce polyolefin.

2.11 Application of plasto oil as fuel

Exceeding energy demand due to growing population, global warming, waste policy, and unstable price of fossil fuels have attracted the researcher to emphasize on developing sustainable alternative energy sources to meet the

energy demand and replace fossil fuels. Plaso oil obtained from waste plastic could be used in various applications including heavy industry boilers, steel factories, fuel oil pumps, hot water generation, and other industrial heating applications, such as IC engines. However, waste plastic pyrolysis oil (PO) can be used as fuel in the transportation sector. Various studies have been carried out on producing gasoline-range liquid fuels. However, in the last few years, studies have been carried out to produce the diesel range (C_{13}- C_{20}) fuel through the thermal recycling of waste plastic for their application in diesel engines from light-duty vehicles to heavy-duty vehicles.

2.11.1 Plasto oil as fuel in compression ignition engine

As per the United Nations report, India has become the world's largest population country with 1,426,296,793 population by 27 April 2023. The growing population has a higher demand for energy in daily life. Researchers are unremittingly doing studies to attain sustainable alternative fuels and meet the energy demand of the growing population. Recycling of waste plastic to energy products is one excellence superimposed over another. Therefore, the pyrolysis of plastic waste is a promising way to address the issue of MMPW recycling. In addition, the process produced plasto oil, which may apply to the compression ignition (CI) engine. Therefore, various research studies were conducted to analyze the characteristics of CI engines fueled by plasto oil. However, due to their low environmental impact, great efficiency in fuel conversion, and durability, CI engines dominate the world's power-generating sectors. Various studies conducted to find the effect of the CI engine with PO and diesel blends. Revu Krishn Mohan et al. studied a light-duty diesel engine with PO. They observed diminished BTE and higher BSFC than diesel. This may be caused by higher density and lower calorific value of PO. A detailed study has been carried out on plastic oil blends in diesel engines and found that BTE decreases by 13.06 % with neat plasto oil on increasing the plastic blends. However, cylinder pressure increased by 5.9 % with plasto oil at a higher engine load (R. K. Mohan et al., 2023). This is caused by the higher viscosity of the PO, leading to inadequate

atomization, which delays the combustion and heightens the combustion rate within the cylinder (Viswanath K. Kaimal et al., 2015). M. Mani et al. study on the plasto oil blend resulted in an engine fueled with plasto oil, increasing the BTE up to 80% engine load. However, BTE decreased by 1.9% than diesel. This may cause of higher heat release rate. Consequently, increasing the exhaust gas temperature (EGT) for PO. This may result in the reduction of brake thermal efficiency at a high engine load for plasto oil (Mani et al., 2011). Sachin Kumar et al. examined the 40 vol% of the PO and 60 vol% diesel as fuel in CI engi, resulting in BTE being 16.73 % lower than diesel. This may cause a lower calorific value of 40% PO than reference diesel. However, NO_x and CO emissions increase with the plasto oil blends. The NO_x may cause the availability of the O_2 content in the plasto oil, resulting in proper combustion and a rise in the temperature of the cylinder. Meanwhile, CO formation is attributed to poor fuel mixing and improper combustion (Kumar et al., 2013). A study was conducted on the PO fuel in CI engine and observed that plastic oil produced a lower BTE of up to 3-4% than conventional diesel. This may cause higher aromatic compounds in the PO, which require high energy to break them. Moreover, there is an increase in emissions, including NO_x, HC, CO and CO_2. Based on the test findings, a blend of 60-70% PO operating at 80-90% engine load has the potential to deliver high engine performance in the long run (Kalargaris et al., 2017). Hence, plasto oil in the CI engine has an adverse effect on the engine characteristics. Further studies and their results have been given in Table 2.6.

Table 2.6: Plasto oil effect on CI engine characteristics

Fuel used	Major finding	Reference
Waste plasto oil (WPO) and diesel blends (10, 20, 30, 40 vol%)	BTE was 13.58%, 17.25%, 13.06% and 16.73%, lower than diesel on increasing the plasto oil blends, respectively. The mechanical efficiency of the 10% WPO with 90% diesel is higher than diesel at all engine load. NO_x, HC, and CO emissions increased as the plastic oil proportion in the blends increased.	(Kumar et al., 2013)
Waste plasto oil, Diesel, diethyl ether (DEE)	The BTE of the PO was 27.5%, 11.0% less than diesel. Blending diethyl ether with 5, 10, and 15 vol.% increases the BTE by 1.45%, 6.90% and 9.25%, respectively, than plasto oil. For DEE blends compared to PO, there was a reduction in cylinder peak pressure and heat release rate, accompanied by prolonged delay period. 15% blending of DDE with plastic reduces the amount of smoke opacity and NO_x by 25% and 29%, respectively.	(Kaimal & Vijayabalan, 2016)
Waste plasto oil and diesel	The engine could operate stably on plastic oil at 75%, 85% and 100% load. BTE was 2 - 3% lower than conventional diesel at higher engine load. NOx, CO, and HC emissions exhibited an increase.	(Kalargaris et al., 2017)

Waste plasto oil and diesel blends (10, 20, 30, 40, 50 vol%)	BTE was 30.01% for diesel and 29.88%, 31.61%, 31.29%, 31.27%, and 31.22% for 10%, 20%, 30%, 40% and 50%, respectively. Crude WPO in diesel blends by up to 50% decreases the volume efficiency with increased EGT. NO_x , CO and HC were higher than diesel.	(R. K. Singh et al., 2020)
Waste plasto oil, N- hexanol and diesel (WPO, D50WPO30H20, D50WPO20H30, D50WPO10H40)	BTE of WPO was 6.31% lower than diesel. Adding the hexanol by 20% (D50WPO30H20) increased the BTE by 3.42% more than diesel and 10.39% higher than WPO. D50WPO30H20 produced 9% and 14.28% lower NO_x than diesel and WPO, respectively. D50WPO30H20 produced 30% and 68.18% lower smoke than diesel and WPO.	(S. P. Venkatesan et al., 2020)
Waste plasto oil and diesel (WPO, WPO80D10)	BTE was lower for plastic oil and plasto oil blends. CO emission was increased with plasto oil and its blends. NO_x was higher for WPO, while WPO80D20 reduced the NO_x emission.	(T. S. Singh et al., 2020)
Waste plasto oil and diesel (5, 10, 15 vol%)	The double bond in the unsaturated compound results in high HRR by 0, 7 and 14% for blends 5, 10, and 15 vol%, respectively Increased in combustion delay and BTE was 25% lower than diesel. NO_x was 12, 21 and 26% higher and HC was 35, 80 and 90% higher than conventional diesel at higher engine loads for blends 5, 10, and 15 vol.%, respectively.	(Mangesh et al., 2020)

Waste plasto oil and diesel (40 vol %) and 100ppm TiO_2	BTE was 6.45% lower than the diesel for 40% plasto oil, Adding the 100 ppm TiO_2 BTE increased by 5.17 % more than 40% plastic oil blends, while decreased by 1.6% more than diesel. The addition of nanoparticles leads to lower HC and CO emissions by enhancing the combustion, leading to more thorough combustion.	(Praveenkumar et al., 2020)
Waste plasto oil and diesel (10, 20, 30 vol %) Low heat rejection engine (LHR)	The less heat rejection engine produced 25.93% BTE, 10.75%, 12.95 and 15.65 % higher than the 10, 20, and 30 vol.% plasto oil blends. Exhaust gas temperature was 1.12%, 2.93%, and 4.74%, higher than diesel. LHR WPO20 emits less CO by 5% than diesel at 75% engine load. LHRWPO10 emits lower hydrocarbon emissions by 7 - 16.2 % at various engine loads and 2% less HSU of smoke at moderate engine loads.	(Sambandam et al., 2020)
Waste plasto oil, Diesel and 25 ppm Al_2O_3	Adding 25 ppm of Al_2O_3 in PO25D75 blends increases the BTE and brake power by 35%. CO_2 and HC emissions were reduced by 60% and 45% by diesel. NO_x emission was reduced by 9% and 15% compared to diesel and WPO emissions.	(Sekar et al., 2021)

Waste plasto oil, Methanol, di ethyl ether (DEE) and diesel (PO40, PO40M25, PO40M20DEE5)	BTE of the PO40 was 12.10% lower and PO40M25 was 3.48% lower than diesel. Adding the DEE (PO40M20DEE5) increased the BTE by 6.8% compared to diesel. The P40M20DEE5 blend decreased smoke HC, and CO by 22.13%, 15.59 and 16.09, and respectively, while NO_x emissions increased by 4.1% compared to the P40 blend. However, concentrations of NO_x were lower than in diesel.	(Mariappan et al., 2021)
Waste plasto oil, Diesel and diethyl ether	Adding the 5% vol of the diethyl ether with 85% diesel and 10% waste, plasto oil produced the closer BTE to the diesel and higher than other blends of plasto oil at 75% engine load condition. NO_x, CO, and HC emissions increased with increasing the PO proportion.	(Selvam et al., 2022)

Hence, Various studies have been carried out on the CI engine fueled with PO blends with conventional diesel fuel and other additives. It has been noted that blending PO with diesel reduced engine power and increased emissions. These emissions are mostly caused by non-stoichiometric combustion, nitrogen dissociation, and contaminants in both the fuel and the air. Consequently, researchers are interested in modifying the CI engine to improve its characteristics.

2.12 Emissions and its formation from CI engine

2.12.1 Carbon monoxide emissions

CO is a colorless, odorless, toxic gas resulting from a fuel-rich equivalence ratio. When there is insufficient oxygen in the combustion chamber to convert the carbon molecule into carbon dioxide (CO_2), some fuel is not burned, and some

carbon is converted to CO. CO is not only considered an unwanted emission, but it also represents a waste of chemical energy.

$$CO + \frac{1}{2}\, O_2 \rightarrow CO_2 + Heat$$

Higher CO formation occurs at higher engine loads or instantaneous emissions, which may cause a rich A-F mixture. Even when the A-F mixture is lean or stoichiometric, it generates a small amount of CO due to the chemical kinetic effect. CO is very harmful to living beings, depending on exposure level and duration. Initial symptoms may include weakness, nausea, confusion, and dizziness. Although carbon monoxide is strongly affixed to the blood, haemoglobin can rapidly absorb it. This may result in asphyxiation.

2.12.2 Hydrocarbons emissions

Hydrocarbon emissions (HC) result from incomplete combustion caused by insufficient oxygen and low temperatures, preventing hydrocarbons from fully converting into H_2O and CO_2. It occurs when the A-F mixture is lean and the fuel deposits or accumulates near the cylinder wall. Alkane, alkene, and aromatic compounds are present in the fuel. The conventional CI engine has a higher combustion temperature, resulting in lower HC formation. However, low flame propagation speed causes misfire or incomplete combustion. In fuel-lean zones, combustion is limited; some fuel is left over in the cylinder and a lesser fuel is trapped on the nozzle tip, i.e., the sac volume does not burn completely and produces the HC emission. HC emission also occurs in the crankcase, venting, and fuel systems. Similar to other pollutants, HC emissions also have detrimental effects on human health, hence contributing to the development of ground-level ozone, which is highly hazardous.

2.12.3 Oxide of Nitrogen

Nitrogen oxide occurs only in engine exhaust combined with nitrogen dioxide and nitric oxide. Nitrogen reacts with oxygen at higher temperatures only. Therefore, higher temperatures and the availability of oxygen are the key reasons for NO_x

formation. Combustion in CI engines takes place by igniting highly compressed hot air, which typically has a temperature between 900-1400 K (Alrazen et al., 2018). The compressed air inside the engine cylinder is directed via the air intake manifold, while fuel is injected just before the completion of the compression stroke. In general, atmospheric nitrogen is naturally sustained and is carried by exhaust and other gases. However, suppose the temperature of combustion exceeds 1600 K. Under such circumstances, nitrogen undergoes a chemical reaction with the existing oxygen to produce nitrogen Oxide (NO) and nitrogen dioxide (NO_2), with NO accounting for about 85% of the overall NO_x output. Both gases possess unique physical and chemical characteristics. NO is colorless and odorless, but NO_2 has a reddish-brown with a pungent smell. Irrespective of their color and fragrance, these gases threaten human well-being, resulting in 1.3 million heart and lung problems annually in India (Shi et al., 2005; Silitonga et al., 2013).

2.12.4 Particulate matter

Particulate matter (PM) comprises solid carbon soot particles formed during combustion within the fuel-rich zones of the cylinder. These emissions, known as exhaust smoke, produce unpleasant odorous contaminants. These particles are produced during the combustion process because of the formation of small particles that may be detrimental to the respiratory system and lungs of humans. The primary factor responsible for PM production was inadequate combustion. According to Agarwal et al. PM is composed of 31% carbon, 7% unburned fuel, 25% oil, 14% sulphate, 13% water, 13% ash, and other substances. PM emission from the CI engine is 8-10 times higher than that SI engine (Agarwal et al., 2007).

Moreover, there are three categories of PM from CI engines: inorganic fraction, soluble organic fraction, and soot, with soot accounting for 85-90% of the total emissions. If not treated appropriately, breathing these may cause asthma, lung cancer, and other cardiovascular problems, as well as death.

2.13 Emissions control in CI engine

In the CI engine, the exhaust gases consist of organic and inorganic solid, liquid, and gaseous compounds, primarily influenced by factors including the design of the engine, operating conditions, quality of fuel, and emission control technologies. However, unavoidable emissions, specifically NO_x and particulate matter, are typically associated with CI engine. NO_x and PM are the major cause of concern and significant global challenges. Attempts to control the emissions, such as engine modification and emission control technologies, have significantly improved the environmental performance of CI engine over the years. Several techniques have been introduced to reduce the NO_x and PM, as shown in Figure 2.8.

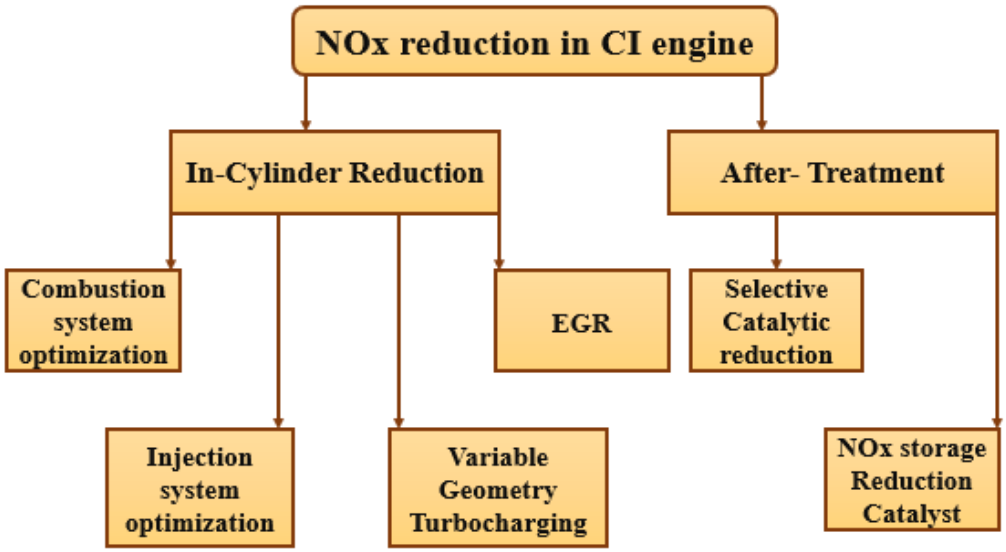

Figure 2.8: NO_x reduction technologies in CI engine

The essential techniques that played a significant role in improving engine emissions in the last two decades are discussed below-

2.13.1 Turbocharging

A turbocharger is a commonly used device in CI engine. A turbocharger comprises a turbine and a compressor directly connected to a single shaft. The exhaust gas undergoes expansion in the turbine, generating power that propels the

compressor. The compressor increases the density and pressure of the incoming air charge before delivering it to the engine intake manifold. The higher airflow mass in the turbocharged engines than the naturally aspirated results in emission reduction. Higher air mass flow is provided to the engine by turbocharging. More than 50% of excess air at rated power conditions can be employed in the CI engine. Turbocharged engines attain higher density and air temperature during fuel injection than traditional normally aspirated engines. This results in a shorter ignition delay time, reducing the fuel quantity used in the premixed phase. Turbocharging allows for the retardation of fuel injection time, resulting in a reduction of NO_x emissions without impacting fuel economy. Conventional turbochargers have limits in pressure ratio characteristics at low engine rpm. However, this challenge can be addressed by employing a variable geometry turbocharger.

2.13.2 De- NO_x catalyst

A huge amount of oxygen is accessible in the exhaust gas of a CI engine. It uses excessive air during operation and provides an oxidizing environment for exhaust pollutants. To be converted into innocuous compounds, NO_x and CO pollutants must be reduced and oxidized in the atmosphere. The SI engine's stoichiometric A-F ratio will support oxidizing and reducing atmospheres in the exhaust system. On the other hand, the diesel engine is only rich in an oxidizing environment. As a result, a novel, non-conventional reducing catalyst is necessary to lower the atmosphere of the exhaust system. Reductants are the name given to this reducing catalyst. In diesel engine exhaust systems, ammonia and hydrocarbons are employed as a reducing agent or reductant. NO_x reduction may be accomplished in two methods, as mentioned below.

2.13.3 NO_x storage–reduction (NSR) catalyst

NO_x storage reduction catalysts, also known as the NO_x trap or NO_x absorber, have been developed as an aftertreatment technique to minimize the NO_x emission for application in engine. NO reacts with oxygen and converts it into NO_2 in the presence of platinum (Pt) reductant.

$$NO + O_2 \xrightarrow{Pt} NO_2$$

This NO_2 reacts with the alkaline BaO (barium oxide)

$$NO_2 + BaO \longrightarrow BaO.NO_2$$

The degradation of this barium nitrate into a harmless substance requires a significant amount of hydrocarbons. In a diesel engine, the injection system allows for a sudden increase in fuel after reaching the top dead centre. In an SI engine, the fuel injection system is synchronized or configured to operate at a rich air-fuel ratio for just one second.

2.13.4 Selective Catalytic reaction (SCR)

SCR technology has been used to turn NO_x into a safe byproduct by using ammonia as a reducing agent. The practical use of the SCR process is to use urea as the source of ammonia since it is more readily accessible and safer to handle and store. The two steps that make up this method's completion are mentioned below.

Urea Hydrolysis

$$(NH_2)_2CO + H_2O \longrightarrow CO_2 + 2\,NH_3$$

NO_x Conversion

$$4NO + 4\,NH_3 + O_2 \longrightarrow 4\,N_2 + 6\,H_2O$$

$$6\,NO_2 + 8\,NH_3 \longrightarrow 7\,N_2 + 12\,H_2O$$

A 30-40% urea concentration is employed in water. A vanadium and titanium oxide mixture was used as an SCR catalyst coated on the ceramic honeycomb structure. The exhaust gases containing NO_x emission vary with engine load, so continuous urea injection variation is required. The concentration of NO_2 in exhaust NO_x is about 10%. A molar ratio of 0.9 of NH_3/NO_x is required to convert NO_x efficiently. A higher amount of ammonia is provided to complete the task. However, there will be a portion of ammonia that stays unreacted, known as

ammonia slip. A strategy is used to dynamically control the ammonia dose to reduce the amount of ammonia slip. Figure 2.9 depicts the advanced SCR catalyst system for heavy-duty diesel engine.

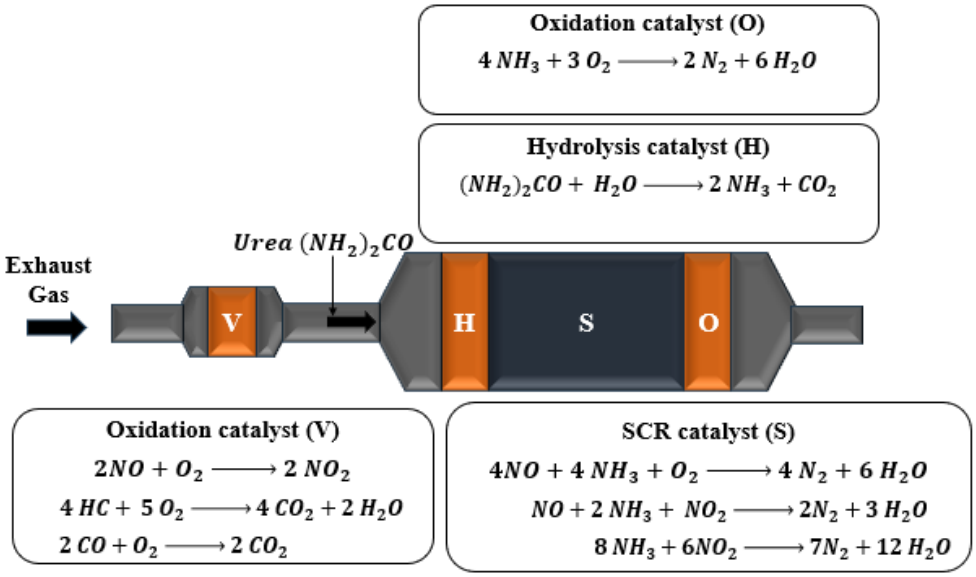

Figure 2.9: Advance SCR catalyst system using pre-oxidation catalyst

(Koebel M. et al. 2020)

2.13.5 Plasma catalyst system (PCS) for NO_x reduction

This concept is inspired by the power generation sector, where flue gases containing NO_x undergo plasma treatment to convert them into acids, which are then combined with ammonia to produce ammonium nitrate. Currently, this technology is used for automotive purposes (Chun et al., 2000). In this reduction process, plasma is utilized to convert the NO component into NO_2, which is subsequently reduced to N_2 with a catalyst by the HC present in the exhaust gases. An advantage of this system is that it achieves NO_x conversion without requiring hydrocarbon oxidation, like an NSR catalyst. Moreover, it does not facilitate the conversion of SO_2 to SO_3 and sulphuric acid, which is crucial for the catalyst's susceptibility to poisoning. The optimal conversion efficiency is achieved when the ratio of hydrocarbons (HC) to nitrogen oxides (NO_x) is between 3:1 and 6:1, within a temperature range of 300 ºC.

2.13.6 Diesel particulate filter

This emission control technology has been in use since 1980. A diesel particulate filter (DPF) is a customized device, which is designed to eliminate particulate matter (PM) or soot from the emissions of diesel engines. Diesel engines emit substantial amounts of particulate matter during the combustion process, which may significantly contribute to air pollution and have detrimental impacts on human health. The DPF system uses filters, such as alumina-coated wire mesh, ceramic fiber and ceramic monoliths in the exhaust system. The honeycomb structure is widely used for exhaust gas filtering, with gases passing through porous wall cells. It is sometimes referred to as a ceramic wall-flow filter. Figure 2.10 illustrates the configuration of the ceramic wall filter. There is an open and plugged end to the alternating rows (cells). Upstream, gases enter via open cells; during filtration, they alter the route flow by entering neighboring cells; downstream, gases exit through open cells. The effectiveness of filtration is based on the porosity (pore size) and density of the filter. Therefore, it is necessary to optimize the size and density of the pores to attain the highest efficiency level.

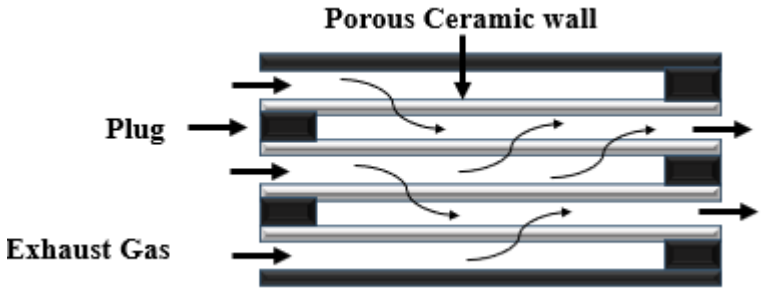

Figure 2.10: Ceramic wall-flow filter for diesel particulate and exhaust gas flow (Xiangjin Kong et al. 2019)

A filter with lower density will not function as expected, while a filter with high density leads to a decrease in the pressure of exhaust gases throughout the filtering process. Achieving efficiency close to 98% is within reach. Porous cordierite ceramic ($2MgO_2.Al_2O_3.5SiO_2$) is frequently chosen for DPF (Diesel

Particulate Filter) applications due to its chemical inertness, low coefficient of thermal expansion, and high melting temperature (1400 ºC).

2.13.7 Regeneration of diesel particulate filter

This approach is relatively easy for filtering and collecting particulate matter in the trap. Although several techniques are available for filtering exhaust emissions, the issue pertains to a significant decrease in pressure during the filtering process caused by the accumulation of soot particles, which negatively impacts fuel efficiency. Based on design considerations and study, a soot loading of 10 g/l of filter capacity leads to a 3-4 times increase in pressure drop, resulting in a backpressure increment of 350 mm of water. A vehicle speed of 65 Km/h causes a 1% decrease in fuel efficiency. Therefore, the DPF renewal became imperative. The purpose of the regeneration procedure is to restore the filter to its initial clean condition after the filtration process. During regeneration, the accumulated soot in the filter is oxidized into carbon dioxide without causing damage to the filter. This occurs primarily via the processes of cracking and melting at elevated temperatures. The regeneration process may be carried out using two methods: the active system and the passive system. An extra heat source engine is used in an active system to enhance the exhaust gas temperature. Hence facilitating the oxidation of soot during the beginning process. The temperature is raised by adjusting the engine's throttle and using an electric heater or burner before the filter. In the passive regeneration system, a catalyst is integrated to reduce the combustion temperature of soot particles, aligning it with the average temperature of the exhaust gas. This catalyst is introduced into the fuel either as an additive or by applying a layer onto the surface of the filter substrate.

2.14 Need of HCCI/PCCI engine

In the current scenario, electric vehicles are becoming increasingly popular. However, diesel engines remain prevalent for mass transportation, public transport, maritime vessels, small-scale power, and distant energy generation. This might be ascribed to its major benefits, such as increased torque, increased

fuel economy, improved performance, cost-effective diesel, and lower carbon emissions. Nevertheless, modern diesel engines have difficulties in controlling the emission of NO_x and PM pollutants because of heterogeneous air-fuel (A-F) mixture combustion. The heterogeneous charge formation in diesel engines is primarily caused by the short period of air-fuel mixing and the inadequate fuel injection characteristics. HCCI technology is a viable solution for addressing issues related to producing heterogeneous charges, which leads to NO_x and PM formation. This technology aims to enhance fuel economy, improve engine performance, and reduce emissions. In several countries, strict regulations on diesel emissions are becoming the primary concern for Original Engine Manufacturers (OEMs), leading them to prioritise the development of technology to reduce emissions.

The objective was to decrease NO_x emissions from 3.6 g/kWh under Euro-IV standards to 0.5 g/kWh under Euro-VI standards. India has announced its intention to transition from Bharat Stage IV (BS-IV) to BS-VI, necessitating a decrease of around 76% in nitrogen oxide (NO_x) emissions to meet BS-VI standards. Researchers are presently focused on cylinder combustion methods to reduce future emissions, such as low combustion temperature, homogeneous charge combustion, and EGR. Because of the low equivalence ratio, HCCI engines achieve combustion at low temperatures, resulting in lower NO_x emissions and soot formation. Soot is mostly produced during the first stages of combustion in the fuel-rich portion of the heterogeneous mixture. However, with HCCI technology, where the mixture is uniform throughout, soot formation is nonexistent. HCCI technology has various advantages, but it also confronts significant hurdles, including regulated auto-ignition, rapid pressure increases during combustion, cold starting, and higher carbon-based emissions. Therefore, an effort has been made to examine the barriers to HCCI technology and viable remedies.

2.15 Summary of literature

The following conclusion is drawn based on the extensive study of the pyrolysis process and its application in the CI engine.

Pyrolysis can transform municipal mixed plastic waste into plasto oil, solid char, and gases. However, the resulting products possess considerable calorific value and are often utilized by recycling and energy industries. The quality of the liquid fuel is greatly influenced by the catalyst employed. Therefore, a bimetallic catalyst, such as Ni, Fe, or a Fe-Ni combination, may be utilized as a supported catalyst to enhance the yielding and quality of PO.

Variables including plastic-type, contamination levels, reactor design, pyrolysis conditions, and residence time can also impact the output of liquid hydrocarbons. These factors may influence the catalytic pyrolysis mechanism, as well as the yield and distribution of products. It is crucial to accurately identify and manage these influences to ensure the sustainability of the process.

Pyrolyzed plastic oil can be used as a substitute fuel in a diesel engine without alternation because plastic oil and diesel have approximately the same physicochemical characteristics.

Various researchers have studied plastic oil application in CI engine and concluded that, for the combustion phenomenon, PO has a more extended ignition delay period and a higher heat release rate than conventional diesel. However, blending PO with diesel fuel reduces BTE.

Plasto oil also has a more significant impact on environmental pollution. Application of plastic oil in CI engine produced higher emissions than conventional diesel. This may cause aromatic compounds in plasto oil, which leads to the incomplete combustion of the plasto oil.

Overall, utilizing a low-cost catalyst in pyrolysis, known as catalytic pyrolysis, could be recommended to enhance the liquid yield. Distillation techniques was employed to eliminate contaminants and enhance the quality of PO. The

purification process improves the physiochemical properties of PO, including viscosity, density, and calorific value. Additionally, there has been no study conducted on the vaporization of plastic oil in PCCI engine mode with EGR, which could potentially lead to better emission behavior of PCCI engines while maintaining comparable engine efficiency.

CHAPTER 3: MATERIALS AND METHODS

This chapter entails the systematic approach used to conduct experiments as part of the study and a description of the equipment used. The outline contains feedstock preparation and characterization, pyrolysis conversion processes setup, and product characterization.

3.1 Feedstock preparation

In the study, MMPW was collected from the Shishambara waste management plant, Dehradun, which was used as feedstock. A pictorial view of the municipal solid waste (MSW) dumping yard is shown in Figure 3.1. The MMPW was collected manually from the MSW. It has been found that MMPW contains various types of plastic waste produced from household, industrial, and agricultural sources. It was mainly composed of LDPE (30-40 wt.%), HDPE (12 - 18 wt.%), PP (15-20 wt.%), PET (2 wt.%) and PS (10-12 wt.%) and PVC (2-4 wt.%).

Figure 3.1: Municipal mixed plastic waste collection (Shishambara waste management plant, Dehradun)

In the study, PVC and other plastic waste were sorted due to the adverse effect on the plasto oil yield products, which produced hazardous chlorine as a processed product of HCl (Chintala et al., 2018). This MMPW contains chips/biscuit packets, plastic carry bags, polyester film, detergent containers, disposable packaging, medical devices, laboratory equipment, baby feeding bottles, shopping bags, plastic trays, plastic bottles, etc. These wastes were collected, cleaned, dried, and shredded into tiny pieces (2-3 mm) and stored for pyrolysis /thermal degradation.

3.2 Characterization of the MMPW

3.2.1 Proximate analysis

Proximate analysis determined the % value of the volatility, ash, moisture content, and fixed carbon available in the feedstock (MMPW). The analysis explains the amount of ash (DIN51719), volatile matter (DIN51720), moisture (DIN51718), and fixed carbon (ASTM E775-78) present in the MMPW. The thorough process used to identify each of these compositions is described here. A desiccator, an aluminium or silica crucible, an oven with reasonable temperature control (±2 °C), a muffle furnace with substantial temperature control, and an analytical balance with good sensitivity (±0.5 mg) are the essential apparatus for proximate analysis.

Moisture Content: 1 gm of the MMPW sample was kept in the pre-weighed crucible and passed to the drying oven at 107 ^{o}C for one hour; the weight was measured after cooling in the desiccator. The moisture content was calculated by using Equation 3.1 (Mitchual et al., 2014).

$$Moisture\ Content = \frac{w_i - w_d}{w_i} \times 100 \qquad \text{Eqn. (3.1)}$$

Where,

w_i, is the initial MMPW weight.

w_d, is the MMPW weight after subjecting to 107 ^{o}C.

Volatile Matter: The dried MMPW was weighed and introduced into the pre-weighed crucible, covered by a lid, and kept in the muffle furnace at 700 ^{o}C for 10 minutes. The weight difference and the volatile matter were measured by using Equation 3.2. (Mitchual et al., 2014).

$$Volatile\ matter = \frac{w_d - w_v}{w_d} \times 100 \quad \text{Eqn. (3.2)}$$

Where,

$W_{d,}$ is the weight of dried MMPW.

W_v, is the weight of the MMPW after subjecting to 700 ^{o}C

Ash content: The MMPW is heated to 950 ^{o}C and allowed to burn completely to a constant weight. The residual ash's weight represents the sample's ash content, which can be calculated using Equation 3.3 (Mitchual et al., 2014).

$$Ash\ content = \frac{w_a}{w_v} \times 100 \quad \text{Eqn. (3.3)}$$

Where,

$Wa_{,}$ is the weight of ashes.

W_v, is the weight of the MMPW after subjecting to 700 ^{o}C

Fixed carbon: fixed carbon in the MMPW was determined by the difference of 100% and the total addition of the volatile matter, ash and moisture available in the MMPW by Equation 3.4 (Mitchual et al., 2014).

$$Fixed\ carbon = 100\% - (Moisture\ + Volatile\ matter + Ash) \quad \text{Eqn. (3.4)}$$

3.2.2 Elemental analysis / CHNS-O analysis

CHNS-O analysis determines the amounts of C, H, N, S, and O present in MMPW. The CHNS-O analysis was performed using a CHNS-O analyzer (Flash 2000 series, Thermo scientific) on ASTM D5373 as shown in Figure 3.2. This method places 1 gm of the sample in the combustion capsule designed for high-temperature combustion. The combustion capsule is placed in the combustion

chamber of the CHNS-O analyzer, where the sample has been heated up to 1000 ^{o}C temperature in the presence of excess O_2. During the combustion process, the sample completely oxidizes, producing combustion gases comprising water vapour (H_2O), CO_2, sulfur dioxide (SO_2), NO_x, and other volatile compounds. Following this, the combustion gases pass through a series of scrubbers or traps to eliminate moisture, acidic gases, and other contaminants, leaving the desired combustion gases (CO_2, N_2, SO_2 and others). The filtered combustion gases are routed via the CHNSO analyzer's detecting system. Each element in the combustion gases is identified and measured using specialized detection technology, such as thermal conductivity detection (TCD), flame ionization detection (FID), or infrared (IR). Calibration curves or standards with known amounts of each element determine the quantity of C, H, N and S. However, oxygen was obtained by Equation 3.4. The HHV of the PO was calculated using Dulong's formula, as given by Equation 3.5.

$$Oxygen\ (\%) = 100\% - (\ C\ \% + H\ \% + N\ \% + S\ \%) \qquad \text{Eqn. (3.4)}$$

$$HHV\ \left(\frac{MJ}{kg}\right) = 0.338C\ + 1.428(H - \frac{O}{8})\ +\ 0.95S \qquad \text{Eqn. (3.5)}$$

Figure 3.2: CHNS-O analyser

3.2.3 Thermogravimetric analyser

Thermogravimetric analysis (TGA) was conducted at IIT Roorkee, using SII 6300 EXSTAR TG/DTA 6300 on ASTM E1131. A pictorial view of the TGA analyser is depicted in Figure 3.3. A thermal analyzer has been used to measure the optimum temperature for thermal degradation. The mass loss of the sample is determined function as a of temperature. A weight of 10 mg of MMPW was placed in a platinum crucible and started to heat the MMPW from atmospheric temperature to 1000 ^{o}C at a 10 ^{o}C/min heating rate in the presence of nitrogen flow with 200 ml/min. The MMPW mass loss curve of TGA was recorded with temperature, which may cause semi-volatile compounds, polymer degradation, ash content, moisture, and carbon black present in the MMPW.

Figure 3.3: TGA analysis instrument (IITR)

3.3 Catalyst preparation

The study used two different catalysts, fuller earth (FE) was supplied by Ecoscience Lab (I) Pvt. Ltd. Mumbai, India, and commercial FCC catalyst was provided by Corporate R&D center of Bharat Petroleum Corporation Ltd. Noida, India. The catalyst was chosen based on its ease of availability and lower price than others. The catalysts received were calcined at 500 ^{o}C for 3 hours without oxygen to remove the volatile substances.

3.4 Characterization of catalyst

3.4.1 X-Ray Fluorescence

X-ray fluorescence (XRF) is a nondestructive analytical technique used to determine a catalyst's inorganic mineral composition. XRF was carried out using the XRF- Siemens SRS – 3000 instruments, which worked on the ASTM E1621 method. Figure 3.4 depicts a pictorial view of the XRF analyzer. This instrument based on the principle of exciting the core electron within an element, followed by the emission of characteristic signals. The instrument consists of Rh anode as an X-ray tube, and an energy dispersive detector was used for the XRF analysis to identify and quantitatively estimate the inorganic minerals present in the catalyst.

In this method, the catalyst was ground as much as possible to make fine powder using mortar to ensure uniformity and dried in an oven at 105 ^{o}C temperature. Before introducing the catalyst sample, XRF warmed up and calibrated using the reference materials to determine the elemental composition and ensure the instrument's accuracy. Place the catalyst sample into the sample tray and set the parameters such as excitation energy, measurement time, X-ray tube voltage, and current to optimize the excitation of elements in the catalyst. A 100 μm thick titanium metallic filter was connected to the Rh X-ray tube. Aluminium collimators with 6 and 3 mm inner diameters were mounted to the X-ray tube and detector, respectively. The X-ray tube and detector were positioned at 45 degrees. The detector and sample holder were positioned on a Z-stage to regulate the distance between the detector and the sample surface. The x-ray tube was set to 40 kV, 0.3 mA, and a measurement duration of 500s.

Figure 3.4: XRF analysis instrument (WIHG, Dehradun)

3.4.2 X-ray diffraction analysis

In X-ray diffraction (XRD), the crystallinity and phase composition of the catalyst were identified using the D8 ADVANCE ECO - Bruker instrument following ASTM E2860 standards. The pictorial view of the instruments is depicted in Figure 3.5. An XRD with a filter of 1D Cu K radiation (wavelength 1.5404) was used to produce XRD patterns. In the process, 1 gm of the catalyst sample was ground into fine powder for the homogenous sample and spread thinly and evenly onto the sample holder. Before analysis, the XRD instrument turned on the sample, and warm-up was allowed. Align the X-ray source, sample holder, and detector following the instrument's alignment standards for optimum diffraction signal capture. D/teX Ultra 250, an X-ray diffractometer, is used as the detector. The instrument had an operating voltage of 40 kV and a current of 50 mA X-ray diffraction was performed using Bragg's angle scan axis from 5° to 80° at a 2°/min scan speed. Now begin the data collection procedure, during which the X-ray beam is focused on the sample and diffraction patterns are recorded by the detector. When the sample is rotated, the detector is moved to scan the range of diffraction angles. Process the raw diffraction data to produce a usable diffraction

pattern. This may include background removal, smoothing, and adjustment for instrumental variables like absorption and scattering.

Figure 3.5: XRD instrument

3.4.3 Scanning electron microscope analysis

The pictorial view of Scanning electron microscope (SEM) instrument, as shown in Figure 3.6, generates highly magnified images by using electrons rather than light to create an image. The instrument model Carl Zeiss EVO 18 on ASTM E1508 is used for morphology and elemental mapping of the catalyst. The catalyst sample is mounted onto the stub by using conductive adhesive. The sample was coated with a thin layer of conductive material using a sputter coater to prevent a charging effect during imaging. An electron gun generates an electron beam at the top of the microscopy. The electron beam moves vertically through the microscope, which is in a vacuum. The beam passes via electromagnetic fields and lenses, concentrating on the sample. When the beam strikes the sample, electrons and X-rays are expelled. Detectors collect X-rays, backscattered electrons, and secondary electrons and transform them into a signal shown on a screen like a television screen.

Figure 3.6: SEM analysis instrument (UIT, Dehradunn)

3.4.4 Temperature-programmed desorption of ammonia

The temperature-programmed desorption of ammonia (NH_3-TPD) was measured by a FineSorb-3010 from Material Analysis & Research Centre, Bengaluru, employed with a thermal conductivity detector (TCD) to analyse the surface acidity of the catalyst. The pictorial view of the TPD is shown in Figure 3.7. Before characterization, the catalysts were pretreated at 120 °C in He for 2 h and then cooled to 80 °C. First, the ammonia was adsorbed on the catalysts for 40 min, and then the catalysts were swept with argon. The reactor was heated from 80 °C to 700 °C at a heating rate of 10 °C/min with constant flow of NH_3. NH_3 molecules will interact with acidic sites on the catalyst surface as the temperature increases and lead to their desorption. Mass spectroscopy or thermal conductivity detector observed the desorbed ammonia molecule. The desorption profile (signal intensity vs. temperature) offers insights into the nature and strength of the acidic sites on the catalyst surface.

Figure 3.7: Temperature-programmed desorption of ammonia instrument

(MARC Banglore)

3.4.5 Brunauer-Emmett-Teller (BET)

The BET technique derives the sample surface area by measuring the physisorption of the gas. The study BET model Quantachrome Instruments v11.05 on ASTM D3037-93 as shown in Figure 3.8 has been used to analyse the catalyst's surface area and pore size. The sample is made in finely powdered form and free of large aggregates. Ensure the sample has been thoroughly degassed to eliminate any adsorbed gases or moisture that may interfere with the analysis. This is commonly accomplished by heating the sample under vacuum at a high temperature for several hours. Now, place the sample into the sample chamber of the BET instrument. The surface area is measured at a steady temperature. The temperature required depends on the inert gas used. Small gas molecules are drawn to the solid sample's surface, opening a porous structure and producing an adsorbed gas monolayer. After forming the gaseous monolayer, the sample is heated in a non-nitrogen environment. This enables the release of adsorbed nitrogen gas molecules from the sample's surface. The liberated gas molecules measured the surface area and porosity of the sample.

Figure 3.8: BET instrument (MARC Banglore)

3.5 Experimental setup for pyrolysis

The pyrolysis setup includes a reactor, heater, condenser and an oil collection tank. The reactor consists of a cast iron cylinder surrounded by a heating coil consisting of nichrome wire, which has a 5 kW heating capacity and 240 V single-phase power supply. The reactor has a capacity of 4 kg of feedstock. A digital temperature indicator with a PID controller is attached to the reactor. The programable PID controller maintains the temperature in the reactor provided by the heating coil. The diagram of the digital pyrolysis reactor is depicted in Figure 3.9. However, heat loss is prevented by placing cotton and ceramics between the reactor and the heating coil. The stainless steel condensers are attached to the reactor. As the temperature reaches beyond the desired temperature, the power supply cuts off automatically. The reactor and condenser outlets are linked via a high-temperature-resistant stainless-steel tube. Condensers connected to the chiller to maintain the desired water temperature in the water jacket and attached to the oil collection tank for condensed plasto oil collection. The outlet of the condenser is connected to the balloon to collect the non-condensable gases for further use.

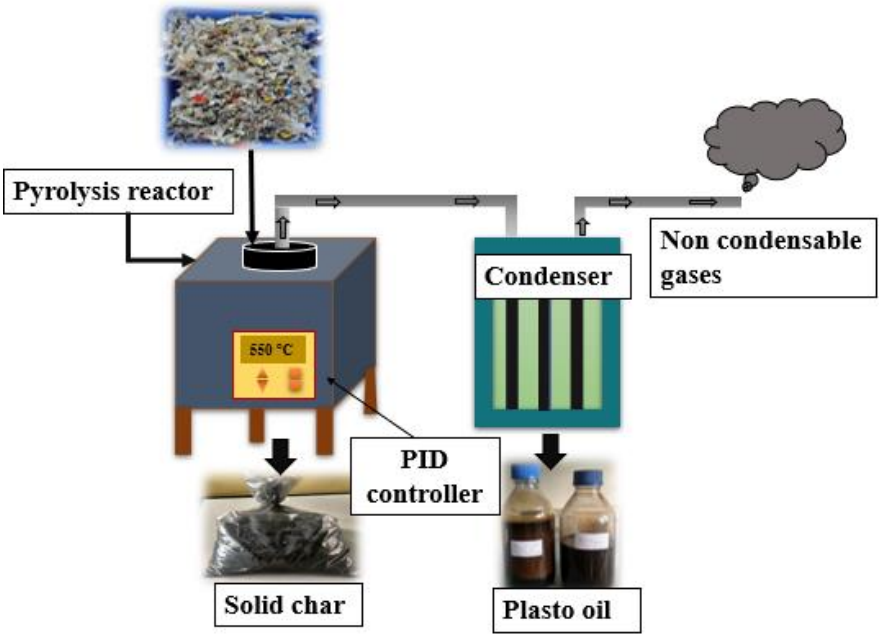

Figure 3.9: Schematic diagram of pyrolysis setup

3.6 Pyrolysis process

A fixed batch pyrolysis reactor established at the Centre for Alternative and Renewable Energy, UPES Dehradun, conducts the pyrolysis process in non-isothermal conditions. Before pyrolysis, the MMPW underwent pretreatment steps, including collection, segregation, drying, and shredding, before being introduced into the pyrolysis reactor. A sample weight of 1kg was introduced to the reactor for each experiment. Before commencing the pyrolysis experiments, the reactor is purged with inert N_2 gas at a flow rate of 500 mL/min and then sealed properly. The whole pyrolysis process is depicted in Figure 3.10.

The experiments were conducted at various temperatures, such as 400 ^oC, 450 ^oC, 500 ^oC, 550 ^oC and 600 ^oC, with a heating rate of 10 ^oC/min and held for 3 hours at required temperature to ensure the completion of the process. The vapor produced in the reactor passes through the condenser and condenses at 6 ^oC temperature. However, non-condensable gases vented from the condenser outlet

and collected into the balloons. After completion of the pyrolysis process, leftover char was collected from the bottom of the reactor and PO was collected and stored in a measuring flask.

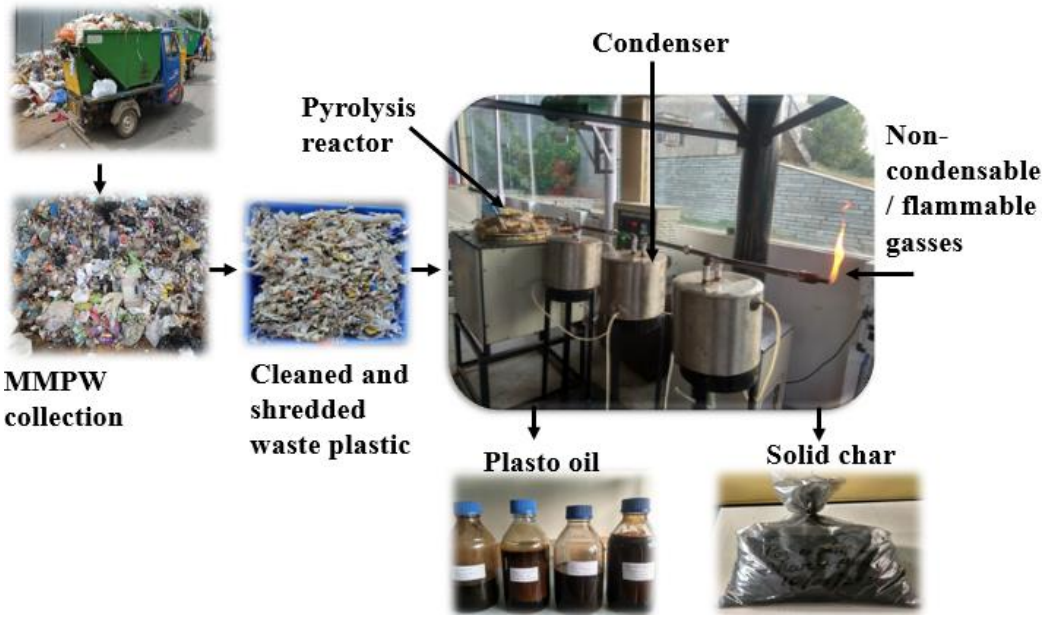

Figure 3.10: Conventional pyrolysis process of the MMPW

3.7 Catalytic Pyrolysis process

The pyrolysis reaction conducted with catalyst is referred to as the catalytic pyrolysis process. The study used two catalysts, fuller earth and commercial FCC catalyst, to achieve optimum liquid yield. The schematic diagram of the catalytic pyrolysis process is illustrated in Figure 3.11. Different proportions of the fuller earth and commercial FCC catalyst (2 wt.%, 4 wt.%, 6 wt.%, 8 wt.% and 10 wt.%) have been used independently in the catalytic thermal degradation process as given in Table 3.1. Hence, a comparative study of both catalysts has been conducted to identify the optimum plasto oil yielding the catalytic pyrolysis process.

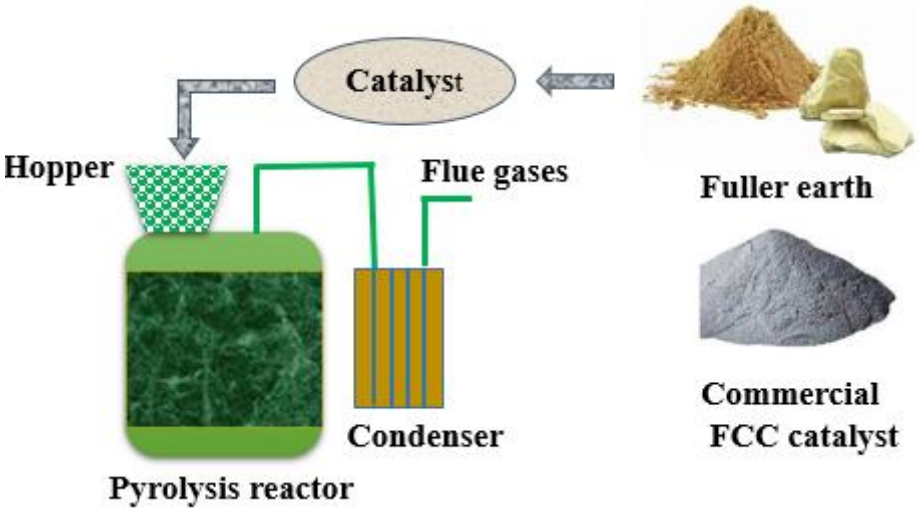

Figure 3.11: Schematic diagram of the catalytic pyrolysis process

Table 3.1: Experimental matrix catalytic thermal degradation process

	Fuller earth	**Commercial FCC catalyst**
Conventional pyrolysis process	0 %	0 %
Catalytic thermal degradation	2 %	2 %
	4 %	4 %
	6 %	6 %
	8 %	8 %
	10 %	10 %

3.8 Fractional distillation of plasto oil

The distillation assembly consists of a heating mantle, two neck round bottom flasks, a thermocouple, a condenser and a collecting vessel, as depicted in Figure 3.12. Distillation is when heavy hydrocarbons available in crude oil transform into lighter hydrocarbons based on their boiling points. PO is poured into the round bottom flask and put on the heating mantle. The heating mantle provides heat to the crude plastic oil, which increases the temperature to evaporate the PO. The vapors in the flask pass through the condenser and are condensed into liquid

form, which is collected into the collecting vessel. Initially, the distillation process was carried out up to 20 ^{o}C to 180 ^{o}C and the process was held for 40 minutes at 180 ^{o}C to obtain the distillated plasto oil of the gasoline range, i.e, plasto oil light (POL). Thereafter, the temperature was increased from 180 to 340 ^{o}C, the process at 340 ^{o}C for 40 minutes, and the distillated plasto oil of diesel range, i.e. called the plasto oil heavy (POH). In the process, it has been observed that the initial boiling point (IBP) of the PO was 90 ^{o}C, and the final boiling point (FBP) was 340 ^{o}C.

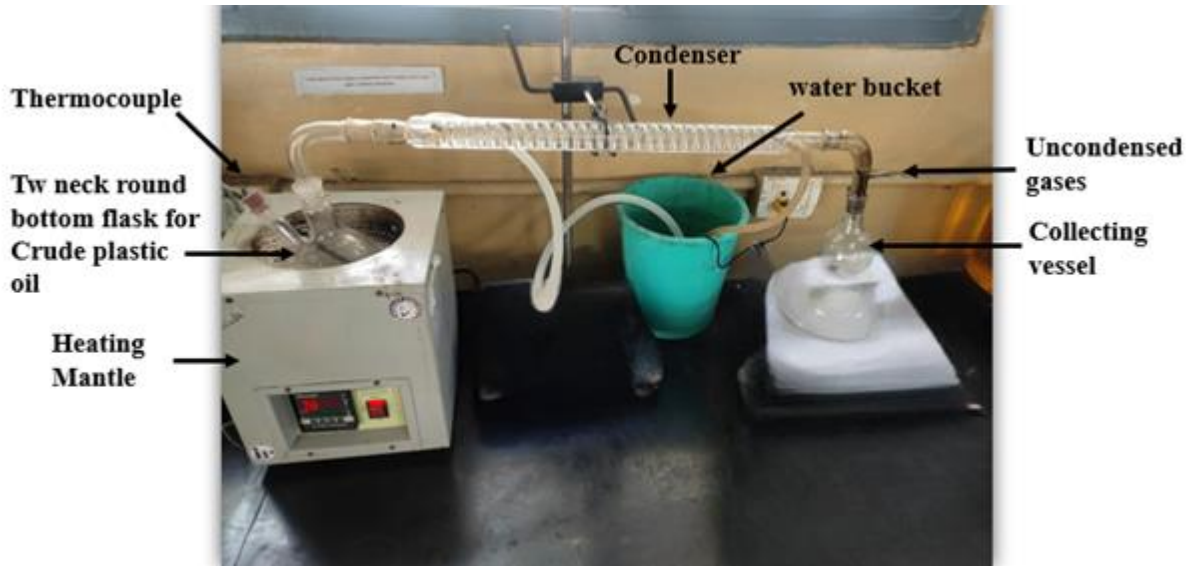

Figure 3.12: Distillation of the plasto oil

3.9 Characterization of the Plasto oil

3.9.1 Physicochemical characteristics

Physicochemical characteristics of crude plastic oil and distillate plastic oil, such as density, viscosity, gross calorific value, flash point, fire point, cloud point, pour point, distillation boiling range and cetane index, determined by the ASTM methods given in Table 3.2.

Table 3.2: Standard methods for physicochemical characteristics

Physicochemical characterization	Methods
Density (kg/m^3)	ASTM D 4052
Viscosity (cSt)	ASTM D 445
Gross heat of combustion (MJ/kg)	ASTM D240
Cloud point (°C)	ASTM D97
Pour point (°C)	ASTM D97
Flash point (°C)	ASTM D93
Fire point (°C)	ASTM D93

3.9.2 Chemical characteristics

3.9.2.1 Fourier transform infrared spectroscopy (FTIR)

The functional group in the pyrolysis oil was analyzed using the FTIR spectroscopy carried out by the model Frontier FT-IR/FIR, Perkin Elmer, as depicted in Figure 3.13 worked on ASTM E168. Both solid (catalyst) and liquid (plasto oil) samples can be analyzed using FTIR spectroscopy. A pallet is prepared for solid samples by pressing with potassium bromide (KBr). However, a small droplet should be placed over the KBr pallet for the liquid sample. Place the prepared sample in the sample container or cell and insert it into the sample compartment of the FTIR instrument. Select the appropriate measurement parameters, such as wavelength range, resolution, and number of scans based on the sample type and expected spectral features. Since KBr is transparent to infrared light at wavelengths between 4000 and 4000 cm^{-1}, it makes an excellent window material. Perform baseline correction, normalization, and other preprocessing processes to improve spectral characteristics and eliminate artefacts. Identify distinct peaks in the spectrum that correspond to functional groups, chemical bonds, or molecular vibrations in the material. Compare the experimental spectrum with reference spectra or databases to help with chemical identification and structural analysis.

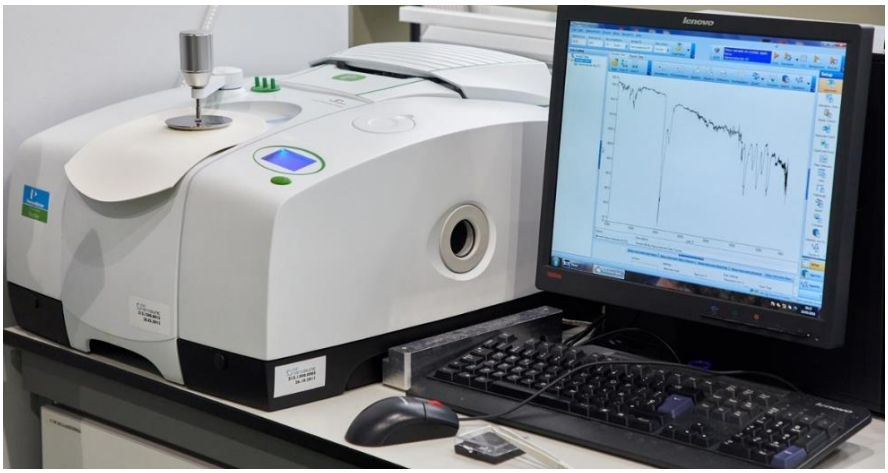

Figure 3.13: FTIR analysis instrument

3.9.2.2 Gas Chromatography and Mass spectroscopy

The Perkin Elmer's Auto system GC-MS analyzer, as shown in Figure 3.14 worked on ASTM D5769 and was used to conduct the GC-MS analysis on plasto oil samples. A steady flow of helium gas (1.51 mL/min) used as a carrier gas. The PO sample was dissolved into a dichloromethane solvent before being injected into the inlet port. The 10 µL PO was injected by splitting method and kept the injected temperature up to 300 ^{o}C to ensure complete vaporization. Set the ionization energy to 70 eV, which is standard for electron ionization. Gaseous components are separated as they pass through the column by winding it within a customised oven with temperature settings ranging from 20 ^{o}C to 320 ^{o}C. A substance that will separate the different chemical components in the sample according to size and polarity is applied to the column surface. Smaller and more volatile sample components will pass through the column more rapidly than others. The separated components go out of the column immediately and enter the MS, which goes through three internal phases as follows -

Ionization source: Components are blasted with electrons, causing them to break up and turn into positively charged ions.

Filter: The ions pass through an electromagnetic field and are selectively filtered according to their mass. Analysts specify a predefined range of masses permitted to pass through when masses leave the ionisation source.

Detector: A computer receives the data, counts the number of filtered ions, and creates a mass spectrum distribution of ions of various sizes.

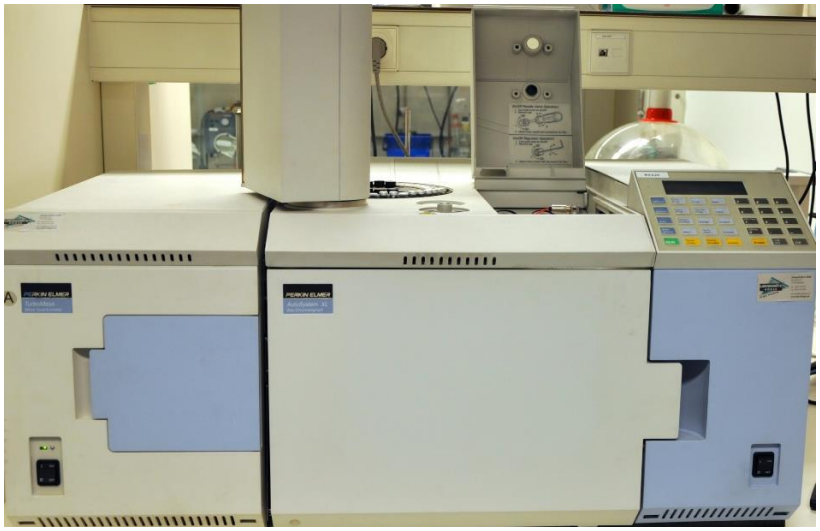

Figure 3.14: GC-MS instrument

CHAPTER 4: RESULT AND DISCUSSION OF SAMPLES

This chapter gives insights into MMPW characterization, such as proximate analysis, elemental analysis, heating value, and TGA Analysis. MMPW characterization is crucial to predict the efficiency of the pyrolysis process and composition of end products, which are summarized in the chapter. However, the catalyst affects the yield of the end products and makes the pyrolysis process more economical by reducing the residence time and increasing the reaction rate. Therefore, Catalyst characteristics such as proximate analysis, elemental analysis, XRF, FTIR, XRD, SEM EDX, BET, and TPD- NH_3 were conducted to find the catalyst's potential in pyrolysis. Moreover, the yield of the pyrolysis plasto oil with and without catalyst and their characteristics, and the effect of the fractional distillation process on physicochemical characteristics are summarized significantly.

4.1 Analysis of the MMPW

4.1.1 Proximate and elemental analysis of MMPW

From Table 4.1. the experimental GCV of MMPW was found to be in good agreement with its theoretical GCV. The results of proximate and ultimate analysis of the MMPW were found to deviate subtly from the reported values, particularly higher in ash content, despite being sourced from the same site earlier from the same site earlier (Pal et al., 2023). Praveen Godkhe et al. carried out the proximate and elemental analysis on municipal mixed plastic waste and reported 93.45 wt.%, 5.34 wt.%, 1.21 wt.% volatile matter, fixed carbon and ash content. However, C, H, N, S and O were 83.23%, 12.45%, 2.71%, 0.41% and 1.21% respectively (P. K. Ghodke, 2021).

Table 4.1: Analysis of MMPW

Properties	**Municipal Mixed Plastic Waste (MMPW)**
Moisture (wt.%)	1.6
Volatile matter (wt%)	91.37
Ash (wt%)	5.57
Fixed carbon (wt%)	1.46
Carbon (wt%) (dry, ash free basis)	81.63
Hydrogen (wt%) (dry, ash free basis)	12.15
Nitrogen (wt%) (dry, ash free basis)	2.69
Sulfur (wt%) (dry, ash free basis)	1.05
Oxygen (wt%) (dry, ash free basis)	2.48
Higher Heating value (MJ/kg)	45.48
Theoretical Higher Heating Value (MJ/kg)	44.55

4.1.2 Thermogravimetric analysis of MMPW

The Thermo gravimetric analysis (TGA) curve of MMPW (Figure 4.1) has shown that wt.% of MMPW left at 99.7 and 200 ^{o}C were 98.5 and 98.1% of its initial weight respectively. Thus, the weight loss of 1.5 to 1.9 Wt.% may be attributed to its moisture content which is in agreement with the 1.6 Wt.% moisture content of MMPW as determined by ASTM E790 method (Table 4.1). Much of the thermal decomposition of the MMPW occurred between 300 and 500 ^{o}C and the Wt.% left at 1010 ^{o}C was 8.9%, which was comparable to the sum of the ash and fixed carbon content of MMPW of 7.03 Wt.% (Table 4.1). Lopez et al. studied municipal plastic waste, resulting in 500 ^{o}C. Temperature is the optimal temperature for the maximum mass loss Similarly, observations were reported by another study (López et al., 2010; R. K. Singh et al., 2019). Praveen Godkhe and Irma Kremer which possibly suggests that the MMPW used in the study had an identical chemical composition to the MMPW used in the literature (P. K. Ghodke et al., 2021; Irma Kremer, et al., 2021).

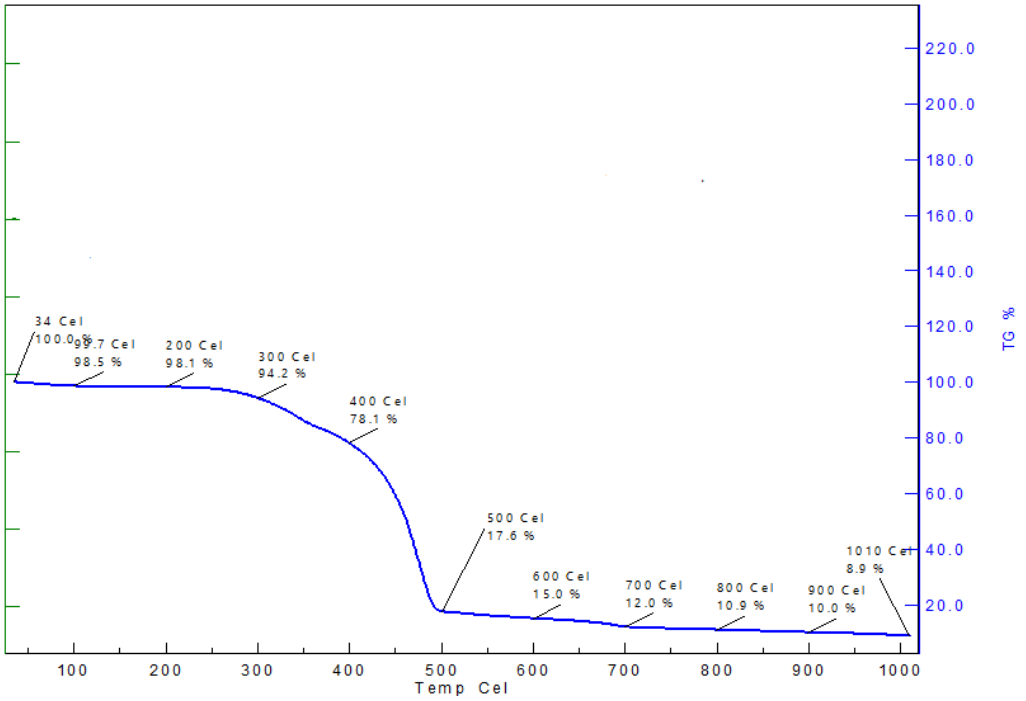

Figure 4.1: Thermogravimetric analysis of the MMPW

4.2 Characterization of catalyst

4.2.1 X-Ray fluorescence

The chemical composition of the catalysts determined by XRF are presented in Table 4.2. The SiO_2 content was less whereas Al_2O_3 , Fe_2O_3 and MgO were higher than the reported values for FE (Subbareddy et al., 2020)

Table 4.2: Chemical composition of the catalysts

Inorganic Materials	Fuller earth	Commercial FCC Catalyst
SiO_2	57.11	40.70
Al_2O_3	15.13	43.76
Fe_2O_3	6.89	0.52
MgO	5.71	0.26
K_2O	2.35	0.20
TiO_2	0.99	0.41
Na_2O	0.75	0.20
CaO	0.37	0.09
P_2O_5	0.06	1.00
MnO	0.05	0.02

since the composition of fuller earth varies depending on the source. While the Al_2O_3 content of commercial FCC was comparable, SiO_2 content was less than the reported values (Ribeiro et al., 2013), may be due to the difference in the proportions of zeolite-Y, matrix and binder.

4.2.2 FTIR analysis of the catalyst

The FTIR spectra of the fuller earth and commercial FCC catalysts are depicted in Figure 4.2. Both the catalysts have shown bands over 3400 – 3500 cm^{-1} and around 1650 cm^{-1}, which were attributed to the stretching and bending vibrations of H-O-H respectively while the bands over 1040 – 1095 and 450 – 480 cm^{-1} were due to the asymmetric stretching and bending vibrations of Si–O respectively (Chen et al., 2019; Subbareddy et al., 2020). The band observed over 830 – 880 cm^{-1} for both the catalysts was due to Al-OH deformation while the band at 2977 cm^{-1} shown by fuller earth may be due to the C-H symmetric stretching, owing to the presence of polyatomic C_n-H-O (Saikia and Parthasarathy et al., 2010).

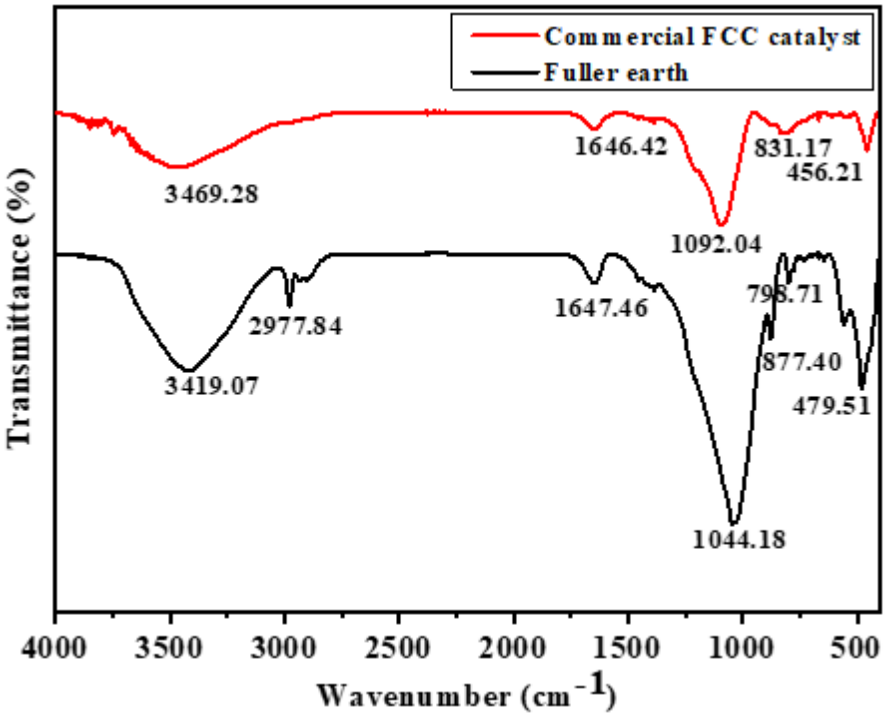

Figure 4.2: FTIR spectra of catalysts

4.2.3 XRD analysis

The x-ray diffraction patterns of fuller's earth and commercial fluidized cracking catalyst (FCC), used as catalysts in the pyrolysis of MMPW are presented in Figure 4.3. The strong peaks observed for fuller's earth at the 2θ positions of 8.6 and 26.9^{o} indicated the presence of palygorskite and quartz respectively as major phases, while weak peaks at 12.5 and 35.2^{o} suggested the presence of kaolinite and montmorillonite as minor phases (Ravikanth et al., 2020).

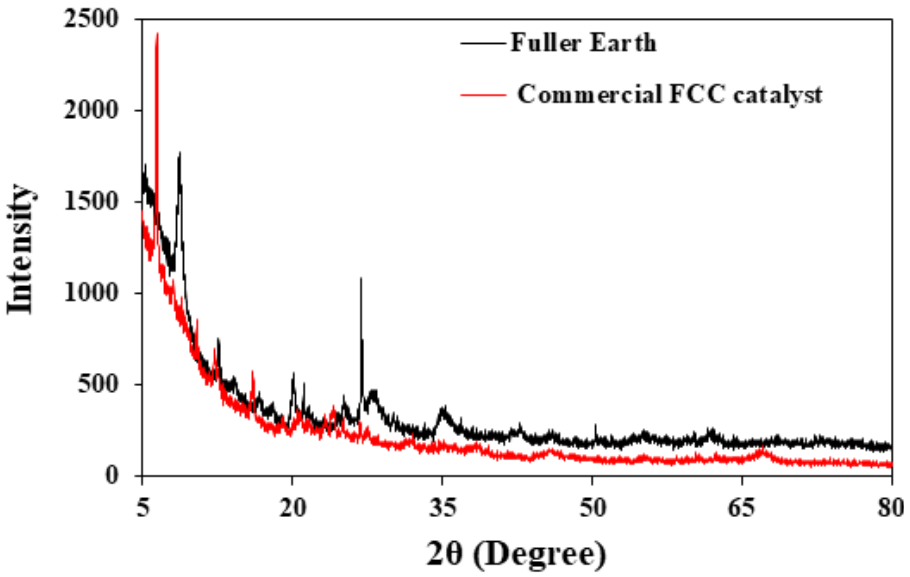

Figure 4.3: XRD pattern of catalyst

The XRD pattern of the commercial FCC catalyst has shown peaks at 2θ positions of 6.4, 10.4, 12.2 and 16.1^{o}, typically of zeolite-Y, the catalytically active phase reportedly present (Salahudeen et al., 2017; Chen et al., 2019).

4.2.4 Scanning electron microscopy

Scanning electron microscopy (SEM) images were used to study the surface morphology or distribution of particles of fuller earth and commercial FCC catalysts at 1k magnifications depicted in Figure 4.4 (a) and (b). SEM image of the fuller earth catalyst (Fig. 4.4a) has shown agglutinated heterogeneous particles, in accordance with the XRD results which confirmed the presence of different phases and is similar to the reported FE SEM images (Atun et al., 2003).

SEM image of the commercial FCC catalyst (Fig. 4.4b) has shown the zeolite-Y crystallites embedded in the matrix (Farshi et al., 2012).

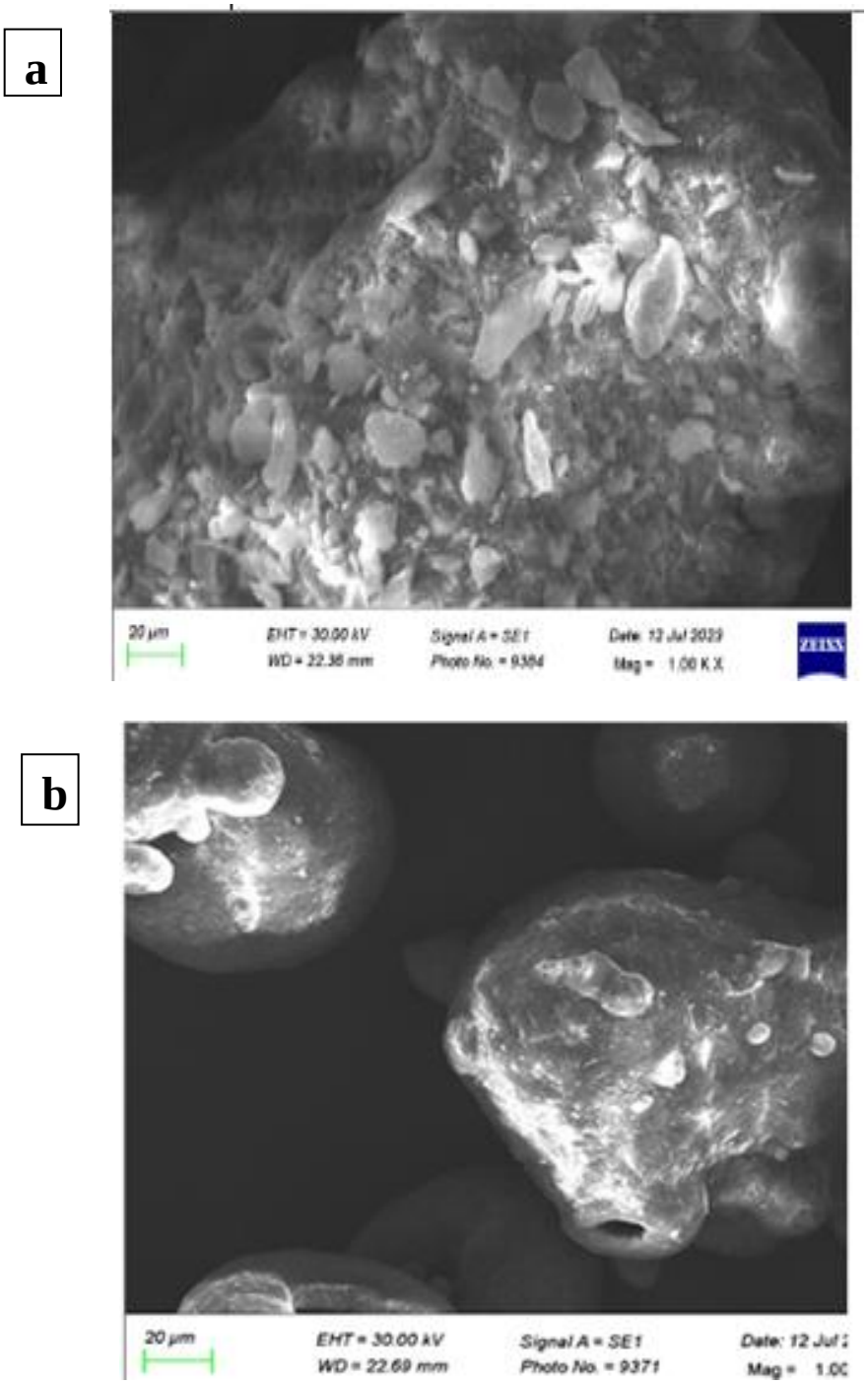

Figure 4.4: SEM image of (a) Fuller earth (b) Commercial FCC

4.2.5 BET and NH_3 -TPD analysis

Nitrogen adsorption-desorption isotherms of the commercial FCC catalyst has shown the combination of IUPAC type II and IV (a) isotherms with the hysteresis loop of type H4 at the relative pressure (p/p_o) of 0.4 onwards (Fig. 4.5a).

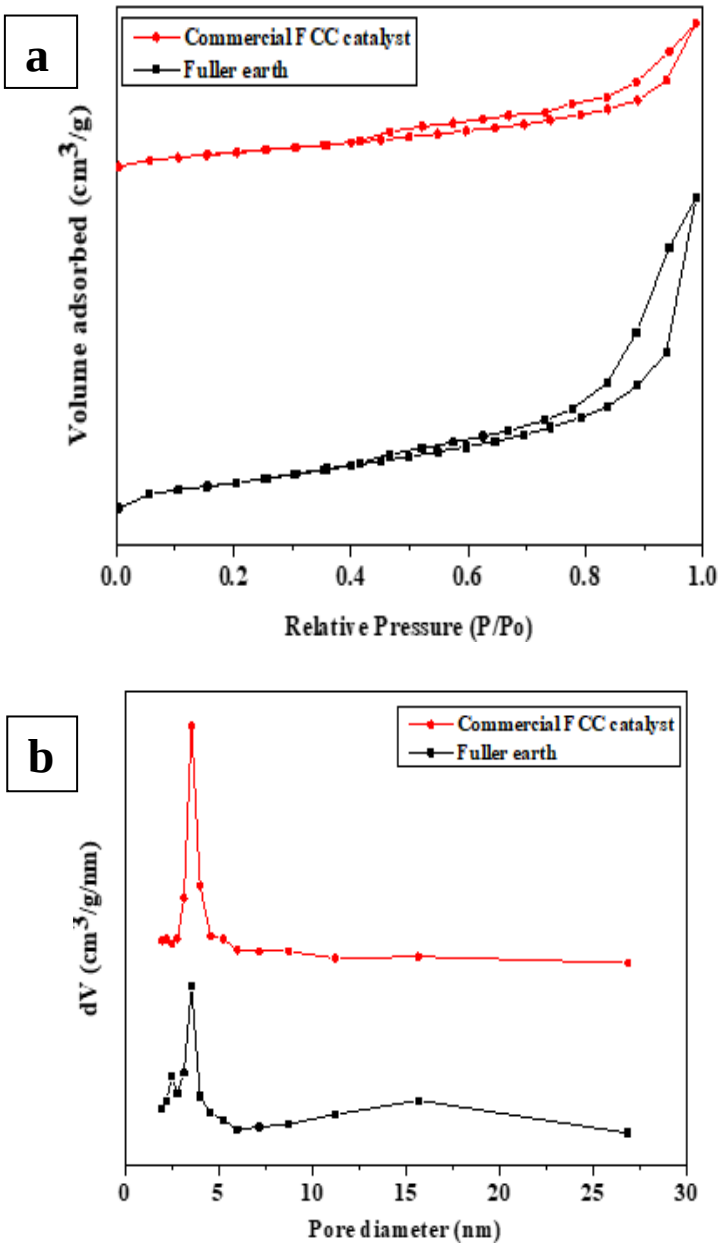

Figure 4.5: (a) Adsorption-desorption isotherm of the catalysts (b) Pore-size distribution of the catalysts

This indicated the presence of both the microporous and mesoporous materials of pores larger than 4 nm (Thommes et al., 2015) which may be of zeolite-Y and matrix respectively, the typical components of FCC catalyst (Zakariyaou et al., 2023), reaffirmed from its pore-size distribution (Fig. 4.5b). Fuller earth has shown the IUPAC type IV(a) adsorption isotherm with type H3 hysteresis loop, typically of clay materials containing mesopores (Thommes et al., 2015). Its pore-size distribution has shown two distinct peaks, unlike commercial FCC catalysts of which one is a sharp peak covering micropores, and smaller mesopores and a broader peak covering larger mesopores of 10 to 25 nm. The physicochemical properties of the catalysts are presented in Table 4.3. Commercial FCC catalyst has higher BET surface area, but lower pore volume compared to fuller earth whereas their average pore diameter is almost the same.

Table 4.3: Physicochemical properties of the catalysts

Catalyst	**BET surface area (m^2/g)**	**Total pore volume (cc/g)**	**Average pore diameter (nm)**	**Acidity (mmol/g)**			
				Weak	Medium	Strong	Total
Fuller earth	94.196	0.290	3.536	0.002	0.015	0.001	0.018
Commercial FCC catalyst	146.039	0.146	3.540	0.004	0.007	0.001	0.014

The NH_3 TPD indicated the presence of three distinct peaks, the first one up to 300^{o}C, second one from 300 to 700^{o}C and third one above 700^{o}C corresponding to weak, medium and strong acidic sites (Fig.4.6). From their values (Table 4.3), the medium acidity of fuller earth was found to be more than double and total acidity was marginally higher than that of the commercial FCC catalyst.

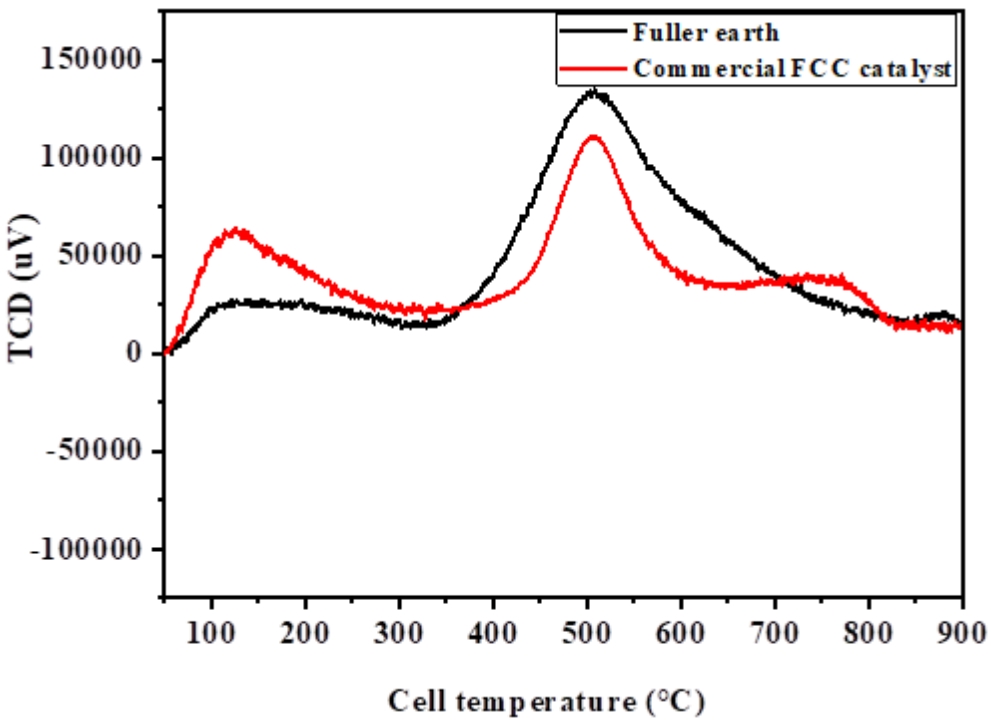

Figure 4.6: NH_3 TPD of catalysts

4.3 Pyrolysis process of the MMPW

In conventional pyrolysis, a digital pyrolysis reactor is used to heat the MMPW in an inert atmosphere. The process was conducted at various temperatures 400, 450, 500, 550, and 600 ^oC at a 10 ^oC/min heating rate for 3 hours. The yield of the pyrolysis products is depicted in Figutre 4.7. The solid, liquid and gaseous products can calculated by Equations 4.1, 4.2 and 4.3, respectively (Parku et al., 2020).

$$Liquid\ (wt.\%) = \frac{weight\ of\ Liquid}{weight\ of\ MMPW} \times\ 100 \qquad \text{Eqn. (4.1)}$$

$$Solid\ (wt.\%)\ = \frac{weight\ of\ solid\ char}{weight\ of\ MMPW} \times 100 \qquad \text{Eqn. (4.2)}$$

$$Gaseous\ (wt.\%) = 100 - (Liquid - Solid) \qquad \text{Eqn. (4.3)}$$

It is elucidated from Figure 4.7, a lower plasto oil yield (42.3 wt.%) was obtained at 400 ^oC temperature while the remaining 26.6 wt.% was gaseous product and

20.1 wt.% was solid char. The lower liquid product may cause insufficient temperature for complete pyrolysis (Islam et al., 1999.). However, on increasing the temperature, the plasto oil yield increased and it has been observed that 550 ^{o}C is the optimal operating temperature to attain the higher yield of PO (53.3 wt%).

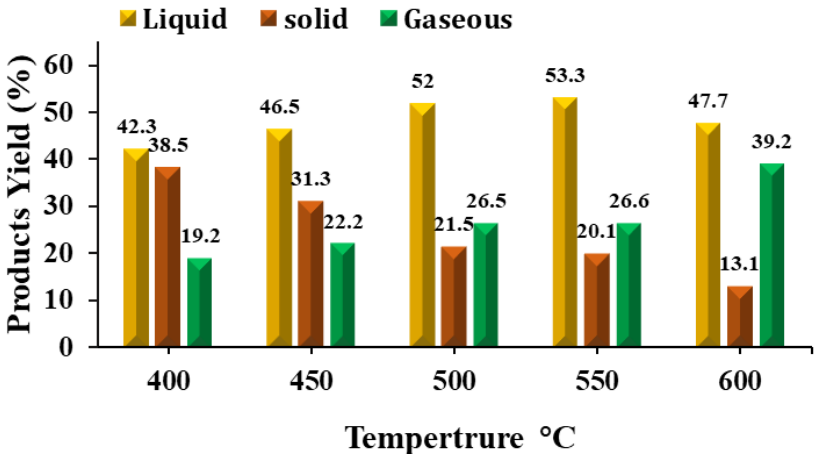

Figure 4.7: Pyrolysis product distribution at different temperatures

Thereafter, the increase in temperature above 550 ^{o}C, plasto oil yield decreased significantly. This may cause a secondary reaction or the heavy molecular weight compound occurrence at higher temperatures, which leads to non-condensable gases (Shadangi et al., 2014).

Hence, it is evident that 550 ^{o}C is the optimized temperature for the pyrolysis of the MMPW. Therefore, a further catalytic reaction was carried out at the same temperature (550 ^{o}C) to obtain the optimum plasto oil yield with less residence time of 3 hours.

4.4 Catalytic pyrolysis process/ Catalytic thermal degradation

In the catalytic thermal degradation process, fuller earth and commercial FCC catalysts in different proportion ranges of 2 wt.%-10 wt.% of the MMPW have been used in the pyrolysis. The process was conducted at 550 ^{o}C with a 10 ^{o}C/min heating rate for 3 hours. In the study, 1 kg of MMPW was introduced to the

reactor. Initially, 25 wt.% of MMPW feeds into the reactor, then a layer of the catalyst with 25 wt.% spread over the MMPW repeatedly, as shown in Figure 4.8.

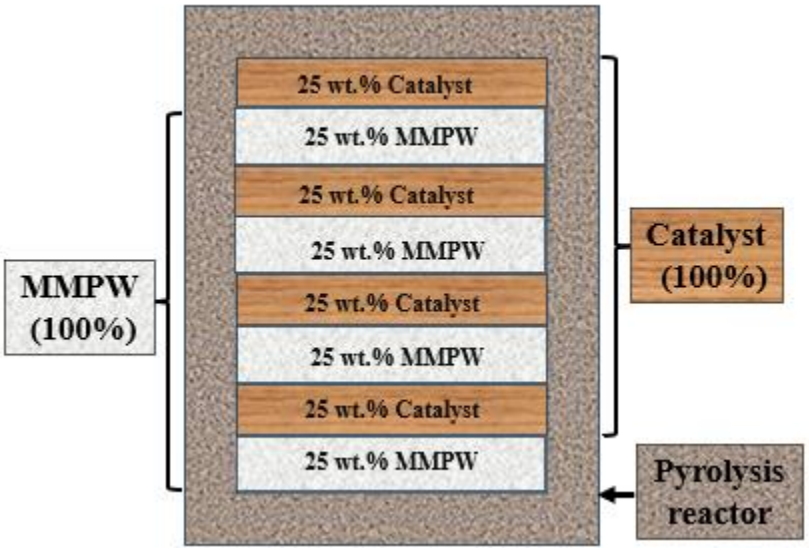

Figure 4.8: Catalyst and MMPW distribution in pyrolysis reactor

The catalytic thermal degradation process of MMPW produced a liquid, solid, and gaseous yield with fuller earth and commercial catalysts are given in Table 4.4.

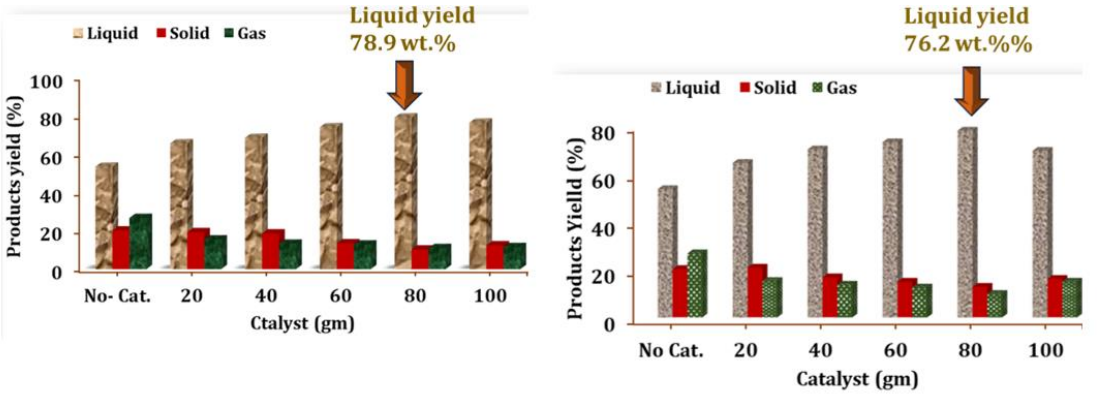

(a) (b)

Figure 4.9: Product yield in catalytic thermal degradation (a) Fuller earth (b) Commercial FCC catalyst

Plasto oil yield increased with the increase in the proportion of fuller earth and commercial FCC catalysts and a decrease in the solid char and gaseous products, as shown in Figure 4.9.

However, it has been found that 8 wt.% (80 gm) fuller earth and Commercial FCC catalyst produced the higher plasto oil yield. Increasing the catalyst proportion reduced the plasto oil yield and increased the gaseous products.

Table 4.4: Product yield distribution with fuller earth and commercial catalyst

Catalyst	**Fuller earth**				**Commercial FCC Catalyst**			
Wt.%	**(%)**				**(%)**			
Catalyst proportion	**Liquid**	**Solid char**	**Gas**	**Catalyst Recovery**	**Liquid**	**Solid char**	**Gas**	**Catalyst recovery**
0	53.3	20.1	26.6	-	53.3	20.1	26.6	-
2	65.4	19.2	15.4	16.8	64.2	20.7	15.1	17.29
4	68.3	18.5	13.2	31.38	69.8	16.65	13.5	36.21
6	73.8	13.4	12.8	51.83	72.8	14.8	12.4	56.96
8	78.9	10.2	10.9	77.35	76.2	12.7	11.1	72.83
10	76.2	12.4	11.4	86.29	69.23	15.98	14.79	92.39

With 8 wt.%, the fuller earth produced higher plasto oil yields than the commercial FCC catalyst. Hence, the higher yield of the obtained plasto oil (8 wt.% of fuller earth) was upgraded to improve for further process.

4.5 Analysis of the plasto oil

4.5.1 Physicochemical characteristics

The Physicochemical characteristics of crude plastic oil produced with different proportions of fuller earth and commercial FCC catalysts are given in Table 4.5.

Table 4.5: Physicochemical properties with and without catalyst

Physical Properties	No - catalyst	Fuller earth (wt.%)					Commercial FCC Catalyst (wt.%)					Diesel
		2	4	6	8	10	2	4	6	8	10	
Density (kg/m^3)	825	816	824	819	835	830	829	823	818	820	824	810-845
Viscosity (Cst)	3.73	3.25	3.52	3.35	3.80	3.12	3.82	3.79	3.45	3.69	3.81	2-4.5
Calorific value (kJ/kg)	41.29	41.03	41.6	42.8	42.3	42.6	41.97	42.87	42.32	42.60	42.39	45.2
Flash point (°C)	57	55	58	53	52	53	61	57	59	54	58	50
Fire point (°C)	64	62	62	58	55	57	65	63	65	59	63	58
Cloud point (°C)	19	16	18	15	17	14	21	18	15	17	20	3
Pour point (°C)	12	11	13	11	12	11	18	11	9	11	13	-1

4.5.2 Chemical characteristics

4.5.2.1 FTIR of the plasto oil

FTIR spectra of the plasto oil with various proportions of the catalyst are depicted in Figure 4.10. Hydrocarbon fuel absorbs infrared light in an FTIR spectrometer, which is an approach that reveals information about its molecular structure and bond strength at discrete wavelengths. Figure 4.10 depicts the 2900-3000 cm^{-1} stretching of the frequency of =C–H, -C-H, C–C, which shows hydrocarbon groups including alkanes, alkenes and alkynes (P. K. Ghodke, 2021). The

wavenumber 2922 cm^{-1} represents alkanes' strong -CH vibrational signal in hydrocarbon fuel. Although the frequency range from 2600-2900 cm^{-1} represents the few oxygenating groups. The wave numbers 2854, 1702, 1456 and 1378 cm^{-1} depicted the alkane C-H stretching, Aliphatic ketone C=O stretching, -C-H scissoring and alkene C=C bending or C-H bending, respectively (Ozdemir et al., 2013)..

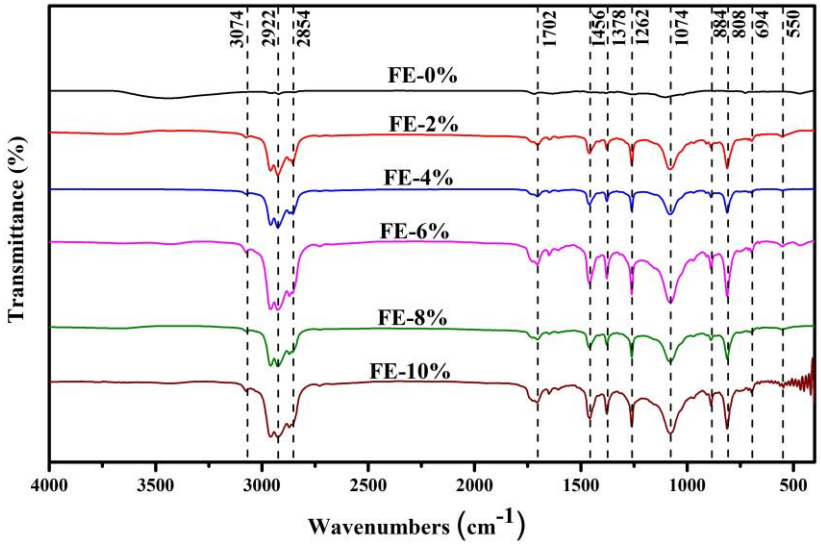

Figure 4.10: FTIR analysis of the plasto oil produced from CTD

Table 4.6 : Summary of FTIR analysis

Wave Number (Cm^{-1})	**Functional group**	**Remark**
3074	=C-H stretching	Alkane
2922	C-H stretching	Alkyl
2854	C-H stretching	Alkane
1702	C=O stretching	Aliphatic ketone
1456	-CH2-	-C-H scissoring
1378	C=C bending or C-H bending	Alkene
1262	C-O stretching	Alkyl ether
> 900	C-H stretching and fingerprint region	Alkane, Alkene, Alkyne

Table 4.6 provides descriptions of the functional groups found in various hydrocarbons, along with details regarding their behavior, strength, and modes of vibration, which encompass bending and stretching.

4.5.2.2 GCMS of the plasto oil

The GCMS analysis of the plasto oil without catalyst and with catalyst (FE 8 wt.%) has been carried out to identify the presence of chemical composition, as depicted in Figure 4.11 and Figure 4.12. However, Table 4.7 and Table 4.8 summarise the chemical compounds in the plasto oil obtained without catalyst and 8 wt. % of fuller earth catalyst, respectively. It has been observed that Plasto oil contains 25-30 compounds. Hydrocarbons were normalized to 100 wt.% of the overall composition using the area percentage determined by mass spectrometry. The major composition of plasto oil is carbon aliphatic (alkane, alkene and alkyl compounds). However, hydroxyl and oxygenated groups were also revealed in the plasto oil. Hydrocarbon fuel comprises straight-chain compounds derived from the MMPW pyrolysis and substituted aliphatic hydrocarbons. During catalytic pyrolysis, hydrocarbons are randomly cracked, producing many hydrocarbon fragments. Chain severing releases a C-C bond in the poly-alkene structure, which forms a stable C=C bond during decomposition. 13-Tetradecane and 7-Dimethoxy-1-tetralone compound contributed the majority of plasto oil without catalyst. However, 10-pentadecane, Tetradecane, and 1,11-dodecane were found in most plasto oil obtained with fuller earth catalysts. The average composition of MMPW hydrocarbon is close to the lower hydrocarbon C_{10} group, indicating that it has more volatile, heating value, and less dense characteristics.

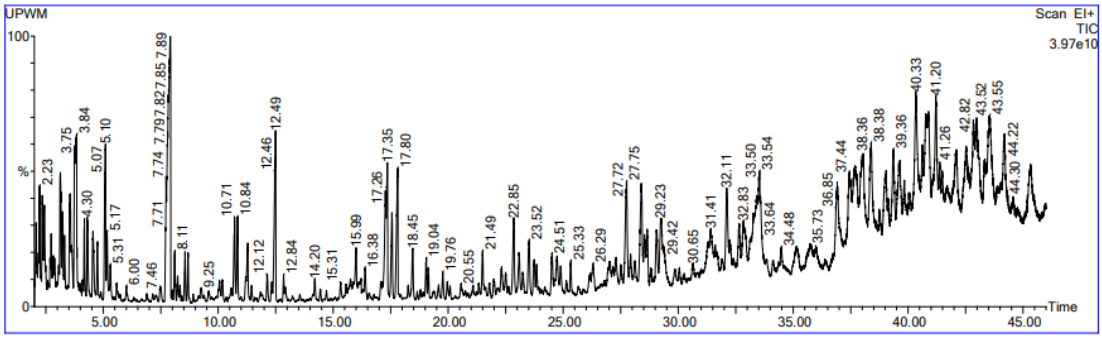

Figure 4.11: GCMS chromatography of plasto oil from MMPW without catalyst

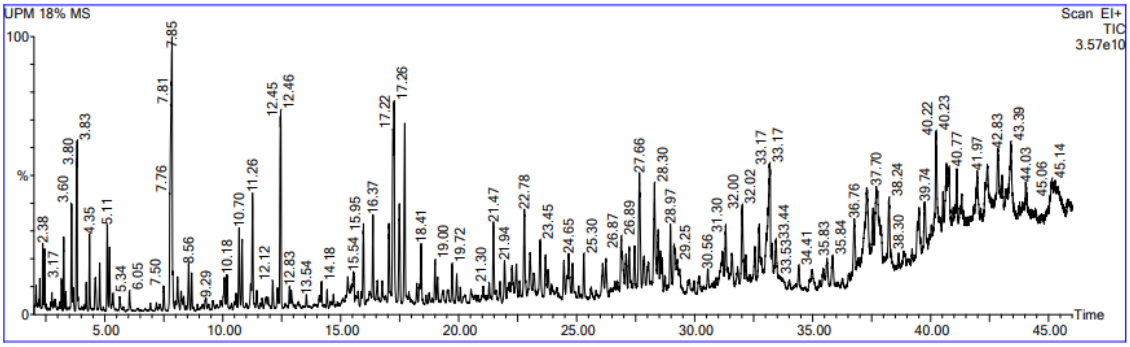

Figure 4.12: GCMS chromatography of plasto oil from MMPW with 8 wt.% FE Catalytic

Table 4.7: Chemical mass composition of plasto oil obtained without catalytic pyrolysis reaction of MMPW

Peak	Compound	Retention time	Area %
1	6 Methoxy-3-pyridinamine	3.84	7.97
2	2-Cycloocten-1-one	3.554	3.73
3	1,8-Dodecadiene	5.10	3.16
4	7-Dimethoxy-1-tetralone	7.92	15.92
5	Cyclododecene	10.71	2.05
6	4-methyl-	11.28	2.07
7	Reticulol	12.49	5.30

8	E-1,9-Hexadecadiene	17.35	3.92
9	1,11-Dodecadiene	17.80	4.18
10	-10-Pentadecenol	23.52	1.38
11	9-Dodecenol	28.39	3.30
12	-2,13-Octadecadien-1-ol	29.06	1.23
13	11(12-Cyclopropyl) dodecen-1-ol	32.84	1.79
14	12-Methyl-oxa-cyclododec-6-en-2-one	33.54	8.71
15	E, Z-2,13-Octadecadien-1-ol	36.91	3.81
16	Z-2,13-Octadecadien-1-ol	38.04	5.89
17	E-2-Octadecadecen-1-ol	39.64	2.40
18	13-Heptadecyn-1-ol	40.76	5.31
19	Oxacyclotetradecane-2,11-dione, 13-methyl-	42.08	4.90
20	13-Tetradecane	43.54	10.14
21	E, Z-2,13-Octadecadien-1-ol	36.91	3.81
22	Z-2,13-Octadecadien-1-ol	38.04	5.89

Table 4.8: Chemical mass composition of plasto oil obtained from catalytic pyrolysis reaction of MMPW

Peak	Compound	Retention time	Area
1	2-Cyclohexen-1-one, 4,5-dimethyl-	3.60	2.37
2	2-Cyclohexen-1-one, 4,5-dimethyl-	3.83	4.10
3	-Dodecen-1-ol	10.70	1.80
4	2-Pentenoic acid, 4-hydroxy-	11.26	2.7
5	9-Decenal	15.3	1.68
6	Cyclooctane, methyl	15.54	2.10
7	Dodecen	16.37	2.05
8	1-12 -Tridecadiene	17.04	2.20

9	1,11-Dodecadiene	17.72	5.17
10	-1,9-Hexadecadiene	18.4	1.67
11	11-Hexadecen-1-ol	22.78	2.20
12	9,17-Octadecadiena	23.4	1.66
13	15-Octadecedien-1-ol acetate	28.29	3.40
14	2-Octadecadecen-1-ol	31.31	1.44
15	Cyclopentadecan	32.01	2.22
16	Oxirane	33.17	5.91
17	5-Octadecedien	36.76	1.76
18	1,9- Octadecadiene	38.23	2.60
19	7-Octadecene	39.5	1.21
20	Cyclooctane	40.77	5.41
21	11- Tricosene	41.97	4.25
22	-10-Pentadecane	43.39	8.47
23	Tetradecane	45.38	6.39

4.6 Fractional distillation of the plasto oil

Fractional distillation of the plasto oil is required to remove the wax and other sand contamination and upgrade the quality of the PO. The plasto oil obtained with 8 wt.% of fuller earth was upgraded by fractional distillation. The distillation process has been carried out at different temperature ranges from 20-180 ^{o}C and 180-340 ^{o}C. The upgraded plasto oil yield obtained at various temperature ranges is given in Table 4.9.

Table 4.9: Distillated plasto oil yield at different temperature ranges

Temperature	**Yield (g/kg)**
20-180 ^{o}C	350
180-340 ^{o}C	580
Residue	70

The distillation process upgrades the plasto oil quality and improves the physicochemical properties. The physicochemical characteristics of the upgraded plasto oil are given in Table 4.10.

Table 4.10: Physicochemical properties of the upgraded plasto oil

Physicochemical properties	Distillate plasto oil temperature range		Diesel	Gasoline
	20-180 (°C) (POL)	180-340 (°C) (POH)		
Density (kg/m^3)	794	812	836	780
Viscosity (Cst)	2.31	2.98	3.1	1.7
Calorific value (kJ/kg)	43.76	42.59	45.2	46.97
Flash point (°C)	34	41	50	29
Fire point (°C)	40	48	58	44
Cloud point (°C)	4	6	3	2
Pour point (°C)	-2	1	-1	-4
Cetane number	NA	51	56	NA

4.7 Summary

This chapter concludes that MMPW can decompose effectively via pyrolysis at 200-550 °C, breaking down long-chain hydrocarbons. FTIR analysis shows the presence of various plastics (PE, PP, PET) and functional groups like carbonyls and aliphatic hydrocarbons. Using commercial Equilibrium and Fuller earth catalysts, a higher liquid yield was achieved with 8 wt.% Fuller earth, its larger pore volume and medium acidity, leading to more liquid hydrocarbons and fewer gases. The oil was refined through distillation, yielding POL (20-180 °C) and POH (180-340 °C). POH was tested in a modified CI engine due to its properties similar to diesel.

CHAPTER 5: ENGINE EXPERIMENTAL SETUP

5.1 CI engine setup

The experiments were conducted using a single-cylinder, four-stroke compression ignition (CI) engine in the Engine Research Laboratory (ERL) at UPES, Dehradun. The engine was equipped with a water-cooled eddy current dynamometer for precise loading. The load cell was used to measure the applied load, and other sensors and instruments were used to measure the characteristics of the CI engine. The technical specifications of the CI engine are given in Table 5.1.

Table 5.1: Technical specification of the CI engine

Parameters	**Dimensions**
Make	Kirloskar Oil Engine Ltd
Cylinder bore diameter	87.5 mm
Piston stroke	110 mm
Cubic capacity	661 cc
Compression ratio	18:1
No. cylinder/injector	One
Engine speed	1500 rpm
Type of injection	DI
Capacity of fuel injection pressure	220 bar
Capacity of fuel injection timing	12 ^{o}CA bTDC
Power rating	7 HP (3.5 kW)
Electronic control unit	Nira i7r (with solenoid injector driver) with programmable ECU software and calibration cable

The schematic diagram of the conventional engine setup is depicted in Figure 5.1. The entire test equipment consists of a conventional CI engine, water pump, eddy current dynamometer, rotameter, and a data collection system (DAQ), along with other sensors for measuring engine parameters. The DAQ includes a load cell, RPM indicator, load indication, crank angle sensor, and an air surge tank. All engine parameters are monitored, and results are recorded in the DAQ and saved to the computer system. The test equipment allows for the study of cylinder pressure, net heat release rate, and performance parameters under different engine loads.

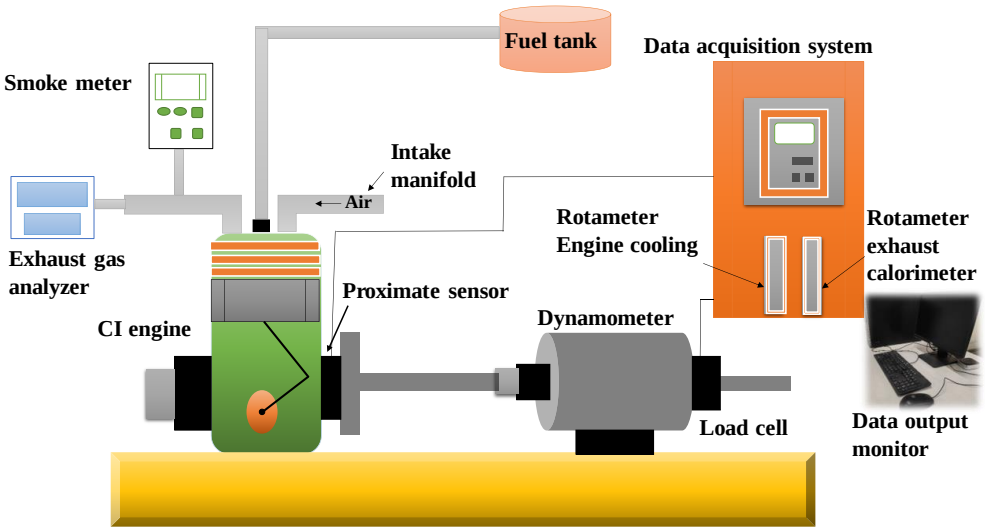

Figure 5.1: Schematic diagram of the CI engine

Different proportions of plasto oil (PO) in conventional CI engines have been used with diesel blending. Volumetric experiments were conducted using different ratios of plastic oil to diesel fuel. The mechanical stirrer was used for 30 min at 500 rpm to mix PO-diesel properly. The fuels used in the CI engine were PO25D75 – 25 vol.% plasto oil and 75 vol.% diesel, PO50D50 – 50 vol.% plasto oil and 50 vol% diesel, PO75D25 – 75 vol.% plasto oil and 25 vol.% diesel, PO100 (neat plasto oil). The experiments were performed on the conventional CI engine fueled with different fuels and the output parameters evaluated from the experiments are mentioned in Table 5.2.

Table 5.2: Experimental matrix for conventional CI engine

Engine	Fuel	Engine load	Output parameter
Single-cylinder compression ignition engine	Diesel (D100) PO25D75 PO50D50 PO75D25 Neat plasto oil (PO100)	25%, 50%, 75%, 100%	Engine Performance ▪ BTE ▪ BSFC ▪ EGT Engine Combustion ▪ NHRR ▪ CP Engine Emissions ▪ CO ▪ HC ▪ CO_2 ▪ NOx ▪ Smoke opacity

5.2 PCCI engine setup

The experiments were performed on the PCCI engine by modifying the existing conventional CI engine set up at APEX Innovation Pvt. Ltd. Sangli, Maharashtra. The technical specifications of the PCCI engine were the same as those given in Table 5.1. The schematic diagram of the PCCI engine setup is depicted in Figure 5.2. There are few modifications made in conventional CI engine. The existing manifold carried out the atmospheric air and EGR inside the intake manifold. However, in PCCI mode, an additional inlet is provided on the manifold to allow the fuel to vapour through the fuel vaporizer system. Therefore, fuel vapour and air are mixed in the modified manifold. This partially premixed air-fuel and exhaust gas mixture was introduced to the engine cylinder,

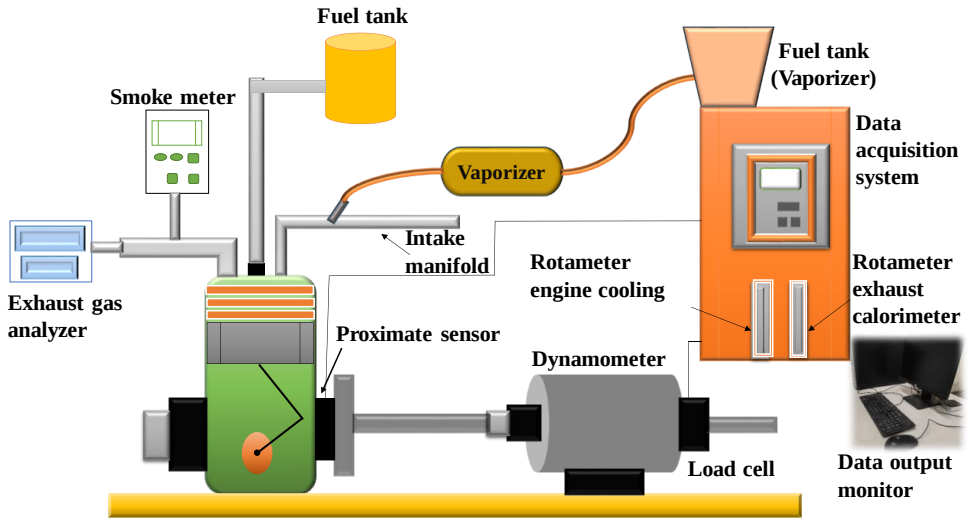

Figure 5.2: Schematic diagram of PCCI engine

The fuel vaporizer used in the study has an inlet and outlet; the inlet is connected with the separate fuel (Plasto-oil heavy) container, and the outlet was associated with the modified intake air manifold. Hence, a small fraction/ partial amount of fuel is injected in vapour form in PCCI operation, and the amount of vapour and timing is controlled by the ECU, while the remaining fuel is provided by the direct injection (Main injection) through the governor operation. Figure 5.3 illustrates the experimental setup of the fuel vaporizer.

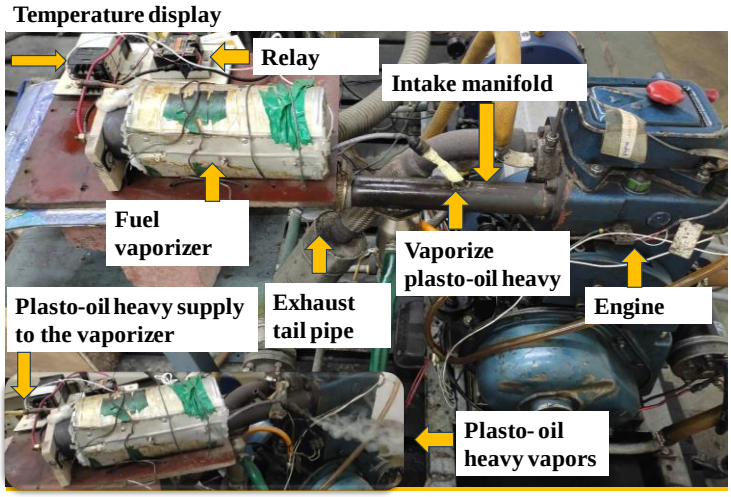

Figure 5.3: Experimental setup for PCCI engine

In the PCCI engine, the experimentations were performed with varying fuel quantities of plasto oil heavy (POH) of 2 ml/min and 3 ml/min with different engine loads with and without EGR at constant rpm. The output parameter obtained is given in Table 5.3.

Table 5.3: Experimental matrix for the PCCI engine

Run	Main fuel injection	Constant fuel (POH) vapour	EGR	Engine load (%)	Output parameter
1	Diesel	-		25, 50, 75, 100	Engine Performance ▪ BTE ▪ VE ▪ EGT. Engine Combustion ▪ NHRR ▪ Pressure-Crank angle Engine Emissions ▪ CO ▪ HC ▪ NOx ▪ Smoke opacity
2	Diesel	-	10%		
3	Diesel	2ml/min	-		
4	Diesel	2ml/min	10%		
5	Diesel	3ml/min	-		
6	Diesel	3ml/min	10%		
7	POH10D90	-	-		
8	POH10D90	-	10%		
9	POH10D90	2 ml/min	-		
10	POH10D90	2ml/min	10%		
11	POH10D90	3ml/min	-		
12	POH10D90	3ml/min	10%		
13	POH20D80	-	-		
14	POH20D80	-	10%		
15	POH20D80	2ml/min	-		
16	POH20D80	2ml/min	10%		
17	POH20D80	3ml/min	-		
18	POH20D80	3ml/min	10%		

5.2.1 Engine load measurement

The engine load was measured using a SAJ AG Series eddy current dynamometer from Saj Test Plant Pvt. Ltd., A strain gauge load cell was used to measure the load on the dynamometer, and a shaft fitted with a rotary encoder was used to track speed. The load cell type 60001, created by Senserotronics, was utilized in the experiment.

The dynamometer consists of a rotor connected to the driveshaft and a stator with two coil windings. When direct current flows through these coils, a magnetic field forms in the region where the shaft is rotating. The rotation of the shaft generates

eddy currents, which produce a braking effect. The load generated by the dynamometer was measured using a load indicator, specifically the SV-8 series of Universal Process Indicators. Figure 5.4 shows a labeled depiction of the eddy current dynamometer.

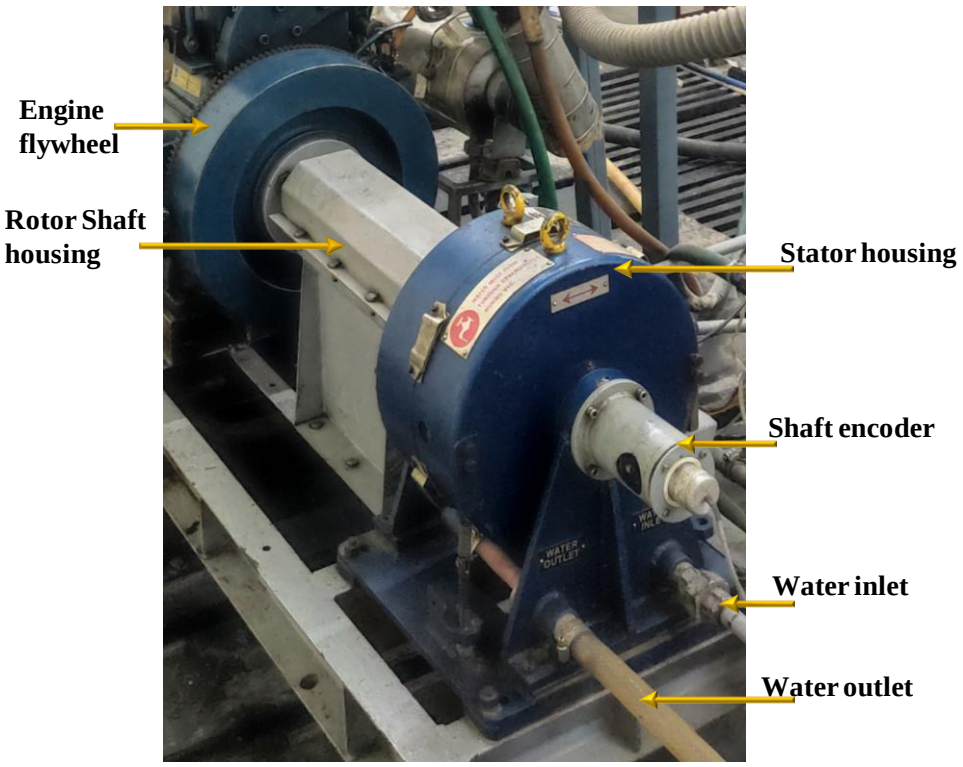

Figure 5.4: Eddy current dynamometer, shaft encoder

5.2.2 Rotameter

A rotameter is used to determine the flow rate of water. It relies on the variable area meter principle, which is based on the buoyancy force principle, the weight of the float, gravity force, and upthrust force. A metallic float is included in the setup and can move up and down inside the tapered tube through which the water flows. Until the water and the float's weight are in balance, the water buoyant force pushes the float upward. The vertical position of the float is a measurement of the instantaneous flow rate, as the scale shows. A centrifugal pump is used to keep the flow rate constant. Figure 5.5 shows a labeled graphic that demonstrates how the rotameter works. According to the engine manual's usual

recommendations, the rotameter water flow was set to 100 liters/ hour (lph), and the calorimeter water flow was set to 250 lph. A drop in water level may raise the possibility of operating an engine at greater loads as the temperature rises, and it can even cause an engine to seize.

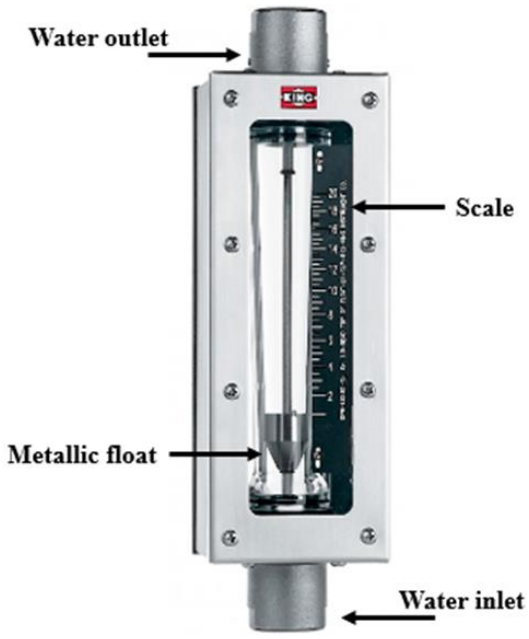

Figure 5.5: Rotameter

5.2.3 Data acquisition system

The engine parameter control panel is called the DAQ. It has an ignition switch, gasoline tank, rotameter, temperature sensors, fuel pipe, manometer, orifice, and dynamometer load unit. The DAQ system facilitates data extraction into the computer system and the graphical analysis of various parameters. The engine load was adjusted using the dimmer stat on the dynamometer.

The fuel tank was placed above the DAQ system, and the fuel consumption was measured using a manometer. Additionally, the DAQ system includes many sensors for analyzing engine parameters, including load cell sensors, differential air pressure transducers, engine/calorimeter inlet and outlet temperature sensors, piezoelectric sensors, and engine exhaust temperature sensors. A piezoelectric sensor is a transducer designed to compute the pressure variation during

compression stroke and combustion stroke and determine engine knocking tendency. The engine/calorimeter inlet/outlet temperature sensor provides information about the engine's operating temperature. An increase in load should be done gradually since temperature increases in proportion to load. Before raising the load, the temperature must be stabilized for the engine to operate efficiently. The differential air pressure transmitter regulates airflow rates within the intake manifold. The DAQ uses the combined data to determine the engine's combustion and performance characteristics, ensuring optimal operation. Figure 5.6 shows a labeled picture of the DAQ. IC engine analysis software was utilized to examine combustion and performance characteristics acquired from DAQ.

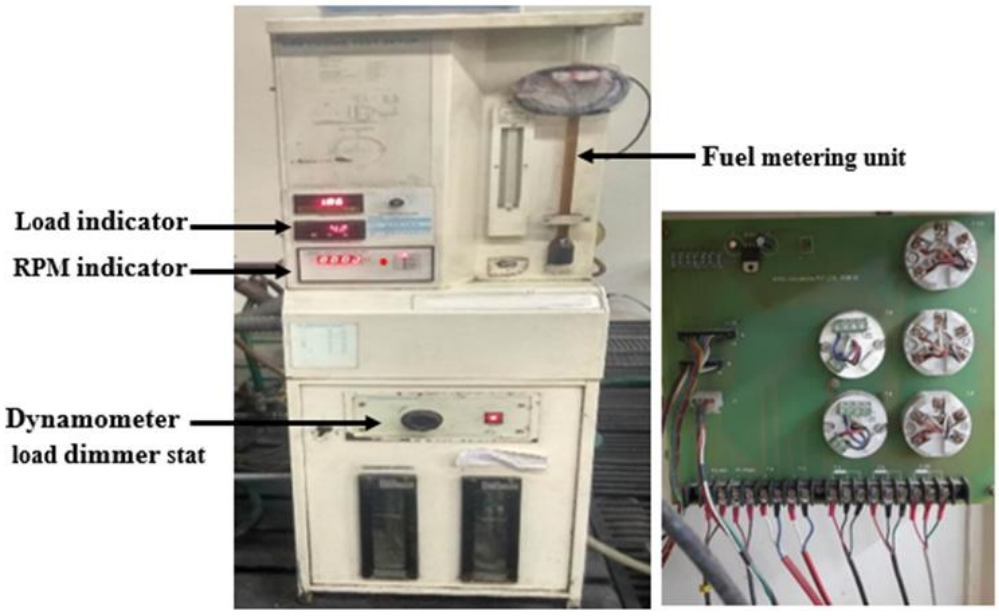

Figure 5.6: Data Acquisition System, transducer, and display interface

5.3 Emission measurement

5.3.1 Emission gas analyser

Emission analysis is an essential engine parameter for measuring the emission of alternative fuel in an engine. It determines CO, NO_x, CO_2, HC, and O_2 levels in exhaust gases based on working conditions. The experiment used the emission gas analyzer shown in Figure 5.7, the AVL DIGAS 444 gas analyzer manufactured by

AVL Engineering, to measure the emissions. Before the analyzer begins measuring the emissions, it must adhere to a few standard operating processes. The gas analyzer comprises two main components: the probe, responsible for collecting sample exhaust gas, and the analyzer itself, which includes sensors to deliver accurate results. The exhaust gas enters the sample cell unit of the analyzer through the cell inlet. The cell unit is situated between the infrared source and the dedicated infrared detector for each gas, except O_2 and NO_x. A decrease in infrared (IR) energy caused by the blockage of gas wavebands is quantified to determine emissions. Measurements of NO_x and O_2 rely on the output from electrochemical sensors, which result from chemical reactions between the test gases and analyzer chemicals. The probe is connected to the analyzer via a hollow rubber hose. Before measuring emissions, a leak test is performed to identify any leaks in the pipe connecting the probe. Following the leak test, the analyzer requires some time for calibration. Once calibrated, initiate the measurement process by inserting the probe into the exhaust outlet. Exhaust gas was examined at different engine load levels.

Figure 5.7: AVL DIGAS 444 gas analyzer

5.3.2 Smoke Meter

Smoke poses a significant threat to researchers while testing the new fuel in a diesel engine. Higher smoke opacity reduces engine performance and increases PM emissions. This study used an AVL-437 smoke meter to assess smoke opacity, as shown in Figure 5.8. The smoke meter is attached at the end of the exhaust piping. The smoke meter was calibrated by drawing ambient air. Before analysis,

the quality of the filter paper was tested. The smoke intensity is determined by the severe strain on the filter paper caused by the exhaust gases drawn into the smoke meter by the pump.

Figure 5.8: AVL 437 smoke meter

5.4 Fuel vaporizer

A fuel vaporizer is a device that converts liquid fuel into vapour before it enters the combustion chamber of an engine. More effective mixing of the vapourised fuel with the air may result in enhanced combustion, higher fuel efficiency, and lower pollutants. A heater is used in the vaporizer to evaporate the liquid fuel and form the external air-fuel mixture in the HCCI engine (Ganesh et al., 2008; Ganesh et al., 2010). A study showed that it is feasible to place the fuel vaporizer on the air intake manifold with minor modifications in the air intake manifold. Aggarwal et al. utilized an electrically operated fuel vaporizer, where a fuel injector sprays atomized fuel into it. The resulting fuel vapor is then mixed with air to form the external air-fuel mixture (Agarwal et al., 2013). Fuel with a higher boiling point and lower volatility is more appropriate in vaporization. The fuel vaporizer must operate at a temperature higher than the fuel's boiling point to effectively generate an external mixture (Ganesh et al., 2011) Numerous studies have been carried out with electrically heated vaporizers (Ganesh et al., 2008; Ganesh et al., 2010; A. P. Singh et al., 2012). However, it is also possible to vaporize the fuel in the intake manifold by using the high intake air temperature associated with EGR (D. S. Kim et al., 2006; H. Liu et al., 2011). Several

researchers designed the electrically heated vaporizer, and band heaters were used to heat the primary vaporizing chamber outside (Ganesh et al., 2008; Ganesh & Nagarajan et al., 2010). The ceramic pipe in this vaporizer is filled with a high-temperature substance that contains liquid fuel, and the heating element consisting of nichrome is coiled around the pipe to transfer heat alone. An ECU was employed to control the mass flow rate and fuel amount supplied to the vaporizer through a straight pipeline. However, a limitation of this method was that the residence time of the vapor was not as anticipated, and the time available for vaporizing the liquid fuel was inadequate, mainly because of the direct path of the liquid fuel flow. Consequently, a larger amount of fuel was present at the outlet of the vaporizer.

In this research study, a fuel vaporizer technique was used. The fuel vaporizer comprises heating material and a higher thermal conductivity copper pipe. The copper pipe is wound over the heating material in a circular path to carry the liquid fuel as shown in Figure 5.9. However, various researchers have studied the straight path to carry fuel. They found that a small amount of fuel is not vaporized properly and accumulates in the intake manifold to catch the path of the air and vapour mixture (Ganesh et al., 2010; Maurya et al., 2014).

This intended approach caused an increase in the residence duration of the vapour. Consequently, only a small amount of liquid fuel was present at the exit of the fuel vaporizer, ensuring complete vaporization as it reached the combustion chamber. In this experiment, POH vapour was produced by the externally powered fuel vaporizer, a temperature controller regulated to ensure a steady temperature during engine loads. For plasto oil heavy to turn into vapour, the temperature of the fuel must rise over its flash point, which is between 85 and 90 ^{o}C. Copper (Cu) was used for the main vaporizing chamber because it has a higher thermal conductivity (384 W/m-k). To prevent the spontaneous ignition of plasto oil heavy within the vaporizing chamber, the temperature of the Cu tube was carefully controlled at 290 ^{o}C, strategically situated between the oil's boiling

point (170 °C) and its auto-ignition temperature (290 °C). This temperature regulation was achieved using a temperature controller with a relay. A heating element made by nichrome facilitated the heating of the copper (Cu) tube.

Furthermore, glass wool was employed as a thermal insulator around the copper tube to reduce heat dissipation in the environment. The fuel vaporizer has a ceramic heating element in its center, and Nichrome conducts the primary heating. Figure 5.9. provides a sectional view of the fuel vaporizer. Insulation for the fuel vaporizer was achieved using glass wool. The Cu pipe dimensions were 2400 mm in length and 6 mm in diameter.

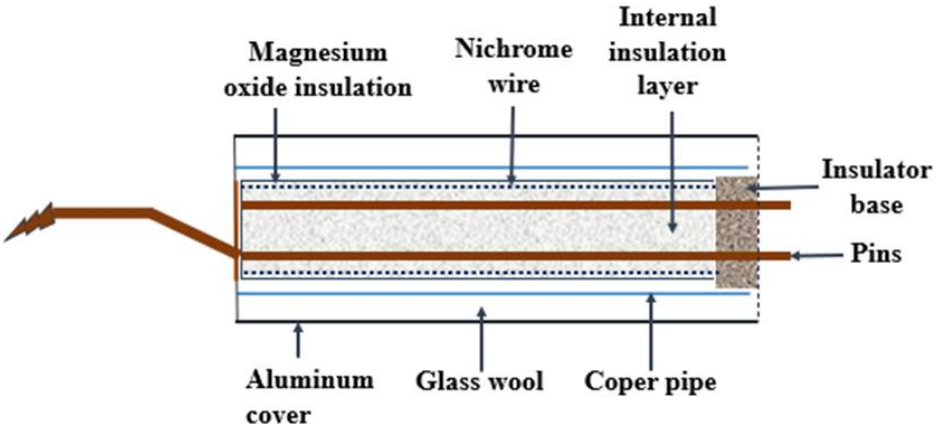

Figure 5.9: Cut-section view of the fuel vaporizer

warm-up time and the cut-off temperature are the parameters that must be regulated for the vaporizer to function compellingly. Thermotech's PID-41S temperature controller has been used in the study. The PID controller took 13 minutes to warm up to 290 °C. The addition of a T-joint substantially eliminated gasoline backflow. A T-junction was inserted into the main gasoline line, with one arm directly attached to the nozzle and the other connected to the engine return line, to guarantee that any excess fuel was routed back to the fuel tank. Figure 5.10 illustrates the fuel vapour injection patterns.

Figure 5.10: Vapour injection pattern

The properties of the plasto oil heavy (POH) have been used for the fuel vaporizer given in Table 5.4.

Table 5.4: Physicochemical characteristics of plasto oil heavy

Physicochemical properties	**Methods**	**Plasto oil heavy (POH)**
Density (kg/m^3)	ASTM D 4052	812
Kinematic Viscosity @ 30 °C (m^2/S)	ASTM D445	2.98
Calorific value (MJ/kg)	ASTM D 240	42.59
Flash point and Boiling point (°C)	ASTM D93	41
Thermal Conductivity of POH (W/m-k)	ASTM D 2717	0.10
Specific heat (J/kg-K)	ASTM D 2890	1903
Latent heat of Vaporisation (kJ/kg)	ASTM D 5501	283
Thermal conductivity of copper (W/m-k)	ASTM C 177	401
Wire diameter (mm)	---	6

5.5 Data analysis

This section details the data processing related to engine performance and combustion. It provides an analysis of cylinder pressure, NHRR, and BTE. The

PCCI engine was performed with EGR and a fuel vaporizer. Additionally, the section discusses related characteristics such as EGR and premixed ratios.

5.5.1 In Cylinder pressure

In-cylinder pressure (CP) is a crucial parameter for diagnosing and regulating engine combustion offering valuable insights into the combustion process in engine cylinders. The combustion parameters of an engine were examined throughout the compression stroke and expansion stroke of the cycle. During combustion, CP fluctuates depending on the volume of the cylinder, combustion dynamics, and heat transfer to the walls. AVL piezoelectric pressure transducers with a capacity of 100 bar (GH14D/AH01) were utilized to detect CP. An appropriate adaptor was used to position the AVL pressure transducer in the cylinder head. The quartz measuring element and the charge amplifier within the plug are integrally connected to capture the fluctuation in pressure throughout the combustion duration. Additionally, a 10 mm hole in the head of the cylinder is connected to the combustion chamber to monitor the pressure during combustion. This setup safeguards the transducer from potential damage caused by flame impingement. The pressure transducer produces the appropriate charge output based on the pressure within the engine cylinder. The crank angle encoder measured the CP with various crank angle positions.

The following conditions must be met to get an accurate in-cylinder pressure reading-

- Accurate mounting of the probe in the cylinder head.
- The pressure vs volume phasing is accurate within 0.2.
- The calibration is affected by temperature variations in the transducer.
- The compression and expansion process should be well-fitted by a polytrophic.
- Relationship, PV^n = Constant, with $n = 1.3 \pm 0.5$ for conventional fuels.

5.5.2 Net heat release rate

In a CI engine, the cylinder functions as a single open system. When the intake and exhaust valves are closed, the A-F mixture enters the combustion chamber

through the system boundary via mass flow. A single-zone model was used to calculate the NHRR. The first law of thermodynamics, expressed as the energy equation for an open system, can be stated as follows:

$$dQ + \sum m_i h_i = dW = dU$$

If the flow in the crevice is negligible, then the equation can be written as

$$\frac{dQ}{d\theta} - \frac{dQ_w}{d\theta} + m_{inj} h_f = P\frac{dV}{d\theta} + \frac{dQ}{d\theta}$$

Where-

U = Sensible internal energy

hf = Sensible enthalpy of injected fuel

Q = Heat release during combustion

Qw = Heat rejected out of the cylinder

If h_f is negligible, the equation can be written as-

$$\frac{dQ}{d\theta} = P\frac{dV}{d\theta} + \frac{C_v}{R}\left[P\frac{dV}{d\theta} + V\frac{dP}{d\theta}\right] + \frac{dQ_w}{d\theta}$$

$$\frac{dQ}{d\theta} = \frac{\gamma}{\gamma - 1}\left[P\frac{dV}{d\theta}\right] + \frac{\gamma}{\gamma - 1}\left[V\frac{dP}{d\theta}\right] + \frac{dQ_w}{d\theta}$$

Where $\gamma = 1.35$

5.5.3 Exhaust gas recirculation

A fuel vaporizer is used to reduce the NO_x emission from the engine. However, further reduction is needed to fulfill stringent emission standards. Therefore, it is essential to maintain control over the peak combustion temperatures to lower NO_x emissions in the exhaust. The effective method of exhaust gas recirculation (EGR) can enable lower NO_x emissions. NO_x emission depends on the combustion temperature; if the combustion temperature is higher and reaches 2000 K, it leads to NO_x formation. When EGR is combined with diesel engine intake air, it raises the temperature of the inlet charge, which may impact the combustion process and

compressed-charge temperature. Increasing the temperature of the intake charge reduces the density and mass of the charge that enters the engine cylinders. The exhaust gas is mostly composed of nitrogen, carbon dioxide, and water vapour. When the exhaust gas is recirculated back into the combustion chamber, it works as a diluent, thus reducing the O_2 concentration in the combustion chamber. Additionally, exhaust gas possesses a higher specific heat than fresh air. Consequently, EGR increases the intake charge's heat capacity and diminishes the temperature and rise for the same amount of heat release.

$$EGR\ (\%) = \frac{Volume\ of\ EGR}{Total\ charge\ inatke\ into\ cylinder} \times 100$$

EGR ratio may be defined using CO_2 concentration.

$$EGR\ (\%) = \frac{[CO_2]_{Intake} - [CO_2]_{Ambient}}{[CO_2]_{Exhaust} - [CO_2]_{Ambient}}$$

5.5.4 Standard error measurement

In the experimental study on the CI engine, the possibility of an error occurring within the readings is overwhelmingly probable. Random inaccuracies may occur in the study, researcher error is also reasonably standard. Therefore, Table 5.5 reported the instrumental errors and experimental errors as well. Uncertainty-measured parameters ($x_1.\ x_2,\ x_3\ \ldots\ x_n$) such as temperature sensors, pressure transducers, etc. The overall uncertainty of the experiments can be computed by the given equation 5.1 (A. K. Das et al., 2020). The uncertainty of the engine parts, BTE, CO, HC, CO_2, and NO_x, is shown in Table 5.5.

Total uncertainty (%).

$$q = \sqrt{\left[\sum\left(\frac{dQ}{dx_n}\Delta x_n\right)^2\right]} \qquad \text{Eqn. (5.1)}$$

q = f ($x_1.\ x_2,\ x_3\ \ldots\ x_n$) (q is the function of $x_1.\ x_2,\ x_3\ \ldots\ x_n$).

$x_1.\ x_2,\ x_3\ \ldots\ldots\ldots x_n$ measured variable.

$dq\ dx_1.\ dq\ dx_2,\ dq\ dx_3\ \ldots\ldots\ dq\ dx_n$: Partial differential of q (calculated parameter)

Table 5.5: List of equipment including their make, range, accuracy

Apparatus	**Make**	**Approximate Range**	**Precision**	**Approximate Uncertainty (%)**
An analyzer for Gases	AVL	CO: 0%-10% HC: 0.0-20,000 ppm NOx: 0.0-5000 ppm	± 0.01 % ± 1ppm ± 1ppm	± 0.50 ± 0.70 ± 0.30
RPM indicator with speed sensor	Selection process control	4.0 rpm-9999 rpm	±0.050%	± 2.0
Mechanical crankshaft angle gauge	Kubler	0^{o} -360^{o}	± 1^{o}CA	± 0.20
Stress gauge (Load cell)	Sensortronics	0.0 kg-50 kg	± 0.1 kg	± 0.10
An indication of the load being carried	ABUS Technologies	0.0 kg-100 kg	± 0.20%	± 0.20
BSFC	-	-		±1.764
BTE	-	-		± 0.45
Smoke	-	-		± 0.50%

CHAPTER 6: ENGINE PERFORMANCE AND EMISSIONS

6.1 Investigation of CI engine characteristics fueled with plasto oil

The engine underwent testing with PO and diesel blends. Volumetric experiments were conducted using varying proportions of plasto oil to diesel. A mechanical stirrer was employed for 30 min at 500 rpm to mix PO-diesel properly. The fuels used in the CI engine were as follows: PO25D75 – comprising 25% plasto oil and 75% diesel, PO50D50 – comprising 50% plasto oil and 50% diesel, PO75D25 – comprising 75% plasto oil and 25% diesel, PO100 – Neat plasto oil.

6.1.1 Engine Performance

6.1.1.1 Brake thermal efficiency

The brake thermal efficiency is the significant engine parameter that addresses the effective conversion of fuel chemical energy into thermal energy and, correspondingly mechanical output. The BTE of the engine can also be determined by Equation 6.1. The deviation of BTE at various engine loads is depicted in Figure 6.1. It has been observed that BTE increases with increasing the loads of the engine. This may cause a fall short in heat loss, leading to the subsequent increase in power due to the improvement in the presence of oxygen in combustion (Shrivastava et al., 2020; Rajak et al., 2020). It has been observed that the BTE of the plasto oil blends produced lower BTE at all engine load conditions than the reference diesel. The BTE of the engine was 31.28% for reference diesel fuel at a higher engine load. However, introducing plasto oil with diesel blends and neat plasto oil such as PO25D75, PO50D50, PO75D25, and PO100 reduced the BTE by 2.50%, 3.70%, 5.08%, and 6.90%, respectively than reference diesel at higher engine load. The inferiority owing to the high viscosity and lower calorific value (CV) of the plasto oil blends This may be attributed to the poor spray formation by poor atomization and vaporization of the

plasto oil blends during premixed combustion (Tesfa et al., 2010; Sambandam et al., 2020). Thokchom Subhaschandra et al. studied on CI engine fueled with 20 vol% plasto oil and 80 vol.% diesel, resulting in lower BTE than diesel. This may cause lower heat content, increased viscosity and heavier hydrocarbon chains (C_{10}-C_{30}) in plasto oil (T. S. Singh et al., 2020).

$$\eta\ (\%) = \frac{\text{Brake power (KW)} \times 3600}{\text{Fuel flow } \left(\frac{\text{Kg}}{\text{hr}}\right) \times \text{Calorific value } \left(\frac{\text{KJ}}{\text{Kg}}\right)} \times 100 \qquad \text{Eqn. (6.1)}$$

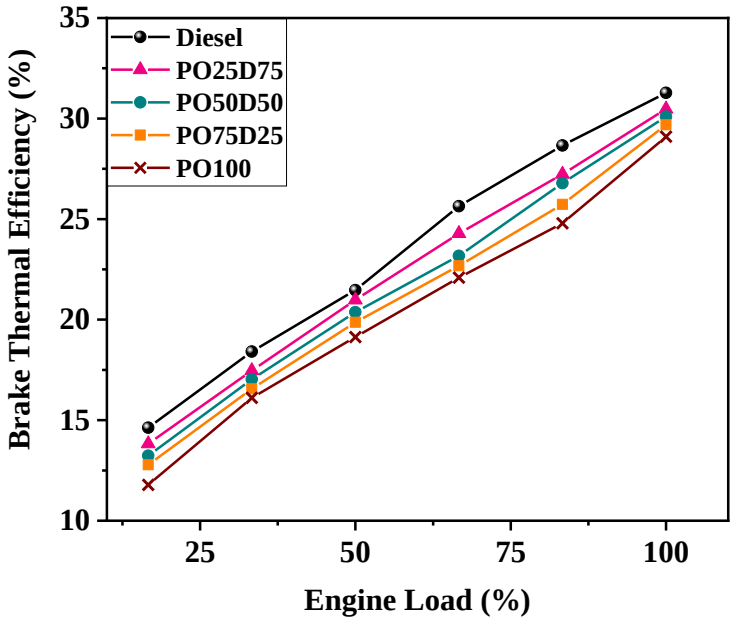

Figure 6.1: Variation in BTE at various engine loads

6.1.1.2 Brake-specific fuel consumption

The BSFC is the ratio of the rate of fuel consumption to the adequate power produced by the engine. The BSFC can also be determined by Equation 6.2. The variation of BSFC at various engine loads is shown in Figure 6.2. The BSFC varies from 0.486 kg/kWh at minimum engine load to 0.357 kg/kWh at higher for reference diesel (D100). Moreover, it varies for plasto oil blends such as PO25D75, PO50D50, PO75D25 and PO100 from 0.501 kg/kWh to 0.369 kg/kWh, 0.517 kg/kWh to 0.378 kg/kWh, 0.537 kg/kWh to 0.387 kg/kWh and 0.558 kg/kWh to 0.391 kg/kWh respectively, which is 3.36%, 5.88%, 8.40% and 9.50% higher than reference diesel. It has been observed that BSFC decreased

with increasing the load. This is caused by the acceleration of the combustion process at higher engine load, attributed to improved fuel atomization, increased fuel mixing, and elevated in-cylinder temperatures, which may elucidate the latter phenomenon of occurrence at higher engine load (Devaraj et al., 2015). Moreover, it has been observed that Plasto oil has higher BSFC than other fuels. This may cause of higher viscosity and lower calorific value of plasto oil, which requires excess fuel to produce the essential heat in the combustion chamber (Saha et al., 2021).

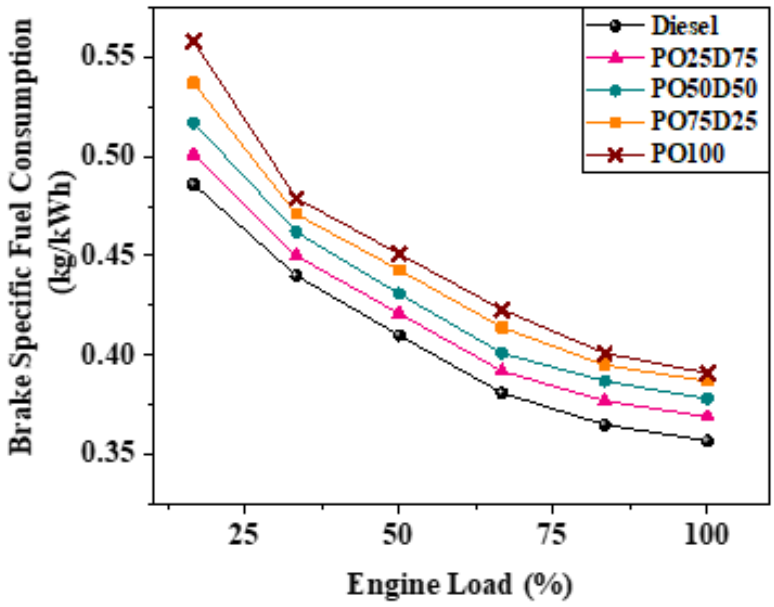

Figure 6.2: Variation in BSFC at various engine loads

Venkatesan et al. probed the effect of the BSFC on plasto oil and diesel blends and found that 30% of plasto oil with diesel has 5-6% higher BSFC than neat diesel. This could be due to higher volatile aromatic hydrocarbon molecules in the plasto oil (H. Venkatesan et al., 2018). Consequently, the air-fuel mixture may not be optimized, leading to higher fuel consumption and an inability to maintain the necessary heat for the brake power output.

$$\text{BSFC} = \frac{\text{mass flow rate (kg/h)}}{\text{brake power (kW)}} \qquad \text{Eqn. (6.2)}$$

6.1.1.3 Exhaust gas temperature

The exhaust gas temperature (EGT) of the plasto oil and diesel blends at different engine loads is shown in Figure 6.3. The EGT of diesel (D100) was 140.11 ^{o}C at a low engine load and reached 310.16 ^{o}C at a high engine load. Similarly, PO and PO-diesel blends increased with various engine loads. EGT increased from 143.91 ^{o}C to 313.09 ^{o}C, 149.05 ^{o}C to 327 ^{o}C, 153.88 ^{o}C to 331.38 ^{o}C and 158.46 ^{o}C to 334.58 ^{o}C for PO25D75, PO50D50, PO75D25 and PO100 respectively at 25% to 100% engine load. It has been found that the higher proportion of the PO increased the EGT and increased with engine load conditions. The average EGT of neat plasto oil is 7.8% higher than the reference diesel at maximum engine load. The reason for increasing EGT was the prolonged combustion process caused by the lower calorific value of the PO than diesel, which required excess fuel to produce the extra power or heat essential to take up the extra engine load

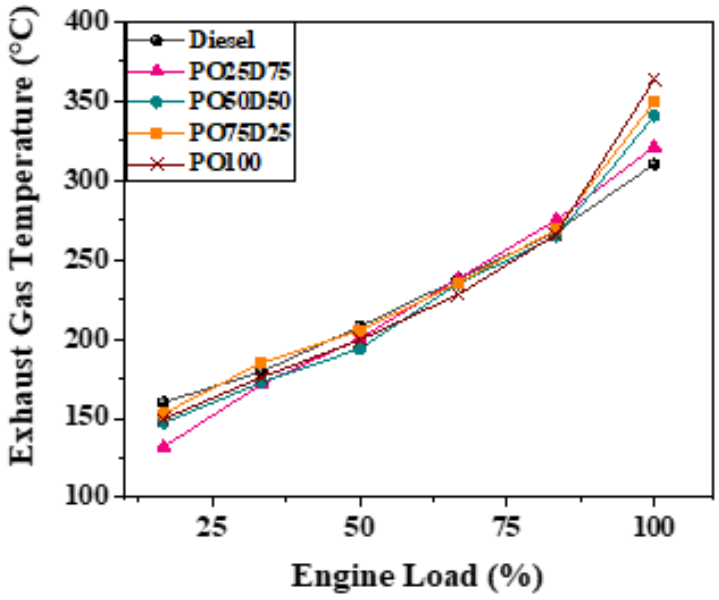

Figure 6.3: Variation in EGT at various engine loads

(Viswanath K. Kaimal et al., 2015). Sachin Kumar et al. evaluated the EGT for the diesel and plasto oil blends and found that a 40% plastic blend with diesel produced 16.33% higher EGT than neat diesel (Kumar et al., 2013). This may

cause lower engine BTE, causing less energy conversion to mechanical output (Shahir et al., 2018).

6.1.2 Engine combustion characteristics

6.1.2.1 Cylinder pressure

In a CI engine, the maximum cylinder pressure (CP) is caused by fuel combustion during the premixed phase, predominantly determined by atomization, vaporization, droplet mixing, and chemical reactions. The deviation of CP with the crank angle of the engine for diesel and plasto oil blends is depicted in Figure 6.4. The higher CP was 54.07 bar/^{o}CA for diesel at a higher engine load. However, cylinder pressure for PO25D75, PO50D50, PO75D25 and PO100 was 52.88 bar/^{o}CA, 53.29 bar/^{o}CA, 54.7 bar/^{o}CA, and 53.01 bar/^{o}CA, respectively, at maximum engine load. Increasing the plasto oil proportion with diesel decreased the cylinder pressure. This could be due to plasto oil blending with the diesel, which increased the viscosity and decreased the self-ignition property.

Consequently, this setup leads to inadequate spray formation and diminished vaporization, which hampers proper combustion, leading to lower peak cylinder pressure in both neat plasto oil and PO-diesel blends (Kaimal & Vijayabalan, 2017; Karishma et al., 2022). The peak CP for all plasto oil blends is delayed and occurs after the top dead center (TDC). The delay is attributed to a deficiency of the fuel for auto-ignition, leading to delays in the combustion process, with the combustion diffusion phase becoming predominant. Furthermore, the lower cetane value contributes to the delay in fuel combustion, which, upon combustion, releases high heat, consequently increasing CP. Additionally, the very identical viscosity of diesel and PO aids in the regulated injection of ignition fuel into the combustion chamber. This facilitates proper mixing of A-F, resulting in enhanced combustion efficiency and increased cylinder pressure. (Rajak et al., 2022). Manigandan Sekar et al. analyzed the effects of PO blends with diesel on the CI engine and found a higher peak pressure of 68 bar/^{o}CA . This could be because of a higher calorific value and viscosity. However, a combination of 25% plasto oil

and 25% Al_2O_3 with 75% diesel achieved 71 bar pressure owing to the better-oxygenated content available in the fuel, which increased the rate of combustion (Sekar et al., 2021).

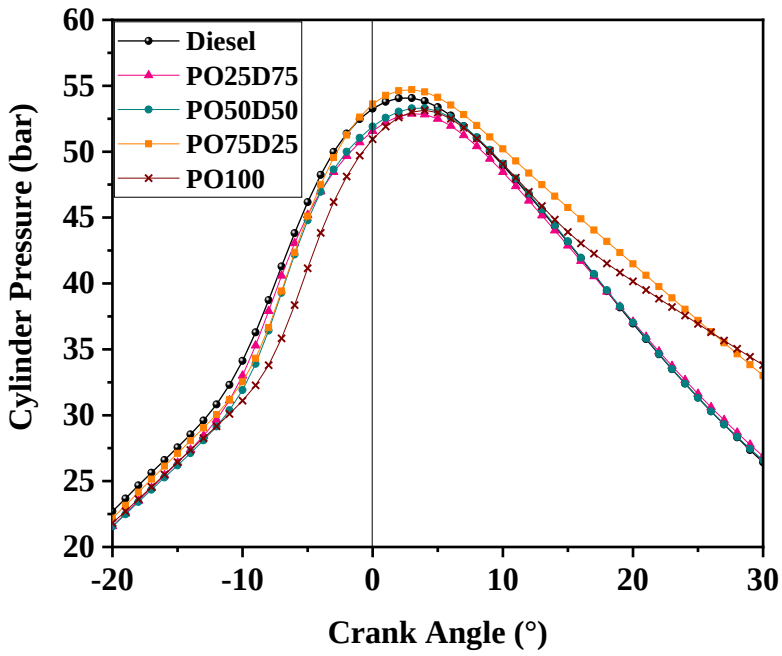

Figure 6.4: Variation of cylinder pressure with various crank angles full engine load

6.1.2.2 Net heat release rate vs crank angle

Figure 6.5 illustrates the net heat release rate (NHRR) for plasto oil and diesel blends at higher engine loads. The heat release curve has two phases: premixed combustion and diffusion combustion. Delayed heat release was observed for PO blends in comparison to diesel, with the duration of heat release being extended for the blends (Thiyagarajan et al., 2019). The maximum NHRR for diesel is 50.5 J/^{o}CA at higher engine load. Increased plasto oil in blends produced a maximum heating rate of 51 J/^{o}CA, 50.5 J/^{o}CA, 53.9 J/^{o}CA and 54.8 J/^{o}CA for 25%, 50%, 75% and 100% respectively at maximum load. This is caused by the high proportion of plasto oil leading to an incomplete combustion and longer ignition delay. The longer delay of ignition time is the primary cause of the higher NHRR of the plasto oil blends. The adiabatic flame temperature increased with increasing

aromatic content, leading to an immediate release of heat (Damodharan et al., 2019). M. Mani et al. studied PO and diesel blends and revealed that the NHRR of plasto oil was 3.2% higher than diesel (Mani et al., 2011).

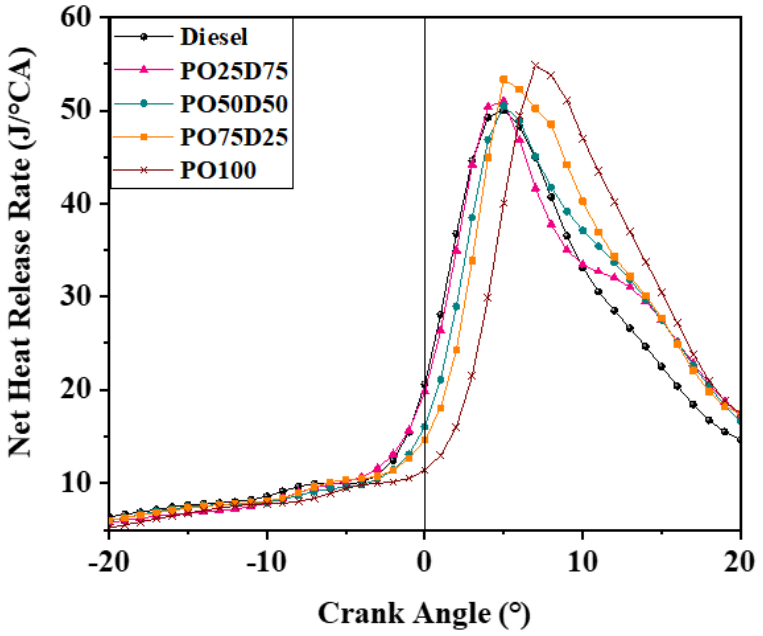

Figure 6.5: Variation of NHRR with various crank angles at full engine load

This may cause of longer ignition delay period. Plasto oil, characterized by its ring structure, contains higher aromatic compounds and a higher adiabatic flame temperature. Additionally, the presence of oxygen in plasto oil, at a concentration of 3.3 wt.%, enhances the combustion process by reducing the cylinder equivalency ratio. However, it's worth noting that the study suggests PO100 may not be suitable for prolonged usage due to its tendency to generate more heat and combust faster, potentially posing a risk of engine failure.

6.1.3 Engine emission characteristics

6.1.3.1 Carbon monoxide

Carbon monoxide (CO) is a byproduct formed during imperfect fuel combustion. The A-F ratio primarily influences CO formation in relation to stoichiometric proportions. Rich combustion conditions lead to the production of CO, with emissions increasing almost linearly to the deviation from stoichiometry

(Kumaravel et al., 2016). The deviation in CO for all fuels at various loads is depicted in Figure 6.6. The result signifies that CO emission is higher for all the plasto oil blends at higher engine loads. It has been observed that CO was 0.02% for diesel at full engine load. However, at maximum engine load, CO emission was 0.03%, 0.034%, 0.04%, and 0.043% at 25%, 50%, 75% and 100% plasto oil fraction. The finding highlights the severe deterioration in combustion observed in PO100 at higher load. This deterioration may stem from lower cetane numbers and higher aromatic compounds in plasto oil, leading to prolonged ignition delay and shorter combustion periods. Hence, incomplete combustion, inadequate mixture preparation, and insufficient oxygen availability are critical factors contributing to CO emission formation (Fiore et al., 2020).

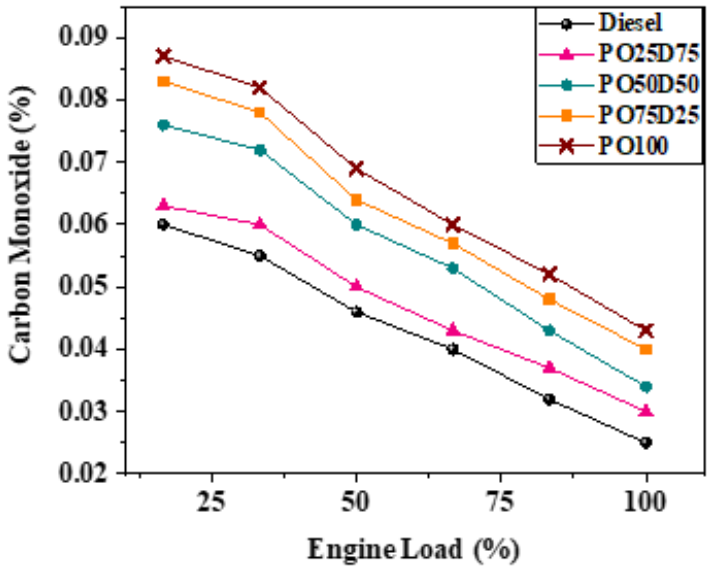

Figure 6.6: Variation of carbon monoxide emissions at various engine loads

Diesel engines exhibit significantly less CO emission owing to their high cylinder temperature and low equivalence ratio. Moreover, the CI engine operates on a lean mixture, lowering CO emissions (R. K. Singh et al., 2020). Venkatesan, S et al. studied plasto oil fueled in CI engine, revealing that plasto oil resulted in a 2.83% higher CO emission than diesel fuel (S. P. Venkatesan et al., 2020). This

may result in insufficient A-F mixture preparation, localized rich zones, and a lack of oxygen compounds in PO.

6.1.3.2 Hydrocarbons emissions

Hydrocarbon (HC) emission formation depends on incomplete fuel combustion, the formation of overly lean mixtures, and low in-cylinder temperatures (Imtenan et al., 2015). Moreover, Viscosity, voltality and cold zones contributed to hydrocarbon emissions. High viscosity promotes large droplets of fuel, while decreased vapour pressure leads to inadequate combustion, thereby increasing the HC emissions. However, low vapour pressure causes inadequate combustion, increasing unburned hydrocarbon emissions. During low loads, the high A-F ratio and low temperatures allow for the simple discharge of unburnt hydrocarbons into the exhaust (Kumar et al., 2013). The deviation in hydrocarbon emission at different engine loads for diesel and PO blends is represented in Figure 6.7. It has been observed that the HC was 18 ppm at a higher engine load for diesel. For plasto oil with blend ratios of 25%, 50%, 75% and 100% shown, the value of 20 ppm, 23 ppm, 31 ppm, and 37 ppm respectively at full engine load. Increasing the plasto oil ratio in diesel leads to an uptick in HC emissions because of incomplete combustion process leftover HC. Two main factors contribute to the generation of hydrocarbons in plasto oil blends. First, the blended plasto oil fails to penetrate deeply into the combustion chamber, leading to fuel buildup along the wall of the cylinder in crevices, where it remains unburnt. Second, unreactive unsaturated hydrocarbons in the fuel persist throughout the combustion process without breaking down, ultimately emitted with the exhaust gases (R. K. Singh et al., 2020; Jacob et al., 2022). Moreover, PO blends may have a higher possibility of impinging on the cylinder wall, cause of their higher viscosity and lower cetane number than diesel. This prolonged igniting delay may cause higher formation of HC emissions (T. S. Singh et al., 2022). In a study on CI engine Sambandam et al. observed that plasto oil emits more HC than diesel. This is caused by the presence of higher aromatic content in PO (Sambandam et al., 2020). This characteristic reduces the duration of combustion and prolongs the ignition delay,

exacerbating the issue of incomplete combustion, and leading to increased UHC emissions.

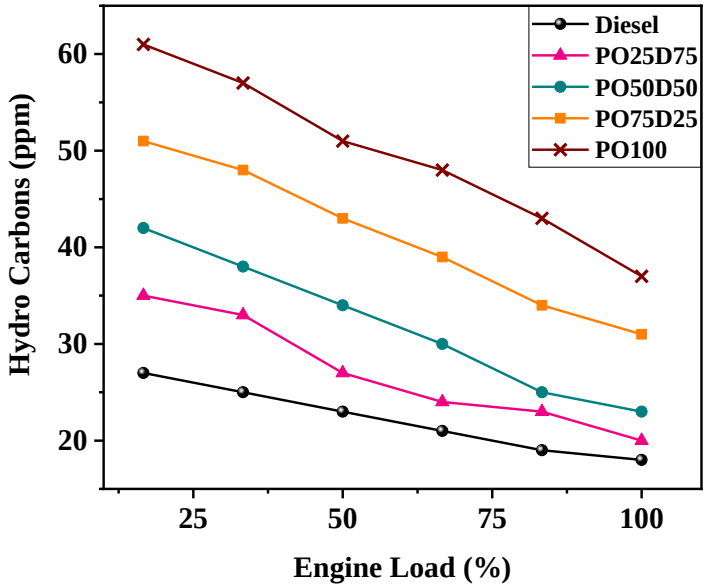

Figure 6.7: Variation of hydrocarbon emissions at various engine loads

6.1.3.3 Carbon dioxide emission

The CO_2 emission formation depends on the fuel combustibility in the combustion chamber. The appropriate fuel combustion, arising from the complete oxidation of carbon atoms within the fuel, causes CO_2 emission. While emission legislation does not regulate it and is not deemed harmful, CO_2 significantly contributes to greenhouse gas emissions and exacerbates climate change (Mariappan et al., 2021). The deviation in CO_2 emission at different engine loads for PO and diesel blends is depicted in Figure 6.8. The higher CO_2 was 13.43% at maximum engine load, for plasto oil blends such as PO25D75, PO50D50, PO75D25 and PO100 produced 12.67%, 11.97%, 10.87% and 10.52 % respectively. It has been observed that diesel produced higher CO_2 emissions by 3.63% than neat plasto oil (PO100). This could potentially lead to incomplete fuel combustion caused by delayed ignition of fuel. Although more fuel is being used in the combustion process at higher engine load, a higher proportion of plasto oil content still results in a reduction in carbon dioxide emissions, indicative of the effectiveness of this

approach in enhancing combustion efficiency. (Pal et al., 2019). Sachin Kumar et al. examined various blends of plasto oil ranging from 10% to 40%. They found that increasing the proportion of PO in diesel decreased carbon dioxide emissions, which are caused by inefficient fuel oxidation (Kumar et al., 2013).

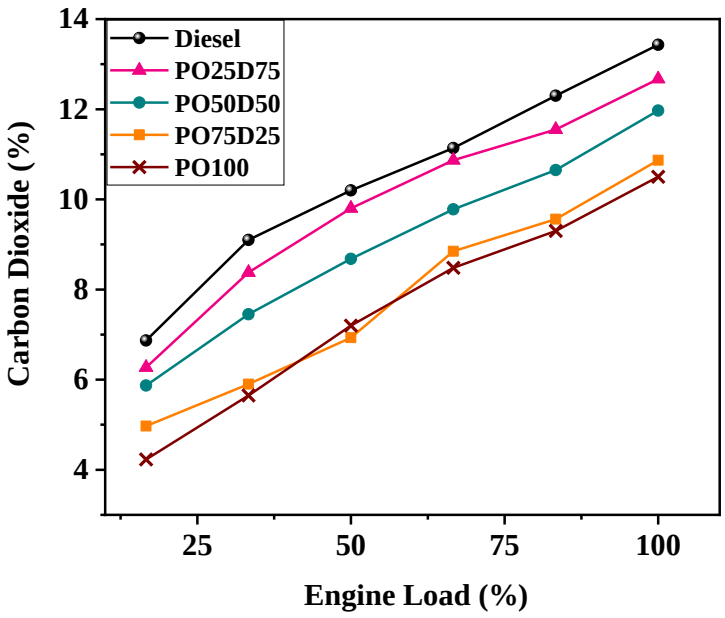

Figure 6.8: Variation of carbon monoxide emissions at various engine loads

6.1.3.4 Oxides of nitrogen

Nitrogen oxide (NO_x) emissions are primarily composed of nitric oxide (NO) and nitrogen dioxide (NO_2). NO_x is formed when nitrogen present in the air is oxidized during the A-F mixture combustion. The ambient temperature and air-fuel ratio are the two important factors influencing nitrogen oxide formation. When combustion is complete, the temperature increases, enabling more free O_2 atoms to interact with N_2 increasing the rate of NO_x formation (Zhu et al., 2011), (Damodharan et al., 2019). However, increased NO_x emissions result from the thermal process triggered by the heightened cylinder temperature and fuel oxygen concentration (Bhurat et al., 2021). The deviation of NO_x emissions with varying engine loads for plasto oil blends is depicted in Figure 6.9. The NO_x emission was 367 ppm for the diesel at higher engine load. However, an increasing proportion of the plasto oil produced 306 ppm, 387 ppm, 427 ppm and 481 ppm for

PO25D75, PO50D50, PO75D25, and PO100, respectively. NO_x emission produced by neat plasto oil was 31.06% higher than diesel at maximum engine load.

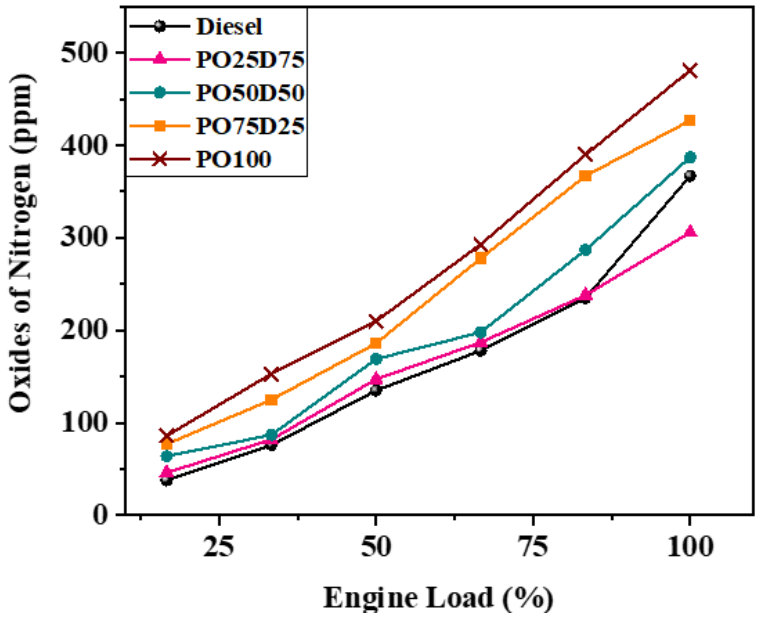

Figure 6.9: Variation of NO_x emissions at various engine loads

This is caused by the oxygenated compounds resulting in proper fuel combustion and increased NO_x formation (İlkil et al., 2012). Kalargaris et al. reported higher NO_x emissions for plasto oil and diesel blends. The study observed that plasto oil produced 2% higher NO_x than diesel fuel. This is caused by the higher amount of premixed combustion and nitrogen in the plasto oil, contributing to increased NO_x formation (Kalargaris et al., 2017).

6.1.3.5 Smoke opacity

Smoke opacity is composed of solid soot particles suspended in the exhaust gases. The deviation in the smoke opacity formation with various engine loads for plasto oil and diesel blends is illustrated in Figure 6.10. The result signifies that diesel produced 53.60% smoke opacity at full engine load. However, an increasing proportion of the plasto oil produced 52.5%, 52.1%, 51.93% and 51.20% smoke opacity for PO25D75, PO50D50, PO75D25, and PO100 respectively at maximum

engine load conditions. The smoke opacity generated by plasto oil was diminished by 4.47% than diesel. The smoke is influenced by carbon atoms and the volume of fuel injected.

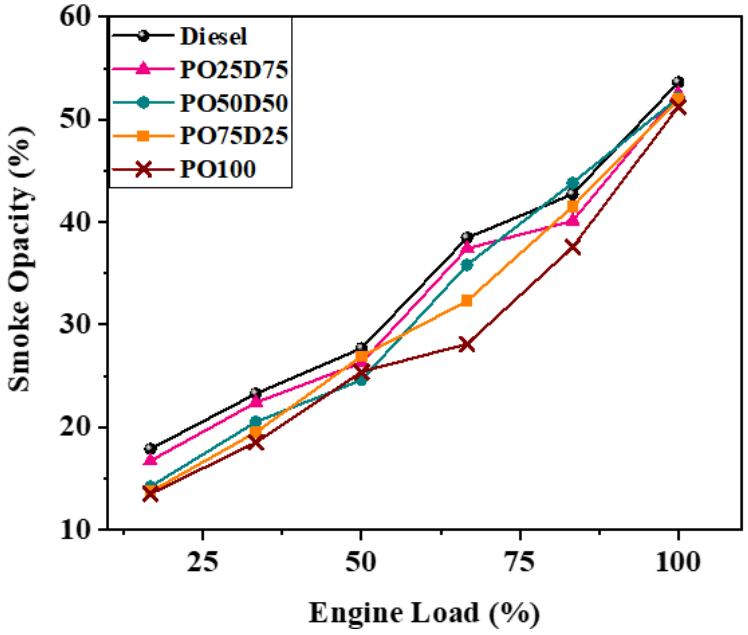

Figure 6.10: Variation of smoke opacity at various engine loads

Plasto oil typically contains fewer aromatic groups than diesel, which may lead to a reduction in soot particles caused by a lower concentration of compounds in the plasto oil (Khairil et al., 2020). Another contributing aspect could be that plasto oil contains naphtha and shorter carbon chain compounds, which may affect the formation of soot particles in the exhaust. Arjharn et al. studied the plasto oil in a CI engine and revealed that diesel produced 16% more smoke opacity than plasto oil. This difference may be due to the combustion of aromatic compounds in diesel compared to the lower concentration of such compounds in plasto oil (Arjharn et al., 2022).

6.2 Investigation of PCCI engine characteristics with plasto oil heavy (POH)

The experiments were performed on plasto oil heavy (POH) blending with diesel as a fuel in conventional CI and PCCI engines at Apex Innovation Pvt. Ltd. Sangli, Maharashtra. The POH blends with diesel as follows: POH10D90 –

comprising 10 vol.% POH with 90 vol.% diesel and POH20D80 comprising 20 vol.% POH with 80 vol.% diesel. Initially, diesel, POH10D90 and POH20D80 fuels were used in conventional CI engine mode without EGR and 10% EGR. However, in the PCCI engine mode, a fuel vaporizer was used to vaporize the POH and obtain the homogenous air-fuel mixture by the external mixture formation approach. The PCCI engine was run with two fuel vapour rates of 2 ml/min and 3 ml/min as a pilot injection (PI) with diesel, POH10D90 and POH20D80 as direct injection (DI) without EGR and with 10% EGR at different engine loads. The governor regulated the fuel's direct injection and maintained the constant engine speed. The start of pilot injection (SoPI) was 40^{o} bTDC, and the main injection (direct injection) was 24^{o} bTDC.

6.2.1 Engine performance

6.2.1.1 Brake thermal efficiency

The deviation in BTE at different engine loads in conventional CI engine mode (direct injection) and PCCI mode is shown in Figure 6.11**.** It is evident that BTE increased with increasing the engine load, which demonstrates the combustion process's ability to efficiently transform the fuel energy into mechanical output while minimizing heat loss (Rajak et al., 2020). Initially, diesel, POH10D90 and POH20D80 were employed in the conventional CI engine mode operation and produced BTE were 30.37%, 29.97% and 29.58% respectively at maximum engine load. It was noted that POH1OD90 and POH20D80 produced lower BTE by 1.31% and 2.60% than reference diesel. This may be caused by the lower calorific value of POH-diesel blends. Moreover, EGT and heat release rate demonstrated an increase for the blends at a full engine load. This may lead to higher heat loss and lower BTE (Arunkumar et al., 2019). Combining 10% EGR, BTE was 28.98%, 28.75%, and 28.24% for diesel, POH10D90, and POH20D80 respectively. It was noted that BTE was reduced with EGR due to the O_2 deficiency in the combustion chamber caused by replacing the fraction of air with exhaust gas (Ganesh et al., 2008; Pathak et al., 2021). Figure 6.11 (a) illustrates that neat diesel brake thermal efficiency was 30.37% at maximum engine load in

conventional CI engine mode operation. However, 2 and 3 ml/min fuel vapour induction with DI of diesel showed minimum penalty of BTE, which decreased by 2.96 % and 4.64 % respectively, compared to the diesel-fueled in conventional mode at higher engine load. Combining 10% of EGR with 2 and 3 ml/min POH vapour reduced BTE by 9.41% and 11.19% respectively, at higher engine load. Figure 6.11 (b) and (c) shows the BTE of POH10D90 and POH20D80 was 28.75 % and 28.24% respectively. The BTE produced by the induction of 2 ml/min and 3 ml/min POH vapour with POH10D90 (DI) decreased by 3.42% and 6.33% respectively at higher engine load than POH10D90 used in conventional engine mode. Similarly, introducing the 2 and 3 ml/min POH vapour with POH20D80 (DI) reduced the BTE by 4.63% and 7.20% respectively at full engine load compared to the fuel POH20D80 used in a conventional engine.

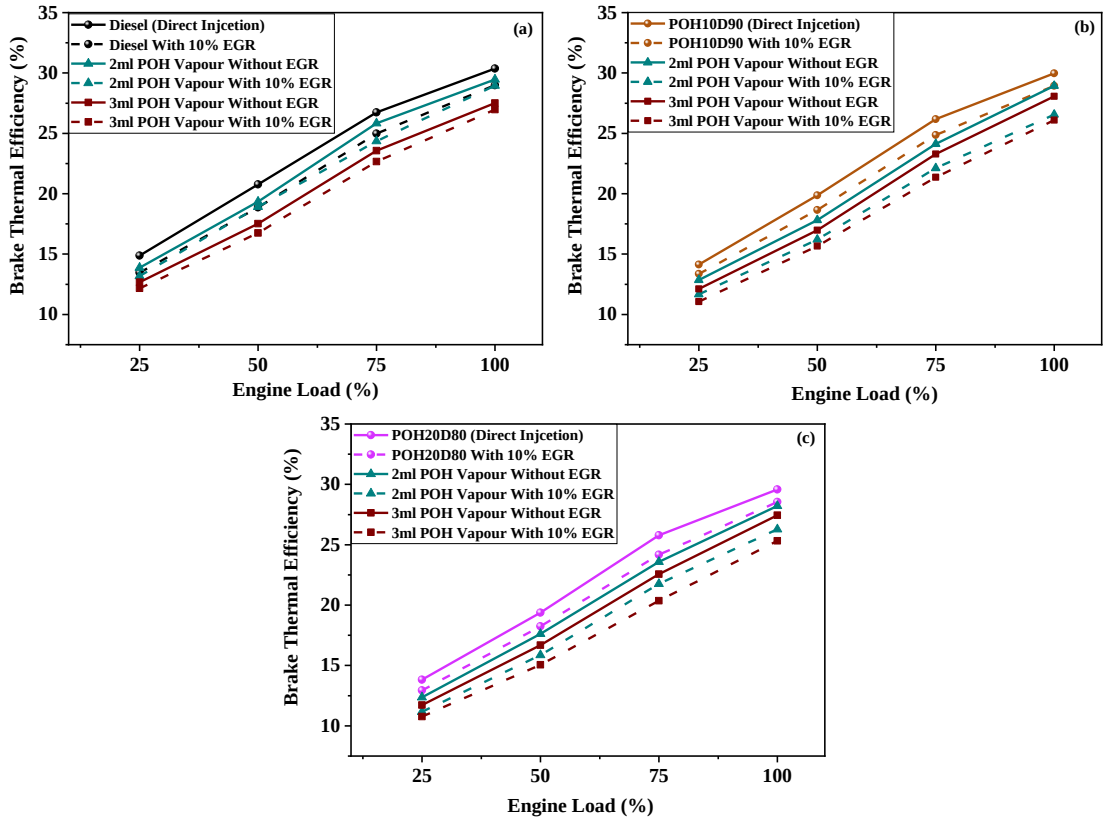

Figure 6.11: Deviation in brake thermal efficiency at increasing engine loads(a) Diesel (b) POH10D90 (c) POH20D80

It has been observed that introducing the POH vapour decreased the BTE for diesel, POH10D90 and POH20D80. This could be due to the external mixture of POH vapour and air in the intake manifold. which could undergo condensation due to the difference in temperature between the two fluids (intake air and POH vapour). Consequently, reduced fuel availability ensues, impacting charge formation and resulting in a decline in BTE with PCCI combustion (Ganesh et al., 2011). The BTE decreased with increasing the vapour induction, leading to increased fuel dilution. At higher engine load BTE for 2 and 3 ml/min POH vapour with POH10D90 and POH20D80 was lowered by 11.37% and 12.24%, 11.01% and 13.11% respectively with 10% EGR as compared to the POH10D90 and POH20D80 fuel in conventional DI mode. Exhaust gases reduce the average combustion temperature within the combustion chamber, resulting in decreased BTE across all engine loads (Jayabal et al., 2020). However, the external mixture formation of POH vapour and air adds diluting elements that lower the essential combustion circumstances and adversely affect the BTE.

6.2.1.2 Exhaust gas temperature

The exhaust gas temperature (EGT) variation with different engine loads for conventional CI engine and PCCI engine modes is shown in Figure 6.12 (a), (b) and (c). EGT increases with increasing the engine load. The increase in EGT signifies the higher energy required to produce the substantial engine power required to handle the additional load. The EGT of an engine is affected by oxygen content and fuel cetane number (Kumar et al., 2013). In conventional CI engine mode, the maximum EGT was 384.47 ^{o}C produced by the POH20D80, which was 4.16% and 6.88 % higher than the POH10D90 and diesel respectively at maximum engine load. The higher EGT could be attributed to the engine's lower BTE. The lower thermal efficiency indicates that less energy input from the fuel gets converted into mechanical output, leading to higher EGT (Nagarajan et al., 2002). However, EGT decreased by 6.16%, 20.63% and 19.3% for diesel, POH10D90 and POH20D80 respectively by introducing the 10% EGR at higher engine load. Figure 6.12 (a) depicted that EGT for 2 and 3 ml/min of POH vapour

with diesel (DI) was 331.99 ºC and 290.8 ºC respectively, which was 7.97% and 18.97 % lower than the diesel fuel in conventional CI engine. EGT was reduced by 22.63% and 31.61% at higher engine load for 2 and 3ml POH vapour with 10% EGR. This could be due to the presence of non-reactive inert gases such as CO_2 and water vapor, which possess relatively higher heat capacities than other constituents of exhaust gas and absorb the heat generated during combustion. Consequently, they lower the cylinder's overall temperature (Agarwal et al., 2013). Figure 6.12 (b) depicts the EGT for POH10D90 and POH20D80 with engine load. It has been observed 2 and 3ml POH vapour induction with POH10D90 EGT decreased by 25.63% and 31.87% respectively than the POH10D90 fueled in conventional CI engine.

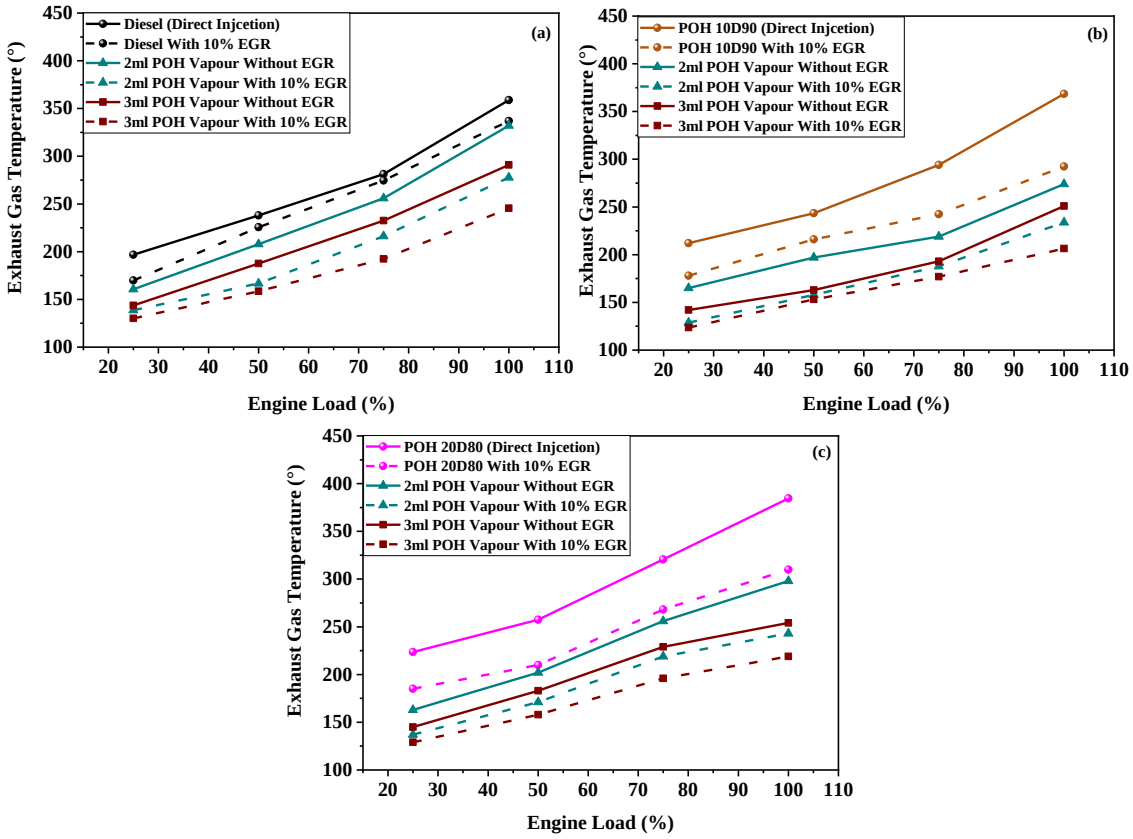

Figure 6.12: Deviation in exhaust gas temperature at increasing engine loads (a) Diesel (b) POH10D90 (c) POH20D80

Similarly, Figure 6.12 (c) illustrated that for 2 and 3 ml POH vapour induction with POH20D80 EGT was reduced by 22.40% and 33.93% at higher engine load as compared to the conventional engine mode operation with POH20D80 fuel. It was noted that EGT reduced in PCCI mode due to the lean A-F mixture, which leads to a lower combustion temperature (Bhurat et al., 2022). However, at maximum engine load, 2 and 3 ml/min induction of POH vapour with POH10D90 reduced the EGT by 36.56% and 43.90% respectively with 10% EGR as compared to the POH10D90 in conventional CI engine mode. Similarly, direct injection of POH20D80 with 2 and 3 ml/min EGT was reduced by 36.79% and 43.03% respectively with 10% EGR. This may cause a lean A-F mixture, which lowers the combustion peak temperature. POH vapour enhanced homogeneity, initially EGT was reduced due to the lean air-fuel charge decreasing the combustion temperature (Ganesh et al., 2008). However, the intake air temperature causes a phase shift that precludes contribution to fuel combustion. Combining of EGR contributes to charge dilution, resulting in a lean A-F mixture (Agarwal et al., 2013).

6.2.1.3 Volumetric efficiency

Volumetric efficiency (VE) depicts the engine breathing capacity, which is influenced by the exhaust gas recirculation and the vapour induction. The deviation in the VE with respect to the engine load is shown in Figure 6.13. It has been observed from the trends that VE is reduced when the POH vapour and EGR rates are increased. In a conventional CI engine, air flows through the manifold during the suction stroke. However, charge formation takes place during fuel is injected into the combustion chamber at the compression stroke. The intake air fills the whole space in the manifold, resulting in high VE. However, the short duration of charge mixing leads to the incomplete utilization of the intake air during combustion and leaving a significant amount of the air ineffective.

In Conventional CI engine mode, a study of diesel, POH10D90 and POH20D80 was carried out and it has been observed that volumetric efficiency was 81.23%,

78.34% and 77.39% at minimum engine load, which decreased by ~2 % at higher engine load for diesel, POH10D90 and POH20D80 respectively. It is noted from the trends that VE decreased by increasing the engine load. This is caused by the cut-off ratio increase, which leads to a gradual, continuous reduction in volumetric efficiency (R. K. Singh et al., 2020). Moreover, the lesser calorific value of the fuel increased fuel consumption and generated high heat and pressure to sustain engine power. Consequently, this results in a reduction in volumetric efficiency for maximum engine load conditions (R. K. Singh et al., 2019). At higher engine load, volumetric efficiency has decreased by 9.95%, 9.22% and 9.10% for diesel, POH10D90 and POH20D80 respectively with 10% EGR. EGR reduces the oxygen availability for combustion, lowers the peak temperature in the engine cylinder and affects the density of the A-F mixture, causing a reduction in volumetric efficiency (Saha et al., 2021). Figure 6.13 (a), (b) and (c) illustrated that in PCCI mode, 2 and 3ml/min induction of POH vapour with diesel reduced the volumetric efficiency by 2.26% and 6.45%, at a higher load than conventional CI mode operation with diesel fuel. However, direct injection of POH10D90 with 2 and 3 ml induction of POH vapour reduced the volumetric efficiency by 2.97 and 7.28% compared to POH10D90 fueled in a conventional CI engine. Similarly, for the POH20D80 volumetric efficiency was found to be 3.70% and 8.16% lower for 2ml and 3ml/min POH vapour induction compared to conventional engines operated with POH20D80 fuel.

However, combining 10% EGR in PCCI engine mode, volumetric efficiency decreased by 13.33% and 15.22% with varying POH vapour from 2 to 3 ml/min with diesel at maximum engine load compared to conventional CI engine fueled with diesel. Similarly, POH10D90 with 2 and 3ml induction of POH vapour reduced the volumetric efficiency by 11.71% and 15.63% respectively with 10% EGR compared to the POH10D90 in a conventional CI engine. However, in the PCCI engine, POH20D80 (DI) with 2 and 3ml induction of POH vapour reduced the volumetric efficiency by 13.06% and 16.80% respectively with 10% EGR as compared to the POH20D80 fueled in a conventional CI engine. It is evident from

the trends that EGR has a more significant impact on the reduction in VE, which is higher than the POH vapour induction with fuel. In PCCI mode, the volume of fuel vapour in the intake manifold, along with the additional space taken up by recirculated exhaust gas, restricts the intake airflow rate, lowering volumetric efficiency (Alemayehu et al., 2022). Pre-mixing starts with the suction stroke and lasts until the combustion starts, allowing for a longer time of homogenous charge generation. Unlike conventional (DI), this process eliminates excess air, contributing to high NO_x emissions .

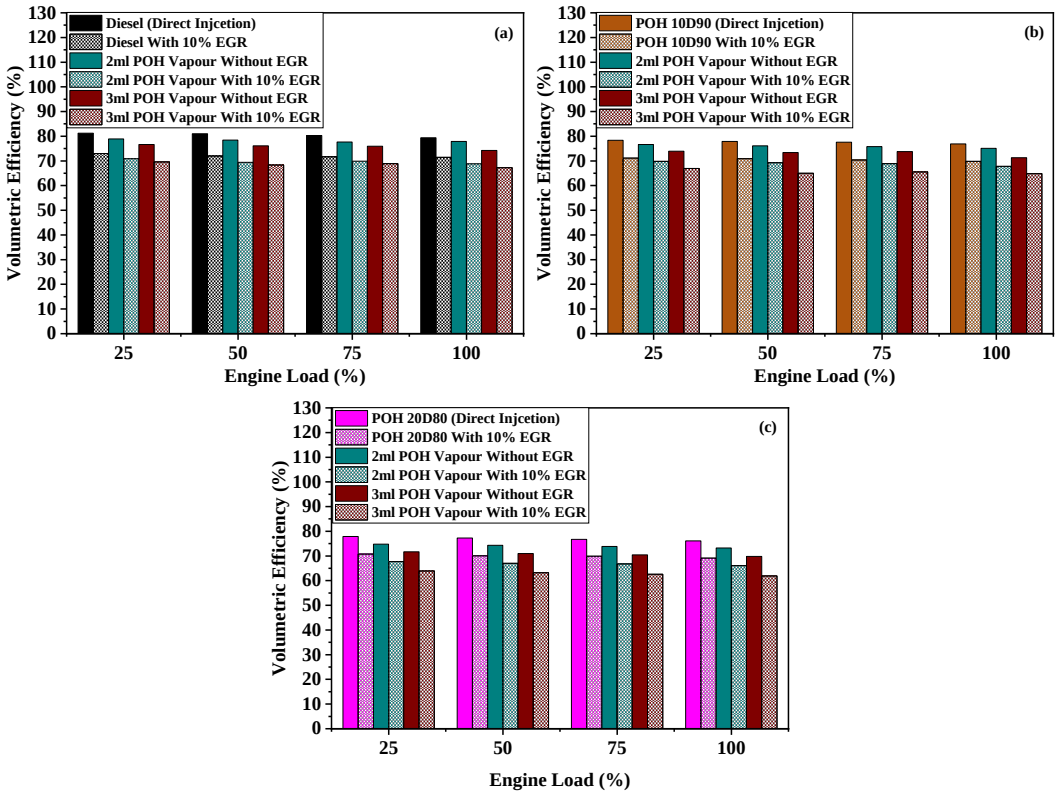

Figure 6.13: Deviation in volumetric efficiency at increasing engine loads (a) Diesel (b) POH10D90 (c) POH20D80

6.2.2 Engine combustion characteristics

6.2.2.1 Cylinder pressure vs crank angle

The fuel burning rate significantly influences the combustion pressure within the engine cylinder during the premixed phase. Figure 6.14 (a), (b) and (c) show the variation in peak cylinder pressure (CP) with various crank angles. In conventional engine mode, the Higher peak pressure was 68.87 bar produced by the POH20D80 followed by 67.89 bar and 66.86 bar for the POH10D90 and diesel at higher engine load conditions. It has been observed that CP increased on increasing the proportion of the POH in diesel. This may cause the lower calorific value and lower cetane number, which require more fuel at the same time to achieve the desired engine power (Sayin et al., 2010). However, introducing the 10% EGR at high engine load cylinder pressure tends to decrease by 4.84%, 4.08 and 3.85 % for diesel, POH10D90 and POH20D80 respectively, compared to without EGR engine operation. This could be because the recirculated exhaust gases lower the combustion chamber cylinder charge temperature by acting as a heat-absorbing agent (Mani et al., 2010). In PCCI engine mode, 2ml and 3ml POH vapour induction with diesel (DI) is shown in Figure 6.13 (a). It has been observed from the trend that increasing the POH vapour quantity from 2ml to 3ml cylinder pressure reduced by 3.02 and 5.29% respectively than diesel in conventional CI mode at maximum engine load. Similarly, Figure 6.13 (b) depicted the 2 and 3ml POH vapour with POH10D90 as the main fuel injection reduced the CP by 5.80% and 7.27% respectively at maximum engine load than POH10D90 in conventional CI engine mode. Similarly, 2 and 3 ml POH vapour with direct injection of POH20D80 reduced the cylinder pressure by 2.91 and 4.31% respectively at full engine load, compared to the POH20D80 fueled in conventional CI engine mode.

However, combining 10% of EGR with 2ml and 3ml of POH vapor reduced the cylinder pressure by 8.82 to 11.02 % for POH10D90 and 9.29 to 13.67% for POH20D80 at full engine load condition as compared to the POH10D90 and POH20D80 fueled in conventional CI engine respectively. POH vapour induction

contributes significantly to peak pressure reduction. Increased diesel vapour amount results in a change in peak in-cylinder pressure closer to TDC. Ganesh et al. (Ganesh et al., 2008) studied diesel fuel vapour in HCCI engine mode. They showed that peak cylinder pressure was obtained at TDC with the induction of diesel vapour, which showed better mixture formation in PCCI engine mode than conventional CI. However, increasing the POH vapour beyond 3ml deviates from the combustion process and may tend to lean towards the rich mixture, causing the A-F mixture to pre-ignite. This might raise the peak in-cylinder pressure during combustion. The study conducted on full vapour induction is not allowed to operate the engine at full engine load (Bhiogade et al., 2016).

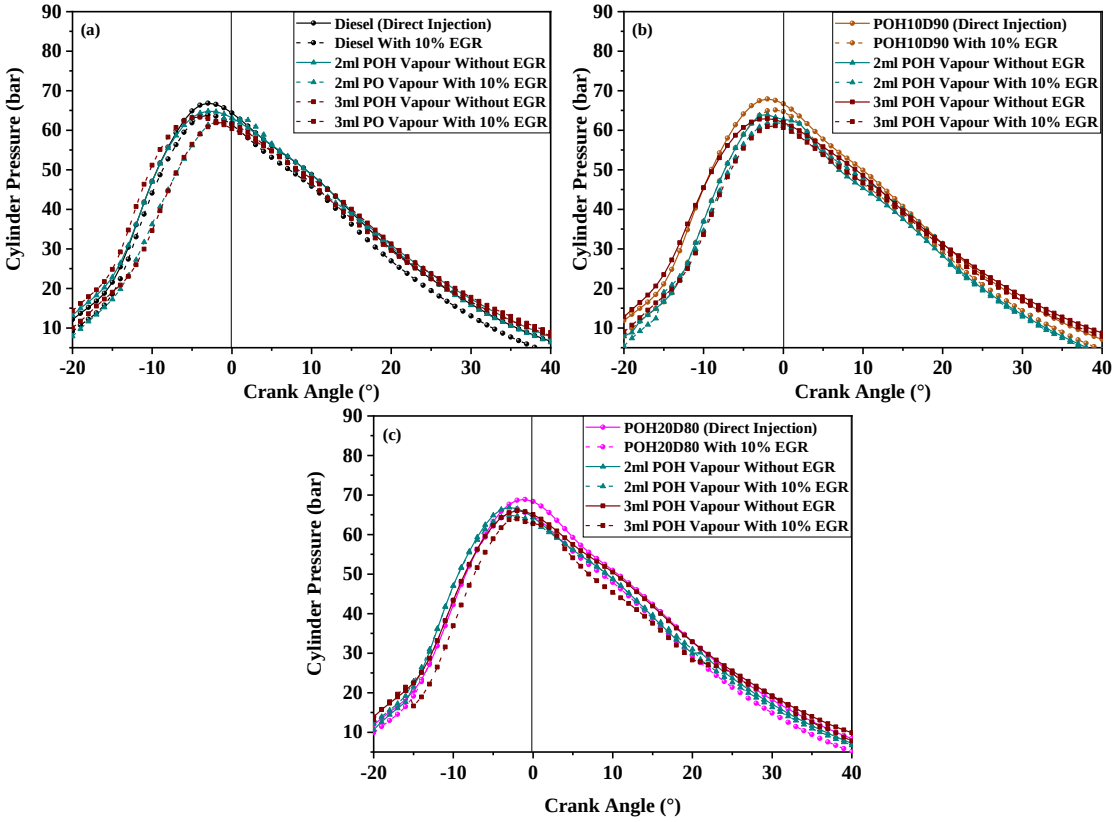

Figure 6.14: Deviation in cylinder pressure with the crank angles at higher engine load (a) diesel (b) POH10D90 (c) POH20D80

6.2.2.2 Net heat release rate

The engine exhibits a high heat release rate caused by the injection process, followed by atomization, vaporization, and mixing of fuel. Figure 6.15 (a), (b) and (c) depicted the deviation of NHRR with crank angle. In conventional CI engine mode, NHRR was 51.46 J/^{o}CA, 52.38 J/^{o}CA and 54.55 J/^{o}CA for diesel, POH10D90 and POH20D20 respectively at full load. It has been found that the heat release rate increased by increasing the POH proportion. This may be due to the heterogeneity of POH fuel. A high heat release rate results from the accumulation after flame generation and the formation of a rich air-fuel mixture near the injector (Arunkumar et al., 2019). Figure 5.15 (a) illustrates that in PCCI engine mode, NHRR was 48.53 and 45.82 J/^{o}CA for 2 ml and 3 ml POH vapour induction with diesel (DI) at higher engine load. However, combining 10% EGR NHRR was reduced by 8.23% and 17.75% in PCCI engine mode than conventional CI engine fueled with diesel. Figures (b) and (c) depicted that, in PCCI mode for 2ml and 3ml POH vapour induction with POH10D90, NHRR was 48.89 and 44.91 J/^{o}CA. However, for 2ml and 3ml POH vapour induction with POH20D80, NHRR was 50.48 and 46.16 J/^{o}CA with POH20D80, which was reduced by 7-15% approximately than the referenced fuel in conventional CI engine mode operation at higher load.

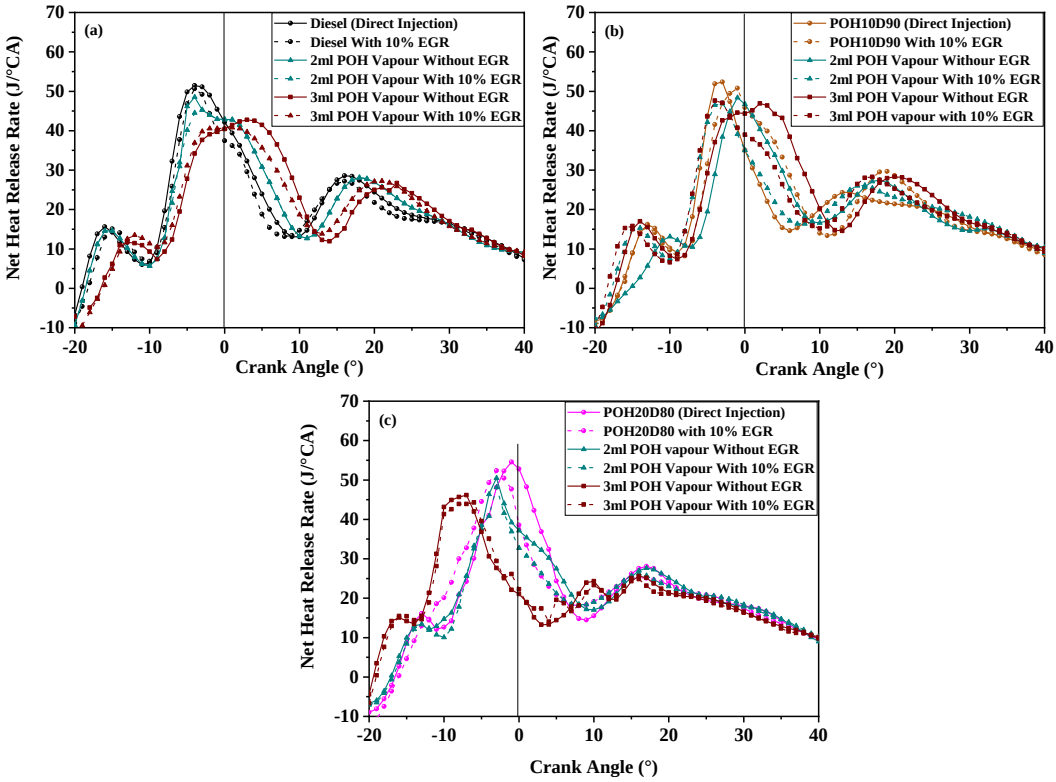

Figure 6.15: Deviation in NHRR with the crank angles at higher engine load (a) Diesel (b) POH10D90 (c) POH20D80

The gas-to-gas diffusion in the fuel induction approach reduces the delay period caused by heterogeneity. Additionally, the limited entry of direct injection (DI) fuels through injection prevents the formation of rich mixtures, resulting in a lower NHRR (Bhurat et al., 2022). At higher engine load, NHRR reduced by 10.42% and 17.92% for 2ml and 3ml vapour induction with POH10D90 (DI) than POH10D90 fueled in a conventional engine. Similarly, NHRR was reduced by 11.69% and 18.77% for 2ml and 3ml POH vapour induction with POH20D80 as compared to the POH20D80 fueled in a conventional engine. It was noted that introducing the 10% EGR reduced the NHRR significantly in conventional CI and PCCI engine. This could be due to the replacement of oxygen by CO_2 reducing oxygen concentrations in the combustion chamber. Consequently, there is a prolonged ignition delay, allowing more time for fuel and oxygen to mix, potentially increasing pre-mixed fuel quantity. However, the reduction in oxygen

content diminishes the intensity of pre-mixed fuel combustion and reduces the NHRR (Ladommatos et al., 1998).

6.2.3 Engine emissions

6.2.3.1 Carbon Monoxide

The variation in CO with varying engine loads for conventional and PCCI mode are depicted in Figure 6.16. The incomplete combustion of fuels leads to increases the CO emissions during the combustion due to lower O_2, inadequate air mixing, and incomplete preparation of the A-F mixture. Carbon monoxide emission poses a hazard and requires regulation since it is a byproduct of incomplete combustion and is an intermediate in the combustion process (Agarwal et al., 2015). In conventional CI engine, CO emission produced by the diesel, POH10D90 and POH20D80 was 0.07%, 0.08 and 0.084% respectively at full engine load condition. It has been found that increasing the POH blends with diesel produced higher CO emissions. The lack of oxygen molecules in POH causes incomplete combustion and increases the formation of CO emissions (Sayin et al., 2011). However, at higher engine load, CO emission was 0.084%, 0.07 and 0.1 %, with 10% EGR for diesel, POH10D90 and POH20D80, respectively. Figure 6.16 (a) depicts the PCCI engine mode operation with diesel with 2 ml and 3 ml POH vapour induction. It has been observed from the trend that 2ml and 3ml POH vapour induction increased CO emission by 0.097% and 0.112% respectively. While using the 10% EGR with varying POH vapour, CO emission increased by 0.127% and 0.134% respectively at maximum engine load. Similarly, Figure 6.16 (b) shows the trend of 2ml and 3ml POH vapour induction with POH10D90 produced CO was 0.10% and 0.119% at higher engine load. However, Figure 6.16 (c) depicts that CO was 0.106% and 0.120% for 2 ml and 3 ml POH vapour POH20D80 respectively. It has been observed that CO was higher with increasing POH vapour at all loads. This may cause an increase in the homogeneity of POH vapours, but it also reduces the volumetric efficiency, altering the required air-fuel ratio and leading to inadequate combustion (Bhurat et al., 2022).

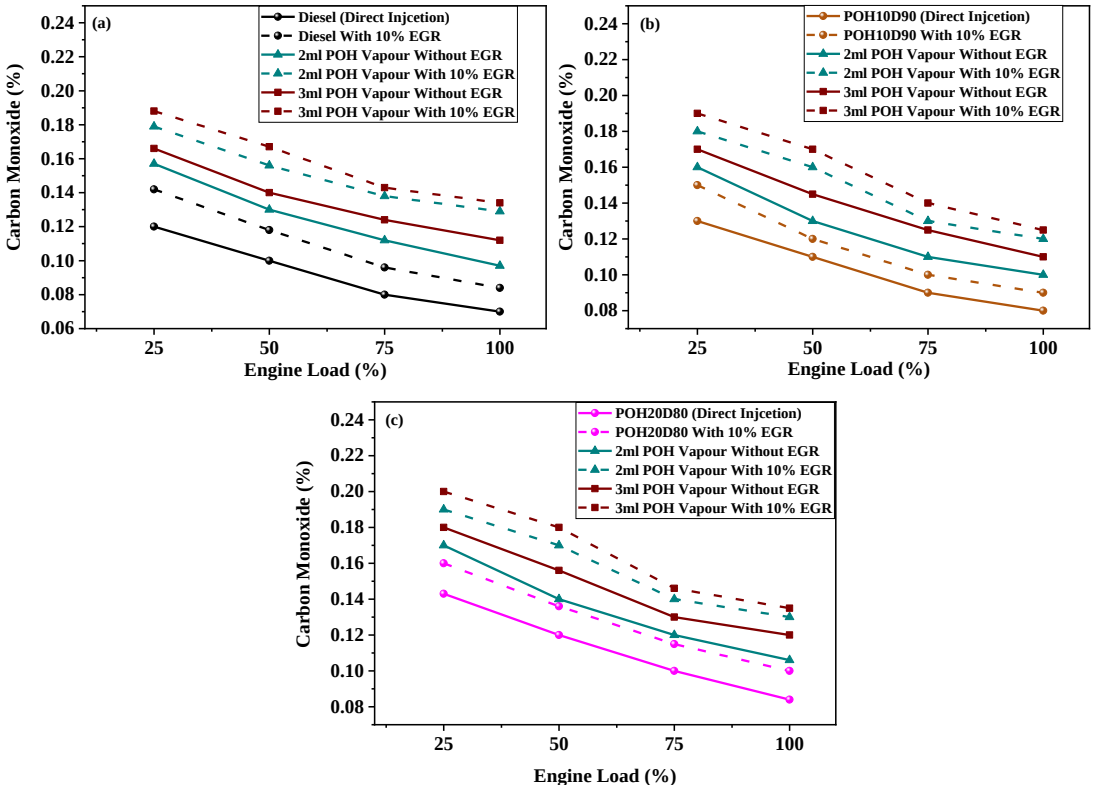

Figure 6.16: Deviation in carbon monoxide at increasing engine load (a) Diesel (b) POH10D90 (c) POH20D80

At higher engine loads, combining 10% EGR the CO was increased in PCCI engine mode operation at all engine loads. It is evident that as engine load increases, the air-vapour ratio adjusts to optimize combustion, resulting in less variance in emissions at part load, mid load, and low load conditions. However, at low load, the Exhaust gas recirculation (EGR) system inhibits airflow, resulting in excess fuel vapour and poor combustion conditions. Consequently, this scenario contributes to higher CO emissions (Bhurat et al., 2021).

6.2.3.2 Hydrocarbons

The principal source of HC emissions is flame extinction in the cold combustion chamber along the cylinder walls. These emissions are also affected by the viscosity and volatility of the fuel. High viscosity results in larger droplet size and reduces the vapour pressure. HC emissions refer to the incomplete combustion of

fuel. At low load, the excess flow of air, low EGT, and lean A-F mixture areas may survive and escape into the exhaust and contribute to HC emission (Korakianitis et al., 2011). Figure 6.17 depicts the deviation in HC emission with varying engine loads for conventional CI and PCCI engine. Conventional CI engine hydrocarbon emission was 31 ppm for diesel at higher engine load. However, HC emissions increased by 3.22% and 6.45% for POH10D90 and POH20D80, compared to the diesel. This could be due to the unsaturated HC in the fuel causing a longer duration of combustion and leading to incomplete combustion. This occurs because these hydrocarbons release more unburned fuel into the exhaust tailpipe without actively participating in combustion (T. S. Singh et al., 2020). In Figure 6.17 (a), hydrocarbon emissions recorded 33 ppm and 35.8 ppm without EGR and 36.9 ppm and 38.87 ppm with 10% EGR at higher engine load for 2 and 3 ml of POH vapour induction with diesel (DI). Figure 6.17 (b) and (c) show that HC emission was 35.6 ppm and 38 ppm without EGR and 38.7 ppm and 39.8 ppm with 10% EGR for 2 ml and 3 ml induction of POH vapour with POH10D90 at full engine load. However, on increasing the POH blend up to 20 vol.% with 80 vol.% diesel, HC emission was 36 ppm and 39 ppm without EGR and 40.2 ppm and 42.6 ppm with 10% EGR. It is noted that introducing partial fuel vapors increases hydrocarbon emissions. However, HC and CO emissions are the significant drawbacks of fuel vapour induction in combustion, which lowers the combustion temperature due to the lean mixture and produces higher HC emissions (Juttu et al., 2007). EGR plays a significant role in HC emission formation and has dual impacts on HC emissions. Firstly, introducing some unburnt HC from exhaust gas into the subsequent cycle reduces HC emissions. Secondly, lowering the combustion temperature within the cylinder elevates HC emissions (Megaritis et al., 2013).

.

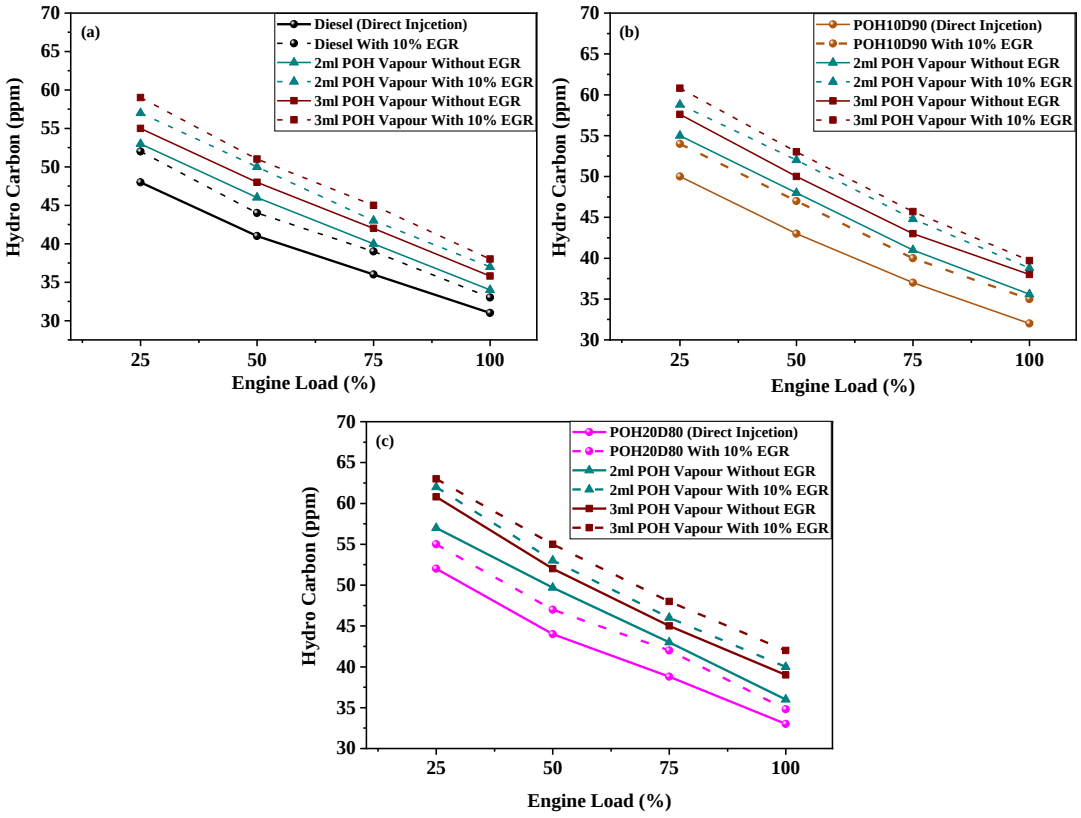

Figure 6.17: Deviation in hydrocarbons at increasing engine load (a) Diesel (b) POH10D90 (c) POH20D80

6.2.3.3 NO_x emissions

Nitrogen oxide emissions contain nitric oxide (NO) and nitrogen dioxide (NO_2) Nitrogen oxide is generated by the oxidation of nitrogen in the air during combustion. The A-F ratio and ambient temperature mainly influence the production of nitrogen oxides. Adequate burning raises the temperature, allowing more free oxygen atoms to react with nitrogen and increasing the rate of nitrogen oxide production. Figure 6.17 (a), (b), and (c) depicted the deviation of NO_x with various engine loads for CI and PCCI engine modes. In conventional CI engine, NO_x was 417 ppm for diesel at higher engine load, while the NOx produced by the POH10D90 and POH20D80 was 2.15% and 5.03% higher than diesel at higher engine load. It was observed that NO_x was higher with POH blends. This

may be due to oxygenated hydrocarbons, which lead to proper combustion and increase the NO_x formation (Maithomklang et al., 2020). However, NO_x formation decreased by 6.47%, 5.27% and 3.35%, respectively, with 10% EGR for diesel, POH10D90 and POH20D80 as compared to diesel at maximum engine load. This may cause of replacement of O_2 molecules by CO_2 in the combustion chamber, which lowers the combustion temperature and reduces NO_x formation (S. Tamilkolundu et al., 2012).

Figure 6.17 (a) depicted the NO_x emission trends for 2ml and 3ml POH vapour induction with diesel (DI). NO_x was 347 ppm and 310 ppm without EGR, while reduced by 28.77% and 31.65% with 10% EGR for 2 ml and 3 ml POH vapour at maximum engine load. Figure 6.17 (b) and (c) depicted the NO_x formation trend for POH10D90 and POH20D80. The NO_x was 378 ppm and 331 ppm for 2ml and 3ml POH vapour induction with POH10D90. However, for 2 and 3 ml POH vapour induction with POH20D80, the NO_x was 389 ppm and 351 ppm respectively at higher engine load. However, introducing the 10% EGR in PCCI mode reduces the NO_x formation. NO_x was decreased by 27.23% and 32.62% for 2 and 3ml POH vapour with POH10D90 as compared to the POH10D90 fuel in a conventional CI engine. Similarly, NO_x was reduced by 35.26% and 38.25% in PCCI mode, compared to the POH20D80 fuel in conventional CI engine. In PCCI mode, the duration for air and fuel vapor premixing surpasses that in conventional direct injection (DI), facilitating the formation of a homogeneous charge.

Additionally, excess air is restricted in PCCI engines due to decreased volumetric efficiency. These combined conditions mitigate the likelihood of nitrogen reacting, attributed to the reduced presence of free oxygen molecules (Ladommatos et al., 1998). EGR can effectively minimize the surplus oxygen in the combustion chamber. This is achieved as HC and CO react with O_2 present in the air, rendering it inaccessible for N_2, consequently decreasing NO_x emissions (El Shenawy et al., 2019). Therefore, combining fuel vapour with EGR offsets the rise in NO_x emissions.

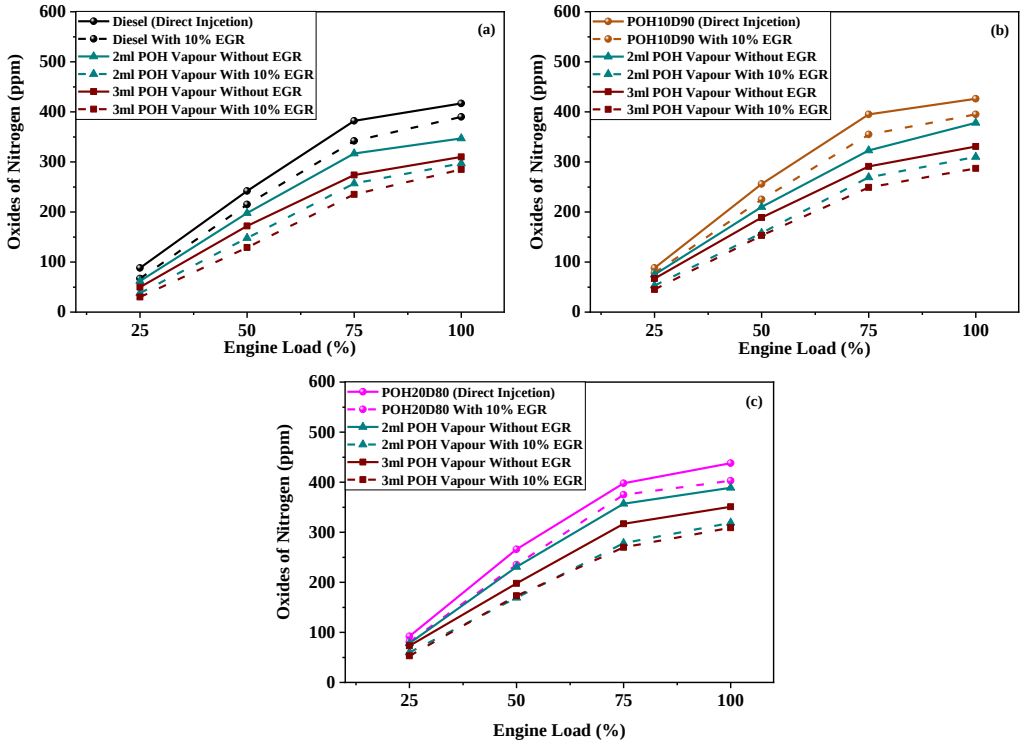

Figure 6.18: Deviation in NOx emission at increasing engine load (a) Diesel (b) POH10D90 (c) POH20D80

6.2.3.4 Smoke Opacity

Rich mixture formation and EGR increase smoke opacity within the exhaust gas (G. Singh et al., 2014). Figure 6.19 (a), (b) and (c) depicted the deviation in smoke opacity at increasing engine load for CI and PCCI engine mode. In conventional CI engine smoke, opacity for the diesel was 51%, followed by 53% and 55% for POH10D90 and POH20D80 respectively at full engine load. An increasing trend of smoke opacity was observed with increasing the POH, which may cause higher carbon present in the POH, forming the soot after combustion. To diminish the smoke opacity, the combustion process should ideally perform at the stoichiometric air-fuel ratio. However, introducing the 10% EGR reduced the smoke opacity by 9.07%, 11.76% and 19.6 % for diesel, POH10D90 and POH20D80, respectively as compared to the reference diesel at maximum engine load. At higher load, smoke opacity escalates due to richer A-F mixture formation. The increased engine load results in the accumulation of soot, partially

burned gases and unburned hydrocarbons, in the exhaust caused by the air insufficiency for optimal combustion, thereby exacerbating smoke opacity. Figure 6.19 (a) depicted that 2 ml and 3 ml POH vapour induction with diesel lowers the smoke opacity by 19.06% and 23% than diesel in conventional engine operation. However, 10% EGR increased the smoke opacity more than POH vapour, while it was lowered by 11.76% and 13.72% more than diesel in conventional mode at a higher engine load. Similarly, Figures 6.19 (b) and (c) show smoke opacity for the POH vapour with POH10D90 and POH20D80 fuel as a direct injection in PCCI mode. It has been observed that 2 ml and 3 ml with POH10D90 results in a reduction of smoke opacity by 16.98% and 22.64% respectively without EGR, and by 9.43% and 13.20% respectively with 10% EGR, compared to POH10D90 fueled conventional CI engine at higher engine loads. Moreover, a study has been carried out on POH20D80 in PCCI engine mode. It has been observed that 2 ml and 3 ml POH vapour induction with POH20D80 produced lowered smoke opacity by 18.18% and 21.81% without EGR and 9.09% and 12.72 % with 10% EGR at higher engine load conditions than the POH2D80 fuel in conventional CI engine mode. The reduction in opacity, relative to conventional Direct Injection (DI), may be caused by the pre-mixing of a homogenous air-vapor mixture. This pre-mixing prevents the rich mixture formation regions typically observed in conventional Compression Ignition (CI) engines (Lü et al., 2005). However, combining 10% of EGR dilution is non-beneficial at part load regarding smoke opacity. This is because CO and HC tend to enrich the mixture, either through the reuse of unburned hydrocarbons or by reducing the essential oxygen from the actual air-fuel charge, therefore using the required quantity of oxygen in the air.

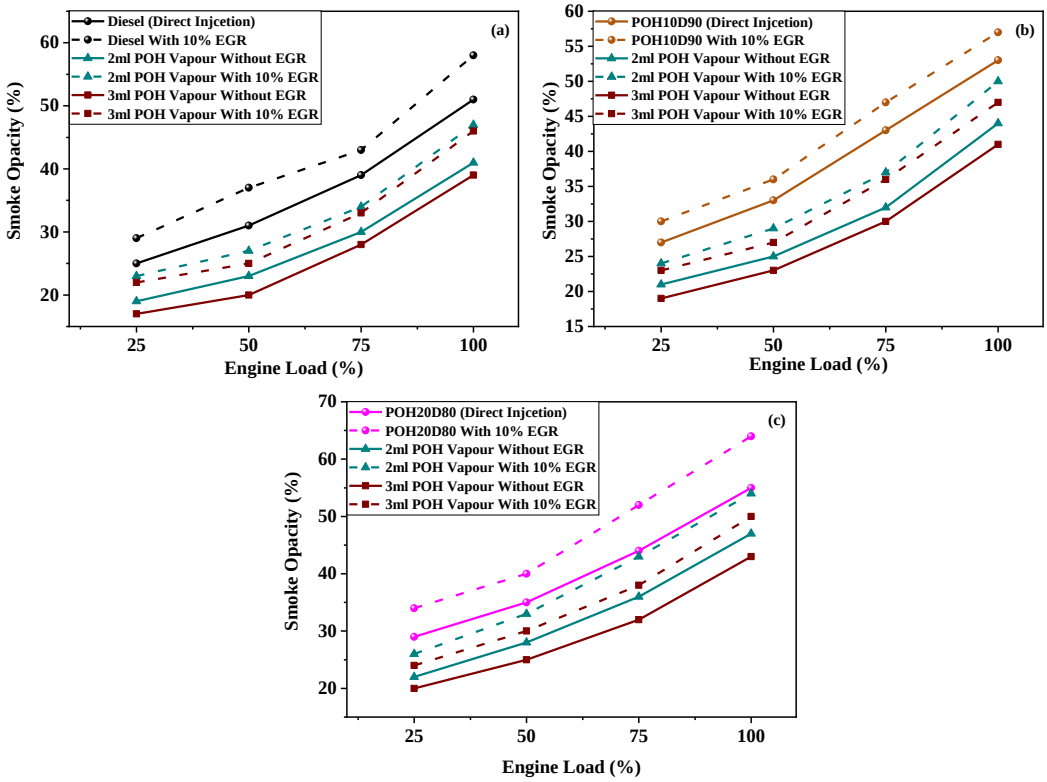

Figure 6.19: Deviation in smoke opacity at increasing engine load (a) Diesel (b) POH10D90 (c) POH20D80

6.3 Summary

The BTE of neat plasto oil was 6.9% lower than diesel due to higher volatility, viscosity, and longer hydrocarbon chains causing poor combustion. However, PO25D75 performed better among blends. In PCCI mode, with 2 ml/min and 3 ml/min POH vapour induction, BTE decreased by 2.96% and 4.64% compared to conventional diesel. NOx emissions were reduced by 16.78% and 25.65%, and smoke by 19.06% and 23% respectively. However, CO emissions were 0.097% and 0.11%, and HC emissions were 33 ppm and 35.8 ppm for 2 ml/min and 3 ml/min respectively, which is higher than the conventional CI engine operation

CHAPTER 7: CONCLUSION AND FUTURE WORK

The present PhD research work contained two parts; the first one is the production of the plasto oil from the MMPW with different catalysts in a fixed batch pyrolysis reactor. A fractional distillation process has been used to separate the plasto oil into plasto oil heavy (POH) and plasto oil lighter (POL) with their temperature range. The second part demonstrates the engine experiments. A 4-stroke single-cylinder compression ignition engine has been used directly in conventional mode and modified to PCCI engine mode by installing the fuel vaporizer on the air intake manifold. The results obtained from the study are presented in the chapter. It begins with the summary of plasto oil production and physicochemical analysis and their corresponding test result, and the results are made subsequently –

i. Pyrolysis is the most prominent and economically feasible technology for recycling municipal mixed plastic waste. Thermal degradation of the MMPW has been carried out at various temperatures of 400 ^{o}C, 450 ^{o}C, 500 ^{o}C, 550 ^{o}C and 600 ^{o}C. It has been noted that the higher yield of the PO was 53.3 wt.% obtained at 550 ^{o}C with 4-hour residence time. Hence, 550 ^{o}C temperature was identified as the optimal temperature for the conventional pyrolysis of MMPW.
ii. Continuing with the second phase of the process, two catalysts including fuller earth and commercial FCC catalyst were employed in different proportions (2 wt%, 4 wt.%, 6wt.%, 8wt.%, 10 wt.%) to increase the reaction rate can lead to increased yields and improved quality of PO. Additionally, adjustments were made to the pyrolysis parameters such as lowered temperature from 550 ^{o}C to 500 ^{o}C. The catalytic thermal degradation process was carried out at 500 ^{o}C with 3 hr. residence time.

It was observed that a significantly higher yield of PO was 78.9 wt.%, which was obtained with 8 wt.% of fuller earth. However, commercial FCC catalyst yielded 3.42 % less PO. The physicochemical characteristics of the plasto oil were analyzed and found to be approximately closer to the reference diesel. Therefore, PO obtained with 8 wt.% of FE catalyst was selected for the application in conventional CI engine with PO and diesel blends.

iii. Different blends of PO and diesel (PO25D75, PO50D50, PO75D25, neat plastic oil) have been used in the conventional CI engine and the BTE of the PO was 6.90% lower than the neat diesel due to the PO increased volatility and viscosity, and longer hydrocarbon chains (C_{10}–C_{30}) caused poor atomization and inefficient combustion in the cylinder. Emissions, including NO_x C and HC, increased with the proportion of PO with diesel. However, increasing plastic oil blends such as PO25D75, PO50D50, PO75D25 and PO100 lower the CO_2 and smoke opacity by 5.60%, 10.87, 19.06%, 21.81%, and 2.05%, 2.79%, 3.11%, and 4.47% respectively at higher engine load, then reference diesel.

iv. The plasto oil used in conventional CI engine contains wax, which is refined by the distillation process from the initial to the final boiling point of PO. The plasto oil light (POL) was obtained at a 350 gm/kg yield with a 20-180°C temperature range. Conversely, the plasto oil heavy (POH) yielded 580 gm/kg at 180 - 340°C temperature range and the remaining 70 gm/kg was residue. Moreover, the physicochemical characteristics of POL and POH were analyzed using ASTM methods, revealing that POL and POH were close to gasoline and diesel respectively. Therefore, POH was opted as fuel for a modified CI engine, with a fuel vaporizer installed on the intake manifold.

v. In PCCI engine mode, experiments were conducted on 2 ml/min and 3 ml /min of POH vapour (pilot fuel injection) induction with diesel, POH10D90, and POH20D80 as direct injection. At 2 and 3 ml POH vapour induction with diesel (DI) produced lower BTE by 2.96 % and 4.64 % than the diesel used in the conventional CI engine at higher engine load. Similarly, the BTE of

POH1010D90 is diminished by 3.42 and 6.33% than conventional CI engine fueled with POH10D90.

vi. To control the combustion in PCCI engine mode, Exhaust gas recirculation (EGR) was used up to 10%. EGR led to the delay in combustion. The combustion process occurs near the TDC rather than before the TDC. This resulted in lower combustion pressure and temperature compared to conventional CI engine.

vii. The CO emission in the PCCI engine was 0.097% and 0.11%, while HC emission was 33 ppm and 35.8 ppm for 2 and 3 ml of POH vapour with diesel (DI) in PCCI mode, which was higher than conventional CI engine operation at full engine load. This caused the lean mixture in the cylinder to reduce the combustion temperature. It was noted that CO and HC emissions remained higher in PCCI engines than in conventional CI engines.

viii. In the PCCI engine at 2 and 3ml vapour induction with diesel (DI), the NO_x emission was 16.78% and 25.65% lower than the diesel in a conventional engine. However, HC was 19.06 and 23% lower for the same conditions. Moreover, POH10D90 in PCCI mode showed that at 2ml and 3ml POH vapour reduced the NO_x emission by 8.59 and 11,73% while smoke emission was reduced by 11.26 and 22.30% than conventional engine fueled with POH10D90 at full engine load. However, the same decreasing trend of NO_x and smoke opacity was noticed at a higher engine load for POH20D80 in PCCI engine mode.

In summary, Pyrolysis of the MMPW-produced plasto oil, This fuel blend exhibits promising potential as a sustainable alternative for compression-ignition (CI) engines. However, in modifying the CI engine an external mixture formation technique can be effectively applied with minimum cost and minor modifications to the already existing intake manifold. The lean mixture and low combustion temperature diminish the NO_x and smoke with minimal effect on BTE.

Future scope

i. Life cycle analysis of the plasto oil in IC engine.
ii. Applications of the Plasto oil in HCCI engine to analyze the Engine Characteristics
iii. Investigating the performance of CI engine fueled by plasto oil blended with nanoparticles under varied injection pressure and timing.

REFERENCES

Abbas-Abadi, M. S., Haghighi, M. N., & Yeganeh, H. (2013). Evaluation of pyrolysis product of virgin high density polyethylene degradation using different process parameters in a stirred reactor. *Fuel Processing Technology*, *109*, 90–95. https://doi.org/10.1016/j.fuproc.2012.09.042

Abbas-Abadi, M. S., Haghighi, M. N., Yeganeh, H., & McDonald, A. G. (2014). Evaluation of pyrolysis process parameters on polypropylene degradation products. *Journal of Analytical and Applied Pyrolysis*, *109*, 272–277. https://doi.org/10.1016/J.JAAP.2014.05.023

Abdul–Latif, A., Menouer, A., Baleh, R., & Deiab, I. M. (2021). Plastic response of open cell aluminum foams of highly uniform architecture under different quasi-static combined biaxial compression-torsion loading paths. *Materials Science and Engineering: B*, *266*. https://doi.org/10.1016/j.mseb.2021.115051

Acomb, J. C., Wu, C., & Williams, P. T. (2014). Control of steam input to the pyrolysis-gasification of waste plastics for improved production of hydrogen or carbon nanotubes. *Applied Catalysis B: Environmental*, *147*, 571–584. https://doi.org/10.1016/j.apcatb.2013.09.018

Adnan, Shah, J., & Jan, M. R. (2015). Effect of polyethylene terephthalate on the catalytic pyrolysis of polystyrene: Investigation of the liquid products. *Journal of the Taiwan Institute of Chemical Engineers*, *51*, 96–102. https://doi.org/10.1016/J.JTICE.2015.01.015

Agarwal, A. K. (2007). Biofuels (alcohols and biodiesel) applications as fuels for internal combustion engines. In *Progress in Energy and Combustion Science* (Vol. 33, Issue 3, pp. 233–271). https://doi.org/10.1016/j.pecs.2006.08.003

Agarwal, A. K., Gupta, T., Shukla, P. C., & Dhar, A. (2015). Particulate emissions from biodiesel fuelled CI engines. *Energy Conversion and Management*, *94*, 311–330. https://doi.org/10.1016/j.enconman.2014.12.094

Agarwal, A. K., Singh, A. P., Lukose, J., & Gupta, T. (2013a). Characterization of exhaust particulates from diesel fueled homogenous charge compression ignition combustion engine. *Journal of Aerosol Science*, *58*, 71–85. https://doi.org/10.1016/j.jaerosci.2012.12.005

Agarwal, A. K., Singh, A. P., Lukose, J., & Gupta, T. (2013b). Characterization of exhaust particulates from diesel fueled homogenous charge compression ignition combustion engine. *Journal of Aerosol Science*, *58*, 71–85. https://doi.org/10.1016/j.jaerosci.2012.12.005

Ahmad, I., Ismail Khan, M., Khan, H., Ishaq, M., Tariq, R., Gul, K., & Ahmad, W. (2015a). Pyrolysis Study of Polypropylene and Polyethylene Into Premium Oil Products. *Http://Dx.Doi.Org/10.1080/15435075.2014.880146*, *12*(7), 663–671. https://doi.org/10.1080/15435075.2014.880146

Ahmad, I., Ismail Khan, M., Khan, H., Ishaq, M., Tariq, R., Gul, K., & Ahmad, W. (2015b). Pyrolysis Study of Polypropylene and Polyethylene Into Premium Oil Products. *Http://Dx.Doi.Org/10.1080/15435075.2014.880146*, *12*(7), 663–671. https://doi.org/10.1080/15435075.2014.880146

Ahmad, N., Ahmad, N., Maafa, I. M., Ahmed, U., Akhter, P., Shehzad, N., Amjad, U. e. salma, & Hussain, M. (2020). Thermal conversion of polystyrene plastic waste to liquid fuel via ethanolysis. *Fuel*, *279*(February), 118498. https://doi.org/10.1016/j.fuel.2020.118498

Ahmed, F., Hossain, S., Hossain, S., Fakhruddin, A. N. M., Abdullah, A. T. M., Chowdhury, M. A. Z., & Gan, S. H. (2019). Impact of household air pollution on human health: source identification and systematic management approach. In *SN Applied Sciences* (Vol. 1, Issue 5). Springer Nature. https://doi.org/10.1007/s42452-019-0405-8

Aisien, E. T., Otuya, I. C., & Aisien, F. A. (2021a). Thermal and catalytic pyrolysis of waste polypropylene plastic using spent FCC catalyst.

Environmental Technology and Innovation, *22*, 101455. https://doi.org/10.1016/j.eti.2021.101455

Aisien, E. T., Otuya, I. C., & Aisien, F. A. (2021b). Thermal and catalytic pyrolysis of waste polypropylene plastic using spent FCC catalyst. *Environmental Technology & Innovation*, *22*, 101455. https://doi.org/10.1016/J.ETI.2021.101455

Alemayehu, G., Nallamothu, R. B., Firew, D., & Gopal, R. (2022). Experimental Investigation on Impact of EGR Configuration on Exhaust Emissions in Optimized PCCI-DI Diesel Engine. *Journal of Engineering*, *2022*, 1–9. https://doi.org/10.1155/2022/5688842

Ali, S. S., Zamir, S., Shakeelur Raheman, A. R., Ansari, K. B., Qyyum, M. A., Al Mesfer, M. K., Danish, M., Khan, M. S., & Al-Muhtaseb, A. H. (2022). Current progress in thermochemical conversion of plastics into jet-fuel hydrocarbons and recommendations for COVID-19 waste management. *Process Safety and Environmental Protection*, *166*, 535–557. https://doi.org/10.1016/J.PSEP.2022.08.050

Alrazen, H. A., & Ahmad, K. A. (2018). HCNG fueled spark-ignition (SI) engine with its effects on performance and emissions. In *Renewable and Sustainable Energy Reviews* (Vol. 82, pp. 324–342). Elsevier Ltd. https://doi.org/10.1016/j.rser.2017.09.035

Al-Salem, S. M., Antelava, A., Constantinou, A., Manos, G., & Dutta, A. (2017). A review on thermal and catalytic pyrolysis of plastic solid waste (PSW). *Journal of Environmental Management*, *197*, 177–198. https://doi.org/10.1016/J.JENVMAN.2017.03.084

Anuar Sharuddin, S. D., Abnisa, F., Wan Daud, W. M. A., & Aroua, M. K. (2016). A review on pyrolysis of plastic wastes. In *Energy Conversion and Management* (Vol. 115, pp. 308–326). Elsevier Ltd. https://doi.org/10.1016/j.enconman.2016.02.037

Arabiourrutia, M., Elordi, G., Lopez, G., Borsella, E., Bilbao, J., & Olazar, M. (2012). Characterization of the waxes obtained by the pyrolysis of polyolefin plastics in a conical spouted bed reactor. *Journal of Analytical and Applied Pyrolysis*, *94*, 230–237. https://doi.org/10.1016/J.JAAP.2011.12.012

Areeprasert, C., Asingsamanunt, J., Srisawat, S., Kaharn, J., Inseemeesak, B., Phasee, P., Khaobang, C., Siwakosit, W., & Chiemchaisri, C. (2017). Municipal Plastic Waste Composition Study at Transfer Station of Bangkok and Possibility of its Energy Recovery by Pyrolysis. *Energy Procedia*, *107*, 222–226. https://doi.org/10.1016/J.EGYPRO.2016.12.132

Arjharn, W., Liplap, P., Maithomklang, S., Thammakul, K., Chuepeng, S., & Sukjit, E. (2022). Distilled Waste Plastic Oil as Fuel for a Diesel Engine: Fuel Production, Combustion Characteristics, and Exhaust Gas Emissions. In *ACS Omega* (Vol. 7, Issue 11, pp. 9720–9729). https://doi.org/10.1021/acsomega.1c07257

Arunkumar, M., Kannan, M., & Murali, G. (2019). Experimental studies on engine performance and emission characteristics using castor biodiesel as fuel in CI engine. *Renewable Energy*, *131*, 737–744. https://doi.org/10.1016/J.RENENE.2018.07.096

Ateş, F., Miskolczi, N., & Borsodi, N. (2013). Comparison of real waste (MSW and MPW) pyrolysis in batch reactor over different catalysts. Part I: Product yields, gas and pyrolysis oil properties. *Bioresource Technology*, *133*, 443–454. https://doi.org/10.1016/J.BIORTECH.2013.01.112

Atun, G., Hisarli, G., Sheldrick, W.S., Muhler, M., 2003. Adsorptive removal of methylene blue from colored effluents on fuller's earth. J. Colloid Interface Sci. 261, 32–39. https://doi.org/10.1016/S0021-9797(03)00059-6

Aznar, M. P., Caballero, M. A., Sancho, J. A., & Francés, E. (2006). Plastic waste elimination by co-gasification with coal and biomass in fluidized bed with

air in pilot plant. *Fuel Processing Technology*, *87*(5), 409–420. https://doi.org/10.1016/j.fuproc.2005.09.006

Bai, B., Liu, Y., Wang, Q., Zou, J., Zhang, H., Jin, H., & Li, X. (2019). Experimental investigation on gasification characteristics of plastic wastes in supercritical water. *Renewable Energy*, *135*, 32–40. https://doi.org/10.1016/J.RENENE.2018.11.092

Bai, B., Wang, W., & Jin, H. (2020). Experimental study on gasification performance of polypropylene (PP) plastics in supercritical water. *Energy*, *191*, 116527. https://doi.org/10.1016/j.energy.2019.116527

Bhateria, R., & Jain, D. (2016). Water quality assessment of lake water: a review. *Sustainable Water Resources Management*, *2*(2), 161–173. https://doi.org/10.1007/s40899-015-0014-7

Bhiogade, G., & Suryawanshi, J. G. (2016). Investigations on premixed charge compression ignition engine with external mixture formation and exhaust gas recirculation technique. *Journal of Mechanical Science and Technology*, *30*(11), 5269–5274. https://doi.org/10.1007/S12206-016-1045-1/METRICS

Bhoi, P. R., & Rahman, M. H. (2022a). Hydrocarbons recovery through catalytic pyrolysis of compostable and recyclable waste plastics using a novel desk-top staged reactor. *Environmental Technology and Innovation*, *27*, 102453. https://doi.org/10.1016/j.eti.2022.102453

Bhoi, P. R., & Rahman, M. H. (2022b). Hydrocarbons recovery through catalytic pyrolysis of compostable and recyclable waste plastics using a novel desk-top staged reactor. *Environmental Technology & Innovation*, *27*, 102453. https://doi.org/10.1016/j.eti.2022.102453

Bhurat, S., Pandey, S., Chintala, V., Jaiswal, M., & Kumar, A. (2021a). Investigation of partially pre-mixed charge compression ignition engine characteristics implemented with toroidal combustion chamber and exhaust

gas recirculation. *Energy Sources, Part A: Recovery, Utilization and Environmental Effects*. https://doi.org/10.1080/15567036.2021.1909675

Bhurat, S., Pandey, S., Chintala, V., Jaiswal, M., & Kumar, A. (2021b). Investigation of partially pre-mixed charge compression ignition engine characteristics implemented with toroidal combustion chamber and exhaust gas recirculation. *Energy Sources, Part A: Recovery, Utilization and Environmental Effects*, *00*(00), 1–19. https://doi.org/10.1080/15567036.2021.1909675

Bhurat, S., Pandey, S., Chintala, V., Jaiswal, M., & Kurein, C. (2022). Effect of novel fuel vaporiser technology on engine characteristics of partially premixed charge compression ignition (PCCI) engine with toroidal combustion chamber. *Fuel*, *315*(August 2021), 123197. https://doi.org/10.1016/j.fuel.2022.123197

Bilal, M., Mehmood, S., & Iqbal, H. M. N. (2020). The beast of beauty: Environmental and health concerns of toxic components in cosmetics. In *Cosmetics* (Vol. 7, Issue 1). MDPI AG. https://doi.org/10.3390/cosmetics7010013

Briassoulis, D., Hiskakis, M., & Babou, E. (2013). Technical specifications for mechanical recycling of agricultural plastic waste. *Waste Management*, *33*(6), 1516–1530. https://doi.org/10.1016/j.wasman.2013.03.004

Bruna Alves. (2023). *Global Plastics Outlook: Policy Scenarios to 2060*.

Bruna alves. (2023). *Plastic waste generation worldwide in 2019, by region*.

Bukkarapu, K. R., Gangadhar, D. S., Jyothi, Y., & Kanasani, P. (2018). Management, conversion, and utilization of waste plastic as a source of sustainable energy to run automotive: a review. In *Energy Sources, Part A: Recovery, Utilization and Environmental Effects* (Vol. 40, Issue 14, pp. 1681–1692). Taylor and Francis Inc. https://doi.org/10.1080/15567036.2018.1486898

Burra, K. G., & Gupta, A. K. (2018). Synergistic effects in steam gasification of combined biomass and plastic waste mixtures. *Applied Energy*, *211*, 230–236. https://doi.org/10.1016/j.apenergy.2017.10.130

Butler, E., Devlin, G., Meier, D., & McDonnell, K. (2011). A review of recent laboratory research and commercial developments in fast pyrolysis and upgrading. *Renewable and Sustainable Energy Reviews*, *15*(8), 4171–4186. https://doi.org/10.1016/j.rser.2011.07.035

Chattopadhyay, J., Pathak, T. S., Srivastava, R., & Singh, A. C. (2016). Catalytic co-pyrolysis of paper biomass and plastic mixtures (HDPE (high density polyethylene), PP (polypropylene) and PET (polyethylene terephthalate)) and product analysis. *Energy*, *103*, 513–521. https://doi.org/10.1016/j.energy.2016.03.015

Chen, D., Yin, L., Wang, H., & He, P. (2014). Pyrolysis technologies for municipal solid waste: A review. *Waste Management*, *34*(12), 2466–2486. https://doi.org/10.1016/j.wasman.2014.08.004

Chen, T., Yu, J., Ma, C., Bikane, K., & Sun, L. (2020). Catalytic performance and debromination of Fe–Ni bimetallic MCM-41 catalyst for the two-stage pyrolysis of waste computer casing plastic. *Chemosphere*, *248*, 125964. https://doi.org/10.1016/J.CHEMOSPHERE.2020.125964

Chen, Xiaopeng, Ren, L., Yaseen, M., Wang, L., Liang, J., Liang, R., Chen, Xiankun, Guo, H., 2019. Synthesis, characterization and activity performance of nickel-loaded spent FCC catalyst for pine gum hydrogenation. *RSC Adv*. 9, 6515–6525. https://doi.org/10.1039/c8ra07943a

Chetna Mohabeer, Novlen Guilhaume, Dorothee Laurenti, Y. S. (2022). *Microwave-Assisted Pyrolysis of Biomass with and without Use of Catalyst in a Fluidised Bed Reactor_ A Review _ Enhanced Reader.pdf*. MDPI. https://doi.org/10.3390/en15093258

Chintala, V., Godkhe, P., Phadtare, S., Tadpatrikar, M., Pandey, J. K., & Kumar, S. (2018). A comparative assessment of single cylinder diesel engine characteristics with plasto-oils derived from municipal mixed plastic waste. *Energy Conversion and Management*, *166*(April), 579–589. https://doi.org/10.1016/j.enconman.2018.04.068

Chintala, V., Kumar, S., Pandey, J. K., Sharma, A. K., & Kumar, S. (2017). Solar thermal pyrolysis of non-edible seeds to biofuels and their feasibility assessment. *Energy Conversion and Management*, *153*. https://doi.org/10.1016/j.enconman.2017.10.029

Chintala, V., Sharma, A. K., Karn, A., Vardhan, H., & Pandey, J. K. (2019). Utilization of biomass-derived pyro-oils in compression ignition (CI) engines–Recent developments. *Energy Sources, Part A: Recovery, Utilization and Environmental Effects*. https://doi.org/10.1080/15567036.2019.1683652

Chintala, V., & Subramanian, K. A. (2014). Experimental investigation on effect of enhanced premixed charge on combustion characteristics of a direct injection diesel engine. *International Journal of Advances in Engineering Sciences and Applied Mathematics*, *6*(1–2), 3–16. https://doi.org/10.1007/s12572-014-0109-7

Choi, S. J., Park, Y. K., Jeong, K. E., Kim, T. W., Chae, H. J., Park, S. H., Jeon, J. K., & Kim, S. S. (2010). Catalytic degradation of polyethylene over SBA-16. *Korean Journal of Chemical Engineering 2010 27:5*, *27*(5), 1446–1451. https://doi.org/10.1007/S11814-010-0281-9

Chun, B.-H., Lee, H.-S., Nam, C.-S., Chun, K. M., Ryu, J. H., & Lee, K.-Y. (n.d.). *Plasma/Catalyst System for Reduction of Nox in Diesel Engine Exhaust*. Vol. 109 *JOURNAL OF FUELS AND LUBRICANTS* (2000), pp. 2744-2748 (5 pages)

Damodharan, D., Rajesh Kumar, B., Gopal, K., De Poures, M. V., & Sethuramasamyraja, B. (2019). Utilization of waste plastic oil in diesel engines: a review. *Reviews in Environmental Science and Biotechnology*, *18*(4), 681–697. https://doi.org/10.1007/s11157-019-09516-x

Damodharan, D., Sathiyagnanam, A. P., Rana, D., Saravanan, S., Kumar, B. R., & Sethuramasamyraja, B. (2018). E ff ective utilization of waste plastic oil in a direct injection diesel engine using high carbon alcohols as oxygenated additives for cleaner emissions. *Energy Conversion and Management*, *166*(January), 81–97. https://doi.org/10.1016/j.enconman.2018.04.006

Das, A. K., Hansdah, D., Mohapatra, A. K., & Panda, A. K. (2020). Energy, exergy and emission analysis on a DI single cylinder diesel engine using pyrolytic waste plastic oil diesel blend. *Journal of the Energy Institute*, *93*(4), 1624–1633. https://doi.org/10.1016/j.joei.2020.01.024

Das, P., & Tiwari, P. (2018). The effect of slow pyrolysis on the conversion of packaging waste plastics (PE and PP) into fuel. *Waste Management*, *79*, 615–624. https://doi.org/10.1016/J.WASMAN.2018.08.021

Davi, G., Luiz, J., Alves, F., Constantino, J., Da, G., Felix, R., Sena, D., Marangoni, C., Antonio, R., & Machado, F. (2019). Thermal investigation of plastic solid waste pyrolysis via the deconvolution technique using the asymmetric double sigmoidal function : Determination of the kinetic triplet , thermodynamic parameters , thermal lifetime and pyrolytic oil composition for cl. *Energy Conversion and Management*, *200*(September), 112031. https://doi.org/10.1016/j.enconman.2019.112031

De Weerdt, L., Sasao, T., Compernolle, T., Van Passel, S., & De Jaeger, S. (2020). The effect of waste incineration taxation on industrial plastic waste generation: A panel analysis. *Resources, Conservation and Recycling*, *157*. https://doi.org/10.1016/j.resconrec.2020.104717

Demirbas, A. (2004). Pyrolysis of municipal plastic wastes for recovery of gasoline-range hydrocarbons. *Journal of Analytical and Applied Pyrolysis*, *72*(1), 97–102. https://doi.org/10.1016/J.JAAP.2004.03.001

Devaraj, J., Robinson, Y., & Ganapathi, P. (2015). Experimental investigation of performance , emission and combustion characteristics of waste plastic pyrolysis oil blended with diethyl ether used as fuel for diesel engine. *Energy*, *85*, 304–309. https://doi.org/10.1016/j.energy.2015.03.075

Dey, S., Reang, N. M., Das, P. K., & Deb, M. (2021). A comprehensive study on prospects of economy, environment, and efficiency of palm oil biodiesel as a renewable fuel. *Journal of Cleaner Production*, *286*, 124981. https://doi.org/10.1016/J.JCLEPRO.2020.124981

Donaj, P. J., Kaminsky, W., Buzeto, F., & Yang, W. (2012). Pyrolysis of polyolefins for increasing the yield of monomers' recovery. *Waste Management*, *32*(5), 840–846. https://doi.org/10.1016/J.WASMAN.2011.10.009

Dong, J., Tang, Y., Nzihou, A., Chi, Y., Weiss-Hortala, E., Ni, M., & Zhou, Z. (2018). Comparison of waste-to-energy technologies of gasification and incineration using life cycle assessment: Case studies in Finland, France and China. *Journal of Cleaner Production*, *203*, 287–300. https://doi.org/10.1016/j.jclepro.2018.08.139

Duque, J. V. F., Martins, M. F., Debenest, G., & Orlando, M. T. D. A. (2020). The influence of the recycling stress history on LDPE waste pyrolysis. *Polymer Testing*, *86*(January), 106460. https://doi.org/10.1016/j.polymertesting.2020.106460

El Shenawy, E. A., Elkelawy, M., Bastawissi, H. A. E., Panchal, H., & Shams, M. M. (2019). Comparative study of the combustion, performance, and emission characteristics of a direct injection diesel engine with a partially premixed

lean charge compression ignition diesel engines. *Fuel*, *249*, 277–285. https://doi.org/10.1016/J.FUEL.2019.03.073

Elordi, G., Olazar, M., Lopez, G., Amutio, M., Artetxe, M., Aguado, R., & Bilbao, J. (2009). Catalytic pyrolysis of HDPE in continuous mode over zeolite catalysts in a conical spouted bed reactor. *Journal of Analytical and Applied Pyrolysis*, *85*(1–2), 345–351. https://doi.org/10.1016/J.JAAP.2008.10.015

Energy institute. (2022). https://www.energyinst.org/exploring-energy/topic/transport

Evode, N., Qamar, S. A., Bilal, M., Barceló, D., & Iqbal, H. M. N. (2021). Plastic waste and its management strategies for environmental sustainability. *Case Studies in Chemical and Environmental Engineering*, *4*. https://doi.org/10.1016/j.cscee.2021.100142

Fadillah, G., Fatimah, I., Sahroni, I., Musawwa, M. M., Mahlia, T. M. I., & Muraza, O. (2021). Recent Progress in Low-Cost Catalysts for Pyrolysis of Plastic Waste to Fuels. *Catalysts 2021, Vol. 11, Page 837*, *11*(7), 837. https://doi.org/10.3390/CATAL11070837

Fang, S., Gu, W., Chen, L., Yu, Z., Dai, M., Lin, Y., Liao, Y., & Ma, X. (2018). Ultrasonic pretreatment effects on the co-pyrolysis of municipal solid waste and paper sludge through orthogonal test. *Bioresource Technology*, *258*(January), 5–11. https://doi.org/10.1016/j.biortech.2018.02.120

Fantozzi, F., Colantoni, S., Bartocci, P., & Desideri, U. (2006). Rotary Kiln Slow Pyrolysis for Syngas and Char Production From Biomass and waste. *ASME Turbo Expo 2006: Power for Land, Sea and Air*, 901–907. https://doi.org/10.1115/1.2720521

Farshi, A., Abri, H.R., 2012. The addition of ZSM-5 to a fluid catalytic cracking catalyst for increasing olefins in fluid catalytic cracking light gas. Pet. Sci. Technol. 30, 1285–1295. https://doi.org/10.1080/10916466.2010.497789

Fekhar, B., Gombor, L., & Miskolczi, N. (2019). Pyrolysis of chlorine contaminated municipal plastic waste: In-situ upgrading of pyrolysis oils by Ni/ZSM-5, Ni/SAPO-11, red mud and Ca(OH)2 containing catalysts. *Journal of the Energy Institute*, *92*(5), 1270–1283. https://doi.org/10.1016/J.JOEI.2018.10.007

Fernandez, E., Santamaria, L., Amutio, M., Artetxe, M., Arregi, A., Lopez, G., Bilbao, J., & Olazar, M. (2022). Role of temperature in the biomass steam pyrolysis in a conical spouted bed reactor. *Energy*, *238*, 122053. https://doi.org/10.1016/J.ENERGY.2021.122053

Figueiredo, A. L., Araujo, A. S., Linares, M., Peral, Á., García, R. A., Serrano, D. P., & Fernandes, V. J. (2016). Catalytic cracking of LDPE over nanocrystalline HZSM-5 zeolite prepared by seed-assisted synthesis from an organic-template-free system. *Journal of Analytical and Applied Pyrolysis*, *117*, 132–140. https://doi.org/10.1016/J.JAAP.2015.12.005

Fiore, M., & Viggiano, A. (2020). Internal combustion engines powered by syngas : A review. *Applied Energy*, *276*(July), 115415. https://doi.org/10.1016/j.apenergy.2020.115415

Fivga, A., & Dimitriou, I. (2018). Pyrolysis of plastic waste for production of heavy fuel substitute: A techno-economic assessment. *Energy*, *149*, 865–874. https://doi.org/10.1016/j.energy.2018.02.094

Fogler, H. (2016). *Elements Of Chemical Reaction Engineering, 4Th Edn*.

Frank Riedewald, Y. P. E. W. S. S. M. S.-G. (2021). Economic assessment of a 40,000 t/y mixed plastic waste pyrolysis plant using direct heat treatment with molten metal: A case study of a plant located in Belgium. *Waste Management*, *120*, 698–707.

Franke, H. J., Shimizu, T., Nishio, A., Nishikawa, H., Inagaki, M., & Ibashi, W. (1999). Improvement of Carbon Burn-up during Fluidized Bed Incineration

of Plastic by Using Porous Bed Materials. *Energy and Fuels*, *13*(4), 773–777. https://doi.org/10.1021/EF980179N

Ganesh, D., & Nagarajan, G. (2010). Homogeneous charge compression ignition (HCCI) combustion of diesel fuel with external mixture formation. *Energy*, *35*(1), 148–157. https://doi.org/10.1016/j.energy.2009.09.005

Ganesh, D., Nagarajan, G., & Ganesan, S. (2011). Performance and emission analysis on mixed-mode homogeneous charge compression ignition (HCCI) combustion of biodiesel fuel with external mixture formation. *SAE Technical Papers*. https://doi.org/10.4271/2011-01-2450

Ganesh, D., Nagarajan, G., & Mohamed Ibrahim, M. (2008a). Study of performance, combustion and emission characteristics of diesel homogeneous charge compression ignition (HCCI) combustion with external mixture formation. *Fuel*, *87*(17–18), 3497–3503. https://doi.org/10.1016/j.fuel.2008.06.010

Ganesh, D., Nagarajan, G., & Mohamed Ibrahim, M. (2008b). Study of performance, combustion and emission characteristics of diesel homogeneous charge compression ignition (HCCI) combustion with external mixture formation. *Fuel*, *87*(17–18), 3497–3503. https://doi.org/10.1016/j.fuel.2008.06.010

Ghodke, P. K. (2021a). High-quality hydrocarbon fuel production from municipal mixed plastic waste using a locally available low-cost catalyst. *Fuel Communications*, *8*(May), 100022. https://doi.org/10.1016/j.jfueco.2021.100022

Ghodke, P. K. (2021b). High-quality hydrocarbon fuel production from municipal mixed plastic waste using a locally available low-cost catalyst. *Fuel Communications*, *8*, 100022. https://doi.org/10.1016/j.jfueco.2021.100022

Ghodke, P. K., Moorthy, K., & Chen, W. (2021). *Production And Characterization of Transportation Fuels From Domestic Plastic Wastes And Mixed Virgin Plastics By Low- Cost Catalytic Pyrolysis*. 1–22.

Ghodke, P., & Krishna, S. V. (2018). *Effect of Heterogeneous Catalyst on Esterification of Pyrolysis Oil*. 219–229. https://doi.org/10.1007/978-3-319-63085-4_30

Ghodrat, M., Abascall Alonso, J., Hagare, D., Yang, R., & Samali, B. (2019). Economic feasibility of energy recovery from waste plastic using pyrolysis technology: an Australian perspective. *International Journal of Environmental Science and Technology*. https://doi.org/10.1007/s13762-019-02293-8

Gu, J.-D. (2021). Biodegradability of plastics: the issues, recent advances, and future perspectives. *Environmental Science and Pollution Research* , *28*, 1278–1282. https://doi.org/10.1007/s11356-020-11501-9/Published

Guan, B., Zhan, R., Lin, H., & Huang, Z. (2014). Review of state of the art technologies of selective catalytic reduction of NOx from diesel engine exhaust. In *Applied Thermal Engineering* (Vol. 66, Issues 1–2, pp. 395–414). Elsevier Ltd. https://doi.org/10.1016/j.applthermaleng.2014.02.021

H wijayanti, C Irawan, N. aulia. (2022). *Copyrolysis of rice husk and plastic bags waste from low-density polyethylene (LDPE) for improving pyrolysis liquid product*. https://doi.org/10.1088/1755-1315/963/1/012012

Hafeez, S., Pallari, E., Manos, G., & Constantinou, A. (2018). Catalytic conversion and chemical recovery. In *Plastics to Energy: Fuel, Chemicals, and Sustainability Implications*. Elsevier Inc. https://doi.org/10.1016/B978-0-12-813140-4.00006-6

Hafeez, S., Pallari, E., Manos, G., & Constantinou, A. (2019). Catalytic Conversion and Chemical Recovery. *Plastics to Energy: Fuel, Chemicals,*

and Sustainability Implications, 147–172. https://doi.org/10.1016/B978-0-12-813140-4.00006-6

Hahladakis, J. N., Velis, C. A., Weber, R., Iacovidou, E., & Purnell, P. (2018). An overview of chemical additives present in plastics: Migration, release, fate and environmental impact during their use, disposal and recycling. In *Journal of Hazardous Materials* (Vol. 344, pp. 179–199). Elsevier B.V. https://doi.org/10.1016/j.jhazmat.2017.10.014

Hakeem, I. G., Aberuagba, F., & Musa, U. (2018). Catalytic pyrolysis of waste polypropylene using Ahoko kaolin from Nigeria. *Applied Petrochemical Research 2018 8:4*, *8*(4), 203–210. https://doi.org/10.1007/S13203-018-0207-8

Han, J., Xiong, Z., Zhang, Z., Zhang, H., Zhou, P., & Yu, F. (2018). The Influence of Texture on Co/SBA–15 Catalyst Performance for Fischer–Tropsch Synthesis. *Catalysts 2018, Vol. 8, Page 661*, *8*(12), 661. https://doi.org/10.3390/CATAL8120661

Harussani, M. M., Sapuan, S. M., Rashid, U., Khalina, A., & Ilyas, R. A. (2022). Pyrolysis of polypropylene plastic waste into carbonaceous char: Priority of plastic waste management amidst COVID-19 pandemic. *Science of the Total Environment*, *803*, 149911. https://doi.org/10.1016/j.scitotenv.2021.149911

Hasan, M. M., Rasul, M. G., Jahirul, M. I., & Sattar, M. A. (2024). An Aspen plus process simulation model for exploring the feasibility and profitability of pyrolysis process for plastic waste management. *Journal of Environmental Management*, *355*. https://doi.org/10.1016/j.jenvman.2024.120557

Hasan, M. M., Rasul, M. G., Khan, M. M. K., Ashwath, N., & Jahirul, M. I. (2021). Energy recovery from municipal solid waste using pyrolysis technology: A review on current status and developments. *Renewable and Sustainable Energy Reviews*, *145*(March), 111073. https://doi.org/10.1016/j.rser.2021.111073

Hedlund, J., Zhou, M., Faisal, A., Öhrman, O. G. W., Finelli, V., Signorile, M., Crocellà, V., & Grahn, M. (2022). Controlling diffusion resistance, selectivity and deactivation of ZSM-5 catalysts by crystal thickness and defects. *Journal of Catalysis*, *410*, 320–332. https://doi.org/10.1016/J.JCAT.2022.04.013

Huang, J., He, C., Li, X., Pan, G., & Tong, H. (2018). Theoretical studies on thermal degradation reaction mechanism of model compound of bisphenol A polycarbonate. *Waste Management*, *71*, 181–191. https://doi.org/10.1016/j.wasman.2017.10.016

Huang, J., Veksha, A., Chan, W. P., Giannis, A., & Lisak, G. (2022). Chemical recycling of plastic waste for sustainable material management: A prospective review on catalysts and processes. *Renewable and Sustainable Energy Reviews*, *154*(May 2021), 111866. https://doi.org/10.1016/j.rser.2021.111866

Hussein, Z. A., Shakor, Z. M., Alzuhairi, M., & Al-Sheikh, F. (2021). Thermal and catalytic cracking of plastic waste: a review. *Https://Doi.Org/10.1080/03067319.2021.1946527*, 1–18. https://doi.org/10.1080/03067319.2021.1946527

İlkiliç, C., & Ilkiliç, C. ˙. (2012). The Emission Characteristics of a CI Engine Fueled with a Biofuel Blend. *Energy Sources, Part A: Recovery, Utilization, and Environmental Effects*, *34*(20), 1901–1912. https://doi.org/10.1080/15567031003773270

Imtenan, S., Masjuki, H. H., Varman, M., Rizwanul Fattah, I. M., Sajjad, H., & Arbab, M. I. (2015). Effect of n-butanol and diethyl ether as oxygenated additives on combustion–emission-performance characteristics of a multiple cylinder diesel engine fuelled with diesel–jatropha biodiesel blend. *Energy Conversion and Management*, *94*, 84–94. https://doi.org/10.1016/J.ENCONMAN.2015.01.047

Inayat, A., Klemencova, K., Grycova, B., Sokolova, B., & Lestinsky, P. (2021). Thermo-catalytic pyrolysis of polystyrene in batch and semi-batch reactors: A comparative study. *Waste Management and Research*, *39*(2), 260–269. https://doi.org/10.1177/0734242X20936746

India - net plastic consumption 2021 | Statista. (2024). https://www-statista-com.eu1.proxy.openathens.net/statistics/1154434/india-net-plastic-consumption/?locale=en

India - per capita plastic consumption in India | Statista. (2024). https://www-statista-com.eu1.proxy.openathens.net/statistics/1344395/india-plastic-consumption-per-capita/?locale=en

India: plastic consumption share by sector | Statista. (2024). https://www-statista-com.eu1.proxy.openathens.net/statistics/1009117/india-plastic-consumption-share-by-sector/?locale=en

Irma Kremer, Thiomir Tomic, Zvonimir katancic, Zlata Hrnjak-Murgic, Matko Erceg, D. R. S. (2021). *Catalytic decomposition and kinetic study of mixed plastic waste.pdf* (pp. 811–827).

Islam, M. N., Zailani, R., Farid, \, & Ani, N. (n.d.). *Pyrolytic oil from ~uidised bed pyrolysis of oil palm shell and its characterisation*.

Jacob, A., Lawrence, J., Soosairaj, A. S., Anandan, J., & Elango, M. (2022). *Exploring the Potential of Microalgae Bioalcohol and Biodiesel in Arresting Particulate Smoke Emissions and Greenhouse Gases using Post-Injection Activated Regeneration Trap*. https://doi.org/10.21203/rs.3.rs-1357066/v1

Jameel, M., Khan, S. A., & Afzal, A. (2021). ADSORPTION STUDIES OF FULLERS EARTH NANOCOMPOSITES FOR THE REMOVAL OF COPPER AND REACTIVE YELLOW 18. *Digest Journal of Nanomaterials and Biostructures*, *16*(1), 261–270. https://doi.org/10.15251/djnb.2021.161.261

Jamradloedluk, J., & Lertsatitthanakorn, C. (2014). Characterization and Utilization of Char Derived from Fast Pyrolysis of Plastic Wastes. *Procedia Engineering*, *69*, 1437–1442. https://doi.org/10.1016/J.PROENG.2014.03.139

Janajreh, I., Adeyemi, I., & Elagroudy, S. (2020). Gasification feasibility of polyethylene, polypropylene, polystyrene waste and their mixture: Experimental studies and modeling. *Sustainable Energy Technologies and Assessments*, *39*(March), 100684. https://doi.org/10.1016/j.seta.2020.100684

Jayabal, R., Thangavelu, L., & Subramani, S. (2020). Combined effect of oxygenated additives, injection timing and EGR on combustion, performance and emission characteristics of a CRDi diesel engine powered by sapota biodiesel/diesel blends. *Fuel*, *276*, 118020. https://doi.org/10.1016/j.fuel.2020.118020

Jia, M., Xie, M., Wang, T., & Peng, Z. (2011). The effect of injection timing and intake valve close timing on performance and emissions of diesel PCCI engine with a full engine cycle CFD simulation. *Applied Energy*, *88*(9), 2967–2975. https://doi.org/10.1016/j.apenergy.2011.03.024

Jung, S. H., Cho, M. H., Kang, B. S., & Kim, J. S. (2010). Pyrolysis of a fraction of waste polypropylene and polyethylene for the recovery of BTX aromatics using a fluidized bed reactor. *Fuel Processing Technology*, *91*(3), 277–284. https://doi.org/10.1016/j.fuproc.2009.10.009

Juttu, S., Thipse, S. S., Marathe, N. V., & Gajendra Babu, M. K. (2007). Homogeneous Charge Compression Ignition (HCCI): A New Concept for Near Zero NOx and Particulate Matter (PM) from Diesel Engine Combustion. *SAE Technical Papers*, *2007-January*(January). https://doi.org/10.4271/2007-26-020

Kaewbuddee, C., Sukjit, E., Srisertpol, J., & Maithomklang, S. (2020). *Evaluation of Waste Plastic Oil-Biodiesel Blends as alternative fuels for diesle engine*. 1–16.

Kaewbuddee, C., Sukjit, E., Srisertpol, J., Maithomklang, S., Wathakit, K., Klinkaew, N., Liplap, P., & Arjharn, W. (2020). Evaluation of Waste Plastic Oil-Biodiesel Blends as Alternative Fuels for Diesel Engines. *Energies 2020, Vol. 13, Page 2823*, *13*(11), 2823. https://doi.org/10.3390/EN13112823

Kaimal, V. K., & Vijayabalan, P. (2016). An investigation on the effects of using DEE additive in a di diesel engine fuelled with waste plastic oil. *Fuel*, *180*, 90–96. https://doi.org/10.1016/j.fuel.2016.04.030

Kaimal, V. K., & Vijayabalan, P. (2017). A detailed investigation of the combustion characteristics of a DI diesel engine fuelled with plastic oil and rice bran methyl ester. *Journal of the Energy Institute*, *90*(2), 324–330. https://doi.org/10.1016/j.joei.2015.11.005

Kalargaris, I., Tian, G., & Gu, S. (2017a). Combustion, performance and emission analysis of a DI diesel engine using plastic pyrolysis oil. *Fuel Processing Technology*, *157*, 108–115. https://doi.org/10.1016/j.fuproc.2016.11.016

Kalargaris, I., Tian, G., & Gu, S. (2017b). Experimental evaluation of a diesel engine fuelled by pyrolysis oils produced from low-density polyethylene and ethylene–vinyl acetate plastics. *Fuel Processing Technology*, *161*, 125–131. https://doi.org/10.1016/j.fuproc.2017.03.014

Kalargaris, I., Tian, G., & Gu, S. (2017c). The utilisation of oils produced from plastic waste at different pyrolysis temperatures in a DI diesel engine. *Energy*, *131*, 179–185. https://doi.org/10.1016/j.energy.2017.05.024

Kaminsky, W., Schlesselmann, B., & Simon, C. M. (1996). Thermal degradation of mixed plastic waste to aromatics and gas. *Polymer Degradation and Stability*, *53*(2), 189–197. https://doi.org/10.1016/0141-3910(96)00087-0

Kaminsky, W., Schmidt, H., & Simon, C. M. (2000). Recycling of mixed plastics by pyrolysis in a fluidised bed. *Macromolecular Symposia*, *152*, 191–199. https://doi.org/10.1002/1521-3900(200003)152:1<191::AID-MASY191>3.0.CO;2-2

Kanda, T., Hakozaki, T., Uchimoto, T., Hatano, J., Kitayama, N., & Sono, H. (2005). *PCCI Operation with Early Injection of Conventional Diesel Fuel*. www.sae.org

Karishma, S. M., Rajak, U., Naik, B. K., Dasore, A., & Konijeti, R. (2022). Performance and emission characteristics assessment of compression ignition engine fuelled with the blends of novel antioxidant catechol-daok biodiesel. *Energy*, *245*, 123304. https://doi.org/10.1016/j.energy.2022.123304

Kasar, P., Sharma, D. K., & Ahmaruzzaman, M. (2020). Thermal and catalytic decomposition of waste plastics and its co-processing with petroleum residue through pyrolysis process. *Journal of Cleaner Production*, *265*, 121639. https://doi.org/10.1016/j.jclepro.2020.121639

Kassargy, C., Awad, S., Burnens, G., Kahine, K., & Tazerout, M. (2018). Gasoline and diesel-like fuel production by continuous catalytic pyrolysis of waste polyethylene and polypropylene mixtures over USY zeolite. *Fuel*, *224*(March), 764–773. https://doi.org/10.1016/j.fuel.2018.03.113

Kataki, R., Bordoloi, N. J., Saikia, R., Sut, D., Narzari, R., Gogoi, L., & Bhuyan, N. (2018). Waste Valorization to Fuel and Chemicals Through Pyrolysis: Technology, Feedstock, Products, and Economic Analysis. *Energy, Environment, and Sustainability*, 477–514. https://doi.org/10.1007/978-981-10-7431-8_21

Khairil, Riayatsyah, T. M. I., Bahri, S., Sofyan, S. E., Jalaluddin, J., Kusumo, F., Silitonga, A. S., Padli, Y., Jihad, M., & Shamsuddin, A. H. (2020). Experimental study on the performance of an si engine fueled by waste

plastic pyrolysis oil–gasoline blends. *Energies*, *13*(6). https://doi.org/10.3390/en13164196

Khan, K., Kumar, G., Sharma, A. K., Kumar, P. S., Mandal, C., & Chintala, V. (2018). Performance and emission characteristics of a diesel engine using complementary blending of castor and karanja biodiesel. *Biofuels*, *9*(1). https://doi.org/10.1080/17597269.2016.1256552

Khan, M. Z. A., Khan, H. A., Ravi, S. S., Turner, J. W., & Aziz, M. (2023). Potential of clean liquid fuels in decarbonizing transportation – An overlooked net- zero pathway? In *Renewable and Sustainable Energy Reviews* (Vol. 183). Elsevier Ltd. https://doi.org/10.1016/j.rser.2023.113483

Kim, D. S., & Lee, C. S. (2006). Improved emission characteristics of HCCI engine by various premixed fuels and cooled EGR. *Fuel*, *85*(5–6), 695–704. https://doi.org/10.1016/j.fuel.2005.08.041

Kim, J. Y., Heo, S., & Choi, J. W. (2018). Effects of phenolic hydroxyl functionality on lignin pyrolysis over zeolite catalyst. *Fuel*, *232*(March), 81–89. https://doi.org/10.1016/j.fuel.2018.05.133

Koebel M., M Elsener., M Koebel (2020). Urea-SCR: a promising technique to reduce NOx emissions from automotive diesel engines. Catalysis Today, 59 (3-4), 335-345. https://doi.org/10.1016/S0920-5861(00)00299-6

Kofi, S., Kofi, E., & Dapaah, S. (2019). Plastic waste to fuel via pyrolysis : A key way to solving the severe plastic waste problem in Ghana. *Thermal Science and Engineering Progress*, *11*(March), 417–424. https://doi.org/10.1016/j.tsep.2019.05.002

Korakianitis, T., Namasivayam, A. M., & Crookes, R. J. (2011). Natural-gas fueled spark-ignition (SI) and compression-ignition (CI) engine performance and emissions. *Progress in Energy and Combustion Science*, *37*(1), 89–112. https://doi.org/10.1016/J.PECS.2010.04.002

K.panda, A. (2018). *Thermo-catalytic degradation of different plastics to drop in liquid fuel using calcium bentonite catalyst.pdf* (pp. 167–176). International journal of industrial chemistry. https://doi.org/10.1007/s1007/s40090-018-0147-2

Krishnamoorthy, V., Dhanasekaran, R., Rana, D., Saravanan, S., & Rajesh Kumar, B. (2018). A comparative assessment of ternary blends of three bio-alcohols with waste cooking oil and diesel for optimum emissions and performance in a CI engine using response surface methodology. *Energy Conversion and Management*, *156*(October 2017), 337–357. https://doi.org/10.1016/j.enconman.2017.10.087

Kumagai, S., Hasegawa, I., Grause, G., Kameda, T., & Yoshioka, T. (2015). Thermal decomposition of individual and mixed plastics in the presence of CaO or Ca(OH)2. *Journal of Analytical and Applied Pyrolysis*, *113*, 584–590. https://doi.org/10.1016/j.jaap.2015.04.004

Kumar, S., Prakash, R., Murugan, S., & Singh, R. K. (2013a). Performance and emission analysis of blends of waste plastic oil obtained by catalytic pyrolysis of waste HDPE with diesel in a CI engine. *Energy Conversion and Management*, *74*, 323–331. https://doi.org/10.1016/j.enconman.2013.05.028

Kumar, S., Prakash, R., Murugan, S., & Singh, R. K. (2013b). Performance and emission analysis of blends of waste plastic oil obtained by catalytic pyrolysis of waste HDPE with diesel in a CI engine. *Energy Conversion and Management*, *74*, 323–331. https://doi.org/10.1016/j.enconman.2013.05.028

Kumaravel, S. T., Murugesan, A., & Kumaravel, A. (2016). Tyre pyrolysis oil as an alternative fuel for diesel engines – A review. *Renewable and Sustainable Energy Reviews*, *60*, 1678–1685. https://doi.org/10.1016/J.RSER.2016.03.035

Ladommatos, N., Abdelhalim, S., Zhao, H., & Hu, Z. (1998). *Effects of EGR on heat release in diesel combustion*. https://www.sae.org/publications/technical-papers/content/980184/

Lakshmi Sandhya Rani, S., & Vinoth Kumar, R. (2022). Fabrication and characterization of ceramic membranes derived from inexpensive raw material fuller's earth clay. *Materials Science and Engineering: B, 284*. https://doi.org/10.1016/j.mseb.2022.115877

Larrain, M., Van Passel, S., Thomassen, G., Kresovic, U., Alderweireldt, N., Moerman, E., & Billen, P. (2020). Economic performance of pyrolysis of mixed plastic waste: Open-loop versus closed-loop recycling. *Journal of Cleaner Production, 270*. https://doi.org/10.1016/j.jclepro.2020.122442

Lazzarotto, I. P., Ferreira, S. D., Junges, J., Bassanesi, G. R., Manera, C., Perondi, D., & Godinho, M. (2020). The role of CaO in the steam gasification of plastic wastes recovered from the municipal solid waste in a fluidized bed reactor. *Process Safety and Environmental Protection*, *140*, 60–67. https://doi.org/10.1016/j.psep.2020.04.009

Lee, U., Chung, J. N., & Ingley, H. A. (2014). High-Temperature Steam Gasification of Municipal Solid Waste, Rubber, Plastic and Wood. *Energy and Fuels*, *28*(7), 4573–4587. https://doi.org/10.1021/EF500713J

Lei, J., Yuan, G., Weerachanchai, P., Lee, S. W., Li, K., Wang, J. Y., & Yang, Y. (2018). Investigation on thermal dechlorination and catalytic pyrolysis in a continuous process for liquid fuel recovery from mixed plastic wastes. *Journal of Material Cycles and Waste Management*, *20*(1), 137–146. https://doi.org/10.1007/s10163-016-0555-3

Leng, S., Wang, X., Wang, J., Liu, Y., Ma, F., & Zhong, X. (2015). Waste Tire Pyrolysis for the Production of Light Hydrocarbons over Layered Catalysts. *Energy Technology*, *3*(8), 851–855. https://doi.org/10.1002/ente.201500031

Lin, H. T., Huang, M. S., Luo, J. W., Lin, L. H., Lee, C. M., & Ou, K. L. (2010). Hydrocarbon fuels produced by catalytic pyrolysis of hospital plastic wastes in a fluidizing cracking process. *Fuel Processing Technology*, *91*(11), 1355–1363. https://doi.org/10.1016/j.fuproc.2010.03.016

Liu, H., Zhang, P., Li, Z., Luo, J., Zheng, Z., & Yao, M. (2011). Effects of temperature inhomogeneities on the HCCI combustion in an optical engine. *Applied Thermal Engineering*, *31*(14–15), 2549–2555. https://doi.org/10.1016/j.applthermaleng.2011.04.020

Liu, X., Burra, K. G., Wang, Z., Li, J., Che, D., & Gupta, A. K. (2020). On deconvolution for understanding synergistic effects in co-pyrolysis of pinewood and polypropylene. *Applied Energy*, *279*(x), 115811. https://doi.org/10.1016/j.apenergy.2020.115811

López, A., de Marco, I., Caballero, B. M., Adrados, A., & Laresgoiti, M. F. (2011). Deactivation and regeneration of ZSM-5 zeolite in catalytic pyrolysis of plastic wastes. *Waste Management*, *31*(8), 1852–1858. https://doi.org/10.1016/J.WASMAN.2011.04.004

López, A., de Marco, I., Caballero, B. M., Laresgoiti, M. F., & Adrados, A. (2010). Pyrolysis of municipal plastic wastes: Influence of raw material composition. *Waste Management*, *30*(4), 620–627. https://doi.org/10.1016/j.wasman.2009.10.014

López, A., de Marco, I., Caballero, B. M., Laresgoiti, M. F., Adrados, A., & Aranzabal, A. (2011). Catalytic pyrolysis of plastic wastes with two different types of catalysts: ZSM-5 zeolite and Red Mud. *Applied Catalysis B: Environmental*, *104*(3–4), 211–219. https://doi.org/10.1016/j.apcatb.2011.03.030

Lopez, G., Erkiaga, A., Amutio, M., Bilbao, J., & Olazar, M. (2015). Effect of polyethylene co-feeding in the steam gasification of biomass in a conical

spouted bed reactor. *Fuel*, *153*, 393–401. https://doi.org/10.1016/J.FUEL.2015.03.006

Lopez, Gartzen, Maider Amutio, Gorka Elordi, Maite Artetxe, Haritz Altzibar, M. O. (2010). A conical spouted bed reactor for the valorisation of waste tires. *The 13th International Conference on Fluidization - New Paradigm in Fluidization Engineering, Art. 87*.

Lopez-Urionabarrenechea, A., De Marco, I., Caballero, B. M., Laresgoiti, M. F., & Adrados, A. (2012). Catalytic stepwise pyrolysis of packaging plastic waste. *Journal of Analytical and Applied Pyrolysis*, *96*, 54–62. https://doi.org/10.1016/j.jaap.2012.03.004

Lu, J. S., Chang, Y., Poon, C. S., & Lee, D. J. (2020). Slow pyrolysis of municipal solid waste (MSW): A review. *Bioresource Technology*, *312*(June), 123615. https://doi.org/10.1016/j.biortech.2020.123615

Lü, X. C., Chen, W., & Huang, Z. (2005). A fundamental study on the control of the HCCI combustion and emissions by fuel design concept combined with controllable EGR. Part 2. Effect of operating conditions and EGR on HCCI combustion. *Fuel*, *84*(9), 1084–1092. https://doi.org/10.1016/j.fuel.2004.12.015

Lubongo, C., Congdon, T., McWhinnie, J., & Alexandridis, P. (2022). Economic feasibility of plastic waste conversion to fuel using pyrolysis. *Sustainable Chemistry and Pharmacy*, *27*, 100683. https://doi.org/10.1016/J.SCP.2022.100683

Luo, W., Fan, Z., Wan, J., Hu, Q., Dong, H., & Zhang, X. (2021). Study on the reusability of kaolin as catalysts for catalytic pyrolysis of low-density polyethylene. *Fuel*, *302*(January), 121164. https://doi.org/10.1016/j.fuel.2021.121164

Madhumitha Jaganmohan. (2024). *Distribution of global plastic materials production in 2022, by region*.

Mahdavi, H., Eden, N. T., Doherty, C. M., Acharya, D., Smith, S. J. D., Mulet, X., & Hill, M. R. (2022). Underlying Polar and Nonpolar Modification MOF-Based Factors that Influence Permanent Porosity in Porous Liquids. *ACS Applied Materials & Interfaces*, *14*(20), 23392–23399. https://doi.org/10.1021/ACSAMI.2C03082

Mangesh, V. L., Padmanabhan, S., Tamizhdurai, P., & Ramesh, A. (2020). Experimental investigation to identify the type of waste plastic pyrolysis oil suitable for conversion to diesel engine fuel. *Journal of Cleaner Production*, *246*, 119066. https://doi.org/10.1016/j.jclepro.2019.119066

Mani, M., Nagarajan, G., & Sampath, S. (2010). An experimental investigation on a DI diesel engine using waste plastic oil with exhaust gas recirculation. *Fuel*, *89*(8), 1826–1832. https://doi.org/10.1016/j.fuel.2009.11.009

Mani, M., Nagarajan, G., & Sampath, S. (2011). Characterisation and effect of using waste plastic oil and diesel fuel blends in compression ignition engine. *Energy*, *36*(1), 212–219. https://doi.org/10.1016/j.energy.2010.10.049

Mariappan, M., Panithasan, M. S., & Venkadesan, G. (2021a). Pyrolysis plastic oil production and optimisation followed by maximum possible replacement of diesel with bio-oil/methanol blends in a CRDI engine. *Journal of Cleaner Production*, *312*(March), 127687. https://doi.org/10.1016/j.jclepro.2021.127687

Mariappan, M., Panithasan, M. S., & Venkadesan, G. (2021b). Pyrolysis plastic oil production and optimisation followed by maximum possible replacement of diesel with bio-oil/methanol blends in a CRDI engine. *Journal of Cleaner Production*, *312*(March), 127687. https://doi.org/10.1016/j.jclepro.2021.127687

Mastral, F. J., Esperanza, E., Garciía, P., & Juste, M. (2002). Pyrolysis of high-density polyethylene in a fluidised bed reactor. Influence of the temperature

and residence time. *Journal of Analytical and Applied Pyrolysis*, *63*(1), 1–15. https://doi.org/10.1016/S0165-2370(01)00137-1

Maurya, R. K., & Agarwal, A. K. (2014). Experimental investigations of performance, combustion and emission characteristics of ethanol and methanol fueled HCCI engine. *Fuel Processing Technology*, *126*, 30–48. https://doi.org/10.1016/j.fuproc.2014.03.031

Megaritis, A., Yap, D., Energy, M. W.-, & 2007, undefined. (2007). Effect of water blending on bioethanol HCCI combustion with forced induction and residual gas trapping. *Energy*, *32*(12), 2396–2400. https://www.sciencedirect.com/science/article/pii/S0360544207001004?casa_token=9hRKQDZiKYMAAAAA:CzXhBuPugcgjRr9blSl6ztHFrqeTVGhdl8lvRLrx6FUBdVt-mK2TJZ4KkGDtVFIw5xe7Y9oqjZkk

Miandad, R., Barakat, M. A., Aburiazaiza, A. S., Rehan, M., & Nizami, A. S. (2016). Catalytic pyrolysis of plastic waste: A review. *Process Safety and Environmental Protection*, *102*, 822–838. https://doi.org/10.1016/j.psep.2016.06.022

Miandad, R., Rehan, M., Barakat, M. A., Aburiazaiza, A. S., Khan, H., Ismail, I. M. I., Dhavamani, J., Gardy, J., Hassanpour, A., & Nizami, A. S. (2019). Catalytic pyrolysis of plastic waste: Moving toward pyrolysis based biorefineries. *Frontiers in Energy Research*, *7*(MAR), 27. https://doi.org/10.3389/FENRG.2019.00027/BIBTEX

Mitchual, S. J., Frimpong-Mensah, K., & Darkwa, N. A. (2014). Evaluation of Fuel Properties of Six Tropical Hardwood Timber Species for Briquettes. *Journal of Sustainable Bioenergy Systems*, *04*(01), 1–9. https://doi.org/10.4236/jsbs.2014.41001

Mohan, I., Yao, Z., Das, A. K., Prakash, R., & Kumar, S. (2023). Performance, emission and combustion characteristics of liquid fuel produced through catalytic co-pyrolysis of waste LDPE and Pongamia pinnata seeds: An

experimental investigation in CI engine. *Results in Engineering*, *20*, 101499. https://doi.org/10.1016/J.RINENG.2023.101499

Mohan, R. K., Sarojini, J., Rajak, U., Verma, T. N., & Ağbulut, Ü. (2023). Alternative fuel production from waste plastics and their usability in light duty diesel engine: Combustion, energy, and environmental analysis. *Energy*, *265*. https://doi.org/10.1016/j.energy.2022.126140

Moorthy Rajendran, K., Chintala, V., Sharma, A., Pal, S., Pandey, J. K., & Ghodke, P. (2020). Review of catalyst materials in achieving the liquid hydrocarbon fuels from municipal mixed plastic waste (MMPW). *Materials Today Communications*, *24*(October 2019), 100982. https://doi.org/10.1016/j.mtcomm.2020.100982

Mortezaeikia, V., & Tavakoli, O. (2022). Thermogravimetric Kinetics of Catalytic and Non-Catalytic Microwave-Assisted Pyrolysis of Waste Abs Plastic. *SSRN Electronic Journal*. https://doi.org/10.2139/ssrn.4121110

Munir, M. T., Mardon, I., Al-Zuhair, S., Shawabkeh, A., & Saqib, N. U. (2019). Plasma gasification of municipal solid waste for waste-to-value processing. *Renewable and Sustainable Energy Reviews*, *116*(April), 109461. https://doi.org/10.1016/j.rser.2019.109461

Murakami, T., Suzuki, Y., Nagasawa, H., Yamamoto, T., Koseki, T., Hirose, H., & Okamoto, S. (2009). Combustion characteristics of sewage sludge in an incineration plant for energy recovery. *Fuel Processing Technology*, *90*(6), 778–783. https://doi.org/10.1016/j.fuproc.2009.03.003

Musale, H. K., Bhattacharyulu, Y. C., Bhoyar, R. K., Student, P. G., & Professor, A. (2013). " Design Consideration Of Pyrolysis Reactor For Production Of Bio-Oil ". *International Journal of Engineering Trends and Technology*, *5*(2), 83–85.

Nagarajan, G., Rao, A. N., & Renganarayanan, S. (2002). Emission and performance characteristics of neat ethanol fuelled Dl diesel engine.

International Journal of Ambient Energy, *23*(3), 149–158. https://doi.org/10.1080/01430750.2002.9674883

Nalluri, P., Prem Kumar, P., & Ch Sastry, M. R. (2020). Experimental study on catalytic pyrolysis of plastic waste using low cost catalyst. In *Materials Today: Proceedings* (Vol. 45, pp. 7216–7221). https://doi.org/10.1016/j.matpr.2021.02.478

Nasution, F., Husin, H., Mahidin, Abnisa, F., Tirta Yani, F., Maulinda, L., & Ahmadi. (2022). Conversion of pyrolysis vapors derived from non-biodegradable waste plastics (PET) into valuable fuels using nickel-impregnated HZSM5-70 catalysts. *Energy Conversion and Management, 273*, 116440. https://doi.org/10.1016/J.ENCONMAN.2022.116440

Ncube, L. K., Ude, A. U., Ogunmuyiwa, E. N., Zulkifli, R., & Beas, I. N. (2021). An overview of plasticwaste generation and management in food packaging industries. *Recycling*, *6*(1), 1–25. https://doi.org/10.3390/recycling6010012

Ni, H. G., Lu, S. Y., Mo, T., & Zeng, H. (2016). Brominated flame retardant emissions from the open burning of five plastic wastes and implications for environmental exposure in China. *Environmental Pollution*, *214*, 70–76. https://doi.org/10.1016/j.envpol.2016.03.049

Nitter Kathrine. (2022). *Plastic waste is a resource that doesn't have to end up in the oceans*. https://norwegianscitechnews.com/2022/06/plastic-waste-is-a-resource-that-doesnt-have-to-end-up-in-the-oceans/

Obeid, F., Zeaiter, J., Al-Muhtaseb, A. H., & Bouhadir, K. (2014). Thermo-catalytic pyrolysis of waste polyethylene bottles in a packed bed reactor with different bed materials and catalysts. *Energy Conversion and Management, 85*, 1–6. https://doi.org/10.1016/J.ENCONMAN.2014.05.075

Okolie, J. A., Nanda, S., Dalai, A. K., Berruti, F., & Kozinski, J. A. (2020). A review on subcritical and supercritical water gasification of biogenic, polymeric and petroleum wastes to hydrogen-rich synthesis gas. *Renewable*

and Sustainable Energy Reviews, *119*, 109546. https://doi.org/10.1016/J.RSER.2019.109546

Onu, P., Vasile, C., Ciocîlteu, S., Iojoiu, E., & Darie, H. (1999). Thermal and catalytic decomposition of polyethylene and polypropylene. *Journal of Analytical and Applied Pyrolysis*, *49*(1), 145–153. https://doi.org/10.1016/S0165-2370(98)00109-0

Onwudili, J. A., Muhammad, C., & Williams, P. T. (2019). Influence of catalyst bed temperature and properties of zeolite catalysts on pyrolysis-catalysis of a simulated mixed plastics sample for the production of upgraded fuels and chemicals. *Journal of the Energy Institute*, *92*(5), 1337–1347. https://doi.org/10.1016/j.joei.2018.10.001

Orozco, S., Artetxe, M., Lopez, G., Suarez, M., Bilbao, J., & Olazar, M. (2021a). Conversion of HDPE into Value Products by Fast Pyrolysis Using FCC Spent Catalysts in a Fountain Confined Conical Spouted Bed Reactor. *ChemSusChem*, *14*(19), 4291–4300. https://doi.org/10.1002/cssc.202100889

Orozco, S., Artetxe, M., Lopez, G., Suarez, M., Bilbao, J., & Olazar, M. (2021b). Conversion of HDPE into Value Products by Fast Pyrolysis Using FCC Spent Catalysts in a Fountain Confined Conical Spouted Bed Reactor. *ChemSusChem*, *14*(19), 4291–4300. https://doi.org/10.1002/CSSC.202100889

Osman Y. Yansaneh, S. H. Z. (2022). *Recent Advances on Waste Plastic Thermal Pyrolysis_ A Critical Overview _ Enhanced Reader.pdf*. https://doi.org/10.3390/pr10020332

Ozdemir, C., Şahinkaya, S., Kalıpcı, E., Oden, M. K., Çepelioğullar, Ö., & Pütün, A. E. (2013). *Utilization of Two Different Types of Plastic Wastes from Daily and Industrial Life*.

Pal, S., Chintala, V., Sharma, A. K., Ghodke, P., Kumar, S., & Kumar, P. (2019). Effect of injection timing on performance and emission characteristics of

single cylinder diesel engine running on blends of diesel[1] S. Pal, V. Chintala, A. K. Sharma, P. Ghodke, S. Kumar, and P. Kumar, “Effect of injection timing on performance and emi. *Materials Today: Proceedings*, *17*, 209–215. https://doi.org/10.1016/j.matpr.2019.06.420.

Pal, S., Kumar, A., Sharma, A.K., Ghodke, P.K., Pandey, S., Patel, A., 2022. Recent Advances in Catalytic Pyrolysis of Municipal Plastic Waste for the Production of Hydrocarbon Fuels. Processes. https://doi.org/10.3390/pr10081497

Palomar-Torres, A., Torres-Jimenez, E., Kegl, B., Bombek, G., Volmajer-Valh, J., & Lešnik, L. (2022). Catalytic pyrolysis of plastic wastes for liquid oils’ production using ZAP USY zeolite as a catalyst. *International Journal of Environmental Science and Technology 2022*, 1–14. https://doi.org/10.1007/S13762-022-04023-Z

Palos, R., Rodríguez, E., Gutiérrez, A., Bilbao, J., & Arandes, J. M. (2022). Cracking of plastic pyrolysis oil over FCC equilibrium catalysts to produce fuels: Kinetic modeling. *Fuel*, *316*, 123341. https://doi.org/10.1016/J.FUEL.2022.123341

Pandey, S., Bhurat, S., & Chintala, V. (2019). Combustion and emissions behaviour assessment of a partially premixed charge compression ignition (PCCI) engine with diesel and fumigated ethanol. *Energy Procedia*, *160*, 590–596. https://doi.org/10.1016/j.egypro.2019.02.210

Pannetier, P., Morin, B., Clérandeau, C., Laurent, J., Chapelle, C., & Cachot, J. (2019). Toxicity assessment of pollutants sorbed on environmental microplastics collected on beaches: Part II-adverse effects on Japanese medaka early life stages. *Environmental Pollution*, *248*, 1098–1107. https://doi.org/10.1016/j.envpol.2018.10.129

Park, K. B., Choi, M. J., Chae, D. Y., Jung, J., & Kim, J. S. (2022). Separate two-step and continuous two-stage pyrolysis of a waste plastic mixture to

produce a chlorine-depleted oil. *Energy*, *244*, 122583. https://doi.org/10.1016/j.energy.2021.122583

Parku, G. K., Collard, F. X., & Görgens, J. F. (2020). Pyrolysis of waste polypropylene plastics for energy recovery: Influence of heating rate and vacuum conditions on composition of fuel product. *Fuel Processing Technology*, *209*. https://doi.org/10.1016/j.fuproc.2020.106522

Patel, M. A., Kar, A. S., Kumar, S., Das, M. K., Raut, V. V., & Tomar, B. S. (2019). Effect of sulfate on sorption of Eu(III) by Na-montmorillonite. *Radiochimica Acta*, *107*(2), 115–128. https://doi.org/10.1515/RACT-2018-2964/MACHINEREADABLECITATION/RIS

Pathak, S. K., Nayyar, A., & Goel, V. (2021). Optimization of EGR effects on performance and emission parameters of a dual fuel (Diesel + CNG) CI engine: An experimental investigation. *Fuel*, *291*(January). https://doi.org/10.1016/j.fuel.2021.120183

Paula costa, FGilomena Pinto, Ricardo Mata, Paula Marques, Filipe Paradela, & Luis costa. (2021). *Validation of the application of the pyrolysis process for the treatment and transformation of municipal plastic wastes.pdf* (pp. 859–864). A journla of the italian Association of the chemical engineering. https://doi.org/10.3303/CET2186144

Praveenkumar, T. R., Velusamy, P., & Balamoorthy, D. (2020). Pyrolysis oil for diesel engines from plastic solid waste: a performance, combustion and emission study. *International Journal of Ambient Energy*, *0*(0), 1–21. https://doi.org/10.1080/01430750.2020.1818124

Qiu, B., Deng, N., Zhang, Y., & Wan, H. (2018). Application of industrial solid wastes in catalytic pyrolysis. *Asia-Pacific Journal of Chemical Engineering*, *13*(1), e2150. https://doi.org/10.1002/APJ.2150

Qureshi, M. S., Oasmaa, A., Pihkola, H., Deviatkin, I., Tenhunen, A., Mannila, J., Minkkinen, H., Pohjakallio, M., & Laine-Ylijoki, J. (2020). Pyrolysis of

plastic waste: Opportunities and challenges. *Journal of Analytical and Applied Pyrolysis*, *152*. https://doi.org/10.1016/j.jaap.2020.104804

Ragaert, K., Delva, L., & Van Geem, K. (2017). Mechanical and chemical recycling of solid plastic waste. In *Waste Management* (Vol. 69, pp. 24–58). Elsevier Ltd. https://doi.org/10.1016/j.wasman.2017.07.044

Rahimi, A. R., & Garciá, J. M. (2017). Chemical recycling of waste plastics for new materials production. In *Nature Reviews Chemistry* (Vol. 1). Nature Publishing Group. https://doi.org/10.1038/s41570-017-0046

Rahman, M. H., Bhoi, P. R., Saha, A., Patil, V., & Adhikari, S. (2021). Thermo-catalytic co-pyrolysis of biomass and high-density polyethylene for improving the yield and quality of pyrolysis liquid. *Energy*, *225*. https://doi.org/10.1016/j.energy.2021.120231

Ribeiro, A., 2013. Ribeiro_2013.pdf. Geol. Port. Vol. 1 - Geol. Pré-mesozóica Port.

Rajak, U., Panchal, M., Veza, I., Ağbulut, Ü., Nath Verma, T., Sarıdemir, S., & Shende, V. (2022). Experimental investigation of performance, combustion and emission characteristics of a variable compression ratio engine using low-density plastic pyrolyzed oil and diesel fuel blends. *Fuel*, *319*(April 2021). https://doi.org/10.1016/j.fuel.2022.123720

Rajak, U., & Verma, T. N. (2020). Influence of combustion and emission characteristics on a compression ignition engine from a different generation of biodiesel. *Engineering Science and Technology, an International Journal*, *23*(1), 10–20. https://doi.org/10.1016/J.JESTCH.2019.04.003

Rasul Jan, M., Shah, J., & Gulab, H. (2013). Catalytic conversion of waste high-density polyethylene into useful hydrocarbons. *Fuel*, *105*, 595–602. https://doi.org/10.1016/j.fuel.2012.09.016

Ratnasari, D. K., Nahil, M. A., & Williams, P. T. (2017). Catalytic pyrolysis of waste plastics using staged catalysis for production of gasoline range hydrocarbon oils. *Journal of Analytical and Applied Pyrolysis*, *124*, 631–637. https://doi.org/10.1016/j.jaap.2016.12.027

Ruhul, A. M., Kalam, M. A., Masjuki, H. H., Fattah, I. M. R., Reham, S. S., & Rashed, M. M. (2015). State of the art of biodiesel production processes: a review of the heterogeneous catalyst. *RSC Advances*, *5*(122), 101023–101044. https://doi.org/10.1039/C5RA09862A

Rui, Z., Lu, J., Zhang, Z., Guo, R., Ling, K., Zhang, R., & Patil, S. (2017). A quantitative oil and gas reservoir evaluation system for development. *Journal of Natural Gas Science and Engineering*, *42*, 31–39. https://doi.org/10.1016/J.JNGSE.2017.02.026

Ravikanth, P., Sudarshan, V., Rao, A.N., 2020. Xrd Studies on Fuller ' S Earth , Vikarabad - Tandur Area , 22, 2020.

S Tamilkolundu, C. M. (2012). *The Evaluation of blend of Waste Plastic Oil-Diesel fuel for use as alternate fuel for transportation*. 2nd International Conference on Chemical, Ecology and Environmental Sciences (ICCEES'2012) Singapore April.

Saad, J. M., Nahil, M. A., & Williams, P. T. (2015). Influence of process conditions on syngas production from the thermal processing of waste high density polyethylene. *Journal of Analytical and Applied Pyrolysis*, *113*, 35–40. https://doi.org/10.1016/j.jaap.2014.09.027

Saeaung, K., Phusunti, N., Phetwarotai, W., Assabumrungrat, S., & Cheirsilp, B. (2021). Catalytic pyrolysis of petroleum-based and biodegradable plastic waste to obtain high-value chemicals. *Waste Management*, *127*, 101–111. https://doi.org/10.1016/J.WASMAN.2021.04.024

Saha, D., Sinha, A., & Roy, B. (2021). Critical insights into the effects of plastic pyrolysis oil on emission and performance characteristics of CI engine.

Environmental Science and Pollution Research, *28*(33), 44598–44621. https://doi.org/10.1007/s11356-021-14919-x

Salahudeen, N., Ahmed, A.S., Al-Muhtaseb, A.H., Dauda, M., Jibril, B.Y., Viswanadham, N., Saxena, S.K., 2017. Synthesis of RE Y zeolite for formulation of FCC catalyst and the catalytic performance in cracking of n-hexadecane. *Res. Chem. Intermed*. 43, 467–479. https://doi.org/10.1007/s11164-016-2635-3

Sambandam, P., Venu, H., & Narayanaperumal, B. K. (2020). Effective utilization and evaluation of waste plastic pyrolysis oil in a low heat rejection single cylinder diesel engine. *Energy Sources, Part A: Recovery, Utilization and Environmental Effects*, *00*(00), 1–17. https://doi.org/10.1080/15567036.2020.1803453

Sangpatch, T., Supakata, N., Kanokkantapong, V., & Jongsomjit, B. (2019a). Fuel oil generated from the cogon grass-derived Al–Si (Imperata cylindrica (L.) Beauv) catalysed pyrolysis of waste plastics. *Heliyon*, *5*(8), e02324. https://doi.org/10.1016/J.HELIYON.2019.E02324

Sangpatch, T., Supakata, N., Kanokkantapong, V., & Jongsomjit, B. (2019b). Fuel oil generated from the cogon grass-derived Al–Si (Imperata cylindrica (L.) Beauv) catalysed pyrolysis of waste plastics. *Heliyon*, *5*(8), e02324. https://doi.org/10.1016/J.HELIYON.2019.E02324

Sanlisoy, A., & Carpinlioglu, M. O. (2017). A review on plasma gasification for solid waste disposal. *International Journal of Hydrogen Energy*, *42*(2), 1361–1365. https://doi.org/10.1016/j.ijhydene.2016.06.008

Sayin, C. (2010). Engine performance and exhaust gas emissions of methanol and ethanol–diesel blends. *Fuel*, *89*(11), 3410–3415. https://doi.org/10.1016/J.FUEL.2010.02.017

Sayin, C., & Gumus, M. (2011). Impact of compression ratio and injection parameters on the performance and emissions of a di diesel engine fueled

with biodiesel-blended diesel fuel. *Applied Thermal Engineering*, *31*(16), 3182–3188. https://doi.org/10.1016/j.applthermaleng.2011.05.044

Sekar, M., Praveenkumar, T. R., Dhinakaran, V., Gunasekar, P., & Pugazhendhi, A. (2021). Combustion and emission characteristics of diesel engine fueled with nanocatalyst and pyrolysis oil produced from the solid plastic waste using screw reactor. *Journal of Cleaner Production*, *318*(August), 128551. https://doi.org/10.1016/j.jclepro.2021.128551

Selvam, M. A. J., Sambandam, P., & Sujeesh, K. J. (2022). Investigation of performance and emission characteristics of single-cylinder DI diesel engine with plastic pyrolysis oil and diethyl ether blends. *International Journal of Ambient Energy*, *43*(1), 3810–3814. https://doi.org/10.1080/01430750.2020.1860127

Sembiring, F., Purnomo, C. W., & Purwono, S. (2018). *Catalytic Pyrolysis of Waste Plastic Mixture Catalytic Pyrolysis of Waste Plastic Mixture*. https://doi.org/10.1088/1757-899X/316/1/012020

Senthil Kumar, P., Bharathikumar, M., Prabhakaran, C., Vijayan, S., & Ramakrishnan, K. (2017). Conversion of waste plastics into low-emissive hydrocarbon fuels through catalytic depolymerization in a new laboratory scale batch reactor. *International Journal of Energy and Environmental Engineering*, *8*(2), 167–173. https://doi.org/10.1007/s40095-015-0167-z

Senthilkumar, P., & Sankaranarayanan, G. (2016). Effect of Jatropha methyl ester on waste plastic oil fueled DI diesel engine. *Journal of the Energy Institute*, *89*(4), 504–512. https://doi.org/10.1016/j.joei.2015.07.006

Shadangi, K. P., & Mohanty, K. (2014). Production and characterization of pyrolytic oil by catalytic pyrolysis of Niger seed. *Fuel*, *126*, 109–115. https://doi.org/10.1016/j.fuel.2014.02.035

Shahir, V. K., Jawahar, C. P., Vinod, V., & Suresh, P. R. (2018). Experimental Investigations on the Performance and Emission Characteristics of a

Common Rail Direct Injection Engine Using Tyre Pyrolytic Biofuel. *Journal of King Saud University - Engineering Sciences*. https://doi.org/10.1016/j.jksues.2018.05.004

Sharma, A. K., Sahoo, P. K., & Singhal, S. (2016). Comparative evolution of biomass production and lipid accumulation potential of Chlorella species grown in a bubble column photobioreactor. *Biofuels*, *7*(4). https://doi.org/10.1080/17597269.2015.1138040

Sharma, A. K., Sahoo, P. K., Singhal, S., & Joshi, G. (2016). Exploration of upstream and downstream process for microwave assisted sustainable biodiesel production from microalgae Chlorella vulgaris. *Bioresource Technology*, *216*, 793–800. https://doi.org/10.1016/j.biortech.2016.06.013

Sharma, A. K., Sharma, P. K., Chintala, V., Khatri, N., & Patel, A. (2020). Environment-friendly biodiesel/diesel blends for improving the exhaust emission and engine performance to reduce the pollutants emitted from transportation fleets. *International Journal of Environmental Research and Public Health*, *17*(11). https://doi.org/10.3390/ijerph17113896

Sharuddin, S. D. A., Abnisa, F., Daud, W. M. A. W., & Aroua, M. K. (2018). Pyrolysis of plastic waste for liquid fuel production as prospective energy resource. *IOP Conference Series: Materials Science and Engineering*, *334*(1), 012001. https://doi.org/10.1088/1757-899X/334/1/012001

Shi, X., Yu, Y., He, H., Shuai, S., Wang, J., & Li, R. (2005). Emission characteristics using methyl soyate-ethanol-diesel fuel blends on a diesel engine. *Fuel*, *84*(12–13), 1543–1549. https://doi.org/10.1016/j.fuel.2005.03.001

Shrivastava, P., Salam, S., Verma, T. N., & Samuel, O. D. (2020). Experimental and empirical analysis of an IC engine operating with ternary blends of diesel, karanja and roselle biodiesel. *Fuel*, *262*, 116608. https://doi.org/10.1016/J.FUEL.2019.116608

Silitonga, A. S., Masjuki, H. H., Mahlia, T. M. I., Ong, H. C., Chong, W. T., & Boosroh, M. H. (2013). Overview properties of biodiesel diesel blends from edible and non-edible feedstock. In *Renewable and Sustainable Energy Reviews* (Vol. 22, pp. 346–360). https://doi.org/10.1016/j.rser.2013.01.055

Silva, R. R. A., Marques, C. S., Arruda, T. R., Teixeira, S. C., & de Oliveira, T. V. (2023). Biodegradation of Polymers: Stages, Measurement, Standards and Prospects. *Macromol*, *3*(2), 371–399. https://doi.org/10.3390/macromol3020023

Singh, A. P., & Agarwal, A. K. (2012). Combustion characteristics of diesel HCCI engine: An experimental investigation using external mixture formation technique. *Applied Energy*, *99*, 116–125. https://doi.org/10.1016/j.apenergy.2012.03.060

Singh, G., Singh, A. P., & Agarwal, A. K. (2014). Experimental investigations of combustion, performance and emission characterization of biodiesel fuelled HCCI engine using external mixture formation technique. *Sustainable Energy Technologies and Assessments*, *6*, 116–128. https://doi.org/10.1016/j.seta.2014.01.002

Singh, R. K., Ruj, B., Sadhukhan, A. K., & Gupta, P. (2019a). Impact of fast and slow pyrolysis on the degradation of mixed plastic waste: Product yield analysis and their characterization. *Journal of the Energy Institute*, *92*(6), 1647–1657. https://doi.org/10.1016/j.joei.2019.01.009

Singh, R. K., Ruj, B., Sadhukhan, A. K., & Gupta, P. (2019b). Impact of fast and slow pyrolysis on the degradation of mixed plastic waste: Product yield analysis and their characterization. *Journal of the Energy Institute*, *92*(6), 1647–1657. https://doi.org/10.1016/J.JOEI.2019.01.009

Singh, R. K., Ruj, B., Sadhukhan, A. K., & Gupta, P. (2022). Conventional pyrolysis of Plastic waste for Product recovery and utilization of pyrolytic gases for carbon nanotubes production. *Environmental Science and Pollution*

Research, *29*(14), 20007–20016. https://doi.org/10.1007/s11356-020-11204-1

Singh, R. K., Ruj, B., Sadhukhan, A. K., Gupta, P., & Tigga, V. P. (2020a). Waste plastic to pyrolytic oil and its utilization in CI engine: Performance analysis and combustion characteristics. *Fuel*, *262*(May), 116539. https://doi.org/10.1016/j.fuel.2019.116539

Singh, R. K., Ruj, B., Sadhukhan, A. K., Gupta, P., & Tigga, V. P. (2020b). Waste plastic to pyrolytic oil and its utilization in CI engine : Performance analysis and combustion characteristics. *Fuel*, *262*(November 2019), 116539. https://doi.org/10.1016/j.fuel.2019.116539

Singh, R. K., Ruj, B., Sadhukhan, A. K., Gupta, P., & Tigga, V. P. (2020c). Waste plastic to pyrolytic oil and its utilization in CI engine : Performance analysis and combustion characteristics. *Fuel*, *262*(November 2019), 116539. https://doi.org/10.1016/j.fuel.2019.116539

Singh, T. S., Rajak, U., Verma, T. N., Nashine, P., Mehboob, H., Manokar, A. M., & Afzal, A. (2022). Exhaust emission characteristics study of light and heavy-duty diesel vehicles in India. *Case Studies in Thermal Engineering*, *29*, 101709. https://doi.org/10.1016/J.CSITE.2021.101709

Singh, T. S., Verma, T. N., & Singh, H. N. (2020). A lab scale waste to energy conversion study for pyrolysis of plastic with and without catalyst: Engine emissions testing study. *Fuel*, *277*(April), 118176. https://doi.org/10.1016/j.fuel.2020.118176

Sipra, A. T., Gao, N., & Sarwar, H. (2018). Municipal solid waste (MSW) pyrolysis for bio-fuel production: A review of effects of MSW components and catalysts. *Fuel Processing Technology*, *175*(October 2017), 131–147. https://doi.org/10.1016/j.fuproc.2018.02.012

Sivagami, K., Divyapriya, G., & Selvaraj, R. (2021). Catalytic pyrolysis of polyolefin and multilayer packaging based waste plastics : A pilot scale

study. *Process Safety and Environmental Protection*, *149*, 497–506. https://doi.org/10.1016/j.psep.2020.10.038

S.M. Al-Salem. (2019). Thermal pyrolysis of high density polyethylene (HDPE) in a novel fixed bed reactor system for the production of high value gasoline range hydrocarbons (HC). *Process Safety and Environmental Protection*, *127*, 171–179. https://doi.org/10.1016/j.psep.2019.05.008

Sogancioglu, M., Yel, E., & Ahmetli, G. (2017). Pyrolysis of waste high density polyethylene (HDPE) and low density polyethylene (LDPE) plastics and production of epoxy composites with their pyrolysis chars. *Journal of Cleaner Production*, *165*, 369–381. https://doi.org/10.1016/j.jclepro.2017.07.157

Sridhar, A., Rahman, M., Infantes-Molina, A., Wylie, B. J., Borcik, C. G., & Khatib, S. J. (2020). Bimetallic Mo-Co/ZSM-5 and Mo-Ni/ZSM-5 catalysts for methane dehydroaromatization: A study of the effect of pretreatment and metal loadings on the catalytic behavior. *Applied Catalysis A: General*, *589*. https://doi.org/10.1016/J.APCATA.2019.117247

Srivastava, V., Vaish, B., Singh, R. P., & Singh, P. (2020). An insight to municipal solid waste management of Varanasi city, India, and appraisal of vermicomposting as its efficient management approach. *Environmental Monitoring and Assessment*, *192*(3). https://doi.org/10.1007/S10661-020-8135-3

Statistical Review of World Energy. (2022). http:// www.bp.com, 2022

Subash, M. chares, Karthikumar, S., Begum, S. N., & Manjula, C. (2022). Optimization studies on decolourization of non-edible cashew oil for industrial application. *Cleaner and Circular Bioeconomy*, *1*. https://doi.org/10.1016/j.clcb.2022.100006

Subbareddy, Y., Kumar, R. N., Sudhakar, B. K., Reddy, K. R., Martha, S. K., & Kaviyarasu, K. (2020). A facile approach of adsorption of acid blue 9 on

aluminium silicate-coated Fuller's Earth—Equilibrium and kinetics studies. *Surfaces and Interfaces*, *19*. https://doi.org/10.1016/j.surfin.2020.100503

Subhaschandra, T., Nath, T., & Neeranjan, H. (2020). A lab scale waste to energy conversion study for pyrolysis of plastic with and without catalyst : Engine emissions testing study. *Fuel*, *277*(February), 118176. https://doi.org/10.1016/j.fuel.2020.118176

Suriapparao, D. V., Boruah, B., Raja, D., & Vinu, R. (2018). Microwave assisted co-pyrolysis of biomasses with polypropylene and polystyrene for high quality bio-oil production. *Fuel Processing Technology*, *175*, 64–75. https://doi.org/10.1016/j.fuproc.2018.02.019

Suriapparao, D. V., Kumar, D. A., & Vinu, R. (2022). Microwave co-pyrolysis of PET bottle waste and rice husk: effect of plastic waste loading on product formation. *Sustainable Energy Technologies and Assessments*, *49*(November 2021), 101781. https://doi.org/10.1016/j.seta.2021.101781

Susastriawan, A. A. P., & Sandria, A. (2020). Experimental study the influence of zeolite size on low-temperature pyrolysis of low-density polyethylene plastic waste. *Thermal Science and Engineering Progress*, *17*(February), 100497. https://doi.org/10.1016/j.tsep.2020.100497

Swift, G. (2015). Degradable Polymers and Plastics in Landfill Sites. In *Encyclopedia of Polymer Science and Technology* (pp. 1–13). Wiley. https://doi.org/10.1002/0471440264.pst457.pub2

Syamsiro, M., Saptoadi, H., Norsujianto, T., Noviasri, P., Cheng, S., Alimuddin, Z., & Yoshikawa, K. (2014). Fuel oil production from municipal plastic wastes in sequential pyrolysis and catalytic reforming reactors. *Energy Procedia*, *47*, 180–188. https://doi.org/10.1016/j.egypro.2014.01.212

Tesfa, B., Mishra, R., Gu, F., & Powles, N. (2010). Prediction models for density and viscosity of biodiesel and their effects on fuel supply system in CI

engines. *Renewable Energy*, *35*(12), 2752–2760. https://doi.org/10.1016/J.RENENE.2010.04.026

Thahir, R., Altway, A., Juliastuti, S. R., & Susianto. (2019). Production of liquid fuel from plastic waste using integrated pyrolysis method with refinery distillation bubble cap plate column. *Energy Reports*, *5*, 70–77. https://doi.org/10.1016/j.egyr.2018.11.004

The Drive. (2023). https://www.thedrive.com/guides-and-gear/how-many-cars-are-there-in-the-world

Thiyagarajan, S., Sonthalia, A., Edwin Geo, V., Ashok, B., Nanthagopal, K., Karthickeyan, V., & Dhinesh, B. (2019). Effect of electromagnet-based fuel-reforming system on high-viscous and low-viscous biofuel fueled in heavy-duty CI engine. *Journal of Thermal Analysis and Calorimetry*, *138*(1), 633–644. https://doi.org/10.1007/S10973-019-08123-W/METRICS

Thommes, M., Kaneko, K., Neimark, A. V., Olivier, J.P., Rodriguez-Reinoso, F., Rouquerol, J., Sing, K.S.W., 2015. Physisorption of gases, with special reference to the evaluation of surface area and pore size distribution (IUPAC Technical Report). *Pure Appl. Chem*. 87, 1051–1069. https://doi.org/10.1515/pac-2014-1117

Ubando, A. T., Chueh, C.-C., Jin, L., Belbessai, S., Azara, A., & Abatzoglou, N. (2022). Recent Advances in the Decontamination and Upgrading of Waste Plastic Pyrolysis Products: An Overview. *Processes 2022, Vol. 10, Page 733*, *10*(4), 733. https://doi.org/10.3390/PR10040733

Vanapalli, K. R., Sharma, H. B., Ranjan, V. P., Samal, B., Bhattacharya, J., Dubey, B. K., & Goel, S. (2021). Challenges and strategies for effective plastic waste management during and post COVID-19 pandemic. *Science of the Total Environment*, *750*. https://doi.org/10.1016/j.scitotenv.2020.141514

Venkatesan, H., Sivamani, S., Bhutoria, K., & Vora, H. H. (2018). Experimental study on combustion and performance characteristics in a DI CI engine

fuelled with blends of waste plastic oil. *Alexandria Engineering Journal*, *57*(4), 2257–2263. https://doi.org/10.1016/j.aej.2017.09.001

Venkatesan, S. P., Jeevahan, J. J., Hemanandh, J., Ganesan, S., Rajakavieswaran, R., & Saravanan, V. (2020). Performance and emission characteristics of diesel engine using waste plastic oil with N-hexanol as an additive. *AIP Conference Proceedings*, *2311*. https://doi.org/10.1063/5.0034393

Viswanath K. Kaimal, P. V. balan. (2015). A detailed study of combustion characteristics of a DI diesel engine using waste plastic oil and its blends. *Energy Conversion and Management* , *105*, 951–956.

Walendziewski, J. (2002). Engine fuel derived from waste plastics by thermal treatment. *Fuel*, *81*(4), 473–481. https://doi.org/10.1016/S0016-2361(01)00118-1

Wan Nurdyana wan mansor et al. (2021). *A review of plastic -derived diesel fuel as a renewable fuel for internal combustion engines: Application , challanges and global potential*. https://doi.org/10.1088/1755-1315/1013/1/012014

Wang, J., & Azam, W. (2024). Natural resource scarcity, fossil fuel energy consumption, and total greenhouse gas emissions in top emitting countries. *Geoscience Frontiers*, *15*(2), 101757. https://doi.org/10.1016/J.GSF.2023.101757

Wang, Q., Zhang, J., Wang, G., Wang, H., & Sun, M. (2018). Thermal and Kinetic Analysis of Coal with Different Waste Plastics (PVC) in Cocombustion. *Energy and Fuels*, *32*(2), 2145–2155. https://doi.org/10.1021/acs.energyfuels.7b03268

Ware, R. L., Rowland, S. M., Rodgers, R. P., & Marshall, A. G. (2017). Advanced Chemical Characterization of Pyrolysis Oils from Landfill Waste, Recycled Plastics, and Forestry Residue. *Energy and Fuels*, *31*(8), 8210–8216. https://doi.org/10.1021/acs.energyfuels.7b00865

Wei, Y., Fakudze, S., Zhang, Y., Ma, R., Shang, Q., Chen, J., Liu, C., & Chu, Q. (2022). Co-hydrothermal carbonization of pomelo peel and PVC for production of hydrochar pellets with enhanced fuel properties and dechlorination. *Energy*, *239*. https://doi.org/10.1016/j.energy.2021.122350

Wen, X., Chen, X., Tian, N., Gong, J., Liu, J., Rümmeli, M. H., Chu, P. K., Mijiwska, E., & Tang, T. (2014). Nanosized carbon black combined with Ni2O3 as "universal" catalysts for synergistically catalyzing carbonization of polyolefin wastes to synthesize carbon nanotubes and application for supercapacitors. *Environmental Science and Technology*, *48*(7), 4048–4055. https://doi.org/10.1021/ES404646E/SUPPL_FILE/ES404646E_SI_001.PDF

Westerhout, R. W. J., Van Koningsbruggen, M. P., Van Der Ham, A. G. J., Kuipers, J. A. M., & Van Swaaij, W. P. M. (1998). Techno-economic evaluation of high temperature pyrolysis processes for mixed plastic waste. *Chemical Engineering Research and Design*, *76*(3), 427–439. https://doi.org/10.1205/026387698524857

Won, H., Heui, D., Jae, J., Shiung, S., Duck, E., & Park, Y. (2020). Bioresource Technology Recent advances in catalytic co-pyrolysis of biomass and plastic waste for the production of petroleum-like hydrocarbons. *Bioresource Technology*, *310*(February), 123473. https://doi.org/10.1016/j.biortech.2020.123473

Wong, S. L., Ngadi, N., Abdullah, T. A. T., & Inuwa, I. M. (2017). Conversion of low density polyethylene (LDPE) over ZSM-5 zeolite to liquid fuel. *Fuel*, *192*, 71–82. https://doi.org/10.1016/J.FUEL.2016.12.008

Wu, P., Sun, J., Abbas, M., Wang, P., Chen, Y., & Chen, J. (2020). Hydrophobic SiO2 supported Fe-Ni bimetallic catalyst for the production of high-calorie synthetic natural gas. *Applied Catalysis A: General*, *590*, 117302. https://doi.org/10.1016/J.APCATA.2019.117302

Wu, Y., Wang, G., Zhu, J., Wang, Y., Yang, H., Jin, L., & Hu, H. (2022). Insight into synergistic effect of co-pyrolysis of low-rank coal and waste polyethylene with or without additives using rapid infrared heating. *Journal of the Energy Institute*, *102*, 384–394. https://doi.org/10.1016/J.JOEI.2022.05.005

Xiangjin Kong., Zhijun Li., Boxi Shen., Yue Wu., Yanke Zhang., Dong Cai. (2019). Simulation of flow and soot particle distribution in wall-flow DPF based on lattice Boltzmann method. Chemical Engineering Science, 202, 169-185. https://doi.org/10.1016/j.ces.2019.03.039

Yadav, R., Sharma, A. K., & Babu, J. N. (2016). Sorptive removal of arsenite [As(III)] and arsenate [As(V)] by fuller's earth immobilized nanoscale zero-valent iron nanoparticles (F-nZVI): Effect of Fe0 loading on adsorption activity. *Journal of Environmental Chemical Engineering*, *4*(1), 681–694. https://doi.org/10.1016/j.jece.2015.12.019

Yadav, V., Sherly, M. A., Ranjan, P., Tinoco, R. O., Boldrin, A., Damgaard, A., & Laurent, A. (2020). Framework for quantifying environmental losses of plastics from landfills. *Resources, Conservation and Recycling*, *161*. https://doi.org/10.1016/j.resconrec.2020.104914

Yang, R.-X., Jan, K., Chen, C.-T., Chen, W.-T., & Wu, K. C.-W. (2022). Thermochemical Conversion of Plastic Waste into Fuels, Chemicals, and Value-Added Materials: A Critical Review and Outlooks. *ChemSusChem*, e202200171. https://doi.org/10.1002/CSSC.202200171

Yansaneh, O. Y., & Zein, S. H. (2022). Latest Advances in Waste Plastic Pyrolytic Catalysis. *Processes 2022, Vol. 10, Page 683*, *10*(4), 683. https://doi.org/10.3390/PR10040683

Zakariyaou, S.Y., Ye, H., Oumarou, A.D.M., Abdoul Aziz, M.S., Ke, S., 2023. Characterization of Equilibrium Catalysts from the Fluid Catalytic Cracking

Process of Atmospheric Residue. *Catalysts* 13, 1–22. https://doi.org/10.3390/catal13121483

Zhang, Q., Dor, L., Fenigshtein, D., Yang, W., & Blasiak, W. (2012). Gasification of municipal solid waste in the Plasma Gasification Melting process. *Applied Energy*, *90*(1), 106–112. https://doi.org/10.1016/j.apenergy.2011.01.041

Zhang, Z., Chen, F., Rezakazemi, M., Zhang, W., Lu, C., Chang, H., & Quan, X. (2018). Modeling of a CO2-piperazine-membrane absorption system. *Chemical Engineering Research and Design*, *131*, 375–384. https://doi.org/10.1016/J.CHERD.2017.11.024

Zhao, F.-Q., Lai, M.-C., & Harrington, D. L. (1995). The Spray Characteristics of Automotive Port Fuel Injection-A Critical Review. In *JOURNAL OF FUELS & LUBRICANTS* (Vol. 104).

Zhao, S., Wang, C., Bai, B., Jin, H., & Wei, W. (2022). Study on the polystyrene plastic degradation in supercritical water/CO2 mixed environment and carbon fixation of polystyrene plastic in CO2 environment. *Journal of Hazardous Materials*, *421*(July 2021), 126763. https://doi.org/10.1016/j.jhazmat.2021.126763

Zhou, H., Saad, J. M., Li, Q., & Xu, Y. (2020). Steam reforming of polystyrene at a low temperature for high H2/CO gas with bimetallic Ni-Fe/ZrO2 catalyst. *Waste Management*, *104*, 42–50. https://doi.org/10.1016/J.WASMAN.2020.01.017

Zhou, N., Dai, L., Lyu, Y., Li, H., Deng, W., Guo, F., Chen, P., Lei, H., & Ruan, R. (2021). Catalytic pyrolysis of plastic wastes in a continuous microwave assisted pyrolysis system for fuel production. *Chemical Engineering Journal*, *418*(March), 129412. https://doi.org/10.1016/j.cej.2021.129412

Zhu, L., Cheung, C. S., Zhang, W. G., & Huang, Z. (2011). Combustion, performance and emission characteristics of a DI diesel engine fueled with

ethanol–biodiesel blends. *Fuel*, *90*(5), 1743–1750. https://doi.org/10.1016/J.FUEL.2011.01.024

zicai chen, Yiqian wang, zhipeng sun. (2021). Application of CoNi intercalated vermiculite catalyst in pyrolysis of plastic. *Journal of Physics: Conference Series*. https://doi.org/10.1088/1742-6596/1885/3032030

Zubris, K. A. V., & Richards, B. K. (2005). Synthetic fibers as an indicator of land application of sludge. *Environmental Pollution*, *138*(2), 201–211. https://doi.org/10.1016/j.envpol.2005.04.013

LIST OF PUBLICATIONS

Shashank Pal, Amit Sharma, Anil Kumar , Shyam Pandey " Recent advance in catalytic pyrolysis of municipal plastic waste for the production of hydrocarbon fuels" processes 2022, 10, 1497 doi: 10.3390/pr10081497 IF - 3.352

Shashank Pal, Anil Kumar et al. "Experimental evaluation of diesel blends mixed with municipal plastic waste pyrolysis oil on performance and emission characteristics of CI engine" Case Studies in Thermal Engineering, Volume 47, July 2023, 103074 DOI: 10.1016/j.csite.2023.103074 IF. 6.2

Shashank Pal, Sunil Kumar, Priyanka, Anil Kumar,.Shyam Pandey, D. Dobrota "Feasibility of Performance Evaluation of Plastic oil in Compression Ignition Engines: A MCDM MULTIMOORA Approach" Fuel. Manuscript Number: JFUE-D-24-04268 IF. 7.4

Shashank Pal, Amit Sharma, Shyam Pandey "A review: Catalytic pyrolysis of Municipal solid plastic waste (MSPW) for production of liquid hydrocarbon fuels" Recent advance in recycling engineering Springer proceeding. pp 165-175 (2022) doi:10.1007/978-981-19-3931-0_13

Shashank Pal, Amit Sharma, Sunil Tiwari, SM Tauseef "Comparative assessment of performance and emission characteristics of DI diesel engine fueled with combined blending of biodiesel butanol and conventional diesel "Springer Proceedings in Earth and Environmental Sciences" pp 495–503 (2021) doi: 0.1007/978-3-030-79065-3_37

Shashank pal, Amit Sharma, Praveen godkhe et al.."Effect of injection timing on performance and emission characteristics of single cylinder diesel engine running on blends of diesel and waste plastic fuels" Materials today proceeding 17 209–215 (2019) doi.org/10.1016/j.matpr.2019.06.420

Shashank Pal, Shyam Pandey et al. "Recycling of Plastic Waste into Transportation Fuels and Value Added Products Renewable Energy Innovations: Biofuels, Solar, and Other Technologies. Page No. 97-122 (2023) doi.org/10.1002/9781119785712.ch4

Shashank Pal, Shyam Pandey, Ram Kunwer, PS Ranjit "An Outlook on Oxygenated Fuel for Transportation Renewable Energy Innovations: Biofuels, Solar, and Other Technologies Page No. 123- 157 (2023)doi.org/10.1002/9781119785712.ch

PhD

ORIGINALITY REPORT

9%	5%	7%	2%
SIMILARITY INDEX	INTERNET SOURCES	PUBLICATIONS	STUDENT PAPERS

PRIMARY SOURCES

1	www.researchgate.net Internet Source	1%
2	encyclopedia.pub Internet Source	1%
3	Swapnil Bhurat, Shyam Pandey, Venkateshwarlu Chintala, Manas Jaiswal, Caneon Kurein. "Effect of novel fuel vaporiser technology on engine characteristics of partially premixed charge compression ignition (PCCI) engine with toroidal combustion chamber", Fuel, 2022 Publication	<1%
4	link.springer.com Internet Source	<1%
5	docplayer.net Internet Source	<1%
6	Ganjar Fadillah, Is Fatimah, Imam Sahroni, Muhammad Miqdam Musawwa, Teuku Meurah Indra Mahlia, Oki Muraza. "Recent	<1%

UPES
UNIVERSITY WITH A PURPOSE

PLAGIARISM CERTIFICATE

1. We Dr. Anil Kumar (Internal Guide), Dr. Shyam Pandey (Co Guide/ External Guide) certify that the Thesis titled

Catalytic Thermal Decomposition of the Muncipal Mixed Plastic Waste into Sustainable Alternative fuel for Modified CI engine

submitted by Scholar Mr/ Ms Shashank Pal having SAP ID 500080562 has been run through a Plagiarism Check Software and the Plagiarism Percentage is reported to be 9 %.

2. Plagiarism Report generated by the Plagiarism Software is attached .

Signature of the Internal Guide

Signature of External Guide/ Co Guide

Shashank Pal

Signature of the Scholar